CHEMICAL REVIEWS

Review

pubs.acs.org/CR

Nanoscaled Metal Borides and Phosphides: Recent Developments and Perspectives

Sophie Carenco,[†,‡,§,∥,⊥] David Portehault,*[,†,‡,§] Cédric Boissière,[†,‡,§] Nicolas Mézailles,[∥,#] and Clément Sanchez*[,†,‡,§]

[†]Chimie de la Matière Condensée de Paris, UPMC Univ Paris 06, UMR 7574, Collège de France, 11 Place Marcelin Berthelot, 75231 Paris Cedex 05, France

[‡]Chimie de la Matière Condensée de Paris, CNRS, UMR 77574, Collège de France, 11 Place Marcellin Berthelot, 75231 Paris Cedex 05, France

[§]Chimie de la Matière Condensée de Paris, Collège de France, 11 Place Marcellin Berthelot, 75231 Paris Cedex 05, France

[∥]Laboratory Heteroelements and Coordination, Chemistry Department, Ecole Polytechnique, CNRS-UMR 7653, Palaiseau, France

CONTENTS

Received: January 16, 2013

   dx.doi.org/10.1021/cr400020d | *Chem. Rev.* XXXX, XXX, XXX–XXX

dx.doi.org/10.1021/cr400020d | *Chem. Rev.* XXXX, XXX, XXX–XXX

1. INTRODUCTION

The quest for nanoscaling has extended beyond traditional metal oxides[1−4] and metal(0),[5] as exemplified by the huge development of "quantum dots" chalcogenide nanoparticles, in terms of both preparative methods and applications.[6−9] During the past decade, less common nanoscaled nitrides and carbides were also investigated. Their tremendous catalytic properties were a driving force for innovative research targeting novel nanomaterials, which resulted from original fabrication routes.[10]

In contrast, metal phosphides and metal borides remain mostly exotic for chemists, despite a specific set of properties that already supplied the worldwide industrial market with phosphide semiconductors[11,12] and catalysts,[13] but also with bulk boride refractory conductive ceramics,[14] hard magnets,[15] superconductors,[16] and hard materials.[14] Fundamental property aspects of bulk metal borides and metal phosphides are also the focus of many researchers: conduction,[17,18] luminescence,[19] field emission,[20] thermoelectric[21] and magnetic[21] properties, ultrahardness,[22,23] and behaviors as diffusion barriers[24] are among the current hot topics. Like for many other materials before, novel properties or performance improvements have emerged from nanoscaling. Especially, catalysis[25−27] and the energy harnessing[28−31] field occupy center stage of investigations into nanoscaled metal borides and metal phosphides. These new and exciting properties stand as the primary driving force for a 10-year-old research effort, focused on the design of new chemical synthesis approaches, which would allow downscaling these materials to the nanoregime.

Although few reviews have treated nanoscaled metal phosphides for specific topics such as lithium batteries,[32] catalysis,[33] or solid state synthesis under pressure,[34] no extensive critical review has been provided. To our knowledge, nanoscaled crystalline metal borides have never been reviewed so far, contrary to amorphous metal−boron alloys.[25,35−37] If this could certainly justify separate reviews on both systems, one could wonder why we are combining both compound families in a single report. The answer lies in the bonding scheme of metal borides and phosphides: most of them share metal−metalloid bonds (M−B or M−P) with a strong covalent component.[38] These bonds are usually stronger than those observed in metal carbides and nitrides.[39] They are also often combined with strong and highly covalent metalloid−metalloid bonds (B−B or P−P). These specific features provide metal borides and metal phosphides with unique properties, complemented by a wide range of compositions, crystal structures, and accessible electronic states,[40] which allow us to envision a myriad of novel discoveries.

Chemical colloidal routes toward nanophosphides are currently developed, and the resulting nanoparticles reach a high degree of sophistication in terms of composition, crystal structure, monodispersity, and morphology, as exemplified by the ones using tri-n-octylphopshine as a "P" source.[41−48] Many innovative approaches have been and still are being explored, including the choice of highly reactive metal and phosphorus precursors.[49,50] However, a sound understanding of reaction pathways is still missing, although it is mandatory to trigger a rational improvement of these routes and to identify new levers for an accurate control of the resulting materials. In comparison, nanoborides seem still in their infancy: colloidal routes have addressed amorphous nanoparticles, but very few attain nanocrystalline state.[51−56] Therefore, materials chemists are relying on more expensive approaches involving hard-to-handle gaseous precursors,[57] pressurized vessels,[34] high energy ball-milling,[58] etc. Besides cost issues, one of the main difficulties of these methods is the challenge of tuning the final nanomaterial characteristics. Indeed, the key experimental levers are not readily accessible and cannot be easily adjusted, thus resulting in mainly sub-micrometer-size particles. Although these systems are not strictly nanoscaled (many of them do not bear any dimension below 100 nm), they will be considered in this review, because they are the object of most current developments. Moreover, their syntheses can stimulate interesting reflections for further downscaling.

The first aim of the present review is to shed light on and to offer a critical look at the routes toward nanoscaled metal borides successfully explored, mainly within the last decade, and to show the exquisite control that can be reached by colloidal syntheses for metal phosphide nanoparticles.

The second aim is to answer an apparently simple question: Why have chemists seemingly just touched upon the fabrication of nanoscaled metal borides, as compared to metal phosphides? We will show that two main answers can be provided. First, the intrinsic bonding scheme of metal borides sets them apart due to the stronger B−B and M−B covalent bonds. These characteristics avoid long-range ordering of the glassy state, unless harsh conditions are provided for crystallization. This often means high temperatures which are not compatible with the isolation of nanostructured systems that are intrinsically metastable. The second answer is the nearly total absence of highly reactive boron sources that could decompose through a simple pathway to provide boron atoms. As a case in point, the crystal structures of usual crystalline forms of elemental phosphorus and boron are pictured in Figure 1. White phosphorus is a molecular species soluble in apolar solvents, highly reactive, and suitable as a P source for synthesis of metal phosphides at low temperature. On the contrary, α-boron is a covalent solid that is strongly inert and resists solubilization, and for which crystallization from the amorphous phase, made of disordered B_{12} clusters, occurs only in extreme pressure and temperature conditions.[59] This simple example illustrates a simple statement: nanomaterials chemists dealing with boron must always struggle with the B source and harsh synthesis conditions. The same holds true for other B based compounds, such as boron nitride and carbon boron nitrides, although these metal-free materials are not considered herein (for a recent review, see ref 60). Up to now, several processes have been examined, while innovative approaches are under development as ground-breaking concepts for a fundamental leap in the direction of nanoscaled borides. In this perspective, the

dx.doi.org/10.1021/cr400020d | Chem. Rev. XXXX, XXX, XXX−XXX

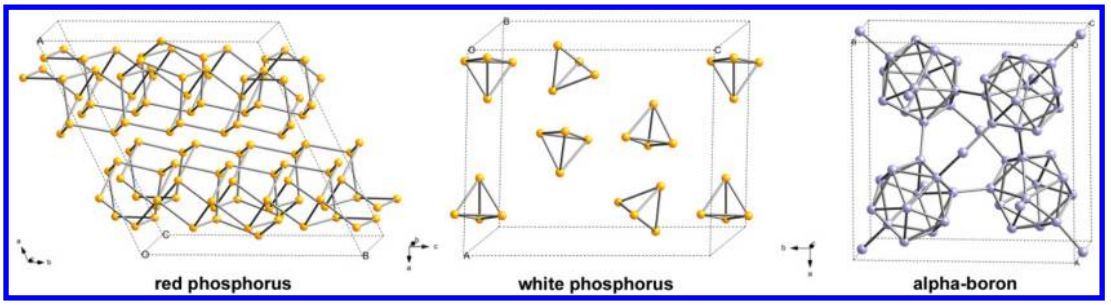

Figure 1. Crystal structures of P and B polymorphs.

background knowledge on metal phosphides might enlighten the boride way.

In order to provide the reader with sufficient background, the second section of this review deals with a short historical survey of metal borides and metal phosphides, a comparative discussion of their main structural and bonding features including most recent works, and their bulk conduction properties, as well as the characterization techniques dedicated to nanoborides and nanophosphides. The third section is a critical report on the different approaches developed for the synthesis of nanoscaled metal borides. The fourth section is a rational survey of the most recent colloidal routes toward metal phosphide nanoparticles. The fifth section examines the different properties that have emerged from nanoscaled metal borides and metal phosphides. Finally, the sixth section aims at identifying the perspectives for the next few years in this scientific area: technological bottlenecks are identified, and several worthy fields of investigation are highlighted. Because the topic of nanoscaled metal borides and metal phosphides is relatively young, this review includes mainly reports from the current century. This survey not only is dedicated to specialists who may find herein a critical look at the related literature, but also aims at raising the interest in some exotic materials of a broader range of scientists belonging to a multidisciplinary community, including solid state and nanomaterials chemistry and physics, organic chemistry, organometallic chemistry, and experimental and theoritical sciences.

2. INTRODUCTORY BACKGROUND

The chemistry and bonding scheme of metal borides and metal phosphides is closely related to the atomic radii and electronegativity of the metalloids: $r(B) = 0.85$ Å, $r(P) = 1.10$ Å, $\chi(B) = 2.0$, $\chi(P) = 2.2$ in the Pauling scale.

2.1. Nomenclature

In the nomenclature proposed by G. de Morveau, A. Lavoisier, C. Berthollet, and A. de Foucroy,[61] "metal phosphide" designates any compound that contains phosphorus and one or several metals, but no oxygen. Its general formula is M_xP_y. According to the modern nomenclature, a phosphide is a compound of phosphorus with one or several less electronegative element(s). However, by extension and by habit, metal−phosphorus compounds where the metal is more electronegative than P, such as Au_2P_3 [$\chi(P) = 2.2$, $\chi(Au) = 2.5$ in the Pauling scale], are still called "metal phosphide".

Boron is a "younger" element, formally identified by J. J. Berzelius in 1824. As a consequence, the metal borides are absent from Morveau et al. nomenclature, where only borate compounds were mentioned. Binary metal boride (MB) general formula is M_xB_y, and like in the metal phosphide (MP) case, MB does not contain oxygen.

Ternary $M_xB_yP_z$ alloys and alloys of MB or MP with another nonmetallic element such as nitrogen, carbon, or sulfur are possible. By convention, the compound is usually named after the most electronegative element.

2.2. Instructive Genesis of Metal Phosphides and Metal Borides

Binary metal borides are encountered with nearly all main-group elements and d-group and rare earth metals. The notable exceptions are zinc, cadmium, mercury, gallium, indium, thallium, tin, and lead.[38,40] Binary combinations with a given element often exhibit various compositions that can range from M_3B to MB_{66}.[38,40] Numerous ternary[62,63] or quaternary[64] compounds are also known. It should be mentioned that elements with low affinity with boron in binary compounds can be incorporated into ternary structures (e.g., Ga and Zn in $Ni_{12}GaB_8$, $Ni_{21}Zn_2B_{24}$).[62,63,65] Phosphorus on the other side is known to form at least one stable combination with every main-group and d-group metals (for example, InP, Cu_3P), while most of the rare earth metals were also found to form phosphide (for example, Eu_4P_3).[66,67] Many metal phosphides accept several stoichiometries, providing a large number of structures for binary metal phosphides. Ternary (and more) structures are also known for several metals (for example, $MnCoP_4$), along with amorphous alloys (for example, Fe_xCr_yP).[68] Interestingly, MBs and MPs were originally man-made materials. First reports of preparation originate from France and Germany.

2.2.1. Metal Borides: A Challenging Topic in Materials Synthesis. The first MBs reported were iron and platinum borides which were prepared by C. Descotils and L. Gemlin at the beginning of the 19th century. Boric acid was reacted with fine metallic powders by carboreduction, which led to carbon contamination. It was recognized as early as in 1827 by Lassaigne that H_2 was thus a better reducing agent to avoid the competitive formation of carbides.[69,70]

Preparative methods for bulk metal borides have been first reviewed in the 1950s and 1960s by a number of reports from Kiessling, Samsonov et al., and Schwarzkopf et al. followed by Gilles and Greenwood.[71−74] Difficulties raised by the preparation of metal borides when they were discovered were quite similar to those encountered nowadays. In particular, scientists are facing the absence of a reactive elemental boron source. Actually, boron had not even been properly isolated when borides were identified. Von Crell, Gay-Lussac, Thenard, and Davy[75−77] discovered elemental boron in its amorphous state with strong contaminations from the reactants during the first decade of the 19th century, by reducing boron oxide B_2O_3 or boric acid ($B(OH)_3$) by potassium or iron or by electrolysis. One century later, Moissan obtained purer boron by reducing boron oxide with magnesium.[78] The first sample of pure elemental boron (>99%) was reported in 1909 by Weintraub.[79]

dx.doi.org/10.1021/cr400020d | Chem. Rev. XXXX, XXX, XXX−XXX

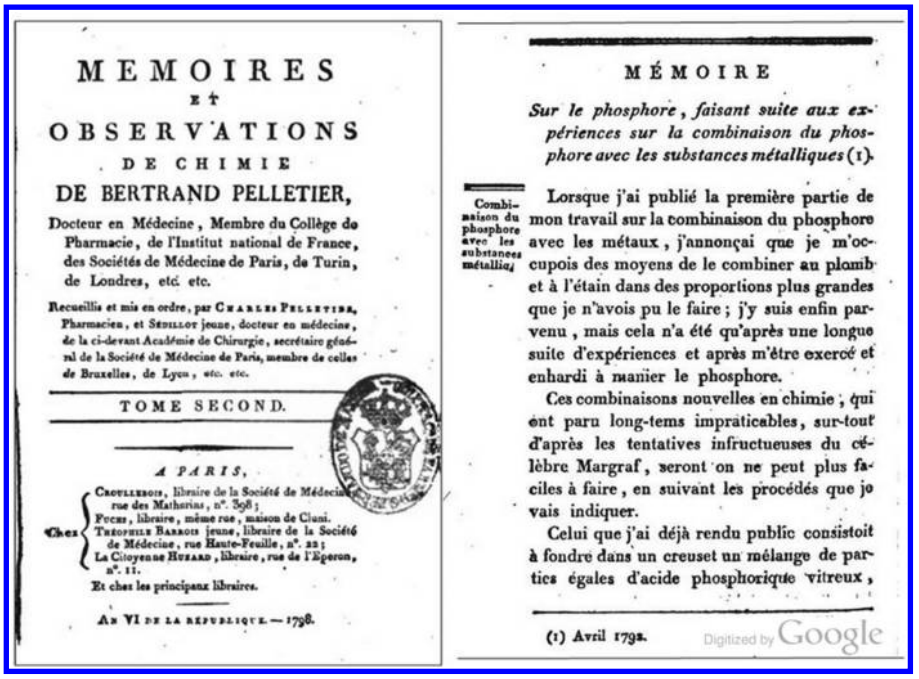
MEMOIRES
ET
OBSERVATIONS
DE CHIMIE
DE BERTRAND PELLETIER,
Docteur en Médecine, Membre du Collège de Pharmacie, de l'Institut national de France, des Sociétés de Médecine de Paris, de Turin, de Londres, etc. etc.
TOME SECOND.
A PARIS,
MÉMOIRE
Sur le phosphore, faisant suite aux expériences sur la combinaison du phosphore avec les substances métalliques (1).
Lorsque j'ai publié la première partie de mon travail sur la combinaison du phosphore avec les métaux, j'annonçai que je m'occupois des moyens de le combiner au plomb et à l'étain dans des proportions plus grandes que je n'avois pu le faire; j'y suis enfin parvenu, mais cela n'a été qu'après une longue suite d'expériences et après m'être exercé et enhardi à manier le phosphore.
Ces combinaisons nouvelles en chimie, qui ont paru long-tems impraticables, sur-tout d'après les tentatives infructueuses du célèbre Margraf, seront on ne peut plus faciles à faire, en suivant les procédés que je vais indiquer.
Celui que j'ai déjà rendu public consistoit à fondre dans un creuset un mélange de parties égales d'acide phosphorique vitreux,
(1) Avril 1792.

Figure 2. Cover and first page of B. Pelletier's report on metal phosphide.[98] Tentative translation: "About Phosphorus, following the experiments on combining phosphorus with metallic compounds. When I first reported on the combination of phosphorus with metals, I stated that I intended to combine it with lead and tin in larger proportions than previously achieved; I finally managed it, though only after a long series of experiments and after being emboldened by extensive practice and manipulation of phosphorus. These new chemical combinations, which seemed for a long time unattainable, especially according to the unsuccessful tries of the famous Margraf, will be readily obtained, following the procedures that I indicate here."

Metal borides are typically synthesized by the solid state reaction between the elemental constituents.[38] The method is still commonly employed in order to obtain novel compositions, structures, and properties.[40] Energetic ball milling can activate the reaction between boron and metals such as chromium, titanium, or zirconium, yielding submicrometer size particles.[80,81] The so-called borothermal reduction is another common route based on the combination of metal oxide and boron.[38] The latter acts as both reductant and boron source and must be used in excess stoichiometry (eq 1) because boron oxide evolves as a side-product. In certain cases, the composition within binary compounds is controlled by adjusting the initial reactant ratio, for instance in the NbB-Nb_3B_4–NbB_2, WB-W_2B_5 and Cr_5B_3–CrB-CrB_2 systems.[82,83]

$$3Nb_2O_5(s) + 22B(s) \rightarrow 6NbB_2(s) + 5B_2O_3 \quad (1)$$

Reactions of boron with metal(0) or metal oxide are usually highly exothermic. As a result, after an initiating step typically above 200 °C,[82,83] temperature self-sustains, if not increases. These so-called self-propagating high temperature syntheses (SHS) have the advantage of low energy consumption, but they must be carefully controlled for safety concerns. Other solid state reactions have been used such as reduction of metal oxide by boron carbide B_4C or carbothermal reduction of metal oxide and boron oxide.[38]

Most of the aforementioned solid state approaches suffer from the incorporation of "foreign" species in the resulting compound. Pollution from the reaction container (crucible), the reactants (carbon, metal additives as reducing agents), and the atmosphere (traces of water and oxygen) is related to the high temperatures required to perform these reactions with inert elemental boron. As a landmark, the reader should bear in mind the very high melting points of the various boron polymorphs (above 2000 °C). The related Tammann temperature (ca. 0.5 times the melting point),[84] above which bulk-to-surface atom migration can occur in the grains, is also high. Very high temperatures (usually between 1000 and 1800 °C) are thus required for solid state reactions between the pure elements, even with amorphous boron. Besides contamination problems, reaching such high temperatures can also be costly and challenging. Moreover, isolating kinetic products in such conditions might turn out to be an illusory task.

Since the 19th century, the inertness of elemental boron and the very high synthesis temperatures required have been the milestones paving the search for alternative synthetic processes that clearly distinguish themselves from the metal phosphide situation. Combining the constitutive elements into metal flux (aluminum, copper, gallium, tin, and their mixtures) efficiently decreases the reaction temperature, provides homogeneous compounds, and allows the growth of single crystals.[85,86] Additional information about this wide ranging topic can be found in the recent review of Kanatzidis, Pöttgen, and Jeitschko.[87] High temperature electrolysis of metal salts in molten alkali borates or boric oxide is also a popular synthetic route.[88] The common drawback of these techniques lies in the possible contamination by the metal bath or the electrolyte.[87]

The use of other, more reactive, boron sources was addressed early on, in 1909 by Weintraub who reduced boron halides by hydrogen for the first production of pure boron (>99%). Pioneering works on room temperature precipitation of amorphous metal–boron alloys in solutions started in the 1950s with the study of metal chloride reduction by borohydrides.[89,90] When heated under inert atmosphere, the amorphous powders undergo crystallization. Bulk Co_2B,[91−93] Fe_2B, and FeB,[94] and mixtures of M, M_2B, and M_3B (M = Co, Ni, Fe),[95,96] were obtained between 400 and 580 °C. Today,

dx.doi.org/10.1021/cr400020d | Chem. Rev. XXXX, XXX, XXX–XXX

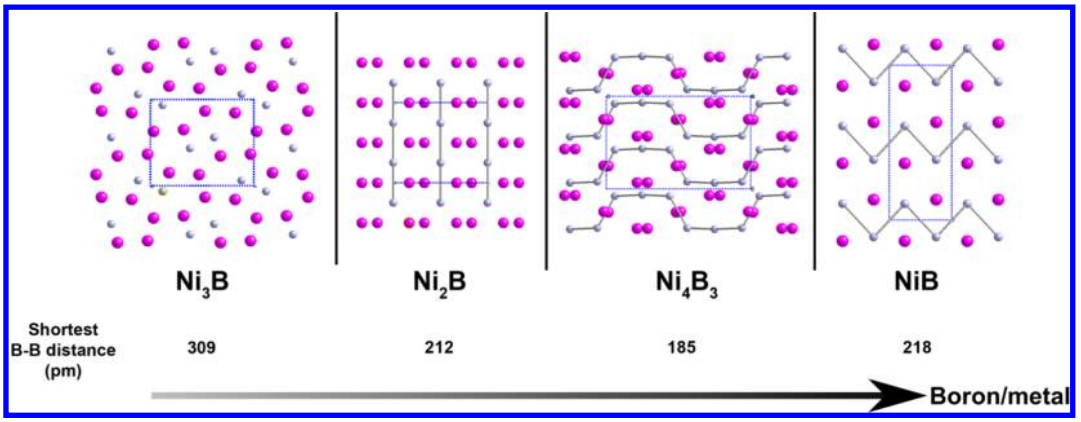

Figure 3. Crystal structures and compositions of nickel borides as an example of metal-rich borides. The displayed Ni_4B_3 structure corresponds to the monoclinic polymorph. Shortest B−B bonds are observed in these compounds. Small spheres represent boron atoms; large spheres represent nickel atoms.

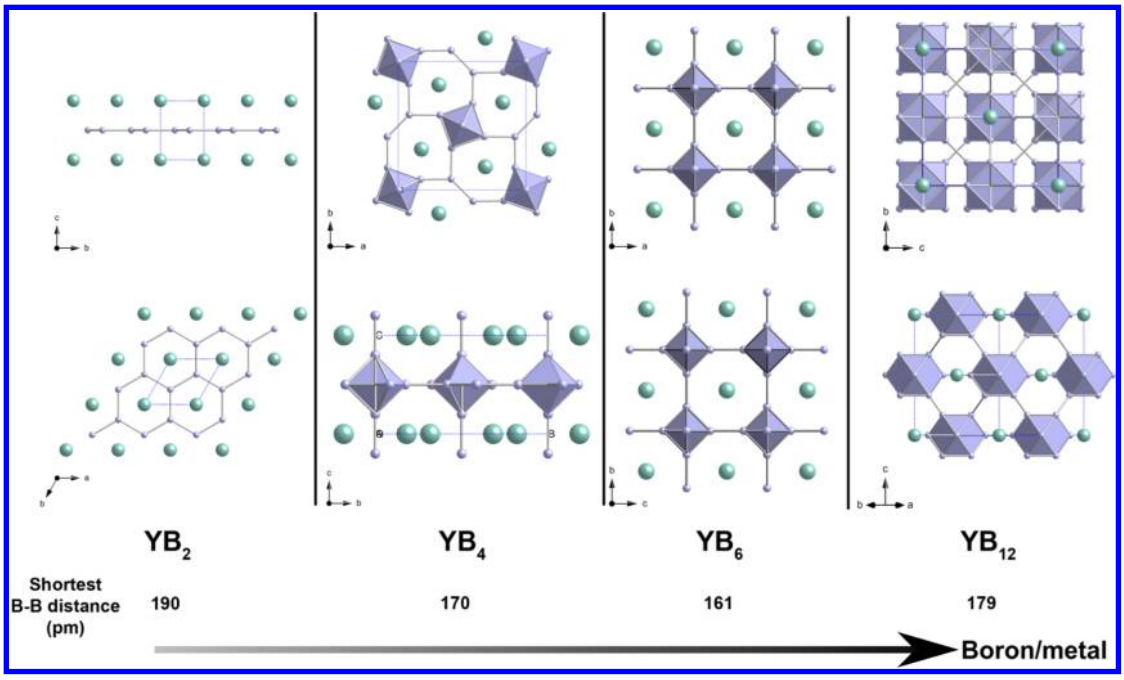

Figure 4. Crystal structures, compositions, and shortest B−B distances of yttrium borides YB_2, YB_4, YB_6, and YB_{12}. Small spheres (polyhedra) represent boron atoms (boron polyhedra); big spheres represent yttrium atoms.

the identification of reactive boron sources like boron halides and borohydrides is still a strong bottleneck for the development of nanostructured borides.

In addition to the difficulties related to the inertness of elemental boron and the high temperatures of synthesis, one should also consider the poor stability of metal-rich borides in air or in the presence of moisture. In this perspective, one understands why platinum boride remained one of the only known borides for decades: this metal both catalyzes the reduction of the starting materials (such as boric acid) in the presence of H_2 and carbon, and yields robust metal borides.

2.2.2. Metal Phosphides: Materials from the New Era of Chemistry. In Berlin, Andreas Marggraf (1709−1782) prepared zinc phosphide, after having isolated pure zinc (the discovery for which he is the most known today).[97] During the same century, in the chaos of the French Revolution in Paris, Bertrand Pelletier (1761−1797) prepared a series of 20 metal phosphides from several experimental routes.[98] Notably, he added small pieces of white phosphorus on silver and nickel heated near their melting point and identified the Ag_2P and Ni_2P compounds, using a balance as the sole quantitative instrument of characterization. He reported these reactions in 1792 (although the report was published after his death by his colleagues in 1798) in a series of writings that, as a 220 year old text, exhibited a particularly modern approach to inorganic chemistry (Figure 2).[98,99] In this report, Pelletier proposed several routes to bulk MPs, including the direct reaction of cuts of P_4 on melted metals.

However, no immediate use was found for metal phosphides, which remained for centuries in the books mainly as curiosities. Nevertheless, since these early reports and until the 1960s, other metal phosphides have been prepared and used in metallurgy and as pesticides, and their structures have been characterized by crystallography.[67]

Indeed, most of the syntheses of metal phosphides were done at high temperature and/or high pressure, suitable for

dx.doi.org/10.1021/cr400020d | Chem. Rev. XXXX, XXX, XXX−XXX

decomposing or vaporizing the precursors and to yield crystalline noncontaminated bulk materials,[68] whose thermodynamic data have been reviewed.[100] They typically involved sequences of annealing and grinding (so-called "heat and beat" method of synthesis). The reactions were conducted either in sealed ampules, in molten metal flux,[87] or by arc melting. Very few syntheses were conducted in a solvent, and in these cases ammonia was used.[101] White phosphorus, red phosphorus, and alkali phosphide were used as phosphorus sources. Alternatively, reduction[102] by H_2 or carbon or electrolysis of phosphates also provided metal phosphides.[68]

2.3. Metal Boride and Metal Phosphide Crystallographic Structures

Crystallographic structures are often classified through the B or P substructures. Because their specific structural features impact directly both the synthesis processes and the resulting properties, a short description is provided in the following section. In a pedagogical purpose, we provide below a few examples of trends that can be found in metal borides and metal phosphides, and by comparison of the two families. Our intent is not to give a full overview of the very rich panel of crystallographic structures, as this was done in the past in extensive ways,[38,40,64,67,71,103−106] and as this does not enter in the scope of describing the nanoscaled recent developments of these materials.

2.3.1. Metal Boride Crystallographic Structures. Metal borides exhibit a huge compositional and structural diversity (ca. 540 entries in the 2010 ICDD database for binary compounds with the exception of H, C, N, P, O, S, Se, F, Cl, Br after removal of the duplicates). Upon an increase in the boron to metal ratio, the B sublattice evolves from isolated clusters to extended one-, two-, and then three-dimensional boron frameworks. Nickel borides are a case in point for metal-rich MBs (from Ni_3B to NiB_2; NiB_3 has also been recently suggested[107]) (Figure 3). Ni_3B contains boron atoms within Ni trigonal prisms which are isolated as suggested by the long B−B distances. Ni_2B is made of linear chains of short B−B bonds; NiB and monoclinic Ni_4B_3 incorporate corrugated B−B chains with boron−boron distances close to those of elemental boron (ca. 175 pm).

The B sublattice experiences growing complexity upon an increase of B content in boron-rich alloys (from MB_2 to MB_{66}). Yttrium borides nicely exemplify this behavior (Figure 4). In metal diboride YB_2, boron atoms associate into a layered hexagonal framework. In YB_4, these boron layers are interconnected. YB_6 has a typical cubic structure made of B_6 octahedra connected together through a B−B bond. YB_{12} is made of connected cuboctahedra, while the structural unit of YB_{25} and YB_{50} is the B_{12} icosahedron.[18] YB_{66} (Figure 5) illustrates the ultimate complexity that metal-rich borides can reach.[18] This structure is also based on B_{12} icosahedra arranged in a 3-dimensional network. B−B bonds in boron-rich borides are short, and their values are very close to those observed in elemental boron.

Diborides of main group and rare earth metals exhibit a layered honeycomb structure. The typical strong ionic character of M−B bonds with such elements in MB_2 (97% and 92% of ionicity in, respectively, MgB_2, AlB_2)[108,109] leads to a $(B^-)_n$ lattice isoelectronic to graphite which explains the sheet-like structure. For transition metal borides of a given stoichiometry, different crystal structures are encountered depending on the metal. This was qualitatively rationalized by Burdett et al.[110,111]

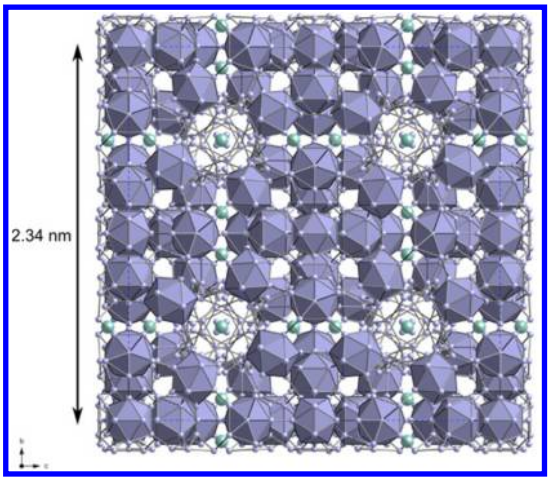

Figure 5. One single cell of YB_{66}. Small spheres (polyhedra) represent boron atoms (B_{12} icosahedra); big spheres represent yttrium atoms.

for transition metal tetraborides MB_4 and diborides MB_2 with M−B bonds of partially covalent nature (e.g., 22%, 52%, and 80% of M−B bond ionicity in, respectively, TiB_2, NbB_2, and HfB_2).[109] For instance, by moving from Ti to Re (Figure 6),

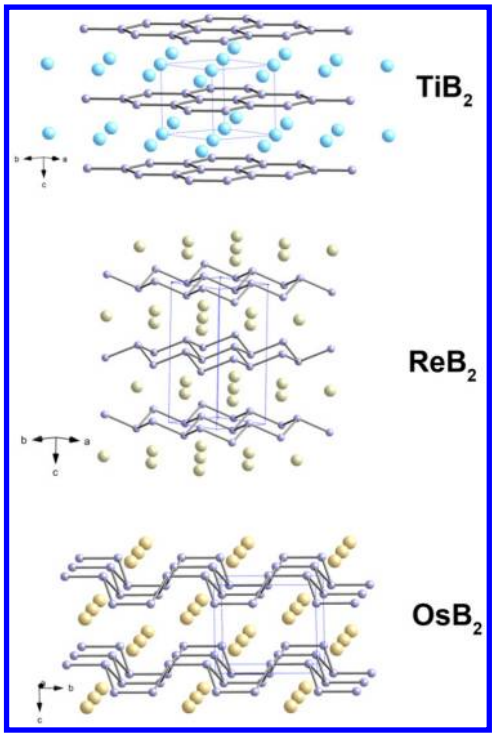

Figure 6. Crystal structures of transition metal diborides TiB_2, ReB_2, and OsB_2. Small spheres represent boron atoms; large spheres represent Ti, Re, or Os atoms.

diborides experience a change from the layered boron honeycomb AlB_2-type structure described above (Ti, V, Cr, Mn, Zr, Nb, Mo, Hf) to puckered boron sheets (Tc, Re). By doing so, the coordination number of the metal decreases from 12 to 8, and the M−M distance through boron sheets increases. This correlates with an increase in the population of an intersheet M−M antibonding band as the d electron count increases. This change in band filling can be accounted, at least partially, for the change in the diboride structure as the metal

dx.doi.org/10.1021/cr400020d | Chem. Rev. XXXX, XXX, XXX−XXX

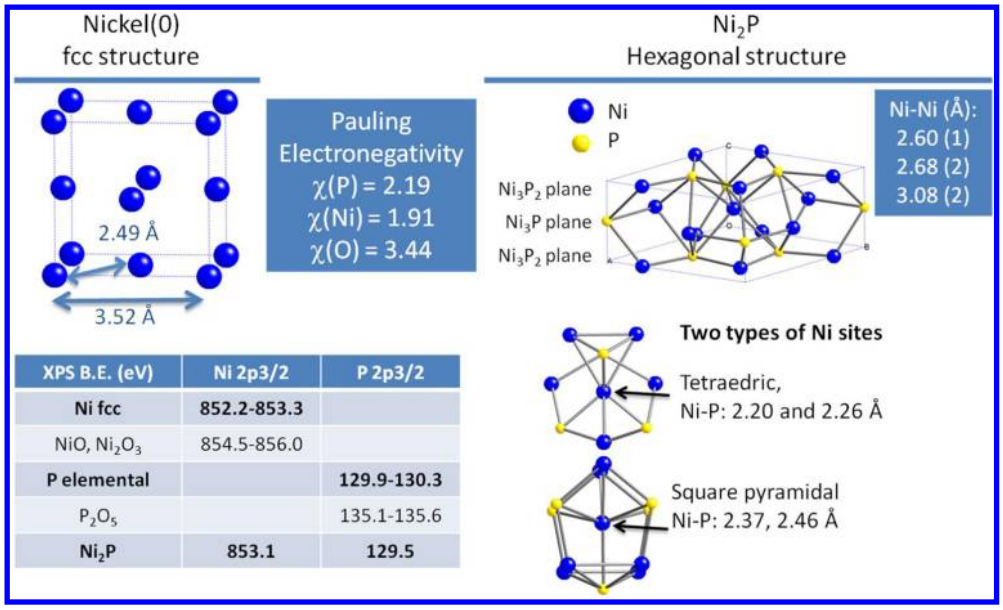

Figure 7. Comparison of Ni_2P and Ni fcc structures. Top Ni_2P structure was adapted with permission from ref 113. Copyright 2004 Elsevier. Bottom Ni_2P structures were adapted with permission from ref 26. Copyright 2009 Elsevier. XPS average binding energy values were taken from NIST XPS Database: http://srdata.nist.gov/xps/Default.aspx.

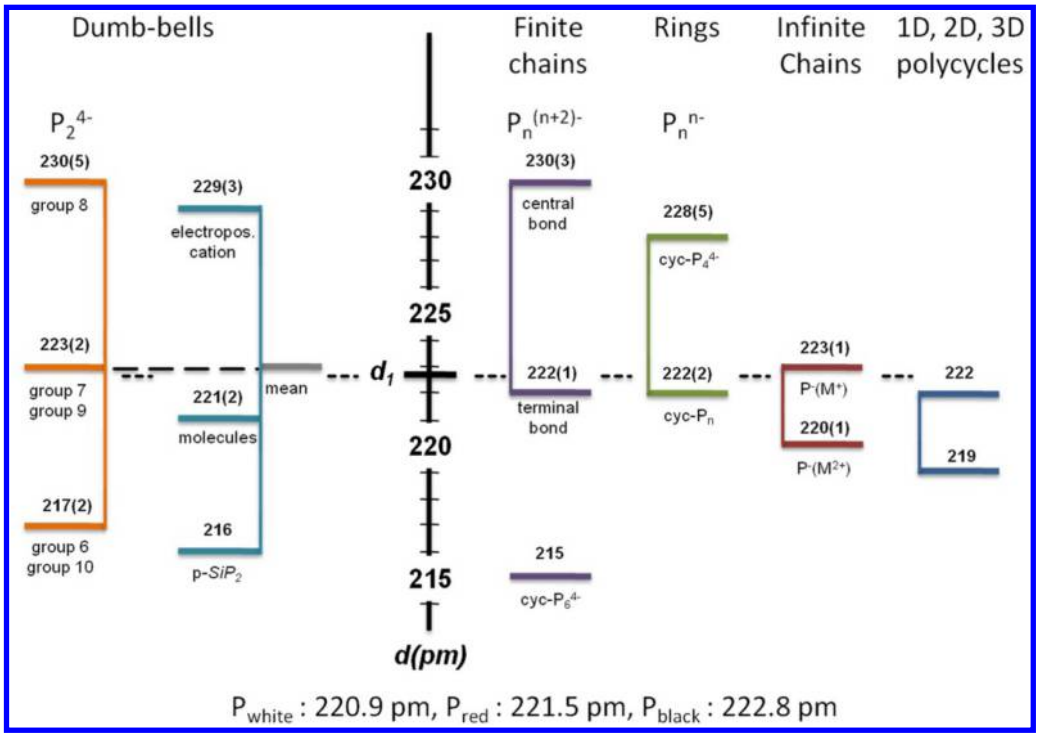

Figure 8. Average P−P bond (pm) in various MP structures. (Adapted with permission from ref 67. Copyright 1988 American Chemical Society.) d_1 corresponds to the P−P distance in P_{black}, which is a near strain-free compound.

group number increases. Interestingly, T. Fehlner proposed an extension of this qualitative solid state approach to the case of molecular metallaboranes.[112] From the point of view of the materials synthesis, it is interesting to note that the typical strength and directionality of B−B bonds usually imply high energy input to trigger the crystallization of boron-rich solids that exhibit extended B−B frameworks.[18]

2.3.2. Metal Phosphide Crystallographic Structures. A very complete description of MPs structures was done by Schnering and Hönle in 1988.[67] As an example of metal-rich phosphides, the structure of Ni_2P is depicted in Figure 7. Ni−Ni bonds are only slightly elongated compared with those of Ni fcc, and Ni−P bonds are short, resulting in a quite dense structure made of a succession of strongly connected Ni_3P_2 and Ni_3P planes along the *c* axis.

In metal phosphides, phosphorus has a lower catenation tendency than boron. For instance, P atoms in Ni_2P are isolated into the metal lattice (d(P−P) = 340 pm, 153% of the mean value in elemental phosphorus),[67] while Ni_2B is made of covalent B−B bond chains (d(B−B) = 212 pm, 121% of the

dx.doi.org/10.1021/cr400020d | Chem. Rev. XXXX, XXX, XXX−XXX

mean value in elemental boron). Similarly, MP_2 contains chains of P−P bonds while MB_2 incorporates B sheets (graphite-like or puckered-like). As for boron, the extent of P networking increases with the metalloid content. P units exhibit a wide variety in terms of building blocks (cages, dumbbell, etc.) and superstructures (1D to 3D chains). The description of structural families in MPs with higher P content is at least as arduous as in MBs. Especially, more diversity is observed for a given stoichiometry, which might be related to the more diffusive orbitals of P compared to B and the hypervalence tendency of phosphorus. As a result, P frameworks show high flexibility. P−P−P angles ranging from 60° to 120° and varying P−P distances were observed, depending on the metal environment and on the M/P ratio. Unsaturated P−P bonds were even found in M_4P_6 phosphides (M = K, Rb, Cs), resulting in planar isometric P_6 rings and very short P−P bonds (215 pm).

As discussed below in subsection 2.5.3, metal−metalloid bonds usually show higher ionicity in MPs than MBs because of the higher electronegativity of P. Consequently, Schnering and Hönle[67] described the P framework according to P units. Such formalism was precluded for most metal borides because of their strongly covalent M−B bonds. The wide variety of P units in terms of charges (ranging from $[P]^{3-}$ to $[P_{15}]^{-}$), substructures (cages, dumbbell, etc.), and superstructures (1D to 3D chains) was highlighted (Figure 8).

The purpose here is not to give a detailed account of all the possible structures. As an example, the case of MP_7 alkali polyphosphides, formulated as $(M^+)(P_7^-)$ and built on P_7^- anions, is illustrated in Figure 9. The smallest cations lead to

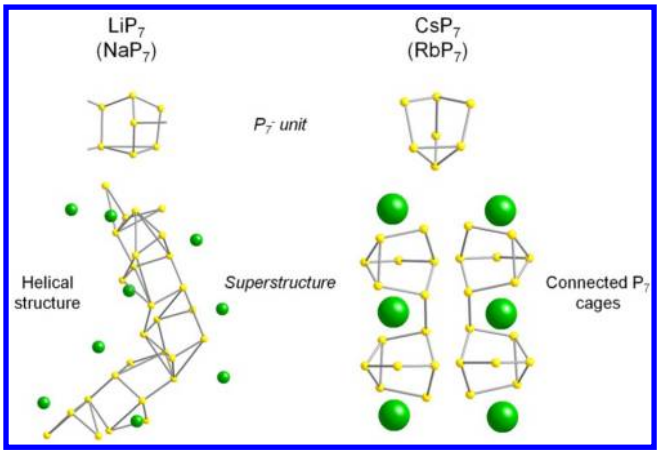

Figure 9. Structural flexibility: the example of MP_7 alkali phosphides. (Adapted with permission from ref 67. Copyright 1988 American Chemical Society.) Yellow represents phosphorus; green represents alkali.

helical chains while the largest ones yield connected P_7 cages. The K^+ cation is both too large for the helical chain cages and too small for the connected P_7 cages: the reaction of potassium and phosphorus (K/P = 1/7) leads to mixtures of phosphides with lower and higher P contents. While a complete description of the existing structures would have been out of the topic of this review, this only example illustrated both the variety of structures and the existence of structural constraints in MPs.

2.4. Quest for Original Structures: Latest Developments

2.4.1. New Developments for Bulk Metal Borides. The main driving force of the research effort on metal borides lies in their specific properties, such as their mechanical behaviors, some of them being superhard or considered as potential ultrahard materials.[22,105,106] Also, superconductivity,[17,18] thermoelectric[21] and specific magnetic behaviors[21] are in the focus of metal boride research. Many of these properties arise from the interplay between a strong extended boron covalent framework and the metal lattice. Therefore, a big part of current work is dedicated to the understanding of the complex interaction between both sublattices. As mentioned above, these phases often require high temperature to undergo crystallization. In such conditions, isolating nanoscaled phases which are metastable in essence is an arduous task. In addition, the use of bulk compounds permits an easier identification of the impact of the crystal structure on the properties, and it discards nanoscaling effects. This is the reason why the search for novel bulk phases of metal borides is so active nowadays.[40,64] Metal flux syntheses,[87] the use of mineralizers in solid state reactions,[114] and combustion syntheses[82,115,116] (self-propagating high-temperature synthesis) are some of the most recent developments in synthetic processes. A growing number of studies is also focused on metal-rich borides, exhibiting magnetic properties in particular.[64] Numerous ternary (e.g., $Ni_{12}AlB_8$, $Ni_{12}GaB_8$, $Ni_{10.6}Ga_{0.4}B_6$,[62] $B_{14}Ga_3Ni_{27}$[63]) or quaternary (e.g., $Ti_9Fe_2Ru_{18}B_8$, $Ti_8Fe_3Ru_{18}B_8$, $Ti_7Fe_4Ru_{18}B_8$[64]) compounds were recently uncovered. Among metal-rich systems, one should mention τ-borides with cubic crystal structure formula $(MM')_{23}B_6$ which represents a large group of about 80 representatives.[117] The main component M is typically a first row 3d transition metal (Ni, Co, Cr) while the choice for M′ is larger (Al, Ga, Sn, Ti, V, Ir, Er, Lu, and so forth).[118−120] A wide nonstoichiometry range is observed in these compounds, and higher boron contents usually result from the substitution of metals by B_4 tetrahedra.[118,120] τ-Borides are often encountered during alloy hardening by boriding or at grain boundaries.[121−124]

2.4.2. New Developments for Bulk Metal Phosphides. Even though the major part of the contemporary work on metal phosphide deals with nanoparticles or nanoscaled forms of matter, bulk metal phosphides are still under investigation. Among major results of the past decades, new bulk phases were prepared, and concerned binary phosphide containing poorly accessible metals such as uranium (UP_4)[125] or made under strenuous conditions such as high temperatures (Ni_5P_2).[126] Ternary phases were, however, the most investigated: Ti_2PTe_2,[127,128] $La_3Zn_{2-x}P_4$ (containing isolated P^{3-} species),[129] Zr_2PTe_2,[130] $BaGa_2P_2$,[131] $Eu_3Ga_2P_4$,[132] $Sm_{15}Ir_{33}P_{26}$,[133] $LnRuP_2$ (Ln = Pr, Nd, Sm, Tb, Dy, Er)[134] and other Ir-rich ternary phosphide,[135] and $NaGe_3P_3$, featuring an unusual $[Ge_3P_7]$ ring where each Ge has a different formal oxidation state,[136] were recently obtained and characterized. The quaternary alloy $Rb_4Sn_5P_4Se_{20}$ was synthesized and described as a metallic composite structure containing conducting Sn_5Se_8 and insulating layers P_2Se_6.[137] Defective structures such as $ZnGeP_2$[138] and $RENi_{2-x}P_2$ (RE = La, Ce, Pr) with nickel deficiency[139] were also studied. In another approach, molecular gas-phase precursor $P(SiH_3)_3$ was utilized for the preparation of monocrystalline Si_3AlP on a Si substrate.[140] Preparations of binary phosphides keep being improved and were achieved for several phases using a lithium metaphosphate melt (AlP, CrP, NbP, MoP, WP)[141] or a solid-stated reduction route (Fe−P binary and ternary alloy powders).[142] Lastly, preferential magnetic alignments were studied in polycrystalline MnP samples.[143]

dx.doi.org/10.1021/cr400020d | Chem. Rev. XXXX, XXX, XXX−XXX

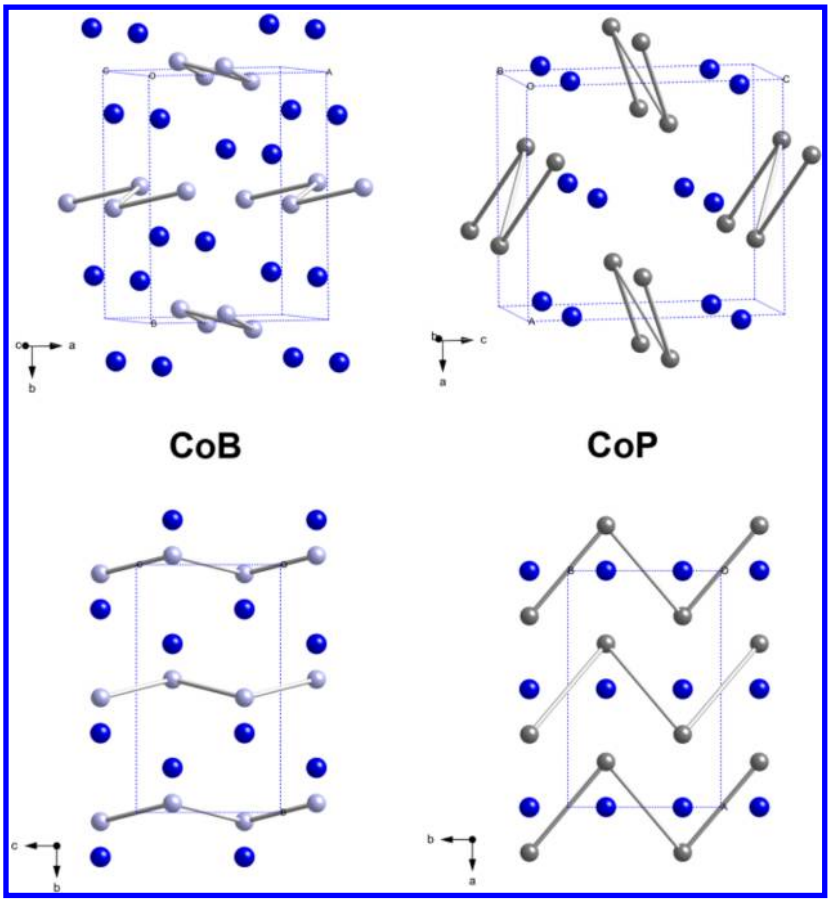

Figure 10. Crystal structure of CoB and CoP. Gray spheres represent boron or phosphorus atoms; blue spheres represent cobalt atoms.

2.4.3. Contribution of Calculations: Thermodynamics, New Phases, and Properties. Thermodynamic knowledge was improved with the publication of updated M−P phase diagrams (Rb−P,[144] K−P,[145] Na−P,[146] Cs−P,[147] Ni−P[148,149]). Relative stabilities of different boride phases have also been investigated.[39,150−155] Among metal phosphides, the Ni−P system was particularly studied in the Ni-rich side.[156] Heat capacity of InP was also determined.[157] Recently, first-principle studies were devoted to the phase transitions of several binary phosphides (Co−P,[158] InP,[159,160] GaP,[160] BP,[160] and AlP[160]) and ternary phosphides such as $LaFe_4P_{12}$[161] and Au_2MP_2 ternary alloys (M = Pb, Tl, Hg).[162]

First principle calculations also become of utmost importance in order to shed some light on structure−property relationships in metal borides and phosphides. Especially, theory is nowadays an invaluable help in the understanding of electronic and mechanical properties of these materials (see subsection 2.5).[105,106,152−155,158,163−165] Such studies are mainly dedicated to well crystallized systems. Only few modelization works have been conducted as to the effect of nanoscaling on the properties of borides.[166] Few theoretical studies were devoted to the electronic structure of amorphous M−B and M−P alloys.[167−175] Another very active research field where theory now has a strong input is the area of superhard materials, especially for boron-containing systems. Ab initio calculations are used not only to evaluate mechanical properties,[105,106] but also to predict or identify new superhard phases based on heavy transition metal borides.[155,176−178]

2.5. Bonding and Electronic Structure in Metal Borides and Phosphides

Interestingly, phosphorus (χ(P) = 2.19) and boron (χ(B) = 2.04) elements exhibit a relatively low difference of electronegativity with most metals, if compared with carbon (χ(C) = 2.55), sulfur (χ(S) = 2.58), nitrogen (χ(N) = 3.04), or oxygen (χ(O) = 3.44). Consequently, electronic delocalization is expected to a varying extent in metal borides and phosphides.

2.5.1. Case in Point: Cobalt Monoboride and Monophosphide. As an illustration and starting point for the comparison between metal borides and metal phosphides, one can consider the case of compositionally and structurally related CoB and CoP (Figure 10). CoB is isostructural to the previously described NiB. It contains zigzag B−B chains. The same metalloid structural unit exists in CoP. In both compounds, the Co−Co distances are similar (260 pm) and close to those observed in elemental cobalt (251 pm). Differences are observed between borides and phosphides for bonds involving metalloid atoms: the B−B bonds (192 pm, 110% of the mean length in elemental boron) are much shorter than the P−P bonds (270 pm, 121% of the mean length in the different allotropes of elemental phosphorus). Modelizations provide deeper insights into the bonding scheme and show strong covalent interactions between boron atoms,[179,180] while only weak covalent bonding occurs between phosphorus atoms[158] as confirmed by XPS measurements.[181] Actually, the nearest neighbors of metalloid atoms are boron atoms in CoB and metal atoms in CoP. This clearly shows that covalency in the metalloid sublattice is much more pronounced in borides. As to metal−metalloid interaction, again, calculations and

dx.doi.org/10.1021/cr400020d | *Chem. Rev.* XXXX, XXX, XXX−XXX

electron density maps suggest higher covalency for metal−boron bonds than metal−phosphorus bonds.[158,179,180,182] XPS data[181] suggest charge separation $[Co^{0.7+}][P^{0.7-}]$ which agrees with the classical view $[Co^{1+}][P^{1-}]$.[67]

The comparison between CoB, CoP, and more ionic compounds (for instance, CoO: Co−Co distances are 301 pm, which is larger than Co−Co in Co, CoB, and CoP) highlights bonding similarities between both metalloid based systems, which can be considered as involving covalent bonds to varying extent between metalloid atoms on one side and metal−metalloid centers on the other side. The most striking difference between the bonding schemes of metal borides and phosphides is the higher covalency occurring in metal borides, especially within the metalloid sublattice. Since considering only one case might be somehow simplistic and could not provide sufficient knowledge background for understanding the relationship between structure, property, and available synthetic pathways, we provide in the following more details about the nature of the bonds and the trends observed in both families.

2.5.2. Metal−Metal and Metalloid−Metalloid Bonds. *2.5.2.1. Metal Borides.* Two general features must be highlighted for metal borides. First, strong electron delocalization often occurs in the M−M sublattice as highlighted by ab initio and DFT calculations.[106,153] This metallic cohesion in the M sublattice prevails as long as the distances between metal atoms are close to those observed in the parent metal (usually MB_x, $x \leq 6$). Second and most importantly, a strong covalency always prevails in the B sublattice with short, rigid, and directional B−B bonds, as long as the boron content enables the formation of an extended boron framework ($x \geq 0.5$ in MB_x). The covalent character of B−B bonds is clearly reflected in the short B−B distances (175−210 pm) close to those observed in elemental boron (ca. 175 pm). Electron localization between boron atoms was also highlighted by numerous first principle calculations.[106,114,155,182] Actually, the main contribution to the cohesion energy of metal borides with extended boron frameworks comes from the B−B bond sublattice.[106]

2.5.2.2. Metal Phosphides. According to XPS,[181−183] XANES,[183] and first principle calculations,[158,182] electron delocalization in the metal sublattice of phosphides is the most common case for lower transition metal phosphides M_3P, M_2P, and MP. Nevertheless, the extent of delocalization is rapidly decreasing as the P content increases, and most of the diphosphides are semiconductors.[11] This trend might be related to the ionic character of MPs for which phosphorus atoms drag most of the valence electron density.[158] Also, strong overlapping between P and M orbitals allows significant electron backdonation from M to P. The poor P−P interaction highlighted for CoP is strengthened in phosphides with higher P content. Similarly, short P−P distances down to a minimum of 215 pm are found in P_4^{6-} finite chain structures such as M_4P_6 (M = K, Rb, Cs), M_3P_4 (M = Sr, Ba), and MP_2 (M = Pr, Nd) (Figure 8).[158]

2.5.3. Metal−Metalloid Bonds: From Covalency to Ionicity. The oxidation degree of the metal in a metal boride or phosphide lattice is easy neither to define, nor to connect with the experimental properties. Some tendencies are highlighted in the following, which shed light on the behaviors of MBs and MPs discussed in section 5.

2.5.3.1. Metal Borides. More often than not, the polarization of M−B bonds is not complete. Actually, the amount and direction of electron transfer between a transition metal and boron has been questioned since the earliest works and monographs dedicated to borides.[38,71,184,185] It is still highly debated nowadays, especially in view of the most recent first principle calculations and state of the art photoelectron spectroscopy. Until recently, the consensus was that two behaviors of electron transfer should be distinguished: from M to B in boron-rich systems (MB_x, $x \geq 2$) and from B to M for metal-rich borides (MB_x, $x \leq 2$).

The case of boron-rich borides is relatively intuitive because it is in agreement with the electronegativity scales as suggested by Pauling.[184−186] This was especially shown for metal hexaborides MB_6 and diborides MB_2. Metal hexaborides MB_6 are a simple case in which the boron network was treated in the framework of the molecular orbital theory by considering 2s and 2p boron orbitals.[38,187] In this model, the orbitals of B_6 octahedra fragments are divided into three families: (i) 7 bonding, and (ii) 6 nonbonding outwardly oriented orbitals and (iii) 11 nonbonding orbitals pointing out of the octahedral vertices. The 7 bonding orbitals require 14 electrons per B_6 unit. The second orbital family ensures bonding between neighboring octahedra and requires 6 electrons per B_6 unit. Therefore, one B_6 unit requires 20 electrons to reach the most stable closed shell configuration. As a result, the metal sublattice must provide 2 additional electrons to each octahedron, leading to the configuration $[M^{2+}][B_6^{2-}]$. Of course, real cases are less simple: the metal strongly influences the band diagram, and complete electron transfer does not always occur.[104,188] As another example, metal diborides discussed above in subsection 2.3.1 should probably be formulated as $[M^{2\delta+}][B^{\delta-}]_2$. In a first approximation, the covalency−ionicity balance of M−B bonds in metal diborides can be linked to relative electronegativities. For strongly electropositive metals such as Mg and Al, ionicity prevails (97% and 92% of ionicity for M−B bonds in, respectively, MgB_2, AlB_2).[108,109] The 3d transition metals lead to higher covalency (22% of ionicity for TiB_2). Inside the first transition series, only a slight ionicity modification is expected because of the low change in electronegativity difference $\Delta\chi$ between metal and boron.[109,189] Instead, M−B bonds in ZrB_2 and HfB_2 show higher ionicity than TiB_2 because of increased $\Delta\chi$.[109,189]

The situation of metal-rich borides is much less straightforward. On the arguments of magnetic and Mössbauer measurements and metal binding energy shifts observed by X-ray photoelectron spectroscopy, the metal was considered to be electronically enriched.[190,191] This argument is still often used to rationalize the differences of catalytic properties between pure metals, metal phosphides, and metal borides, especially for nickel based systems.[192] However, recent works suggest that this statement should be reconsidered. Indeed, most of the first principle calculations[152,153] show that the total electron transfer should occur from metal to boron in relation with relative electronegativities. However, the subgroup of the d electrons is polarized in the opposite direction, providing metal atoms with increased d population while they are globally electronically deficient. Data of high resolution X-ray photoelectron spectroscopy and X-ray Auger electron spectroscopy were thoroughly discussed by S. Diplas et al.[182,193,194] The authors pointed at the risk of misinterpretation about binding energy shifts and showed that more reliable data might be retrieved from metal satellite intensities, initial state and final state Auger parameters. Experimental results for amorphous NiB were in agreement with calculations on the crystalline compound and showed that back-donation occurs in these systems as in transition metal alloys,[179,195−197] due to

dx.doi.org/10.1021/cr400020d | Chem. Rev. XXXX, XXX, XXX−XXX

hybridization between metal s−d and boron s−p orbitals. These recent highlights still require validation on other metals and stoichiometries.[175,179] However, it is interesting to note that this interpretation might conciliate both views because it would be in agreement on one side with the classical electronegativity view,[184−186] on the other side with the XPS, magnetic, and Mössbauer measurements.[38,190] It is noteworthy that Diplas et al.[182,193,194] pointed at the similarity of the d electron density of states between Ni−B, Ni−P on one side and Pt on the other side: metal borides and metal phosphides can behave in some cases in the same manner as noble metals. This is one reason why these systems are highly attractive for catalysis.

2.5.3.2. Metal Phosphides. As already mentioned, metal phosphides are classified according to the nature of the P units: dumbbells, cages, chains, tubes, etc.[67] The structure of Ni_2P was already depicted in Figure 7. XPS surface binding energies (BEs) of Ni $2p_{3/2}$ are in the same range in Ni fcc and Ni_2P, as are P $2p_{3/2}$ BE in elemental P and Ni_2P (Figure 7). These BE values are much smaller than those of oxidized species (Ni_xO and P_2O_5). Therefore, Ni−P bonds and more generally metal−phosphorus bonds bear lower ionicity than metal−oxygen bonds, in relation with lower $\Delta\chi$. XPS[181−183] and XANES[183] measurements suggest that phosphorus in M_3P, M_2P, and MP holds the oxidation state P^{1-}, although the ionic character tends to increase as the P content increases.[158,181,183] Still, P-rich metal phosphides are valence compounds in the sense that valence electrons are essentially localized,[67] so that MPs can be roughly described in the framework of the Zintl−Klemm formalism[67,198,199] in relative agreement with experimental crystal structures.[67,200] Consequently, the P center can be ascribed with a formal charge and can adopt several oxidation degrees ranging from 0 to −3.[67] Such a description, although valid for ionic MBs like alkali borides, usually fails for other metal borides.[103] Indeed, the higher covalency of M−B bonds and the electron delocalization in the metal sublattice prevent an ionic description for B/M elemental ratio lower than 6.

2.5.4. Electrical Behavior of Bulk MBs and MPs. The various electrical behaviors of metal borides reflect the complexity of the chemical bonding in these systems. The case of metal hexaborides is relatively straightforward because of the strong ionicity of the M−B bonds in these compounds. When the band structure is calculated by taking into account only boron atoms using the linear combination of atomic orbitals approximation,[38,187] the closed shell configuration is reached for divalent hexaborides which might behave as insulators. As a matter of fact, CaB_6, SrB_6, and BaB_6 are semiconductors with band gaps much smaller than expected from this simple consideration because the metal impacts the band structure of the boron sublattice. Also, divalent hexaborides, as well as other borides obtained at high temperature, are often subjected to nonstoichiometry or incorporation of impurities during synthesis. It is therefore relatively difficult to retrieve reliable experimental data. Hexaborides of trivalent metals (LaB_6, EuB_6, etc.)[38] are conductors because the additional electron is not monopolized by the boron framework. Interestingly, transition metal borides are metallic compounds, and they are often more conductive than the parent metal.[201] It is noteworthy that the density of states (DOS) of transition metal diborides exhibits a sharp valley close to the Fermi level (Figure 11) which can explain the superior stability versus oxidation of these compounds compared to other metal-like systems.[165,202] When this

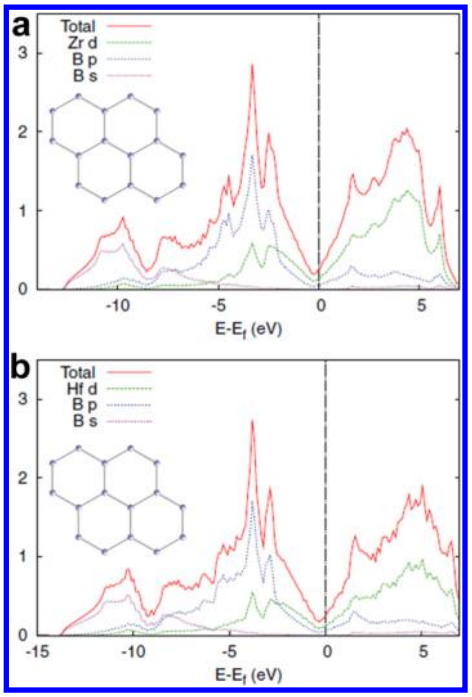

Figure 11. Total and site projected density of states of (a) ZrB_2 and (b) HfB_2. Both compounds have the honeycomb AlB_2 structure. The finite DOS at the Fermi level highlights the metallic behavior of both materials while the sharp valley is accounted for by the excellent thermal and chemical resistance of these ultrahigh temperature ceramics.[165] Reprinted with permission from ref 165. Copyright 2011 John Wiley and Sons, Inc.

pseudogap is located at the Fermi level (TiB_2, ZrB_2, HfB_2), the finite DOS ensures metallic behavior with high electronic conductivity, while empty antibonding states are somehow separated from full bonding states, which results in the typical cohesive features of insulators such as high melting point and chemical inertness. Besides metallic conductivity, metal borides can also possess interesting superconductivity properties. As the flagship of this family of compounds, magnesium diboride MgB_2 has been shown by Nagamatsu et al.[16] in 2001 to exhibit superconductivity. This conventional BCS superconductor has a high critical temperature of 39 K that substantially limits the cryogenic requirements for its use and explains its fast industrial development and commercialization.[203−205]

Most of the metal phosphides are semiconductors or insulators, because their electrons are localized in the vicinity of phosphorus atoms; however, some of them (usually the most metal-rich ones) exhibit a metallic character (Table 1). The electronic properties of the material depend obviously on several factors: (i) the difference of electronegativity between M and P, (ii) the M/P ratio, and (iii) the crystallographic structure which defines the local environment of M and P. The spin configuration also can play a role in some metal phosphides, and complicates their study through ab initio calculation. Moreover, few bulk metal phosphides such as LiFeP and NaFeP are known as superconductive, as recently reviewed.[206]

2.6. From Bulk to Nanoscale MPs and MBs: Characterization Tools

In this section, an overview and discussion of the main characterization techniques for MBs and MPs is provided (Figure 12). Most of them were primarily developed for bulk

dx.doi.org/10.1021/cr400020d | *Chem. Rev.* XXXX, XXX, XXX−XXX

Table 1. Nonexhaustive List of Metallic and Semiconducting Metal Phosphides[11]

	very low band gap phosphides		medium band gap phosphides	
metallic phosphides	phosphide	band gap	phosphide	band gap
TiP, TiP_2			AlP	2.50
VP_2, VP_4			BP	2.20
CrP_4			Cd[Si,Ge,Sn] P_2	[2.20, 1.80, 1.50]
MnP	MnP_4	0.14	Zn[Si,Ge,Sn] P_2	[2.30, 2.20, 2.10]
FeP, Fe_2P	FeP_2	0.37	Zn_3P_2	1.32
ZrP_2	CoP_2, CoP_3	−, 0.45	InP	1.27
MoP_4	NiP_2	0.50	$In_{2/3}PSe_3$	1.55
α-WP_2, WP_4	PdP_2	0.60	GaP	2.24
	PtP_2	0.60	$GaAs_{0.85}P_{0.15}$	1.44

materials but are still efficient when dealing with nanoscaled compounds. Similarly, most of the existing databases deal with the bulk compounds. It is noteworthy that B. Albert and H. Hillebrecht published recently a critical review on bulk boron-rich borides[40] and provided a concise yet precise overview of related characterization techniques. Note that, as a light element, boron requires some specific techniques for accurate analysis of the metal borides.

2.6.1. Chemical Analysis. Although a prerequisite to understand structure−property relationships, the evaluation of the exact composition of metal borides can turn into a complex and time-consuming process because of their typical thermal and chemical inertness.[207] The use of techniques which require specimen dissolution such as inductive coupled plasma optical emission spectroscopy must be considered with care. Hopefully, nanoscaled metal borides are much more reactive than their bulk counterpart, and their analysis is much more straightforward.[51] Quantification of boron by energy-dispersive X-ray spectroscopy (EDS) or wavelength-dispersive X-ray spectroscopy (WDS) is facing the typical problems of low-Z elements analysis: boron has a low fluorescence yield, the emitted X-rays have a low energy and can be absorbed by the specimen itself before reaching the detector, and the B Kα peak overlaps with the C Kα peak (often difficult to avoid from contamination) and L-M-N lines of heavier elements.[208−210] However, the development of low voltage (2−5 kV) scanning electron microscopes, new windows, and sensitive high resolution detectors allows now quantitative evaluation of the boron content in an SEM.[211−214] Ultimately, chemical analysis of magnesium diboride on a scale ranging from micrometers to nanometers was performed through a sophisticated combination of EDS spectroscopy and mapping in an SEM, in a scanning transmission electron microscope (STEM), and with electron energy-loss mapping (electron spectroscopic imaging ESI) through energy-filtered TEM (EFTEM).[208−210]

2.6.2. X-ray and Neutron Diffraction. The resolution of phosphide and boride crystal structures is usually conceived through single crystal or powder X-ray diffraction. Again, boron turns out to be an elusive element. Indeed, B atoms bear poor electron density, and their X-ray atomic scattering factor is consequently low. Positive localization of boron and the determination of partial occupancies are therefore sometimes problematic. Neutron diffraction might be more suited to study the structure of borides because of the high neutron scattering length of ^{11}B.[215] However, ^{11}B enriched samples must be used

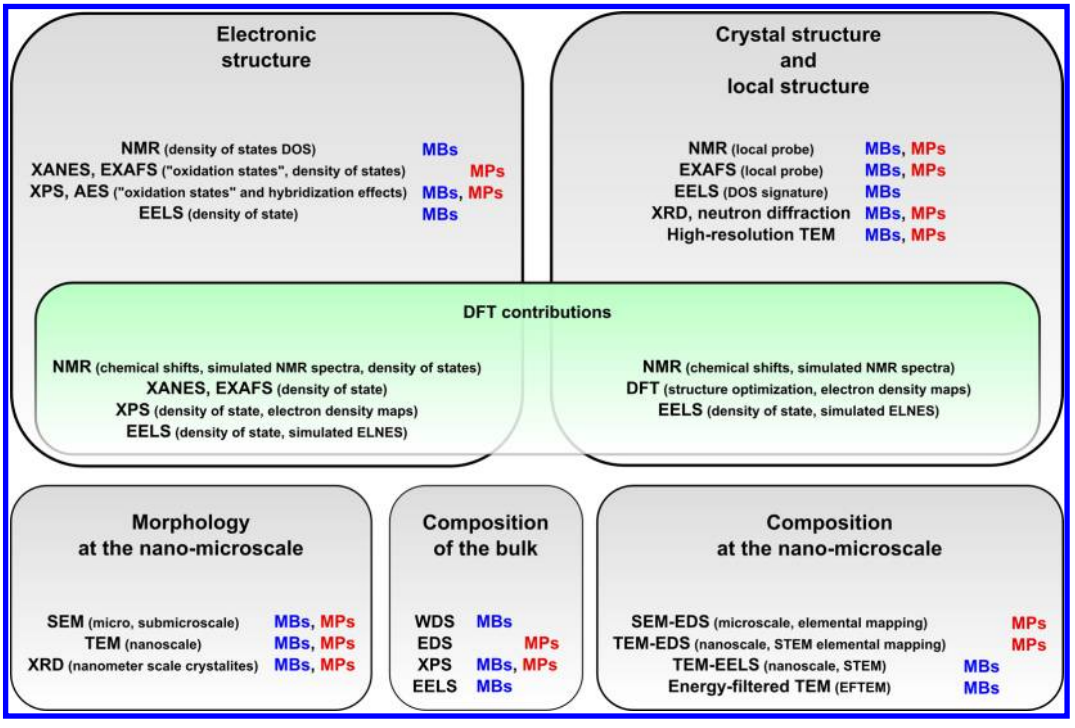

Figure 12. Most suited techniques for the characterization of the electronic structure, crystal and local structures, morphology, and composition of metal borides and metal phosphides both at the macroscale and at the nano/microscale. The most important contribution of DFT calculations to the interpretation of the different techniques is also shown. The metal−metalloid systems (MBs or MPs) which are the most studied by each technique are also tentatively outlined. Boron is a light element and requires some specific techniques for accurate analysis. For instance, EDS is hardly suitable for boron determination while EELS is especially dedicated to boron based compounds.

dx.doi.org/10.1021/cr400020d | Chem. Rev. XXXX, XXX, XXX−XXX

because ^{10}B absorbs neutrons too strongly, which is the reason why boron is often involved in neutron capture applications.[215]

2.6.3. Electron Microscopy. Scanning electron microscopy is essentially dedicated to surface imaging and chemical analysis when coupled with EDS. On the other hand, besides the aforementioned coupling with chemical analysis, transmission electron microscopy supports structure resolution on thin bulk materials with characterizations in diffraction (selected area electron diffraction SAED) or in image modes (high resolution transmission electron microscopy HRTEM, Figure 13).[216] Of course, the resolution of TEM is particularly

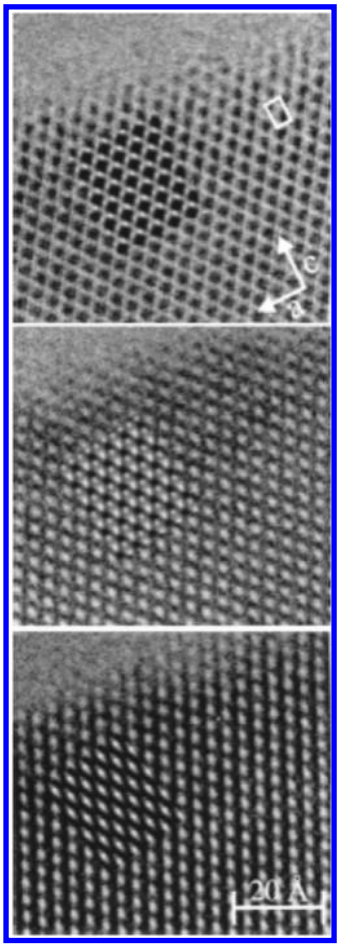

Figure 13. HRTEM images of bulk Na_2B_{29} for different defocus values. Simulated pictures are superimposed.[216] Reprinted with permission from ref 216. Copyright 2000 John Wiley and Sons, Inc.

suited to the analysis of nanoscaled matter. This technique must be used with care when specimens are prone to beam-damage. For instance, amorphous Ni−B alloys were recently studied by HRTEM.[217,218] Nanodomains of elemental nickel segregated in a boron matrix were identified. However, the use of harsh observation conditions (acceleration voltage of 300 kV) might cause crystallization of the inherently metastable amorphous nanoalloy. Alterations during the observation of these reactive systems cannot be ruled out except by studying them under different energy input conditions.

2.6.4. X-ray Photoelectron Spectroscopy (XPS), Auger Electron Spectroscopy (AES), and X-ray Absorption Spectroscopy (XANES, EXAFS). As described above, XPS was used for the investigation of bonding into metal borides and phosphides. Shortly, binding energy shifts for the metal are small and should be considered with care by taking into account not only charge transfer but also hybridization or changes in the coordination.[181−183] More information might be retrieved from metal satellite peaks and Auger parameters obtained from X-ray-induced Auger electron spectroscopy (AES).[181,182,194] Unfortunately, boron does not exhibit a sharp B KLL Auger peak and is not suitable for such analysis.[194] Furthermore, its XPS B 1s peak is experiencing only a slight shift when boron is incorporated into metal borides and is therefore difficult to interpret. As discussed in subsection 2.5, recent studies of nickel−metalloid systems based on XPS and AES were focused on the metal part and combined with first principle calculations.[182,193,194] These results suggested that charge transfer occurs usually from the metal to boron but at a lesser extent than in metal phosphides.[182]

The small number of X-ray absorption spectroscopy (XAS) studies reported on metal borides is probably due to the soft X-ray energy range of the B K edge at 180 eV. In these conditions, most of the incident photons can be absorbed. XAS measurements focused on boron therefore require high flux sources, low pressure, and/or high sensitivity detectors. It is noteworthy that this limitation can be turned into an advantage since it provides a way to discriminate between bulk and surface states by recording XAS spectra through collection of the X-ray fluorescence yield or the total electron yield.[219−221] Surface oxidation can then be highlighted on XANES spectra with a typical boron oxide peak at 194.0 eV.[221] The density of state of metal hexaborides was also probed by interpreting XANES and EXAFS with the help of calculations.[220,221] Actually, the metal center is much easier to probe by XAS and was the object of some studies, even if only few of them were dedicated to crystalline metal borides.[221−225] The strongest research effort in XAS was focused on binary or ternary amorphous alloys to probe pair distributions.[225−230]

Altogether, several experimental techniques have allowed the investigation of the bonding in metal phosphides. XPS and XANES spectroscopy were used for the investigation of MP, M_2P, and M_3P structures.[183,231] As can be seen in Figure 14 (left), binding energies of metal-rich phosphides and the pure metal are very similar. However, the decrease of the satellite intensity testifies of the presence of phosphorus (Figure 14, right). These satellites originate from plasmon loss processes, which are less efficient when the cross-section diminishes. The presence of phosphorus was then explained by a depletion of the valence electrons around the metal, meaning that phosphorus attracts electrons from the metal in these structures.

More generally, there is a correlation between the difference of electronegativity, the stoichiometry, and the spectroscopic properties, especially P $2p_{3/2}$ binding energies and P K-edge absorption energies (Figure 15). Concerning binding energies, it has been shown that intra-atomic (charge variation of the atom) and interatomic (coordination effect) effects are responsible for the shift: intra-atomic ones are generally dominant, but the extended nature of the bonding in MP_2 and MP_3 makes the other ones also significant.[232] Coming back to the case of molecular species, the shift in metal phosphide according to interatomic effect is reminiscent of the high ability of phosphine ligands to bind transition metal centers because of adequate orbitals levels (covalency of the bonds) but also because of extended electron delocalization between the metal and the phosphorus center due to donation and back-donation

dx.doi.org/10.1021/cr400020d | Chem. Rev. XXXX, XXX, XXX−XXX

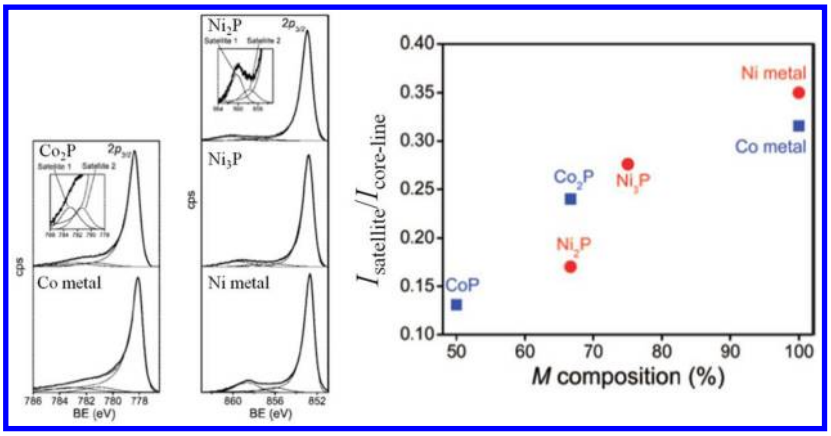

Figure 14. Left: High resolution M $2p_{3/2}$ XPS spectra for Co and Ni based phosphides, compared with the pure metal. Right: Normalized satellite intensity ($I_{satellite}/I_{core\text{-}line}$) vs the composition.[183] Reprinted with permission from ref 183. Copyright 2008 American Chemical Society.

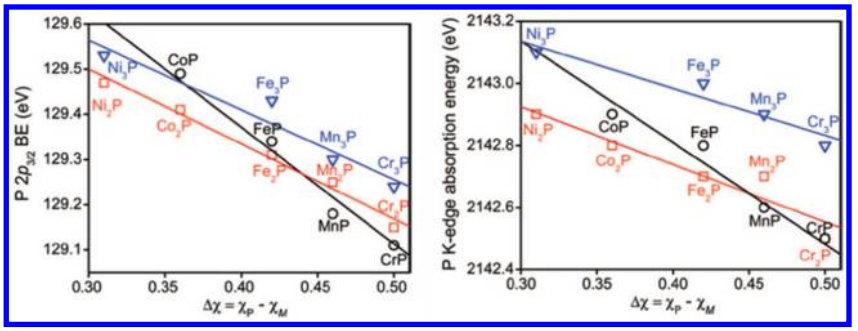

Figure 15. Dependence of P $2p_{3/2}$ binding energy (left) and P K-edge absorption energy (right) on electronegativity difference for MP, MP_2, and MP_3.[183] Reprinted with permission from ref 183. Copyright 2008 American Chemical Society.

in the bonding and antibonding in the diffuse P orbitals. However, Blanchard et al. refute the necessity of back-bonding for the stabilization of the structure on the profit of changes of coordination environment. They conclude to a −1 charge of the phosphorus in the three series discussed (MP, M_2P, M_3P), and suggest that catalytic activity could be tuned by tuning the electron counts, that is, by using ternary alloys.

Similarly, XPS and XANES studies were also done on MP_xAs_{1-x} alloy (M = Co, Fe, Cr) and suggested that the use of arsenic would allow a considerable tunability of the electronic structure without modification of the metal.[183]

2.6.5. Electron Energy Loss Spectroscopy (EELS). Electron energy loss spectroscopy (EELS) is a technique usually mounted on a transmission electron microscope that is especially suited to the characterization of light elements which are difficult to deal with or even to detect by EDS into a TEM or SEM. The primary use of EELS in the field of metal borides is the quantification of boron as well as carbon or oxygen impurities. EELS is a routine technique for chemical analysis of elemental boron,[233−235] MgB_2,[236−238] Fe_3B,[239] SrB_6,[240] CaB_6,[235,241] and LaB_6,[242] among others. Beyond quantification, EELS provides also valuable information about the coordination sphere and the electronic state of boron in metal borides. In particular, the energy-loss near edge structure (ELNES) of the B_K ionization edge is sensitive to the density of unoccupied states above the Fermi level and can be used primarily as a fingerprint of the boron framework (Figure 16).[243−245] The nature of the metal associated with boron can also modify the ELNES spectrum because it changes the DOS, as shown for metal diborides or hexaborides (Figure 16). K. Hofmann, B. Albert et al., and Gao et al. nicely demonstrated the beneficial contribution of DFT calculations to simulate near-edge structure studies and guide experimental interpretation.[246−248] Consequently, ELNES can circumvent the low sensitivity of XRD toward boron and becomes the first tool for structure resolution, while X-ray powder diffraction is used to refine the primary structure.[246,248] Another strong advantage of EELS over other techniques is its coupling with TEM that can provide high spatial resolution with the possibility to record EELS spectrum on areas of the subnanometer scale in scanning TEM (STEM) mode. This technique is especially suitable for nanoscale materials to probe composition inhomogeneity and surface effects (oxidation for instance).[235,240,241,245] Alternatively, energy-filtered TEM (EFTEM) can be used to provide elemental mapping at the nanometer scale.[234,237,249,250]

2.6.6. Nuclear Magnetic Resonance (NMR) Spectroscopy and ab Initio Calculations. With the development of the DFT codes, in particular for the prediction of NMR shifts, joint studies with DFT calculations and NMR measurements have provided structural insights into solid-state materials, such as nanostructured boron-carbon-nitrides by combined ^{13}C, ^{15}N, and ^{11}B NMR;[251] alkaline earth boronates by combined ^{1}H, ^{11}B, ^{13}C, and ^{43}Ca NMR;[252] or GaP nanotubes with ^{69}Ga and ^{31}P NMR.[253]

Boron and phosphorus are particularly well suited for solid-state NMR investigations (static or at magic-angle spinning). ^{11}B and ^{31}P nuclei have spins of, respectively, $^{3}/_{2}$ and $^{1}/_{2}$, high natural abundances of, respectively, 80.1% and 100%, and relatively high gyromagnetic ratios of, respectively, 8.585×10^7 and 10.829×10^7 rad s^{-1} T^{-1}.

dx.doi.org/10.1021/cr400020d | Chem. Rev. XXXX, XXX, XXX−XXX

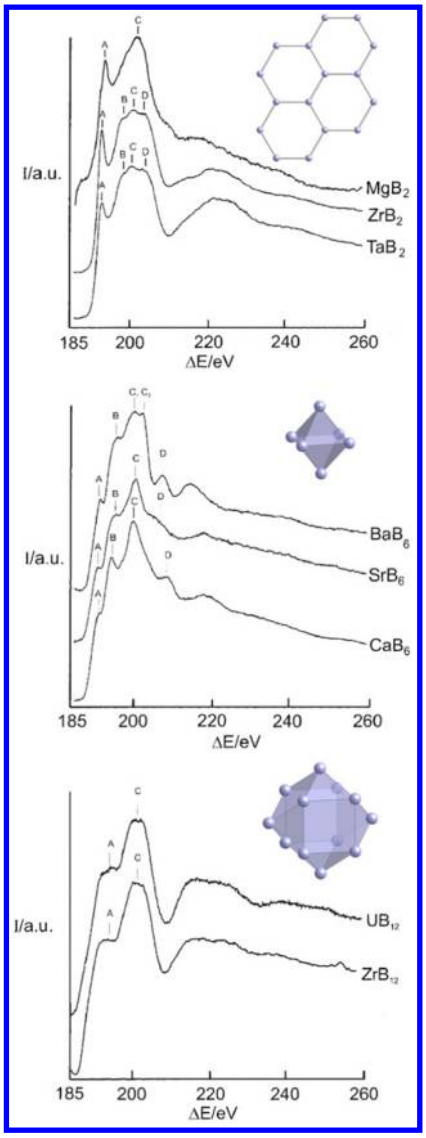

Figure 16. EELS spectra with energy-loss near-edge structure (ELNES) of metal diborides, metal hexaborides, and metal dodecaborides with the representation of boron structural units, respectively, boron sheets, B_6 octahedra, and B_{12} cuboctahedra. Reprinted with permission from ref 243. Copyright 2002 John Wiley and Sons, Inc.

^{11}B is a quadrupolar nucleus and as such leads to relatively broad signals in magic-angle spinning NMR studies. Coupling NMR measurements with the DFT-calculated chemical shifts is therefore a useful approach that provides deep insight into the structure of boron based materials. This was especially demonstrated on boron carbides,[254,255] boron nitride polymeric precursors,[256,257] $LiBH_4$/carbon foams,[258] and hierarchically nanostructured boron-carbon-nitrides.[251] Many metal borides possess high electrical conductivity. This complicates NMR experiments which are particularly difficult to perform on strongly paramagnetic and electrically conductive samples, because of the skin effect, for example. Nevertheless, modern NMR devices and sequences allow us to measure significant signals also from these paramagnetic media. Because of the high conductivity of borides, their solid state NMR spectra often exhibit Knight shifts.[259,260] These shifts, together with spin–lattice relaxation rates and electric field gradients, are not only useful for probing the crystallographic structure, but they also provide valuable information on the charge distribution around the nuclei and the density of state (DOS) close to the Fermi level.[259,261,262] The occurrence of superconductivity was also investigated by ^{11}B NMR on ternary rare earth diborides $RERuB_2$[263−265] and MgB_2.[266−269] Analyses with regard to predictions from DFT calculations have proved to provide deep insights into the DOS structure, for instance of transition metal diborides,[270] metal rare earth hexaborides (LaB_6, PrB_6, SmB_6),[271] rhenium borides,[272,273] yttrium borides,[262,274,275] dodecaborides,[276] lanthanum hexaboride,[277] and rare earth metal silicide borides.[260] Other nuclei than ^{11}B can be used.[278] For instance, superconductivity in MgB_2 was probed by ^{25} Mg NMR,[279,280] local environment for vanadium in vanadium borides was studied by the Knight shifts in ^{51}V NMR spectra,[259,281] and site occupancies of sodium in Na_2B_{29} were obtained by combining different sequences in ^{23}Na solid state NMR (Figure 17).[216] Coupling of ^{11}B (Figure 17), ^{29}Si, and ^{89}Y solid state NMR was also performed.[260] It is noteworthy that crushing the sample into a powder is usually a convenient method to limit conductivity and restrain the skin effect of metal borides. Hopefully, nanoscaled materials are less prone to this behavior and easier to analyze using NMR.[51]

Because of low spin value and large shift range, solid-state NMR investigations (static or at magic-angle spinning) of ^{31}P are especially easy to interpret. Metal phosphides are also less prone to Knight shifts than metal borides because of their lower conductivity. A correlation between ^{31}P NMR shifts and electronic structure calculated by DFT could thus be found for a family of transition-metal phosphides including V, Fe, Co, and Ni atoms, with various M/P ratios.[283] The instance of monoclinic NiP_2, a metal phosphide particularly investigated as a negative electrode for Li batteries, is illustrated in Figure 18. DFT calculation of the bulk structure allowed a good interpretation of the static NMR spectra. Additionally, interpretation of the projected density of state (DOS) confirmed a Ni^{2+} (d^8) oxidation state with an empty band localized in the Ni($d_{x^2-y^2}$) orbital. As a consequence, only very weak δ-type interactions exist in the interlayer direction (Figure 18, right). The study of the reaction of bulk NiP_2 with Li furthermore highlighted that phosphorus was the main redox center for the first-step insertion, which goes through the breaking of the weak interlayer P–P bond.[284] Prior to this study, it was also shown that shuttling between two oxidation states of the phosphorus in CoP_3 electrodes, between Li_3P and LiP compounds, was responsible for their reversible lithium uptakes.[285]

Altogether, these particular cases illustrate the very high redox flexibility of the metal phosphides and its consequences on their reactivity. The redox state of the metal can easily change in the presence of an incoming species, and both the metal and the phosphorus can be involved in reactive steps.

The similarities in terms of bonding scheme between metal borides and metal phosphides clearly validate a comparison between the synthetic approaches of both systems. Maybe the strongest difference between the two families of "covalent alloys" is the extent of covalency which is larger in metal borides. The straightforward consequence is that crystalline metal borides usually require harsher synthetic conditions than metal phosphides. Therefore, materials scientists are still in the early stage of the synthetic process of metal borides in general and nanoscaled metal borides in particular. In the next section, the different approaches toward nanostructured metal borides

dx.doi.org/10.1021/cr400020d | *Chem. Rev.* XXXX, XXX, XXX–XXX

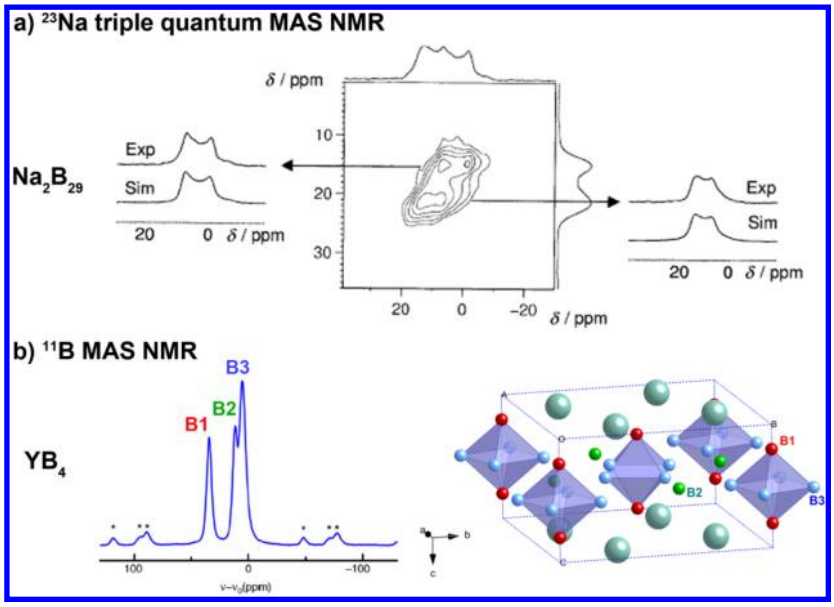

Figure 17. (a) ^{23}Na triple quantum MAS NMR spectrum of Na_2B_{25} (experiment and simulation) highlighting two nonequivalent sodium sites,[216] which disproves the former view of single site "NaB_{15}".[282] Reprinted with permission from ref 216. Copyright 2000 John Wiley and Sons, Inc. (b) ^{11}B MAS NMR spectra of the central $(+^1/_2 \leftrightarrow -^1/_2)$ transition for YB_4.[275] Reprinted with permission from ref 275. Copyright 2009 Elsevier.

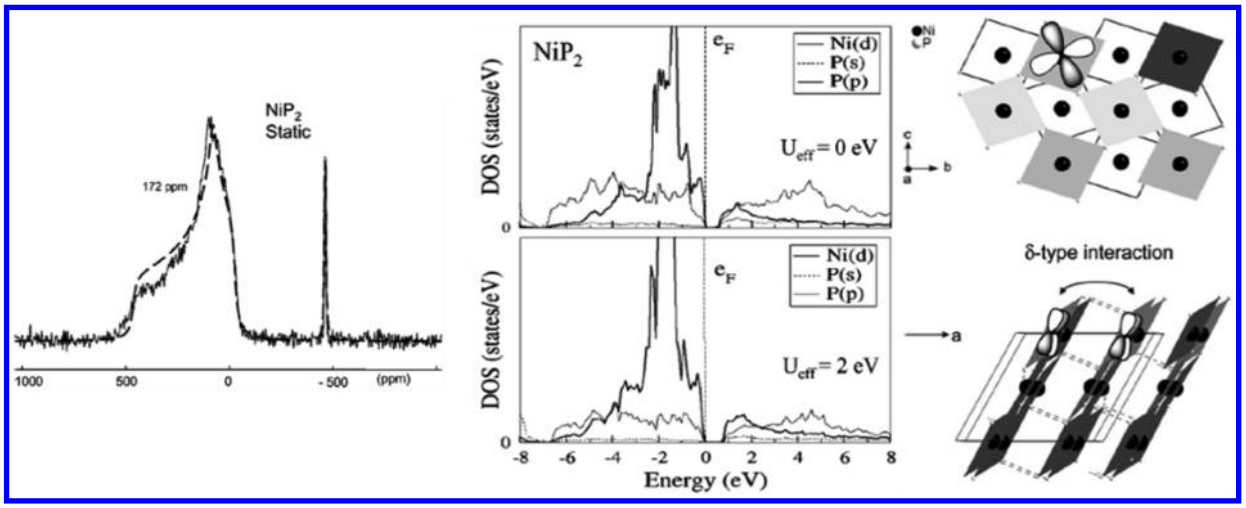

Figure 18. Left: Experimental and calculated static ^{31}P NMR spectra of NiP_2. Middle: DOS calculation. Right: Projection views of the crystal structure in the interlayer direction (top) and in the chain direction (bottom).[283] Reprinted with permission from ref 283. Copyright 2008 American Chemical Society.

known up to now are presented. The following section addresses the specific case of colloidal synthesis of nanoscaled metal phosphides.

3. NANOSCALED METAL BORIDES

As is often the case with nanomaterials, one should keep in mind that materials scientists were dealing with nanostructured metal borides well before the "nanowave" and the systematic use of electron microscopy as the definite proof of their synthesis. In particular, some examples developed in the following subsections highlight "hints" that nanoscaled metal borides were obtained in the 1980s and 1990s.[286] Nevertheless, most of the research efforts targeting nanostructures of metal borides have been made during the past decade.

Several top-down approaches have been studied to yield nanoscaled metal borides. Especially, superconductive MgB_2 nanowires, bridges, and meanders were obtained by electron beam lithography,[287,288] and a combination of photolithography, ion-beam-milling, and focused ion beam.[289] However, most of the ways explored up to now to reach nanoscaled metal borides rely on "chemical" bottom-up approaches, in the sense that they are based on reactions between a metal and a boron molecular or solid precursor. Figure 19 aims at summarizing these different synthetic processes in terms of the temperature used and of the typical length scale of the resulting metal borides. Most of these approaches yield particle size between 30 and 100 nm. A few points deserve highlights. First, only one process recently highlighted, namely colloidal synthesis in salt melts, is suitable to reach sub-10-nm crystalline nanoparticles (nanocrystals).[51] Second, although performed at high temperatures usually favoring crystal growth (1300 °C), some methods (e.g., borothermal reduction and synthesis in metal flux) can yield small nanoparticles of ca. 20−40 nm.[87,250,290] Third, among this variety of syntheses, only three provide

dx.doi.org/10.1021/cr400020d | Chem. Rev. XXXX, XXX, XXX−XXX

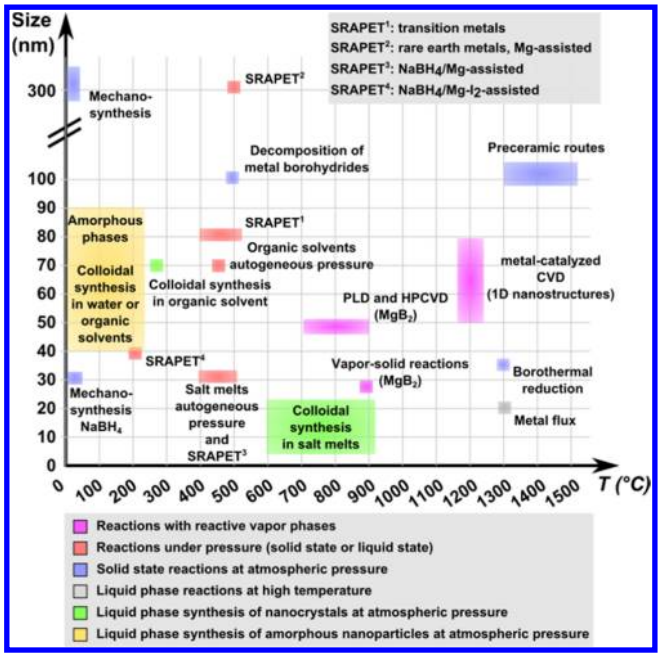

Figure 19. Typical temperature used and particle size achieved by the different techniques of nanoscaled metal borides synthesis: SRAPET, solid state reaction under autogenous pressure at elevated temperature; PVD, physical vapor deposition; CVD, chemical vapor deposition; HPCVD, hybrid physical chemical vapor deposition. The different processes are explored in the next sections.

particle size control (CVD of nanowires,[291] precipitation of amorphous nanoparticles,[292−295] and colloidal synthesis in salt melts[51]). The following section describes the different approaches, points out trends emerging over a few years, and provides a comparative discussion of each processes.

3.1. Variety of Boron Precursors

As discussed above, the electronic state of metal borides is still highly debated and should probably be discussed case by case. Nevertheless, reported syntheses of borides are still dictated by the common belief that both metal and boron should be at their ground oxidation state in order to bind together into boride crystalline frameworks. Up to now, this way of thinking boride crystallization had a direct impact on the choice of boron and metal precursors. The chemical processes involved are indeed selected in order to provide both B(0) and M(0) in the course of the reaction. As a result, only few boron sources were investigated for the production of nanoscaled metal borides. They can be classified according to their composition, which in turn is related to their redox reactivity: boron−metal alloys, elemental boron, boranes (boron hydride clusters), borohydrides, boron halides, boron−oxygen compounds, and molecular single sources. Although amorphous preceramics might be considered as single sources, they are always polymeric and often ill-defined species. Consequently, they are not treated as molecular single sources here, but their use will be covered in subsection 3.4.

3.1.1. Metal−Boron Alloys and Metal Borides. The first class of B donors is composed of metal−boron alloys and metal borides (MgB_2). Copper−boron alloys are poorly stable and decompose in the presence of Cu−Ti alloys to yield more stable titanium diboride TiB_2.[296] MgB_2 was also reported as boron donor for the synthesis of TiB_2 from $TiCl_4$ according to eq 2.[297] In this case, Mg(0) is used as secondary species to ensure reduction of the metal chloride. Although the process is described by the authors as belonging to solid state chemistry routes, it should be noticed that both titanium chloride and magnesium are liquid in the conditions of the experiment (650 °C in sealed vessel). Therefore, the reaction medium is most likely a heterogeneous mixture.

$$TiCl_4(l) + MgB_2(s) + Mg(l) \xrightarrow{650\ ^\circ C,\ \text{sealed vessel}} TiB_2(s) + 2MgCl_2(s) \quad (2)$$

3.1.2. Elemental Boron. The use of boron for the synthesis of nanoscaled borides is most of the time associated with metal(0) as M precursors, so that no redox reaction is required. It is especially used for multiple target molecular beam epitaxy (MBE) (eq 3).[233] In addition, it can also act as a solid template and a reactant to be combined with a gaseous metal. This is especially the case of the synthesis of MgB_2 nanowires produced by reacting Mg vapors with elemental boron nanowires (eq 4).[233,237,298]

$$Ca(g) + 3B(g) \xrightarrow{500\ ^\circ C,\ \text{MBE}} CaB_3(s) \quad (3)$$

$$Mg(g) + 2B(s) \xrightarrow{950-1050\ ^\circ C,\ \text{vapor-solid reaction}} MgB_2(s) \quad (4)$$

For use with oxidized metal sources (metal oxides or chlorides), additional reductants such as Na[55] or Mg[299] are provided to ensure the formation of formal M(0) (eqs 5 and 6).

$$TiCl_4(sol) + 2B(s) + 4Na(s) \xrightarrow{400\ ^\circ C,\ \text{sealed vessel}} TiB_2(s) + 4NaCl(s) \quad (5)$$

$$La_2O_3(s) + 12B(s) + 3Mg(s) \xrightarrow{500\ ^\circ C,\ I_2,\ \text{sealed vessel}} 2LaB_6(s) + 3MgO(s) \quad (6)$$

Although boron is used as both B source and reductant in so-called borothermal reduction of metal oxides for the synthesis of bulk borides, such a process is only scarcely reported for the production of nanostructures. The reason for this lack of investigation in the nanoarea is the strong exothermicity of the reaction which yields high temperature in the medium. Thus, unrestricted crystal growth occurs and nanostructured materials cannot be isolated. Borothermal reduction of oxides was nevertheless recently highlighted as a suitable process to yield nanoscale niobium diboride (eq 7)[250] or cerium hexaboride[290] when the starting materials themselves are nanostructured.

$$NbO_2(s) + 4B(s) \xrightarrow{1300\ ^\circ C,\ \text{solid state}} NbB_2(s) + \frac{1}{2}B_2O_2(g) \quad (7)$$

3.1.3. Boranes. Some boron hydride clusters (Table 2), namely diborane B_2H_6, pentaborane B_5H_9, and decaborane $B_{10}H_{14}$, are widely involved as volatile precursors in chemical vapor deposition processes (CVD). These mild reductive

Table 2. Boranes Used for the Synthesis of Nanostructured Metal Borides

name	formula	melting point (°C)	boiling point (°C)	vapor pressure at 25 °C (Torr)
diborane	B_2H_6	−165.5	−92.5	
pentaborane	B_5H_9	−46.6	58	209[310]
decaborane	$B_{10}H_{14}$	99	213	0.2[311]

dx.doi.org/10.1021/cr400020d | Chem. Rev. XXXX, XXX, XXX−XXX

species can be used with either M(0) (Hf(s) toward HfB_2,[300] Mg(g) toward MgB_2[301−304]), metal oxides,[235,240,241,305] or metal chlorides.[57,291] MgB_2 is a special case where additional reductive atmosphere provided by H_2 is required to avoid oxidation of elemental magnesium and magnesium diboride upon exposure to oxygen traces.[306] N. N. Greenwood intensively studied the thermal decomposition of gaseous boranes which go through a complex series of interconversions between B_xH_y species.[307−309]

3.1.4. Borohydrides. Alkali borohydrides ($LiBH_4$, $NaBH_4$, KBH_4) are economical, solid species which do not suffer from the same safety issues as toxic gaseous boranes. They were considered as early as 1951 for the production of borides and for hydrogen production.[90,312] Alkali borohydrides, especially $LiBH_4$ and $NaBH_4$, are currently intensively studied for chemical H_2 storage.[313] H_2 evolution occurs upon pyrolysis or hydrolysis.

The full pyrolysis process is described by eq 8 and involves a complex stepwise mechanism which is still under investigation.[314]

$$LiBH_4(s) \rightarrow LiH(s) + 1.5H_2(g) + B(s) \quad (8)$$

Hydride abstraction from the BH_4^- anion occurs above 480 °C for $LiBH_4$ which has the lowest decomposition temperature among alkali borohydrides.[314] $NaBH_4$ decomposition starts at ca. 500 °C following eqs 9 and 10.

$$NaBH_4(s) \rightarrow BH_3(g) + NaH(s) \quad (9)$$

$$BH_3(s) \rightarrow B(s) + 1.5H_2(s) \quad (10)$$

Solutions of borohydride in protic solvents are metastable and decompose in the course of minutes or hours. In water, BH_4^- is hydrolyzed into borates or boric acid depending on the pH ($pK_A(B(OH)_3(s)/BO_2^-(aq)) \approx 9.2$) according to eqs 11 and 12.

$$BH_4^-(aq) + 2H_2O(l) \rightarrow 4H_2(g) + BO_2^-(aq) \quad (11)$$

$$BO_2^-(aq) + H_2O(l) + H^+(aq) \rightarrow B(OH)_3(aq) \quad (12)$$

The notation "BO_2^-" is actually an oversimplification because of the complex behavior of boron in aqueous solution. Indeed, borates are often encountered as clusters with nuclearities depending on both concentration and acido-basic conditions.[315] The most famous borate is of course the tetrameric anion $[B_4O_5(OH)_4]^{2-}$ found in the mineral borax. As suggested by eqs 11 and 12, the rate of borohydride hydrolysis depends strongly on pH and increases in acidic medium. Hydrolysis is also catalyzed by additives, especially metal (boride) nanoparticles. This can have a serious impact on the aqueous precipitation of metal borides and will be discussed in detail in subsection 3.8.

In the framework of metal boride synthesis, hydridoborates are used because of their strong reducing reactivity and because the products of their decomposition or oxidation are borane, or even boron, which combine with metals at relatively low temperature (eq 13).[91−94,96]

$$2CoCl_2(aq) + 4NaBH_4(aq) + 9H_2O(l) \xrightarrow{\text{room temperature}} Co_2B(s, \text{amorphous}) + 4NaCl(aq) + 12.5H_2(g) + 3B(OH)_3(aq) \quad (13)$$

Additional reductants can also be used, such as LiH (eq 14).[58] or Mg (eq 15).[316]

$$TiCl_3(s) + 2LiBH_4(aq) + LiH(s) \xrightarrow{\text{room temperature, mechanosynthesis}} TiB_2(s) + 3LiCl(s) + 4.5H_2(g) \quad (14)$$

$$VCl_4(l) + 2NaBH_4(s) + Mg(s) \xrightarrow{\text{650 °C, sealed vessel}} VB_2(s) + 2NaCl(s) + MgCl_2(s) + 4H_2(g) \quad (15)$$

Borohydrides in organic protic solvents such as alcohols readily yield borate ether derivatives $BH_{4-n}(OR)_n^-$[317,318] which are the reactive species for metal reduction and production of metal borides.

3.1.5. Boron Halogenides. Boron chloride BCl_3[319] is another popular gaseous boron source, commonly used for CVD processes. A reductive atmosphere is supplied by a mixture of hydrogen and a vectorizing gas to ensure reduction of the boron halide and the metal chlorides or oxides if required.[320−324] This process is mainly involved in the production of rare earth hexaborides and MgB_2. Titanium diboride was also reported from the reaction between BCl_3 and $TiCl_4$ in the presence of Na vapor (eq 16).[319] Use of BBr_3 was investigated for the synthesis of nanoscaled TiB_2 from titanium(0) under autogenous pressure.[325] The reaction is assisted by sodium(0), presumably to reduce the boron source (eq 17).

$$TiCl_4(g) + 2BCl_3(g) + 10Na(g) \xrightarrow{\text{1000 °C, gas phase combustion}} TiB_2(s) + 10NaCl(s) \quad (16)$$

$$Ti(s) + 2BBr_3(g) + 6Na(l) \xrightarrow{\text{400 °C, sealed vessel}} TiB_2(s) + 6NaBr(s) \quad (17)$$

To our knowledge, boron iodide BI_3 was only reported twice by the same group in the course of metal boride production, for the synthesis of Fe_3B nanowires from FeI_2 at 800 °C.[239,326] No additional reductant was required (eq 18) because of the lower decomposition temperature of BI_3[327] and FeI_2, especially compared to BCl_3.[239] Decomposition of the precursors yields boron(0) and iron(0) according to eqs 19 and 20, which combine together into Fe_3B. Noteworthy, iron as intermediate species might act as a catalyst for BI_3 decomposition and could fasten nucleation and growth of Fe_3B.

$$BI_3(g) + 3FeI_2(s) \rightarrow Fe_3B + 4.5I_2(g) \quad (18)$$

$$BI_3(g) \rightarrow B + 1.5I_2(g) \quad (19)$$

$$FeI_2(g) \rightarrow Fe + I_2(g) \quad (20)$$

3.1.6. Boron−Oxygen Species (Boron Oxide and Boric Acid). Boron oxide and boric acid are also reported as boron sources, although classified as carcinogenic, mutagenic, and reprotoxic chemicals. When heated, B_2O_3 has a significant vapor pressure reaching 344 Pa at 1527 °C.[328] $B(OH)_3$ dehydrates under atmospheric pressure between 150 and 200 °C to yield B_2O_3.[329] If the reaction is conducted with $B(OH)_3$ in a closed vessel above these temperatures, a wet atmosphere is in contact with the reactants. The impact of water as

dx.doi.org/10.1021/cr400020d | Chem. Rev. XXXX, XXX, XXX−XXX

additional species is usually neglected, and $B(OH)_3$ is considered as being equivalent to B_2O_3. Boron (hydr)oxide is combined with oxidized metal species, such as metal oxides, chlorides, carbonates, and nitrates.[54,299,330] As for boron halides, an additional reactant such as carbon or magnesium is added to ensure reduction of both boron and metal components (eq 21[299] and 22[331]).

$$La_2O_3(s) + 6B_2O_3(s) + 21Mg(s) \xrightarrow{500\ ^\circ C,\ I_2,\ \text{sealed vessel}} 2LaB_6(s) + 18MgO(s) \quad (21)$$

$$LaCl_3{\cdot}7H_2O(s) + 3B_2O_3(s) + 21Mg(s) \xrightarrow{500\ ^\circ C,\ \text{sealed vessel}} LaB_6(s) + 1.5MgCl_2(s) + 16MgO(s) + 7H_2(g) \quad (22)$$

Wang et al. observed recently that the formation of LaB_6 from La_2O_3, Mg, and I_2 could be achieved at lower temperature by using $B(OH)_3$ instead of B_2O_3.[299] The authors suggested that water as a side product might have a noticeable role in the enhanced kinetics of the reaction. Water might catalyze the highly exothermic reaction between Mg and I_2, yielding MgI_2 and a strong temperature increase. This would be highly favorable to the reduction of La_2O_3 and the in situ formed B_2O_3. Combination of the resulting lanthanum(0) with boron(0) into LaB_6 would also be fastened by the increase in interior temperature.

3.1.7. Molecular Single Source. Some reports have been provided concerning the use of noncommercial molecular single source precursors composed of both metal and boron for the production of borides. Metal borohydrides [$Hf(BH_4)_4$,[332−337] $Ti(BH_4)_3(dme)$[332] (dme = 1,2-dimethoxyethane), $Zr(BH_4)_4$,[24,332,333,338] $Al(BH_4)_3$,[339] $HFe_3(CO)_9BH_4$[340]] have successfully yielded amorphous transition metal borides through CVD processes in a temperature range 500−650 °C. Other complexes containing borane ligands led to similar results [$B_2H_6Fe_2(CO)_6$,[341] $[B_2H_4Fe_2(CO)_6]_2$,[341] $Cr(B_3H_8)_2$[342]]. Quite intuitively, single sources incorporating different M:B ratios yield in some cases different stoichiometries, as for amorphous Fe−B compounds.[340,341] It is noteworthy that the recently reported $Cr(B_3H_8)_2$[342] is the only MB_xH_y-type transition metal complex without BH_4^- ligands. It can prevent incorporation in the final product of carbon or oxygen from the ancillary ligands. Single sources are not only useful for CVD processes, but they can also be involved into other processes, such as electron beam induced deposition (EBID) for crystalline HfB_2 from $Hf(BH_4)_4$.[337]

3.2. Deposition from a Reactive Vapor Phase

3.2.1. General Considerations on the Thermal Decomposition of Boranes. Chemical vapor deposition was until very recently the only efficient route toward nanoscaled crystalline borides because the involved treatments require relatively low temperature. It is especially dedicated to the production of MgB_2 superconducting thin films and 1D nanostructures of alkaline earth and rare earth hexaborides. CVD processes involving gaseous reactive boron species were first intensively developed for B doping in the semiconductor area. Especially, diborane B_2H_6 is among the most used volatile molecules for such deposits on silicon surfaces. Its reaction with Si(100), as well as Pd, Mo, and Ru substrates, was studied in-depth.[343] The detailed doping mechanism can be described by the formation of intermediate adsorbed BH_3 molecules which dissociate on the surface (eq 23 and 24).

$$B_2H_6(g) + 2\square(\text{surface}) \rightarrow 2BH_3(\text{surface}) \quad (23)$$

$$BH_3(\text{surface}) \rightarrow B(\text{surface}) + 1.5H_2(g) \quad (24)$$

Diborane is also widely used as boriding species for the production of boride films. Dissociative adsorption of B_2H_6 onto hafnium producing BH_4^- as a transient surface species was also reported.[344] To the best of our knowledge, no detailed investigations of the surface reactions occurring during CVD based boride syntheses have been performed.

3.2.2. Boriding Metal Films. Belyanski et al. have shown that (0001)-oriented thin films of HfB_2 with 5−10 nm thickness could be epitaxially grown over a (0001)Hf surface under low pressure.[300,344] The Hf:B stoichiometry could be controlled by adjusting the temperature of the substrate and the postannealing procedure. At a growth temperature of 450 °C, XPS shows that boron is deposited over the Hf surface and that the film is poorly ordered with Hf:B = 1:3. Upon an increase of the temperatures of boriding and annealing, the B(1s) XPS peak sharpens (Figure 20), indicating complete incorporation

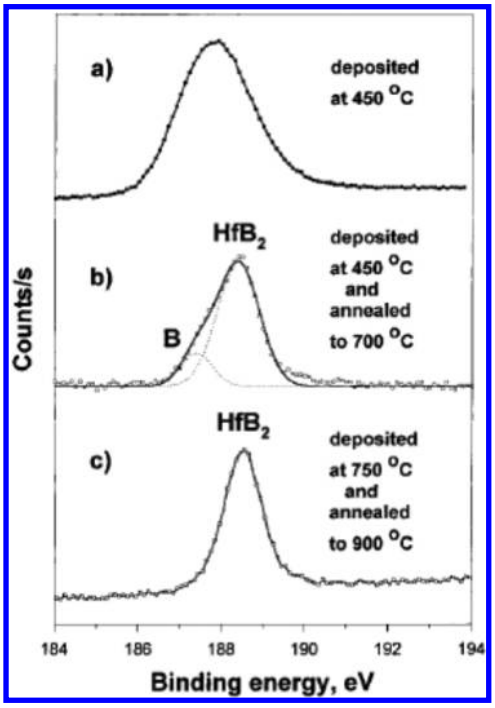

Figure 20. XPS spectra of the B(1s) region of (a) a HfB_x film deposited on a (0001)Hf surface from $Hf(BH_4)_4$ at 450 °C, (b) a film deposited at 450 °C and annealed to 700 °C, (c) a film deposited at 750 °C.[300] Reprinted with permission from ref 300. Copyright 1997 American Chemical Society.

of boron into the HfB_2 structure with a stoichiometric ratio of 1:2. Friedhoff et al. reported more recently the reaction between BCl_3 at a static pressure of 1 bar and wires of various metals including V, Nb, Ta, Ti, Mo, and Zr.[345] In the absence of any additional reactant to reduce efficiently BCl_3, high temperatures between 1200 and 1500 °C were required to carry out the reaction. As a consequence, only micrometer-sized structures were obtained.[345] Metallization of boron nanostructures was also investigated for MgB_2 synthesis (see subsection 3.2.5) and TiB_2.[346]

dx.doi.org/10.1021/cr400020d | Chem. Rev. XXXX, XXX, XXX−XXX

Table 3. Metal-Catalyzed and Self-Catalyzed CVD of Metal Boride One-Dimensional Nanostructures

MB_6	diameter (nm)	reactants/catalyst	temp (°C)/pressure	melting point of the parent metal (°C)	ref
		Metal-Catalyzed CVD			
CaB_6	10−50	$CaO-B_2H_6$/Ni	925/N/A		241
	15−40	$CaO-B_2H_6$/Ni	860−900/N/A		235
SrB_6	10−50	$SrO-B_2H_6$/Ni	760−800/N/A		240
	20−100	$SrO-B_2H_6$/Ni	840−870/N/A		305
BaB_6	20−300	$BaO-B_2H_6$/Ni	840−870/N/A		305
YB_6	ca. 50	$YCl_3-B_{10}H_{14}$/Pd (Pt)	1000 (1090)/ 100 mTorr		57
LaB_6	ca. 50	$LaCl_3-B_{10}H_{14}$/Pd	1000/100 mTorr		57
	ca. 50	$LaCl_3-BCl_3-H_2$/Au	1150/atm		373
	15−100	$LaCl_3-BCl_3-H_2$/metal not specified	1150/atm		242
	nano-obelisks ca. 200 nm at base of the shaft, 10−15 nm at the tip	$LaCl_3-B_{10}H_{14}$/Pt	920−960/ 160 mTorr		291
CeB_6	ca. 50	$CeCl_3-B_{10}H_{14}$/Pd	1000/100 mTorr		57
	ca. 50	$CeCl_3-BCl_3-H_2$/Pt	1125/atm		320
PrB_6	ca. 50	$PrCl_3-B_{10}H_{14}$/Pd	1000/100 mTorr		57
NdB_6	ca. 50	$NdCl_3-B_{10}H_{14}$/Pd	1000/100 mTorr		57
	ca. 50	$NdCl_3-B_{10}H_{14}$/Pd	915−940/		367
SmB_6	ca. 50	$SmCl_3-B_{10}H_{14}$/Pd	1000/100 mTorr		57
GdB_6	ca. 50	$GdCl_3-B_{10}H_{14}$/Pd	1000/100 mTorr		57
	100−1000	$GdCl_3-BCl_3-H_2$/Au	1150/atm		368
TbB_6	ca. 50	$TbCl_3-B_{10}H_{14}$/Pd	1000/100 mTorr		57
DyB_6	ca. 50	$DyCl_3-B_{10}H_{14}$/Pd	1000/100 mTorr		57
HoB_6	ca. 50	$CeCl_3-B_{10}H_{14}$/Pd	1000/100 mTorr		57
Fe_3B	5−50	FeI_2-BI_3/Pt−Pd	800/N/A		239
		Self-Catalyzed CVD			
CaB_6	60−100	$Ca-BCl_3-H_2$	1000/atm	842	323
LaB_6	20−200	$La-BCl_3-H_2$	1070/atm	920	321
CeB_6	20−100	$Ce-BCl_3-H_2$	1125/atm	799	374
PrB_6	100−200	$Pr-BCl_3-H_2$	1050/atm	931	372
	50−300	$Pr-BCl_3-H_2$	1050/atm		322
NdB_6	100	$Nd-BCl_3-H_2$	1150/atm	1016	324
SmB_6	200	$Sm-BCl_3-H_2$	1140/atm	1072	369
	80−100	$Sm-BCl_3-H_2$	1100/atm		371
EuB_6	60−300	$Eu-BCl_3-H_2$	950/atm	822	370

3.2.3. Non-Nanostructured Thin Films. Research efforts on metal boride CVD growth started in the middle of the 1970s with the works of Takahashi et al.,[347,348] Besmann et al.,[349] Pierson et al.,[350,351] and Motojima et al.[352] However, until the end of the 1990s, only few details were provided about the nano-microstructures of the resulting films.

TiB_2 was among the most studied materials for mechanically and chemically resistant coatings. It was typically deposited on steel, graphite, glass, or silicon at substrate temperatures between 400 and 1000 °C.[348,351,353,354] The microstructure of the first films obtained from $TiCl_4$, B_2H_6, and H_2 was not described.[355] Soon after, TiB_2 synthesis from $TiCl_4$, BCl_3, and H_2 resulted mostly in films of micrometer-scale thickness.[348,351,353,354] Stoichiometric and crystallized materials were typically obtained above 800 °C.[348,351,353−355] At lower temperatures, excess of boron was observed and poorly ordered, oxygen sensitive compounds were obtained.[353] TiB_2, ZrB_2, and HfB_2 films were synthesized from single source borohydride complexes $M(BH_4)_4$ (M = Ti, Zr, Hf), with stoichiometries and air sensitivity similar to those observed from multiple sources,[332,333,338] although crystallization occurred in the lower temperature range 500−650 °C.[332,334−336] Amorphous films obtained at lower temperature contain most often boron in excess with M:B ≈ 3,[24] because of the difficult desorption of boranes resulting from the borohydride decomposition. To enhance B_2H_6 desorption during the deposition process, Sung et al. successfully used an atomic hydrogen beam generated by plasma discharge.[24] Amorphous films with compositions close to the stoichiometry, enhanced oxidation resistance, and electrical conductivity could then be achieved at 300 °C, although crystallization of HfB_2 still occurred above 650 °C.

Metals from other groups have been investigated for CVD of borides from single sources. For example, micrometer-thick amorphous films of aluminum−boron alloys were obtained from aluminum borohydride below 660 °C.[339] By changing the ratio between the metal ion and boron into the precursor complex, it was possible to modify the compound stoichiometry, for instance in the Fe−B system at the amorphous state.[340,341] Amorphous Ni−B alloys were deposited from $NiCl_2$ and decaborane or pentaborane as the boron sources and reductants.[356] Postannealing of these films at 800 °C produced Ni_3B microparticles. More recently, Girolami and co-workers proposed complexes containing $B_3H_8^-$ ligands ($Cr(B_3H_8)_2$) as more stable and efficient single sources toward metal boride (CrB_2) films.[342]

dx.doi.org/10.1021/cr400020d | Chem. Rev. XXXX, XXX, XXX−XXX

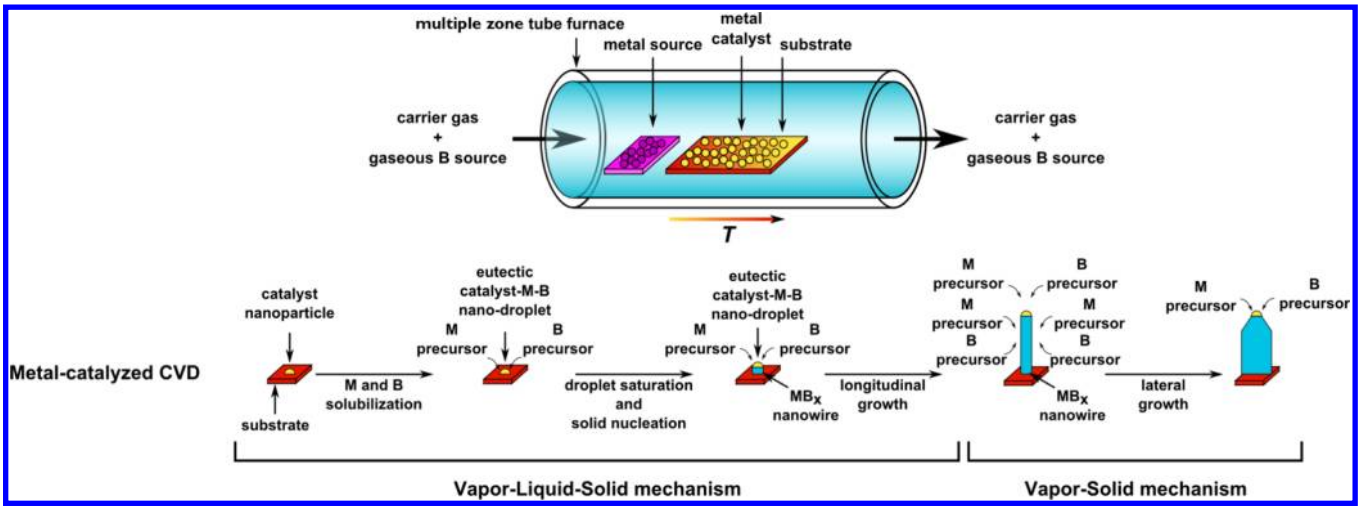

Figure 21. Scheme of a metal-catalyzed CVD process for the synthesis of MB_6 nanostructures.

Other techniques were employed to yield metal boride thin films. For instance, molecular beam epitaxy (MBE) from solid pure element sources was scarcely investigated for growth of MgB_2 films,[357,358] with thicknesses of 20 nm. Yamazaki recently claimed the discovery of crystalline CaB_3 as a new calcium boride deposited by MBE.[359] Although not completely solved, the structure of CaB_3 might be stabilized by the epitaxial growth of the 100 nm thick film on Al_2O_3 (0001). Attempts to synthesize MgB_2 thin films by pulsed laser deposition (PLD) did not provide films of good quality, probably because of the high temperature of the plasma.[360,361] On the contrary, Latini et al. could obtain films of rhenium diboride by PLD without any postannealing step.[362] Magnetron sputtering was also shown as an efficient process, especially for films of rare earth hexaborides (LaB_6) and metal diborides (VB_2, ZrB_2, TaB_2)[363] which grow epitaxially on oriented Si and NaCl surfaces.

3.2.4. CVD for Growth of 1D Nanostructures. Hexaborides are especially studied in the framework of the CVD process. This enthusiasm is certainly related to the well-known field emission properties of these compounds, which are enhanced when the materials are shaped into one-dimensional structures, whose synthesis by CVD is relatively straightforward. When rare earth hexaborides are deposited from solely rare earth chlorides and pentaborane or decaborane between 800 and 1000 °C, microparticles are usually obtained.[364−366] In order to decrease the particle size, a simple strategy consists of the use of preformed metal nanoparticles, so-called "catalysts" although they are used in stoichiometric quantities: each metal nanoparticle increases the nucleation rate of one nanostructure. Because the nucleation and growth steps are substrate-mediated, the catalyzed CVD process yields one-dimensional growth of metal hexaborides, despite their cubic structure. Many occurrences of metal hexaboride nanowires and related nanostructures can be found in the literature (Table 3). The reported growth direction is most often ⟨100⟩,[57,235,240−242,291,305,320,322,324,367−372] more rarely ⟨111⟩[321,373] or ⟨110⟩.[323] Two families can be distinguished within these procedures: namely, metal-catalyzed CVD and self-catalyzed CVD.

3.2.4.1. Metal-Catalyzed CVD. This technique involves an additional metal as catalyst for a so-called vapor−liquid−solid (VLS) mechanism (Figure 21).[375] Usually, a powdered metal precursor (chlorides or oxides) is placed in the cold (ca. 700 °C) upstream section of a tube furnace. At such temperatures it is partially vaporized, carried downstream in the higher temperature region together with the gaseous boron species. Then, the precursors react on a substrate, usually made of silicon or silicon oxide covered with metal nanoparticles (Au, Pd, Pt, Ni). Those act first to fasten the decomposition of the gaseous precursors into boron(0) and metal(0) which are collected into the nanoparticles. The melting point of the catalyst−B(0)−M(0) mixture is lowered compared to pure metal and elements, so that it is liquid at the substrate temperature. Hence, precipitation of the solid occurs from the supersaturated droplets. The solid nuclei is further fed by the catalyst−B(0)−M(0) droplet which migrates to the top of the nanostructures. The choice of an appropriate metal for dissolution of high amounts of precursors is a key issue for efficient nanowire growth. Although these processes were developed a long time ago for hexaboride growth, it is only very recently that Cheung's team demonstrated rational choice of the metal catalyst for high yield of rare earth hexaborides nanowires.[57] The authors showed that the higher the solubility of boron and rare earth metal into the catalyst, the higher the yield and the lower the amount of defects into the nanowires. The best results were obtained by using Pd nanoparticles as catalysts for CVD growth from decaborane and $RECl_3$ at 1000 °C. Homogenous samples of hexaboride MB_6 nanowires (M = Y, La, Ce, Pr, Nd, Sm, Gd, Tb, Dy, and Ho) could be obtained with a diameter of ca. 50 nm and length of few micrometers (Figure 22). On the other hand, Pt provides only low solubility of the precursors and cannot ensure efficient growth of the nanowires (Figure 23a). Another example is nanowires of LaB_6 and GdB_6 obtained from BCl_3/H_2 over poorly efficient Au catalyst. The nanostructures exhibit large diameters and wider polydispersities. When a better catalyst is used, such as Pt at 1125 °C, the diameter is reduced down to 50 nm and the distribution is narrowed.[57]

The reaction temperature is another important factor for the control of the nanostructure and the composition of the resulting solid, for several reasons. First, temperature greatly affects the solubility of precursors into the catalyst. Hence, although Pt is inefficient for hexaboride growth at 1000 °C (Figure 23a),[57] it becomes a suitable catalyst at 1090 °C when Pt can dissolve high amounts of reactants (Figure 23c). Second, temperature also affects the flow and the concentration of

dx.doi.org/10.1021/cr400020d | Chem. Rev. XXXX, XXX, XXX−XXX

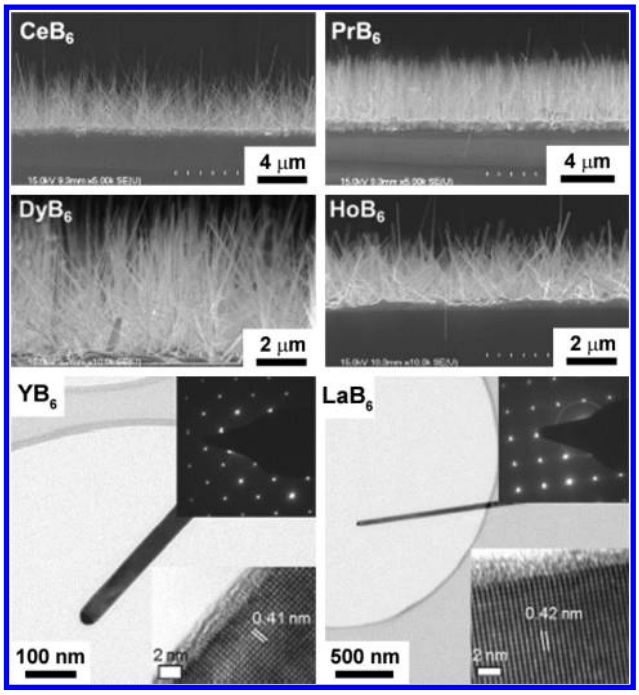

Figure 22. SEM images of Pd-catalyzed CVD-grown rare earth boride nanowire samples on Si wafer substrates. TEM images of YB_6 and LaB_6 nanowires. Insets are (top) SAED patterns and (bottom) HRTEM images of the corresponding nanowires.[57] Reprinted with permission from ref 57. Copyright 2011 American Chemical Society.

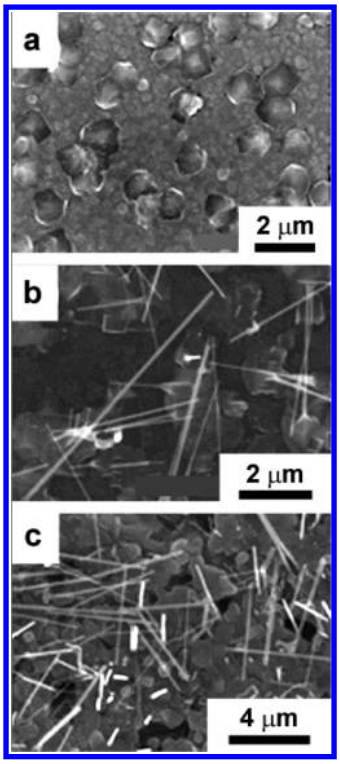

Figure 23. Scanning electron microscopy (SEM) images of YB_6 nanostructures synthesized at 1000 °C with (a) Pt nanoparticles and (b) Pd nanoparticles, and (c) at 1090 °C with Pt nanoparticles.[57] Reprinted with permission from ref 57. Copyright 2011 American Chemical Society.

gaseous precursors at the deposit site. For instance, increasing the temperature of synthesis of NdB_6 from $B_{10}H_{14}$ and $NdCl_3$ over Pd nanocatalysts[367] leads to an evolution from amorphous and boron-rich nanocurls to long straight single crystal NdB_6 nanowires. This was assigned to an increase in the vapor pressure of $NdCl_3$, which is sufficient at high temperature to ensure supersaturation of the liquid Pd−Nd−B droplets and continuous growth of stoichiometric nanowires. Such a rational understanding was made possible by changing only temperature while other parameters were kept unchanged, contrary to other reports.[235,240] Brewer et al. changed the longitudinal coordinate of the deposit site to tune the flow of reactants $B_{10}H_{14}$, $LaCl_3$ over Pt nanoparticles.[291] They were able to grow selectively LaB_6 nano-obelisks upstream where the flow of precursors is high (Figure 24). It was shown (Figure 21) that

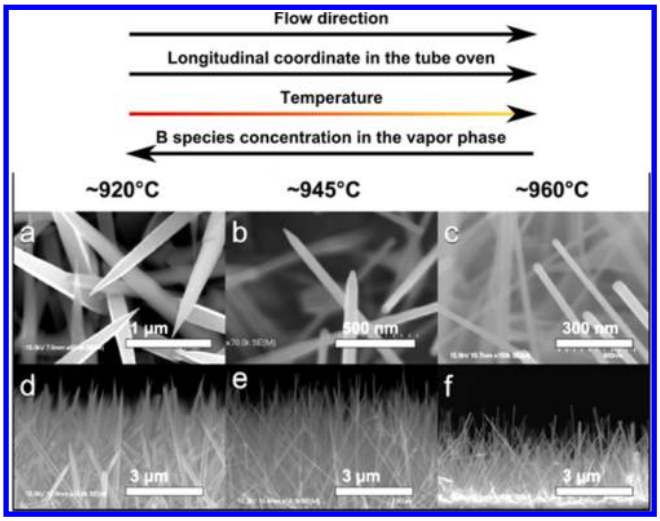

Figure 24. Evolution as a function of the substrate position in the gas stream of LaB_6 nanostructures from nano-obelisks to nanowires. The CVD synthesis was performed from $B_{10}H_{14}$, $LaCl_3$, and Pt nanoparticles. Reprinted with permission from ref 291. Copyright 2007 American Chemical Society.

longitudinal growth occurred first because of the high rate of the VLS mechanism, while transverse growth with diameter increase at the base of the obelisks happened at the second place by slower vapor−solid (VS) reaction. Since most of the precursors were consumed in this high concentration upper section, the downstream reactant feed rate was lower and only yielded nanowires with uniform diameters through the VLS mechanism. An increase in the temperature can also favor VS side-reactions, as was shown for the growth of NdB_6 nanoobelisks.[367] Although it was not demonstrated, one might expect that by adjusting temperature, time, and/or reactant flow, it would be possible to modify the velocity ratio of VLS longitudinal growth and VS lateral growth, so as to tune the aspect ratio of the final nanowires/nanoobelisks. It is noteworthy that in a recent attempt to simplify the codeposition process by avoiding the use of a downstream susbtrate, Amin et al. and Jash et al. reported an alternative VLS process toward BaB_6 and SrB_6 nanowires by reacting B_2H_6 directly on Ni-coated BaO/SrO powders.[240,305] Despite its simplicity, this process suffers from high diameter polydispersity between 20 and 200 nm, presumably because the nucleation and growth steps are not sufficiently separated. When narrow size distributions are required, especially for field emission, growth from metal precursors on separate substrates

dx.doi.org/10.1021/cr400020d | Chem. Rev. XXXX, XXX, XXX−XXX

should be favored with nanowire diameters typically ranging between 10 and 50 nm.

It is worth noting that metal-catalyzed CVD can also be applied in principle to the synthesis of 1D nanostructures of other metal borides, especially those containing transition metals. This was nicely exemplified by Li and co-workers who obtained Fe_3B nanowires by CVD on silicon over Pd/Pt alloy nanoparticles using iodide precursors (Figure 25).[239] Low

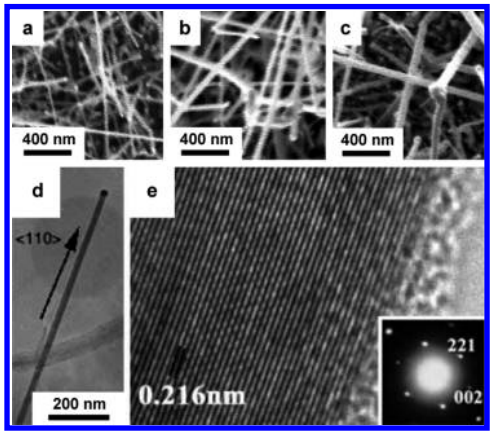

Figure 25. Fe_3B nanowires by CVD on silicon over Pd/Pt alloy nanoparticles.[239] (a–c) SEM evidence of diameter adjustment by increase of the amount of catalyst. (d, e) TEM and HRTEM of single crystal Fe_3B nanowire. Reprinted with permission from ref 239. Copyright 2006 American Chemical Society.

decomposition temperatures were the main reason for the choice of iodides, especially compared to BCl_3. This enabled working at low deposition temperature and recovering nanowires without noticeable sintering. In a following work, the same group took advantage of the high reactivity of the precursors to grow selectively Fe_3B and Fe_5Si_2B nanowires on silicon without any catalyst.[326] To our knowledge, this is the only work reporting the use of iodides FeI_2 and BI_3 as precursors. Up to now and apart from this convincing demonstration, CVD was not applied to transition metal boride nanostructures. The reason might be found in the specific interest in 1D rare earth and alkaline earth hexaboride nanostructures for field emission. Indeed, REB_6 and AEB_6, to a lower extent, have gathered most of the attention of the CVD community.

3.2.4.2. Self-Catalyzed CVD. This technique does not involve any additional metal as catalyst since it relies solely on the reaction between metal(0) and gaseous BCl_3/H_2 (Figure 26).[321−324,369−372,374] Growth of the nanostructures occurs directly on the metal which acts as a catalyst and avoids the use of a separate substrate. Contrary to boridization of metal films, self-catalyzed CVD is performed at atmospheric pressure and temperatures between the melting point and the boiling point of the metal. Therefore, liquid metal droplets are the reactive sites for growth of the 1D nanostructures (Figure 26). This calls for obvious similarities with the VLS mechanism, except that the droplet is not able to dissolve boron(0) to a large extent and feeds directly the hexaboride nanowire (Figure 27). Bigger particles and larger size distributions are usually obtained from self-catalyzed CVD performed at higher T than metal-catalyzed CVD.

3.2.5. CVD, PLD, and HPCVD for MgB_2 Nanostructures. *3.2.5.1. Special Case of MgB_2.* Magnesium has vapor pressure orders of magnitude higher than that of boron. This directly impacts the synthetic procedures at the low pressures used in molecular beam epitaxy or pulsed laser deposition, because MgB_2 is stable (Figure 28) and has a significant growth rate only in a narrow temperature range.[358,376,377] Hopefully, kinetics widen the useful window in terms of temperature and Mg concentration in the gas since there is a significant energy barrier for the decomposition of MgB_2 into Mg vapor and richer borides.[377] Special processes were developed in order to provide high concentration Mg vapor and to reach the right Mg:B stoichiometry in MgB_2. Two families can be distinguished, whether boron is provided as a solid or as gaseous species. In the first case, magnesium vapors react with boron nanostructures through vapor–solid reactions, while in the second case Mg reacts with boron precursors in the gas phase. This later case combines physical vapor deposition (PVD) and CVD in a single process by involving physical evaporation of a metal bulk and chemical decomposition of a boron precursor gas. As such, the process is called hybrid physical chemical vapor deposition (HPCVD).

3.2.5.2. Vapor–Solid Reactions. This family of reactions involves conversion of amorphous boron films under Mg vapor, typically at ca. 900 °C. This process was intensively used at the beginning of the 2000s soon after the discovery of high T_c (39 K) superconductivity of MgB_2.[16] Although the first reports using boron films obtained by PLD do not describe the nanostructure of the resulting MgB_2 thin films,[361,378] later

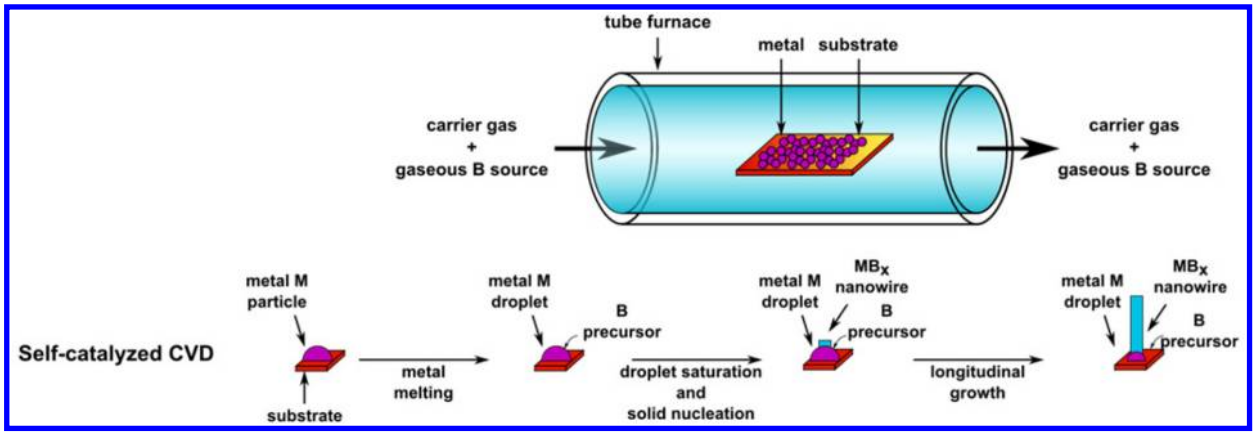

Figure 26. Scheme of a self-catalyzed CVD process for the synthesis of MB_6 nanostructures.

dx.doi.org/10.1021/cr400020d | *Chem. Rev.* XXXX, XXX, XXX–XXX

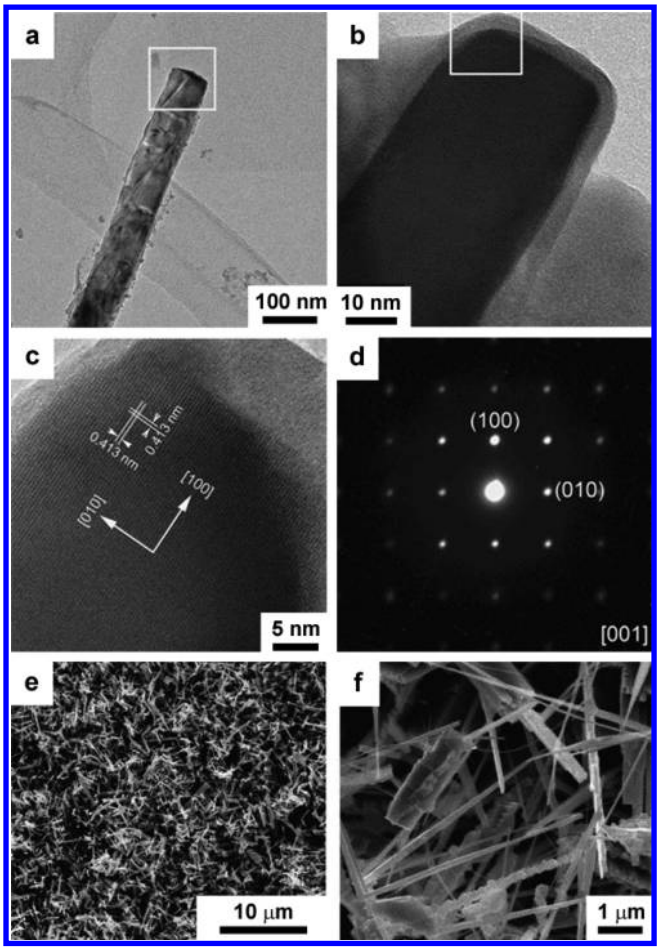

Figure 27. (a–c) TEM pictures, (d) SAED pattern, and (e, f) SEM pictures of PrB_6 nanowires obtained by self-catalyzed CVD from BCl_3 gas.[372] Reprinted with permission from ref 372. Copyright 2009 John Wiley and Sons, Inc.

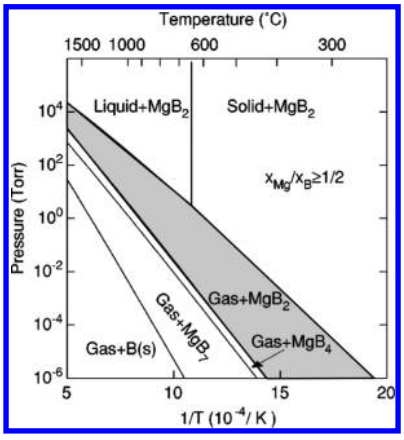

Figure 28. Pressure–temperature phase diagram for the Mg:B atomic ratio $x_{Mg}/x_B \geq 1/2$. The region "Gas + MgB_2" is the thermodynamic growth window for MgB_2 films. Reprinted with permission from ref 376. Copyright 2001 American Institute of Physics.

works have shown that nanoplates could be obtained by this process (Figure 29a).[379] When the initial boron film is nanostructured, the morphology is maintained and the boron nanostructure acts as a so-called "reactive template". Especially, MgB_2 nanowires (Figure 29b–d) can be synthesized from boron nanowires obtained by templating in mesoporous

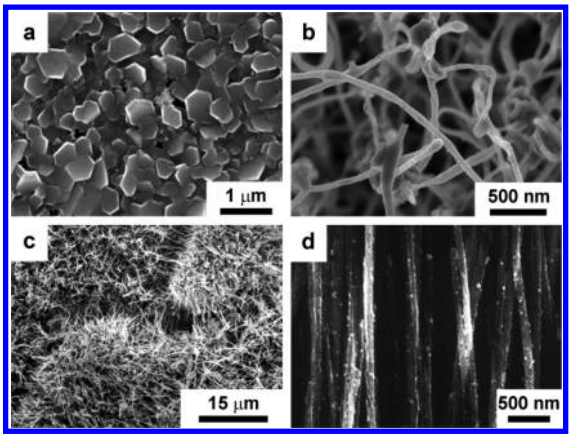

Figure 29. SEM pictures of MgB_2 nanostructures obtained by reactions between Mg vapors and boron nanostructures: (a) submicrometer plates (Reprinted with permission from ref 379. Copyright 2003 Elsevier.), (b–d) nanowires. (Reprinted, respectively, with permission from refs 233 , 237, 298. Copyright, respectively, 2001 John Wiley and Sons, Inc.; 2005 American Institute of Physics; 2007 Elsevier.) Image d shows some white spots indicating MgO nanoparticles originating from oxidation during the heat treatment.

alumina membranes,[380,381] by Au-catalyzed CVD growth from gaseous BI_3,[233,298] or by magnetron sputtering.[234,237,382] In a similar process, amorphous MgB_x films originating from electron beam evaporation of Mg and B sources yield 20 nm-thick MgB_2 nanoplates[306] when exposed to Mg vapors, in the presence of H_2 to prevent Mg oxidation.

3.2.5.3. HPCVD Vapor–Vapor Reactions. MgB_2 nanowires[236] and nanotubes[238] (Figure 30) were formed from

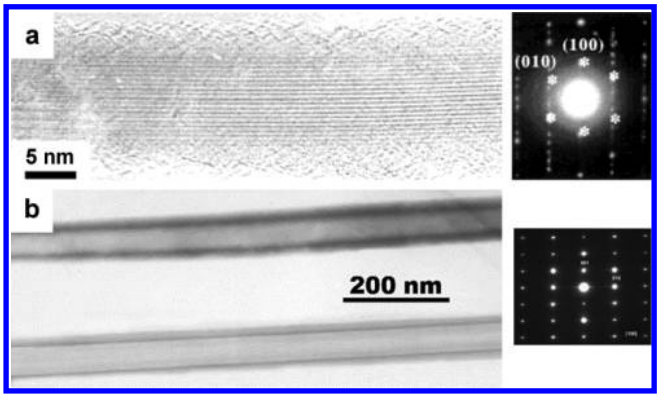

Figure 30. MgB_2 (a) nanowires and (b) nanotubes grown by heating mixed MgB_2/Mg powders on, respectively, MgB_2/Mg (900 °C) and h-BN (850 °C) substrates. Reprinted, respectively, from refs 236 and 238. Copyright, respectively, 2003 American Chemical Society and 2009 Elsevier.

very close procedures, involving heat treatment of mixed MgB_2/Mg powders obtained by mechanically actived reaction between magnesium and boron. Nanowires grew over the initial MgB_2/Mg powder,[236] while nanotubes grew on the surface of the BN crucible.[238] No discussion was provided concerning this discrepancy between the reported morphologies, and it is actually difficult to discriminate between the different substrates (MgB_2/Mg and h-BN), slightly different precursor compositions (MgB_2:Mg = 1.5/2.0 and 1.3:2.0 for, respectively, nanowires[236] and nanotubes[238]), and heat treatments (900 °C during 40 min and 850 °C during 30 min for,

dx.doi.org/10.1021/cr400020d | Chem. Rev. XXXX, XXX, XXX–XXX

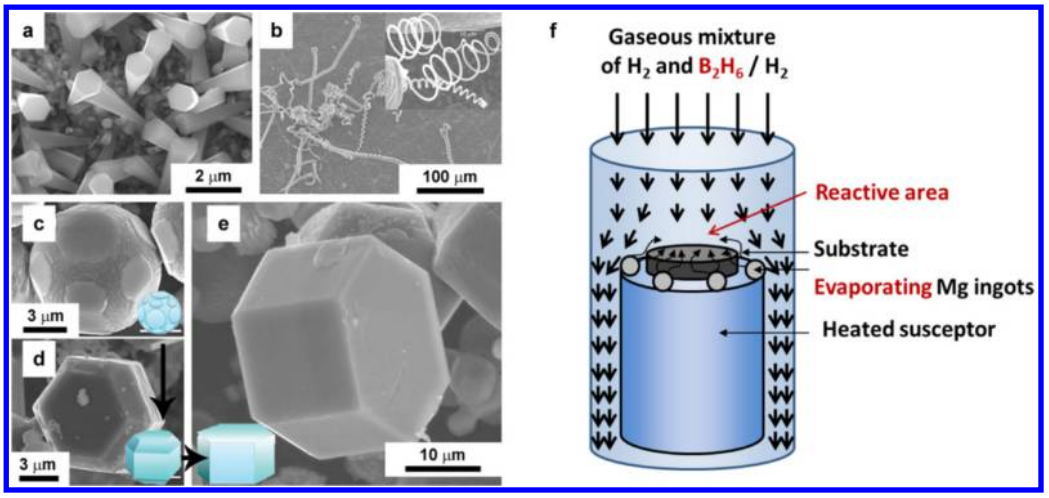

Figure 31. SEM pictures of MgB_2 nanostructures obtained by HPCVD from magnesium ingots under different flows of B_2H_6/H_2 gas. (a) Micropillars grown from Cu substrate (650 °C for 4 min). Reprinted with permission from ref 386. Copyright 2009 American Chemical Society. (b) Nanohelices grown from silicon. Reprinted with permission from ref 388. Copyright 2008 American Chemical Society. (c–e) HPCVD growth evolution of self-standing hexagonal prisms on stainless steel (680–720 °C for 6–12 min). Reprinted with permission from ref 387. Copyright 2011 Royal Society of Chemistry. (f) Scheme of a typical HPCVD system. Adapted with permission from ref 304. Copyright 2007 John Wiley and Sons, Inc. The susceptor temperature is in the range 550–760 °C. The carrier gas H_2 at a pressure of 100 Torr avoids oxidation. A mixture of B_2H_6 (25%) and H_2 is injected into the carrier gas at varying ratios. The reactive area corresponds to stagnant gas which ensures high local Mg content.

respectively, nanowires[236] and nanotubes[238]). However, it is clear that Mg vapors play again a significant role in the growth of these 1D nanostructures. Also, in these cases, the nanostructures grow from sites different from the precursor position. This indicates that gaseous boron containing species are formed and are able to diffuse and react together with Mg vapors at the reaction site. Besides vaporized "single sources" MgB_2[236,238] and MgB_xO_y[383] gels, the use of dedicated gaseous boron sources was reported. Especially, reaction between B_2H_6 and a MgB_xO_y gel at 800 °C yielded MgB_2 nanowires after a few hours.[301] Similarly, $MgAl_xB_y$ nanowires were obtained after treatment of 1% Mg-doped mesoporous alumina under gas mixtures of B_2H_6/H_2 or BCl_3/H_2, although templating was not clearly demonstrated since 1D nanostructures were obtained outside the mesopores.[302] Some Mg–B nanowires with undefined composition were similarly deposited over an MCM-41 zeolite with metallic nickel filling the pores, by using the reaction between B_2H_6/H_2 and Mg vapors from metal ingots.[384] Yang et al. described a convenient alternative method to produce MgB_2 nanowires of 100 nm diameter and 10 μm length.[385] The technique relies on single source thermal decomposition in vacuum, with solid magnesium borohydride $Mg(BH_4)_2$ as the precursor. Upon heating, hydrogen evolution occurs, and the solid phase goes through a series of intermediate steps, with a mixture of Mg and MgB_2 at 380 °C and MgB_2 at 460 °C after 1 h. The very low temperature of synthesis observed here can be explained by the intimate mixture between Mg and B occurring from the single source. Although it is not discussed in the original article, the (P,T) reaction conditions clearly fall in the gas + MgB_2 stability domain highlighted in Figure 28. This suggests that gaseous species might play an important role in the growth of these nanostructures. In all the above-mentioned cases, one-dimensional growth of the nanostructures can only be explained by the diffusion of gaseous Mg outside the initial Mg containing precursors.

3.2.5.4. Tuning between Homogeneous and Heterogeneous Nucleation During HPCVD. Nice examples of the versatility of MgB_2 particle morphologies at the micrometer-scale were reported by HPCVD over the past few years (Figure 31). The common base of these syntheses is the chemical reaction between vaporized Mg from bulk metal ingots and B_2H_6/H_2 gas flow in the temperature range 650–800 °C at low pressure (Figure 31f).[303,304] By using very close heat treatment conditions, Wang et al. obtained micropillars[386] (Figure 31a) grown from Cu, Mg, and stainless steel substrates (650 °C for 4 min), while Chen et al. reported self-standing microprisms (Figure 31c–e) with stainless steel substrates (680–720 °C for 6–12 min).[387] The reason for the different resulting microstructures might be found both in the slightly different heating conditions, but also in the gas mixture composition and flow. Compared to pillars, prisms are obtained at higher temperature, longer time, higher borane composition of the flowing gas, and higher gas flow. All these factors favor high concentration in the vapor phase of Mg and boron precursors, thus enabling high supersaturation in the reactive area which triggers homogeneous nucleation of prisms from the vapor, instead of heterogeneous nucleation on substrates and pillar growth when the gaseous reactant concentration is lowered. It is worth noting that, with a similar HPCVD process, Nath et al. have been previously able to synthesize MgB_2 nanohelices[388] (Figure 31b) on various substrates, including tantalum, silicon, silica, sapphire, and porcelain. However, the lack of detailed experimental conditions prevents in-depth comparison with the works of Wang and Chen.

3.2.6. Alternative Processes toward Other Nanostructured Films. *3.2.6.1. Single Source CVD.* Tuning of nanostructured hafnium diboride films was demonstrated by Jayaraman and co-workers by CVD growth from single source $Hf(BH_4)_4$. By adjusting the pressure of the precursor vapor and the temperature, the authors were able to control the stoichiometry, thickness, roughness, and crystallization state of the films. Below 500 °C, highly conformal, dense amorphous films were obtained (Figure 32a,b), while HfB_2 films with a columnar microstructure were produced above 500 °C (Figure 32c–e).[334–336]

dx.doi.org/10.1021/cr400020d | *Chem. Rev.* XXXX, XXX, XXX–XXX

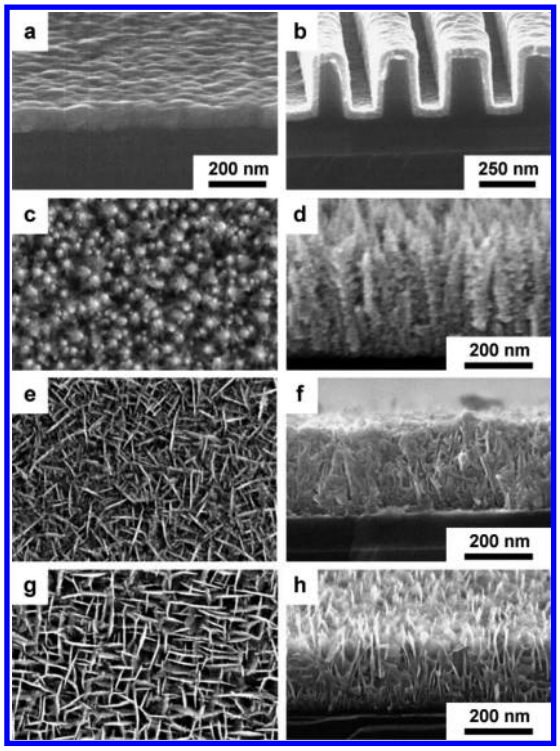

Figure 32. SEM side view of amorphous HfB_x films grown at (a) 200 °C on a planar Si surface and (b) 250 °C on a trenched silica substrate.[334] Reprinted with permission from ref 334. Copyright 2005 American Vacuum Society. SEM plan-view and cross-sectional images of crystalline HfB_2 films grown from the single-source precursor $Hf(BH_4)_4$ (c,d) on SiO_2 at 600 °C, where the preferred orientation is (0001); (e,f) on SiO_2 at 800 °C, where the preferred orientation is $(10\bar{1}0)$; and (g,h) on Si(001) at 800 °C, where the preferred orientation is $(10\bar{1}0)$.[335] Reprinted with permission from ref 335. Copyright 2006 Elsevier.

3.2.6.2. Electron Beam Induced Deposition. EBID usually employs the electron beam of a scanning electron microscope to decompose precursor molecules introduced to a substrate in the gas phase. To enhance the spatial resolution of the process, Ye and co-workers used a negatively biased scanning electron microscope as the electron source.[337] They demonstrated the outstanding resolution of the technique by depositing sub-5-nm nanostructures of HfB_2 on hydrogen-bounded silicon surfaces (Figure 33). Contrary to CVD, decomposition of the single precursor $Hf(BH_4)_4$ and crystallization of the diboride were achieved without heating the substrate.

3.2.6.3. Arc Plasma in Liquid Phase. A recent process toward nanostructures based on magnesium and boron was described by Sano and co-workers who performed arc plasma in liquid argon.[389] This way, bulk MgB_2 was converted into nanotubes, although the exact composition of the product could not be assessed. In this process, a plasma is created between two electrodes immerged in liquid Ar. Because of high local temperature, bulk MgB_2 at the anode passes in the liquid phase and precipitates at the cold cathode with nucleation of the nanostructures.

3.3. Solid State Syntheses

3.3.1. Reduction of Nanostructured Metal Oxides. Reduction of oxides by boron is strongly exothermic and yields high temperatures in the course of the reaction. Grain growth and sintering are then difficult to restrain.[390,391] However, Jha et al. showed recently that niobium diboride could be obtained at the nanoscale through borothermal reduction at 1300 °C of NbO_2 nanocrystals, in order to yield NbB_2 nanowires with a diameter of 40 nm.[250] In a similar manner and at the same temperature, the same group developed the synthesis of cerium hexaboride nanorods.[290] By using nanoparticles (10 nm) of cerium oxide as precursor, the authors obtained submicronic rods with diameters of a few hundreds of nanometers. On the contrary, much smaller nanorods (30×150 nm^2) were synthesized from aggregated nanorods of cerium oxalate (5×20 nm^2). Both studies point out the importance of the metal precursor choice for governing the reactivity and the final morphology: nanostructured precursors are usually more reactive, and lead to more intense nucleation and smaller particles of the metal boride phase. The typical resistance of metal borides to sintering might explain the persistence of nanostructures at temperatures as high as 1300 °C.

Alternatively, Deheri et al.[392,393] and Jadhav et al. proposed approaches to produce nanoscaled $Nd_2Fe_{14}B$ by reducing a nanostructured mixture of Nd−Fe oxides and B_2O_3, respectively, by calcium dihydride at 800 °C[392,393] and hydrogen at 950 °C.[394] The resulting 50−100 nm nanoparticles were strongly aggregated. A hybrid approach was recently proposed for the synthesis of nanoparticles mainly made of $Nd_2Fe_{14}B$,[395] consisting in the aqueous precipitation of amorphous Fe−B nanoparticles through reduction by borohydrides in the presence of Nd^{3+} cations. Neodymium ions are adsorbed on the surface of 2 nm primary particles agglomerated into 60 nm aggregates. Further annealing at 950 °C under hydrogen yields 80 nm particles made of a $Nd_2Fe_{14}B$/Fe−B composite.

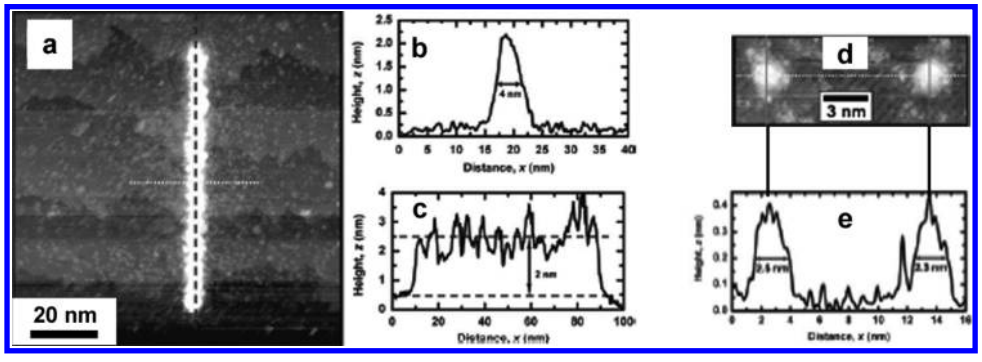

Figure 33. HfB_2 nanostructures made by STM-EBID on a hydrogenated Si(100) surface. (a−c) nanowire and line contours, (d, e) nanodots and line contour.[337] Reprinted with permission from ref 337. Copyright 2010 American Chemical Society.

dx.doi.org/10.1021/cr400020d | *Chem. Rev.* XXXX, XXX, XXX−XXX

Table 4. Solid State Syntheses under Autogeneous Pressure of Metal Borides[a]

metal boride	diameter (nm)	reactants	temp (°C)	duration	metal:boron M:B(:coreactant) ratio	ref
		Alkaline Earth Metal Borides				
CaB_6	few 100s of nm	$CaCl_2/NaBH_4$	500	8 h	1:6	402
		$CaO/B(OH)_3/Mg/I_2$	250	12 h	1:3.2:10.7:1*	299
		$CaCO_3/B(OH)_3/Mg/I_2$	400	4 h	1:6:22:3	299
SrB_6	few 100s of nm	$SrO/B(OH)_3/Mg/I_2$	350	12 h	1:6:22:2	299
BaB_6	few 100s of nm	$BaO/B(OH)_3/Mg/I_2$	350	10 h	1:6:22:2	299
MgB_2	few 100s of nm	$MgCl_2/NaBH_4$	600	8 h	1:5	403
		Transition Metal Borides				
Co_2B*	80*	$CoCl_2/NaBH_4$	500−600	12 h	4:1*	404
VB_2	50−100	$VCl_4/NaBH_4/Mg$	650	8 h	1:2:1	316
		Rare Earth Metal Borides				
LaB_6	few 100s of nm	metal acetate/$NaBH_4$	900	3 h	1:6	405
		$LaCl_3{\cdot}7H_2O/B_2O_3/Mg$	500	4 h	1:6:25	331
		$La_2O_3/B(OH)_3/Mg/I_2$	250	12 h	1:6:22:3	299
	100−200 nm	$La_2O_3/B_2O_3/Mg/I_2$	500	12 h	1:6:5:3	299
	mixture of few 100s of nm cubes and 40 nm nanoparticles	$La_2O_3/B_2O_3/Mg/I_2$	500	0.7 h	1:6:5:3	299
	30 nm	$LaCl_3{\cdot}7H_2O/NaBH_4/Mg$	400	4 h	1:9:11	331
	50 nm	$La_2O_3/NaBH_4/Mg/I_2$	400	12 h	1:6:4:3	299
	50 nm	La_2O_3/amorphous B/ Mg/I_2	500	12 h	1:6:6:3	299
CeB_6	few 100s of nm	metal acetate/$NaBH_4$	900	3 h	1:6	405
		$CeO_2/B(OH)_3/Mg/I_2$	250	12 h	1:6:22:3	299
		$CeCl_3{\cdot}6H_2O/B_2O_3/Mg$	500	12 h	1:6:25	406
	30	$CeCl_3{\cdot}6H_2O/NaBH_4/Mg$	400	48 h	1:8:13	406
PrB_6	few 100s of nm	$Pr_6O_{11}/B(OH)_3/Mg/I_2$	250	12 h	1:6:22:3	299
	ca. 50	$PrCl_3{\cdot}6H_2O/B_2O_3/Mg$	500	12 h	1:6:25	406
	30	$PrCl_3{\cdot}6H_2O/NaBH_4/Mg$	400	48 h	1:8:13	406
NdB_6	few 100s of nm	metal acetate/$NaBH_4$	900	3 h	1:6	405
		$NdCl_3{\cdot}6H_2O/B_2O_3/Mg$	500	12 h	1:6:25	406
		$Nd_2O_3/B(OH)_3/Mg/I_2$	350	12 h	1:6:22:3	299
	30	$NdCl_3.6H_2O/NaBH_4/Mg$	400	48 h	1:8:13	406
SmB_6	few 100s of nm	metal acetate/$NaBH_4$	900	3 h	1:6	405
		$NdCl_3{\cdot}6H_2O/B_2O_3/Mg$	500	12 h	1:8:13	407
		$Sm_2O_3/B(OH)_3/Mg/I_2$	250	12 h	1:6:22:3	299
	nanorods, few 100s of nm in diameter	$NdCl_3{\cdot}6H_2O/B_2O_3/Mg$	500	48 h	1:8:13	407
EuB_6	few 100s of nm	metal acetate/$NaBH_4$	900	3 h	1:6	405
		$NdCl_3{\cdot}6H_2O/B_2O_3/Mg$	500	12 h	1:8:13	407
		$Eu_2O_3/B(OH)_3/Mg/I_2$	250	12 h	1:6:22:3	299
GdB_6	few 100s of nm	metal acetate/$NaBH_4$	900	3 h	1:6	405
		$NdCl_3{\cdot}6H_2O/B_2O_3/Mg$	500	12 h	1:8:13	407
TbB_6	few hundreds of nm	$NdCl_3{\cdot}6H_2O/B_2O_3/Mg$	500	12 h	1:8:13	407

[a] Asterisk indicates an excess of metal source is used for the synthesis of Co_2B[404] and CaB_6.[299] This suggests the presence of metal-containing side-products, although this point is not discussed in the corresponding reports.

3.3.2. Solid State Reactions under Autogenic Pressure. *3.3.2.1. SRAPET Procedure.* Techniques based on solid state chemistry carried out in sealed vials (autoclaves) have been named as solid state reactions under autogenic pressure at elevated temperature (SRAPET) by the group of Gedanken.[34,396−400] The development of SRAPET for metal borides started in the middle of the first decade of the 2000s and since then demonstrated high versatility. Nowadays, this synthetic method is one of the most suitable for the production of a huge variety of submicronic metal borides. The interest in using pressurized containers for improved yield and crystallinity is always explained by the beneficial impact of pressure although it was, to our knowledge, never investigated in-depth.[401] The primary reason for the lack of data concerning the role of pressure is the difficulty to adjust separately the temperature and the pressure, and then to decipher the role of both parameters. Because the formation of borides is a succession of irreversible reactions, the role of the pressure might be found in its impact on the kinetics. Especially, it is striking that all the reactions involved in boride-targeting SRAPET bring into play reactants (B_2O_3, Mg), intermediates (B_2H_6), and/or by-products (H_2) which are highly volatile and strongly impacted by pressure. The first role of the sealed vessels is therefore to confine the species necessary to the completeness of the transformation. The second important effect is the increased concentration of gaseous reactants and intermediates, which provides enhanced reaction rates.

SRAPET processes have been dedicated to a wide range of borides belonging to alkaline earth borides, transition metal borides, and rare earth metal hexaborides. Most of these

dx.doi.org/10.1021/cr400020d | Chem. Rev. XXXX, XXX, XXX−XXX

syntheses are carried at temperatures above 500 °C (Table 4). It is noteworthy that, with a few exceptions, the SRAPET procedure yields mainly submicrometer particles. Alkaline earth borides (CaB_6,[402] MgB_2[403]) and transition metal borides (Co_2B[404]) have been scarcely reported. Rare earth metal hexaborides have been more intensively studied mainly because of the interest in their field emission properties.[299,331,405−407]

3.3.2.2. Size and Temperature Reduction. After the successful use by Selvan et al.[405] of RAPET at 900 °C to produce submicrometer cubes of various REB_6 (RE = La, Ce, Nd, Sm, Eu, Gd) from rare earth acetates and $NaBH_4$, Qian's group tackled the question of size reduction. To do so, the authors used first Mg additive with a 2-fold role, first as a reductant (eq 21 and 22) of metal cations, second as a source for strong in situ heating.[331,406] Indeed, its strongly exothermic oxidation reduces the energy input necessary for completion of the reaction. Heating to 400 °C is therefore sufficient to induce the reaction between rare earth chlorides, $NaBH_4$ and Mg.[331,406] An excess of sodium borohydride and magnesium led to particles of MB_6 (M = La, Ce, Pr, and Nd) with a diameter of ca. 30 nm (Figure 34).[331,406] A similar effect of

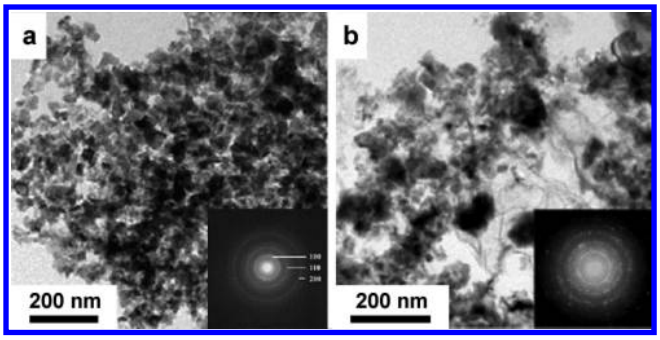

Figure 34. TEM images and SAED patterns of (a) LaB_6 nanoparticles[331] and (b) CeB_6 nanoparticles[406] obtained by the Mg-assisted reaction between rare earth metal chlorides and $NaBH_4$ under RAPET conditions at 400 °C for 4 h and 500 °C for 12 h, respectively. Reprinted, respectively, with permission from refs 331 and 406. Copyright, respectively, 2008 Elsevier and 2009 Elsevier.

additives was observed by using boron oxide as the boron source (eq 22).[331,406,407] Although stoichiometric amounts of metal and boron sources were used, highly reductive conditions were involved, with a nearly double excess of magnesium. Submicrometer cubes of LaB_6, CeB_6, PrB_6, NdB_6, SmB_6, EuB_6, GdB_6, and TbB_6 were obtained from B_2O_3,[331,406,407] compared to 30 nm nanoparticles from $NaBH_4$ (Figure 35).[331,406] In order to explain the impact of the boron source, the authors speculate that the physical state of the precursors might have a strong impact on the reaction course. More precisely, B_2O_3 is liquid in the reaction conditions, while solid $NaBH_4$ starts to decompose above 500 °C (eqs 9 and 10). It is argued that liquid B_2O_3 might coat metal chloride particles and facilitate the growth of metal boride particles.[406] Another reason for the discrepancy in the particle morphology might come from the highly reducing ability of sodium borohydride. This could indeed trigger the reaction between metal chlorides and the boron source at lower temperature than for B_2O_3, thus facilitating the nucleation step and providing a larger amount of small particles. Obviously, both hypotheses are far too simple to explain the whole process, especially because they do not take into account the role of magnesium in the course of the reaction.

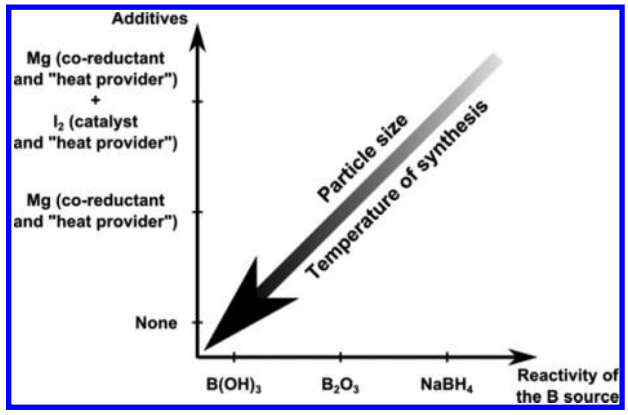

Figure 35. Experimental levers used to control the temperature of synthesis and the size of rare earth hexaborides: coreactants and boron sources. From the data in refs 299, 331, 406, 407.

A further decrease in the synthesis temperature from metal oxide precursors was achieved through the addition of a second coreactant, namely iodine, which leads to reactive intermediates, such as metal iodides or oxyiodides, through exothermic reactions (e.g., between excess magnesium and iodine to yield MgI_2), thus enabling crystallization at temperature set points as low as 250 °C.[299] Depending on the nature of the boron source, particles with sizes ranging from a few tenths to a few hundreds of nanometers were synthesized by addition of Mg and I_2. LaB_6 nanoparticles (50 nm) were obtained with $NaBH_4$ as a boron source. Again, $NaBH_4$ yields smaller particles than less reactive boric acid or boron oxide. An interesting effect of the hydration degree of the precursors was also observed. Indeed, boric acid $B(OH)_3$ yielded crystalline LaB_6 at 250 °C compared to 500 °C with B_2O_3. This temperature decrease was assigned to dehydration of boric acid at 159 °C. The evolving water catalyzes exothermic formation of MgI_2. As a result, crystallization occurs at a lower temperature set point with $B(OH)_3$ than with B_2O_3. Although the syntheses are performed at much lower temperature (250 °C) when I_2 is added, the reported procedure involving metal oxide precursors still yields bigger particles than those based on metal chloride precursors without iodine, presumably because metal oxides are poorly reactive M species. It is also important to note that low temperature reactions involving iodine occur only with low yields ranging between 20% and 50%.

3.3.2.3. Mechanistic Issues. The mechanism of the reaction between metal salts and alkali borohydrides was never experimentally assessed, even in the most recent reports. On the basis of the known decomposition pathway of single $NaBH_4$ at ca. 500 °C (eqs 9 and 10), all the studies on RAPET processes speculate a reaction scheme involving eqs 9, 10, 25, and 26 or similar ones with other metals, yielding net equations like eq 27. Many questions are nevertheless raised. Especially, how borohydride or intermediate borane react with metal chlorides is still an open question: Do they combine directly, do they lead first to metal borohydride intermediates, or do they decompose first into B(0) by reduction of the metal precursor, followed by "alloying" between M(0) and B(0)? Mechanistic studies, for example mass spectrometry analysis of the evolved gases,[314] could be of great interest in the case of metal boride synthesis and are clearly lacking here.

$$MgCl_2(s) + 2B(s) + H_2(g) \rightarrow MgB_2(s) + 2HCl(g) \quad (25)$$

dx.doi.org/10.1021/cr400020d | *Chem. Rev.* XXXX, XXX, XXX−XXX

$$NaH(s) + HCl(g) \rightarrow NaCl(s) + H_2(g) \quad (26)$$

$$MgCl_2(s) + 2NaBH_4(s) \rightarrow MgB_2(s) + 2NaCl(s) + 4H_2(g) \quad (27)$$

3.3.2.4. Comparison between CVD and RAPET. All in all, the use of solid state reactions under autogenous pressure is highly suitable to the synthesis of a wide range of metal borides, especially boron-rich compounds, namely diborides and hexaborides. The latter are most often obtained as cubes when they are produced as sub-micrometer-scale particles, in relation with their cubic structure and the surface energy of the different facets. On the contrary, hexaborides originating from CVD processes are usually produced as one-dimensional nanostructures. The difference in the morphologies obtained from both kinds of procedures can be explained by the role of the substrate in chemical vapor deposition. In this case, growth occurs on the surface which breaks the cubic symmetry, while the metal catalyst fastens and then exacerbates one-dimensional growth. Although not reported yet, combining CVD and RAPET approaches might provide an acute control on the morphology of metal hexaborides. However, two major drawbacks of solid state reactions, even under autogenous pressure, are the slow diffusion of reactants in the vessel and the unfavorable reaction kinetics. Because homogeneous mixtures of initial and/or intermediate species are difficult to reach, size and shape inhomogeneities are inevitably observed in the final samples. This is exemplified in most of the microscopy images describing the products (Figure 34). Also, because the reaction rates are slow in the solid state, extensive growth often occurs, leading to big particles mostly in the submicrometer range. It was however nicely demonstrated by Qian's group that the use of highly reactive boron sources, such as sodium borohydride, together with the assistance of strongly reactive additives can significantly improve the nucleation kinetics and lead to smaller particles in the nano-range (Figure 35). Again, a parallel can be drawn with CVD processes: judicious choices of the boron precursor in terms of reactivity ($NaBH_4$ versus B_2O_3 for RAPET, boranes versus BCl_3 for CVD) and of suitable catalysts or "activating species" (magnesium-assisted processes versus no additive for RAPET, metal-catalysis versus self-catalysis for CVD) are efficient ways to hasten reactions, decrease the temperature of synthesis, and decrease the particle size.

3.3.3. Mechanosynthesis. Mechanosynthesis of metal−boron alloys was developed from the 1990s to provide iron, niobium, copper−titanium borides,[408,409] Fe−B,[410] and Ni−B amorphous alloys. Mechanical activation of boride formation is often combined with a thermal post-treatment above 900 °C to yield crystalline metal borides.[80,81] This is especially the case when elemental metal and boron are used as precursors, e.g., in the Zr−B,[411] Cr−B,[80] or Mo−B systems.[412] In the latter case, broad XRD peaks of a sample obtained at 900 °C suggest nanosized crystallites of single-phase MoB_2, although no microscopy data were provided.[412] The strong advantages of mechanochemical synthesis, namely simplicity and energy saving, are put in the foreground when crystallization of MB systems is triggered without thermal activation. Indeed, submicrometer particles of diborides TiB_2,[413−416] NbB_2,[417,418] and MgB_2;[419] Ni_2B;[420,421] and VB_2[30,31] could be readily obtained after energetic ball-milling during few tens of hours.

When oxidized precursors are used, reductive assistance is provided by the addition of magnesium in excess of 10−40 mol % to overcome residual oxidation. For instance, submicroscaled HfB_2 was reported from $HfCl_4$, B, and Mg after heat treatment at 1100 °C.[422,423] Few examples of submicronic particles were reported without postannealing, including mixtures of Mo_xB_y from MoO_3, B_2O_3, and Mg;[424] ZrB_2 from ZrO_2, B_2O_3, and Mg;[425] and TiB_2 from TiO_2, B_2O_3, and Mg.[426−428] Nevertheless, postannealing is often used to ensure crystallization. In this case, the reaction is so violent into the finely ground mixture of oxidic precursors and magnesium that the process can be referred to as a self-propagating high-temperature synthesis (SHS). Self-heating occurs and adiabatic temperatures close to 1800−2000 °C are quickly reached after ignition of the medium. Because the reaction itself ensures heating, the set-point temperature (or ignition point) is not necessarily high: TiB_2, ZrB_2, and ReB_2 submicronic particles were obtained at 800 °C;[411,429] mixtures of Mo_xB_y species and Mo were produced at a set-point 500 °C;[424] and submicrometer size LaB_6 was obtained from $LaCl_3$, B, and Li.[430] It is noteworthy that when SHS reactions are involved, the particle size (e.g., for ZrB_2 from Zr and B[411]) can be decreased from the microscale to the 40−100 nm range, by adding a dilutant (e.g., NaCl) which limits the temperature increase.

Recently, Kim et al.[58] modified the nature of the boron source by using lithium borohydride to convert $TiCl_3$ and VCl_3 into, respectively, TiB_2 and VB_2, with the reductive assistance of LiH (eq 14). After a few hours and washing in water, the authors could recover polycrystalline nanoparticles of titanium and vanadium diborides, with diameters of 15−60 nm (Figure 36). As in CVD and RAPET procedures, the higher reactivity of $LiBH_4$ combined with LiH compared to other boron sources triggers reaction at lower temperature, larger amount of nuclei, and smaller particles. It is noteworthy that crystalline particles with a diameter ranging from a few tens to a few hundreds of

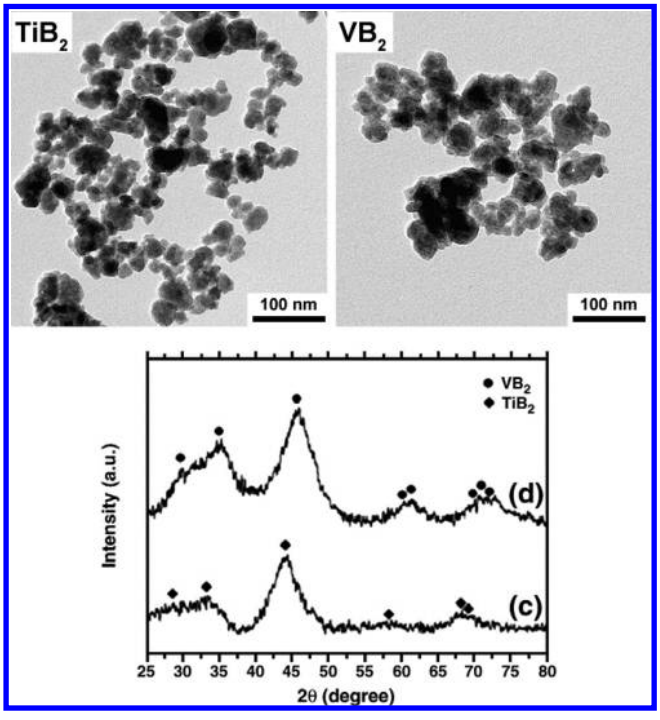

Figure 36. TEM micrographs and XRD patterns of TiB_2 and VB_2 powders prepared by mechanochemical processing on a planetary ball mill for 4 h from $TiCl_3/VCl_3$, $LiBH_4$, and LiH.[58] Reprinted with permission from ref 58. Copyright 2008 Elsevier.

dx.doi.org/10.1021/cr400020d | *Chem. Rev.* XXXX, XXX, XXX−XXX

nanometers can be obtained for metal-rich borides like CoB.[431] These materials crystallize at relatively low temperature (e.g., 600 °C) and are formed after a slight heat post-treatment. By using the same boron precursor, Lu et al. synthesized MgB_2 nanoflakes with 70 nm basal face through MgH_2 as metal source. Post-treatment at 450 °C and the use of a TiB_x catalyst was necessary to ensure crystallization.[432]

Mechanochemical syntheses rely on very simple procedures and are therefore very attractive processes. However, the present state of the art for metal borides does not show high control of the purity, the crystallinity, and the size of the particles. Especially, metal borides obtained from these routes are often contaminated by materials from the container, such as tungsten carbides, iron, or iron borides.[412,422,423] It was indeed suggested that these contaminants may play a decisive role in the nucleation of boride nanoparticles and the final morphology.[422,423] Investigating the route of the reactions is also relatively difficult since the leaching post-treatment modifies the particle morphology and compositions.[426,427] Further in-depth characterizations and engineering are highly sought in order to improve control of the process, especially purity, crystallinity, and size distribution of the final samples.

3.4. Preceramic Routes

Carbothermal reductions of metal oxides and boron oxide, as well as reduction of metal oxides by boron carbide B_4C, have been known for a long time for producing bulk metal borides.[38] In order to get smaller particles, usually in the submicrometer scale, these typical procedures were modified with the main objective of starting from mixtures that could ensure homogeneous nucleation of the metal boride particles. We classify these approaches as "preceramic routes" since they involve the preliminary formation of a metal−boron mixture at the solid state or as a gel, which is homogeneous at the nanoscale and involves at least one noncrystalline, polymeric phase. These procedures are related to the well-known Pechini process for the synthesis of submicro- to nanoscaled metal oxide particles.[433]

3.4.1. Carboreduction in Physical Mixtures of Metal Oxide, Boron Oxide or Boric Acid, and Carbon. Substitution of bulk metal oxide by metal oxide nanoparticles, and ball milling the oxide nanoparticles with boron oxide and carbon, lead to an homogeneous mixture which yields nanoscale metal boride nanoparticles (TiB_2[434]) with remaining carbon after carbothermal reduction at 1500 °C. A similar procedure for sub-micrometer-scale TiB_2 and NbB_2 was shown by using a mixture of metal oxide nanoparticles, boric acid, and cornstarch which is calcinated at 1500 °C.[435,436]

3.4.2. Carboreduction in Mixtures of Metal Oxides and B-Containing Polymers. The second type of preceramics is made of mixtures between metal oxides and B-containing polymers. This route was inspired by the works dealing with boron nitride and boron carbide synthesis from the calcination of boron-containing polymers.[437−441] The procedure for metal borides was developed in the 1990s for diborides of Ti, Zr, Hf, Nb, Ta, especially in the groups of Seyferth[442] and Sneddon.[443,444] Powders of metal oxides are mixed with the polymer in a suitable solvent (e.g., THF).[444] After evacuation of the solvent, the resulting solid is calcined under inert atmosphere at ca. 1400 °C. The polymer decomposes into boron-containing carbonaceous compounds, and then carboreduction of the oxides occurs together with alloying between boron and the metal, yielding metal boride submicronic particles. The polymer must meet some criteria in order to be suitable for this approach: (1) It should bear a suitable B/C ratio to ensure complete reduction of the oxides and transformation into the borides. (2) It should be stable at relatively low temperature and be soluble in a volatile solvent. (3) It should have a high yield of carbonization products to ensure complete carboreduction. (4) It should decompose at relatively low temperature to ensure coating and confinement of the metal oxide particles before they start to grow, which would lead to inhomogeneous mixtures and large particles. Decaborane-diamine,[442] decaborane-dicyanopentane,[443,444] and then polyhexenyldecaborane[445] polymers with increasing stability and char yield were developed. In a similar approach, boride/nitride TiB_2/TiN and HfB_2/HfN composites were obtained from a polyborazilene polymer mixed with the parent metals.[445] Interestingly, the rheological properties of the initial mixture can be tuned by adjusting the glass transition of the polymer or the polymer concentration or by adding some surfactants. The latter possibility was used to ensure homogeneous coating of graphite plates by a TiB_2 layer after calcination.[444]

3.4.3. Carboreduction in Metal and Boron Hybrid Oxo-Gels. The third type of preceramics is composed of hybrid organic−inorganic oxo-gels obtained from molecular sources of a metal and boron. Because of the significant volatility of $B(OH)_3/B_2O_3$ species at high temperature, a slight excess of ca. 10 mol % is required to ensure the formation of metal borides as the sole metal-containing phases. Metal diborides (TiB_2, ZrB_2, TaB_2)[446−450] are the most studied M−B alloys in the framework of this preceramic route. The synthesis is based on a two-step process. First, an amorphous gel is formed from metal alkoxides [i.e., $Ti(O^iPr)_4$, $Zr(OPr)_4$][448−450] or oxychlorides (i.e., $ZrOCl_2$)[447] and a boron alkoxide [$B(OEt)_3$, trimethoxyboroxine][446] or hydroxide $B(OH)_3$.[447−450] The gel is usually obtained by reacting these precursors in a suitable solvent (acetic acid, butanol) in which inorganic polymerization is controlled, often through the addition of complexing agents such as acetates[448−450] or a polyol (glycerol/furfuryl alcohol).[446] These complexants cross-link the metal-oxo species through transesterification of the alkoxides.[446] These organic cross-linkers polymerize together and decompose into carbon when heated at 800 °C. Other ligands like acetylacetonates can be used to control the cross-linking.[448,449] Other carbon sources were experienced, such as sucrose[449,450] or a phenolic resin.[447,448] In a second step, the precursor mixture is heated above 1000 °C. Then, it goes through the crystallization of metal oxide nanoparticles embedded into a carbon matrix. Boron oxide is also probably formed, although it was not observed by XRD. Finally, carbothermal reduction of the metal oxide and the B species occurs together with alloying between the metal and boron, leading to metal borides (Figure 37). The interest in using molecular precursors of carbon, boron, and/or metal is the improved homogeneity of the initial M, B, and C mixture. The intermediate state is then made of particles uniformly distributed into the carbon phase. A large interface between carbon and oxides ensures high reactivity, as exemplified by the onset of carboreduction and formation of TiB_2 occurring at 1000 °C instead of 1250 °C for a physical carbon−titania mixture.[446] Also, the carbon phase acts as a template for restricting nanoparticle growth at high temperature. Indeed, during the synthesis of ZrB_2,[447] complete consumption of carbon above 1500 °C is correlated to a strong decrease of the

dx.doi.org/10.1021/cr400020d | Chem. Rev. XXXX, XXX, XXX−XXX

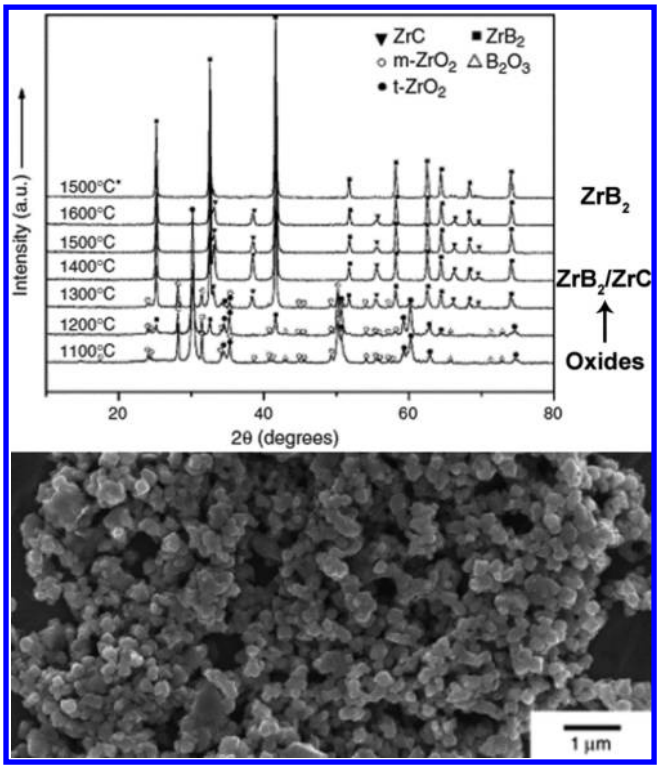

Figure 37. XRD patterns highlighting the course of ZrB_2 formation from calcination of a preceramic powder made of $ZrOCl_2$ and $B(OH)_3$ (Zr:B = 1:2) mixed with phenolic resin. The pattern for "1500 °C*" represents the result from a mixture containing 10 wt % of $B(OH)_3$ in excess. SEM picture of corresponding powder made of pure ZrB_2. Reprinted with permission from ref 447. Copyright 2006 John Wiley and Sons, Inc.

BET specific surface area from 200 to 32 m^2 g^{-1}. We have recently developed a similar procedure for the synthesis of nanostructured Magnéli's substoichiometric titanium oxides.[451] It is noteworthy that the process for metal borides cannot afford highly efficient templating and leads to submicronic particles. The structure of the polymeric precursor might also impact the final morphology of the metal boride particles, as suggested by Zhang et al.[450] who showed that when the initial gel was curred at increasing temperatures, the final morphology of ZrB_2 particles was modified and one-dimensional preferential growth was emphasized (Figure 38).

Nath et al. claimed the sol–gel synthesis of magnesium diboride nanowires.[301] The authors used a mixture of $MgBr_2$, $NaBH_4$, and hexadecyltrimethylammonium bromide (CTAB) as a surfactant in ethanol. After evaporation of the solvent, a gel was obtained and subsequently calcined under diborane flux at 800 °C. This procedure was already described above in subsection 3.2.5. The vapor pressure of magnesium is relatively high in the synthesis conditions, while the gel made of organics is certainly decomposed into a carbonaceous matter containing NaBr as one of the byproducts. As a consequence, MgB_2 nanostructures grow likely through an HPCVD vapor–vapor reaction on the surface of the matrix originating from the gel. The SEM pictures confirm this hypothesis by clearly showing long nanowires grown on a denser substrate. Therefore, formation of MgB_2 is not likely to occur through condensation of molecular species in a condensed phase and is not directly related to the sol–gel process. Interestingly, Hall et al. proposed recently an alternative route toward carbon-doped

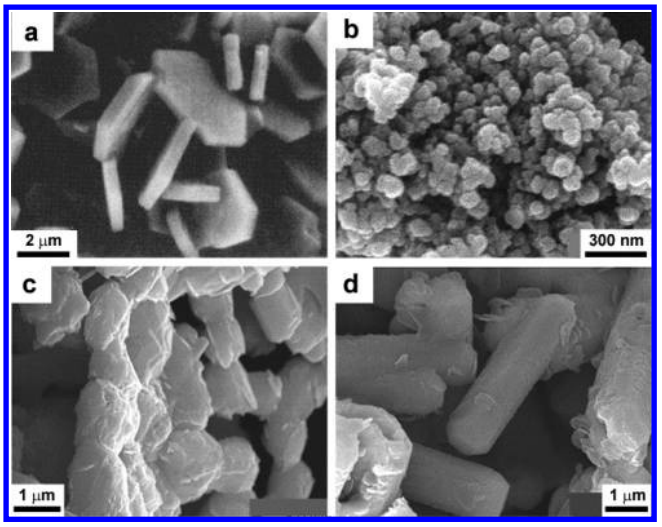

Figure 38. SEM showing submicronic particles of diborides obtained from hybrid metal-oxo gels: (a) TiB_2 from a mixture of titanium isopropoxide, boron triethoxide, furfuryl alcohol, and glycerol heated at 1000 °C.[446] Reprinted with permission from ref 446. Copyright 1992 Royal Society of Chemistry. ZrB_2 from a mixture of zirconium isopropoxide, boric acid (Zr:B = 1 2.3), acetic acid, and sucrose dried at (b) 65 °C, (c) 75 °C, (d) 85 °C and calcined at 1500 °C for 2 h. Reprinted with permission from ref 450. Copyright 2011 Elsevier.

MgB_2, by triggering the reaction between elemental boron and magnesium into a carbon matrix derived from the thermal decomposition of dextran. MgB_2 nanoparticles could be obtained through the confinement effect of the carbon template.[452]

3.5. Liquid Phase Syntheses in High Temperature (>1000 °C) Flux

Molten metal baths have been used mostly for the growth of macroscale single crystals of metal borides.[87] A noticeable exception has been reported by Guo et al. who proposed a short flow process to precipitate 20 nm TiB_2 nanoparticles into molten copper. The procedure lies in the rapid mixing of Cu–Ti and Cu–B melts at 1300 °C followed by quenching. Titanium and boron spontaneously yield TiB_2 nanoprecipitates in bulk copper. By modifying the composition of the initial mixtures, the metal boride content of the resulting Cu–TiB_2 composite was adjusted to 0.45 or 1.6 wt %.[296]

3.6. Liquid Phase Syntheses under Autogenous Pressure

Most liquid phase syntheses of metal borides rely on temperatures ranging from 400 to 650 °C. In these conditions, many solvents and reactants have a high vapor pressure and require closed vessels in order to trigger the reaction and to get a sufficient yield. These protocols are described herein, whether liquid solvents (salt melts or organic compounds) or liquid species acting both as solvents and reactants are used.

3.6.1. Salt Melts under Autogenous Pressure. Following early reports on bulk metal boride fabrication by high temperature electrosynthesis in molten salts, these electrolytes were recently used as flux for the synthesis of nanoscale borides under autogenous pressure. Metal chlorides are readily available, easy to use, and economical solvents. Ma et al.[53] developed the synthesis of CrB nanorods (Figure 39) from $CrCl_3$ and elemental boron in stoichiometric amounts, with the addition of sodium as reductant (Cr:B:Na = 1:1:3). The solvent was aluminum chloride (melting point 192 °C), and the reaction was performed at 650 °C. Later on, the same group

dx.doi.org/10.1021/cr400020d | Chem. Rev. XXXX, XXX, XXX–XXX

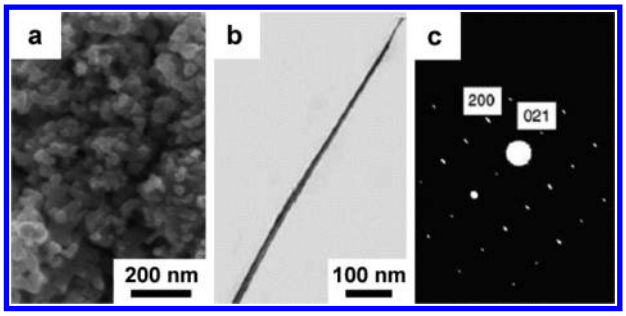

Figure 39. Pictures of nanoscale metal borides obtained at 650 °C under autogenous pressure in molten chlorides. (a) SEM picture of NbB_2 nanoparticles obtained from Nb_2O_5, B_2O_3, and Mg in a 50:50 wt % NaCl:$MgCl_2$ mixture.[54] Reprinted with permission from ref 54. Copyright 2009 Elsevier. (b) TEM picture. (c) Corresponding SAED pattern of a CrB nanorod obtained from $CrCl_3$, B, and Na in $AlCl_3$.[53] Reprinted with permission from ref 53. Copyright 2003 Elsevier.

reported the fabrication of NbB_2 nanoparticles at 650 °C (Figure 39).[54] The flux was a NaCl/$MgCl_2$ mixture of 50:50 weight ratio, melting at ca. 475 °C. In this case, metal and boron oxides were used as precursors with additional magnesium as reductant (Nb:B:Mg = 1:2:9). According to TEM data, the NbB_2 particles exhibited diameters of ca. 30 nm, but the BET specific surface area did not exceed 16 $m^2\ g^{-1}$, suggesting strong aggregation of the nanoparticles.

3.6.2. Organic Solvents under Autogenous Pressure. Besides ionic flux, organic species were also used as liquid media for boride synthesis. Gu and co-workers[55] obtained TiB_2 nanoparticles from $TiCl_4$ and elemental boron in stoichiometric amounts. An excess of sodium (Ti:B:Na = 1:2:4.3) was added to ensure reduction of the metal precursor. The reaction was performed at 400 °C in benzene, and TEM images suggest diameters ranging from 15 to more than 100 nm. Soon after this report, a similar process yielded Ni_2B nanoparticles from anhydrous $NiCl_2$ and $NaBH_4$ in benzene at 420 °C.[56] The stability under pressure of the organic solvent at such temperatures is nevertheless questioned by Gu et al. who suspect partial carbonization of benzene and incorporation of carbon into the final compound.[55]

3.6.3. Liquid Reactants under Autogenous Pressure. Other works rely on liquid precursors and might be considered to belong to reactions in the liquid state or in heterogeneous liquid/solid media. Apart from the physical state of the reactants, experimental procedures are similar to those used for typical RAPET syntheses. That is the case of the TiB_2 synthesis from elemental titanium, gaseous BBr_3, and liquid sodium (Ti:B:Na = 1:2:6) at 400 °C.[325] Liquid $TiCl_4$ and solid $NaBH_4$ (Ti:B = 1:4.8[453] or Ti:B = 1:6.5[454]) were also combined in an autoclave and converted into TiB_2 above 500 °C (Figure 40), but in these conditions $TiCl_4$ is presumably in the vapor state. The same procedure was used for the synthesis at ca. 600 °C of diborides HfB_2,[455] ZrB_2,[456] and NbB_2[457] from the respective chlorides $HfCl_4$, $ZrCl_4$, and $NbCl_5$. Nanoparticles with a diameter of about 20−25 nm were obtained with hafnium and zirconium. The NbB_2 sample was reported as a polydisperse mixture of particles and rods with diameters of, respectively, 10 and 100 nm. Crystalline materials were only obtained with an excess of borohydride (MCl_x:$NaBH_4$ = 1:6−1:8).[455,456] An increase in the $NaBH_4$ concentration produced larger crystallite sizes. This could be ascribed to the increased H_2 (together with B_2H_6 or BH_3) pressure as the amount of borohydride was raised (eq 28, 29 and 30), therefore providing

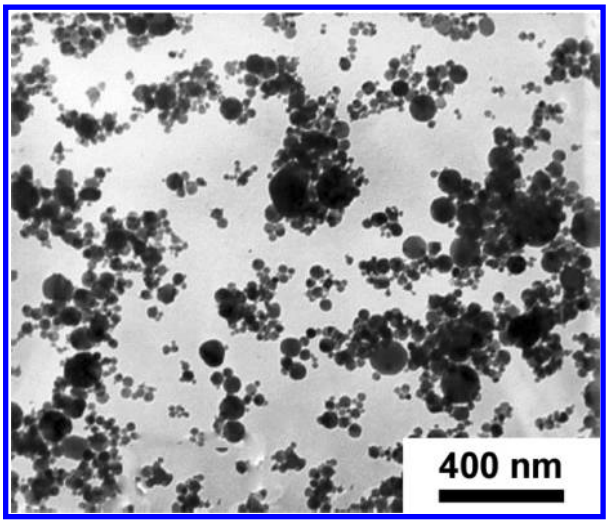

Figure 40. TEM picture of TiB_2 nanoparticles obtained from a mixture $TiCl_4$:$NaBH_4$ = 1:6.5 at 700 °C under autogenous pressure.[454] Reprinted with permission from ref 454. Copyright 2010 Springer.

more reductive condictions. Shi et al.[316] could obtain crystalline VB_2 nanoparticles through a very close procedure from stoichiometric amounts of VCl_4 (liquid at room temperature, boiling point of 154 °C under 1 atm.), $NaBH_4$, and Mg as an additional reductant (VCl_4:$NaBH_4$:Mg = 1:2:1, eq 31) to overcome the low H_2 pressure.

$$ZrCl_4(l) + 2NaBH_4(s) \rightarrow ZrB_2(s) + 2NaCl(s) + 2HCl(g) + 3H_2(g) \quad (28)$$

$$ZrCl_4(l) + 4NaBH_4(s) \rightarrow ZrB_2(s) + 4NaCl(s) + 2BH_3(g) + 5H_2(g) \quad (29)$$

$$ZrCl_4(l) + 8NaBH_4(s) \rightarrow ZrB_2(s) + 4NaCl(s) + 4NaH(s) + 6BH_3(g) + 5H_2(g) \quad (30)$$

$$VCl_4(l) + 2NaBH_4(s) + Mg(s) \rightarrow VB_2(s) + 2NaCl(s) + MgCl_2(s) + 4H_2(g) \quad (31)$$

All in all, although liquid phase processes with organic species under pressure are simple procedures, they are always involving at least partial decomposition of the liquid component. This can be considered as an advantage when the liquid is also the reactant, but this always brings the question of the purity of the final compound. Despite these potential side reactions, the elemental composition of the products is only rarely assessed with care. This will inevitably put under question the resulting properties of the material obtained via these routes, unless in-depth characterization is performed.

3.7. Low Temperature and Atmospheric Pressure Colloidal Syntheses of Crystalline Metal Boride Nanostructures

Up to now, very few studies have been reported to yield nanoscaled crystalline metal borides from liquid phases without the use of sealed vessels. This point is nevertheless of utmost importance if the protocol is to be scaled up. Hereafter are described the only two approaches that, in our opinion, have

dx.doi.org/10.1021/cr400020d | Chem. Rev. XXXX, XXX, XXX−XXX

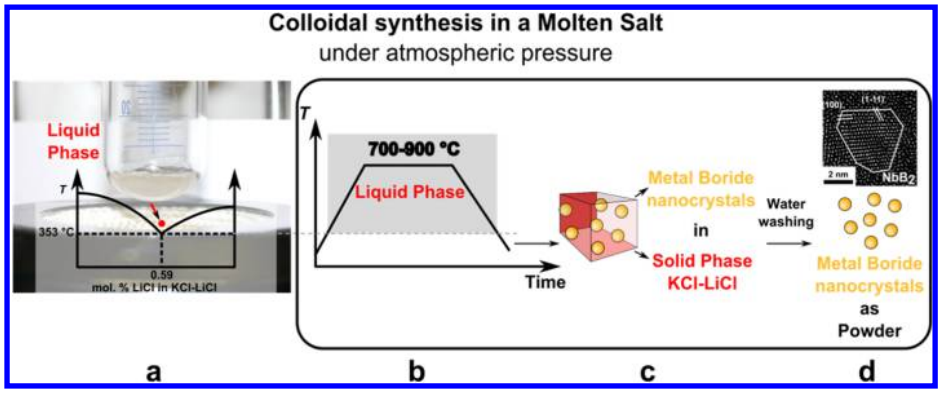

Figure 41. Principle of the colloidal synthesis of metal boride nanocrystals in molten salts. (a) Binary phase diagram of the LiCl−KCl system, and picture of the liquid solvent at the eutectic composition above the melting point. (b) Temperature profile. The reaction between M and B precursors occurs in the liquid phase domain of the ionic solvent. (c) After cooling down, the solvent is frozen and encapsulates the nanocrystals. (d) The inorganic salt is then washed with water, and the resulting powder is dried. The HRTEM picture (from ref 51) of a typical product such as niobium diboride highlights the small size of nanocrystals of approximately 5 nm in diameter. Reprinted with permission from ref 51. Copyright 2011 John Wiley and Sons, Inc.

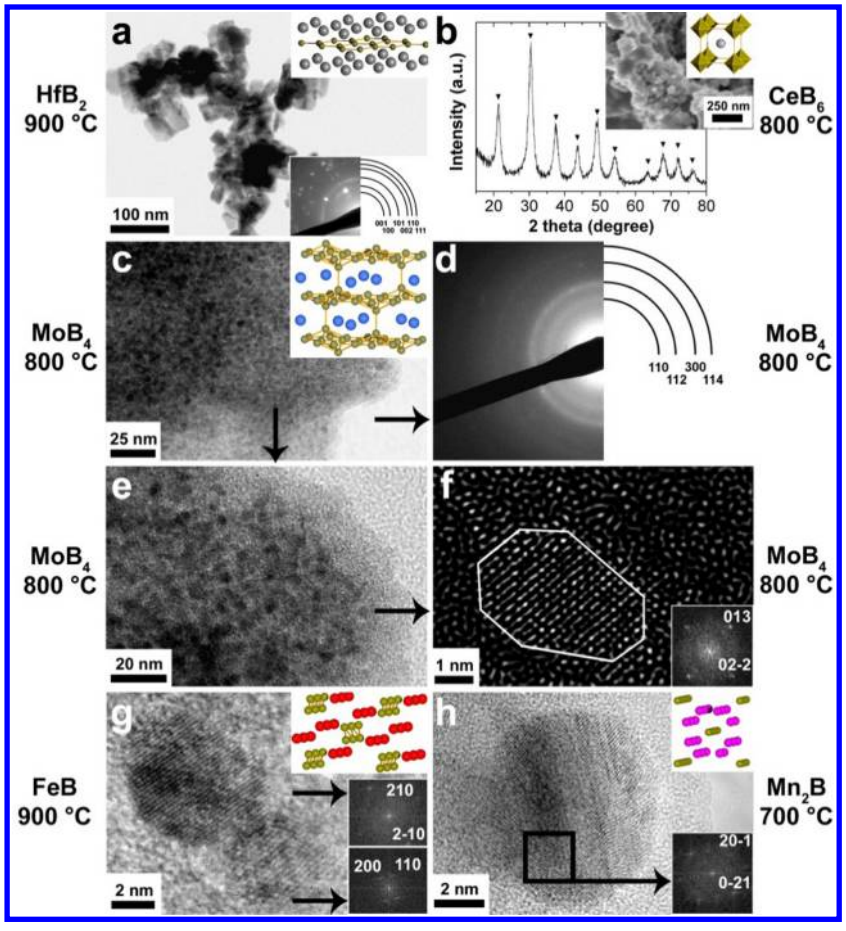

Figure 42. (a) TEM picture and corresponding SAED pattern of HfB_2 nanocrystals. (b) XRD pattern and SEM image of CeB_6 nanoparticles. (c, e) TEM pictures, (d) corresponding SAED pattern, and (f) Fourier filtered HRTEM image of MoB_4 nanoparticles. HRTEM picture and corresponding Fourier transforms of (g) FeB nanoparticles and (h) a Mn_2B nanoparticle. Reprinted with permission from ref 51. Copyright 2011 John Wiley and Sons, Inc.

been demonstrated as efficient ways to obtain nanocrystals of metal borides. The first route relies on salt melts as solvents for the production of nanoparticles in the range 5−10 nm. The second one targets particles in the 100 nm range by using an organic solvent.

3.7.1. Salt Melts under Atmospheric Pressure. Through a recent collaboration, our group developed a new synthetic process toward metal boride nanocrystals.[51] The principle of the method (Figure 41) lies in the colloidal synthesis in inorganic molten salts as room pressure solvent. For instance, the eutectic mixture KCl−LiCl was used. Contrary to low

dx.doi.org/10.1021/cr400020d | Chem. Rev. XXXX, XXX, XXX−XXX

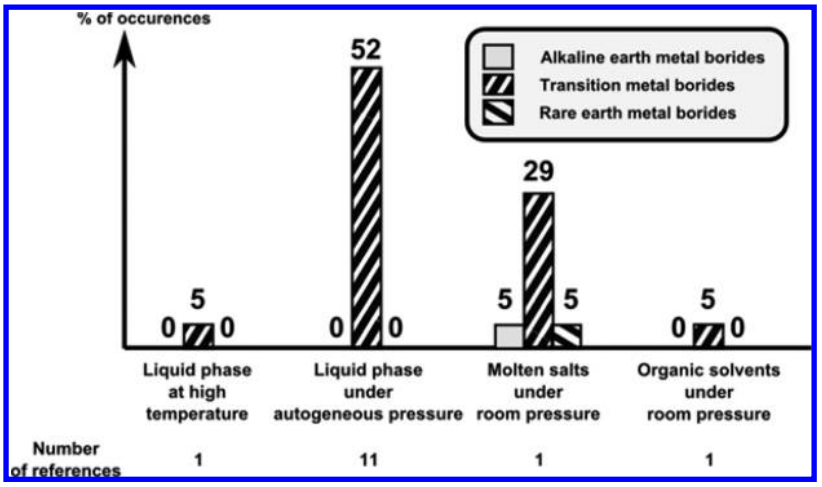

Figure 43. Percentage of reported occurences of crystalline nanoscaled compounds from the main families of metal borides by precipitation at atmospheric pressure in an organic solvent and in molten salts. From the data in refs 51 and 52.

melting point solvents which are often volatile (e.g., $AlCl_3$) above 300 °C, the melt used in the process does not exhibit any significant vapor pressure up to 900 °C and does not require any costly pressurized reactor (autoclaves for use up to 650 °C). The precursors (metal chlorides and sodium borohydride) are grounded with the solvent powder. Upon heating of the reaction medium, the solvent melts at ca. 355 °C (Figure 41), and the precursors react together in the liquid phase. After cooling, a block of salt is recovered, and the solvent and side products of the reaction are washed by water, yielding pulverulent powders after drying, with a yield higher than 90% versus the metal precursor. Nanoparticles with a diameter ranging between 5 and 10 nm are usually obtained. This represents a decrease of at least 1 order of magnitude compared to nanostructured metal borides reported by most other methods. This approach has proven suitable for various metal boride nanocrystals (Figures 42 and 43), most of them being reported at the nanoscale (<100 nm) for the first time.

The crystallization temperature depends on the metal and the stoichiometry of the resulting metal boride. Nanocrystals of boron-rich borides (e.g., NbB_2, CaB_6) are obtained at higher temperature (usually 800−900 °C) than metal-rich borides (e.g., Mn_2B) (600−700 °C). This trend corroborates the difficult ordering of complex boron frameworks because of the high density of strong and directional B−B bonds.

The molten salt process also enables tuning of the nanocrystals' size.[51] Crystalline NbB_2 is obtained from $NbCl_5$ at 800 °C with an initial metal to boron ratio M:B ranging between 1:4 and 1:8 (Figure 44). By increasing the proportion of boron precursor, the nanoparticle size decreases from 10 nm (Nb:B = 1:4) to 5 nm (Nb:B = 1:8), even if the temperature is unchanged. Accordingly, the total surface area of the final material increases from, respectively, 25 to 120 $m^2\ g^{-1}$. The impact of the reactant concentration on the particle size distribution was interpreted in terms of nucleation−growth competition. In this synthesis, the nucleation of the crystalline material is the rate limiting step. An increase in the boron precursor concentration leads to an increased nucleation rate, the production of more particles for the same amount of metal atoms, and then smaller nanoparticles.

When an excess of borohydride is used, an amorphous shell is observed that coats the nanoparticle surface (black arrow in Figure 44a). This shell was identified by solid state ^{11}B NMR

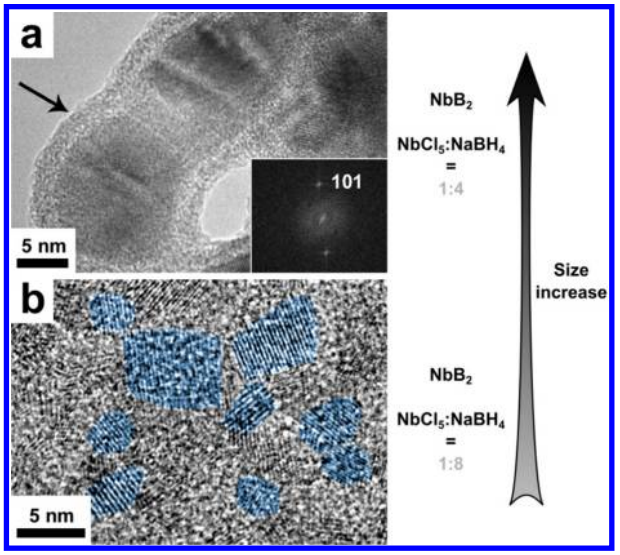

Figure 44. TEM pictures of niobium diboride nanocrystals obtained at 900 °C with $NbCl_5/NaBH_4$ = (a) 1:4 and (b) 1:8. A corresponding Fourier transform is shown in inset of part a. Some nanoparticles are highlighted in part b. The black arrow in part a highlights an amorphous shell embedding the particles. Reprinted with permission from ref 51. Copyright 2011 John Wiley and Sons, Inc.

and elemental analysis as being mainly amorphous boron which is partially oxidized, presumably during water and air exposure after the synthesis. Interestingly, this amorphous boron phase could also have an impact on the size distribution by a templating effect: the higher the amount of boron precursor, the higher the amorphous phase content and the more effective the crystal growth restriction.

It is noteworthy that Nath et al.[301] (see subsections 3.2.5 and 3.4.3) described their sol−gel mediated synthesis of MgB_2 nanowires as occurring from the reaction of $NaBH_4$ with molten $MgBr_2$ (melting point ca. 650 °C) in stoichiometric amounts at 800 °C. Nevertheless, strongly reductive borohydride anions obviously had already reacted with the Mg salt at lower temperature (see subsection 3.3.2 above).[385] Consequently, the occurrence of a salt melt in this specific case is likely to be discarded.

The molten salt process has been demonstrated as an efficient way to obtain various metal boride nanocrystals, with

dx.doi.org/10.1021/cr400020d | Chem. Rev. XXXX, XXX, XXX−XXX

further control on the particle size in the approximate range 5−20 nm. These materials seem air-stable. Therefore, the method is likely suitable for various applications. The salt used in this case might be changed in order to tune the reactivity of the material, although precise mechanistic studies are required to provide a better insight into the reaction pathway. Indeed, our group showed that inorganic molten salt solvents are particularly adapted to the synthesis of very small boron based nanoparticles, not only metal borides,[51] but also boron carbon nitrides.[458]

3.7.2. Organic Solvents under Atmospheric Pressure. As specified above, the use of organic solvents is always restricted by their thermal stability range, often below 400 °C. Such temperatures usually do not provide sufficient energy for crystallization of metal borides. However, a noticeable exception was reported recently by Z. Schaefer and his collaborators.[52] The authors succeeded in synthesizing aggregated Ni_3B particles with a diameter of 50−90 nm. The process relied on tetraethyleneglycol as a high boiling point (280 °C) solvent and on the use of large excess of reductant/boron source (19 equiv of KBH_4 versus $NiCl_2{\cdot}6H_2O$). Aggregates of amorphous nanoparticles formed first at 100 °C, and then evolved into crystalline Ni_3B upon further heating up to 280 °C. Crystallization is accompanied by the smoothing of particle surfaces due to Oswald ripening. According to XPS and magnetic measurements data, the authors suggested that carbon doping occurred and that the samples were contaminated by a slight amount of elemental nickel as a side-product.

3.8. Low Temperature Colloidal Syntheses of Amorphous Metal Borides

The topic of amorphous metal borides and their synthesis is so vast that providing a comprehensive study in this review would be illusory. The readers interested in this wide ranging subject are redirected to dedicated reports.[25,35−37] Instead, the aim of this section is to provide some milestones for understanding the complexity of these systems. To do so, we emphasize some key-studies which help to shed light on these behaviors. Nanoparticles of amorphous metal−boron alloys are most often obtained in solution by reduction of metal salts by borohydride. Apart from some exceptions, the compositions are always in the metal-rich side of the phase diagrams.

3.8.1. Synthesis of Amorphous Metal Boride Nanoparticles in Water. The first works on solution-processed metal borides are probably to be ascribed to studies on reactions between metal salts and borohydrides in aqueous media. Those were first performed during the 1950s on amorphous Ni−B[312] and Co−B systems.[90] Although the size and the morphology of the particles could not be investigated at that time, it is most likely that the products were nanoscaled. Indeed, the intensive work conducted during the 1980s and 1990s on amorphous M−B nanoparticles relies on very similar procedures. Freitag et al.[459] followed by Dragieva et al.[460] showed by TEM that the as-obtained powders were made of spheres of 50−100 nm diameter.[461] These studies were completed by nitrogen sorption experiments.[460] High specific surface areas ranging from 50 to 230 $m^2\ g^{-1}$[460,462] were measured, in agreement with the nanoscale of the particles.

3.8.1.1. Nanoscaled Binary Amorphous Borides. Fe−B,[294,461,463−470] Ni−B,[244,462,465,467,471−473] and Co−B[90−92,465,471,474−477] binary compounds were obtained through reduction of metal chlorides, sulfates, nitrates, or acetates[478,479] by alkali borohydrides, especially by Dragieva et al.,[478,480] Linderoth, Mørup et al.,[294,464,481,482] Yiping et al.,[293,466] and Saida et al.[465] Other amorphous metal borides obtained through metal salt reduction by borohydride, wrongly described as pure metals, were also reported, like Ru−B for instance.[483] For Co−B alloys, the B content reaches values ranging from 25 to 40 atom %,[90−92,465,471] a composition close to Co_2B.[90−92,471] Glavee and co-workers investigated the course of the reaction between cobalt(II) chloride and sodium borohydride in water.[91,92] They proposed eq 32, in agreement with the quantities of evolved hydrogen under anaerobic conditions:

$$2CoCl_2(aq) + 4NaBH_4(aq) + 9H_2O(l) \rightarrow Co_2B(s) + 4NaCl(aq) + 12.5H_2(g) + 3B(OH)_3(aq) \quad (32)$$

As pointed out by Brown et al.[484,485] and Glavee et al.,[91,92] the process is quite complex because of two reasons. First, the mechanism of incorporation of boron into the alloy is unknown. Incorporation of boron arises probably after metal production (eq 33). Metal-catalyzed decomposition of borohydride into alloyed boron then occurs according to eqs 34 and 35. Second, the particles obtained in the course of the reaction act as catalyst for further hydrolysis of borohydride ions into borate (eq 36) or boric acid (eq 37) in an ineffective process toward MB alloys. The strong dependence on pH of these reactions makes the optimization and understanding of the metal boride precipitation difficult. For instance, borohydride hydrolysis modes (eqs 34, 36, 37) are favored and hastened in acidic conditions, contrary to the first step of production of metal particles (eq 33).

$$BH_4^-(aq) + 3H_2O(l) + 2Co^{2+}(aq) \rightarrow 2Co(s) + 3H^+(aq) + 2H_2(g) + B(OH)_3(aq) \quad (33)$$

$$BH_4^-(aq) + H^+(aq) \rightarrow 2.5H_2(g) + B(s) \quad (34)$$

$$2Co(s) + B(s) \rightarrow Co_2B(s) \quad (35)$$

$$BH_4^-(aq) + 2H_2O(l) \rightarrow 4H_2(g) + BO_2^-(aq) \quad (36)$$

$$BO_2^-(aq) + H_2O(l) + H^+(aq) \rightarrow B(OH)_3(aq) \quad (37)$$

When a temporary excess of borohydride is exposed to in situ produced amorphous Co_2B nanoparticles under slightly acidic conditions, for example during slow addition of cobalt chloride to a borohydride solution, then eqs 36 and 37 take place and the borate $Co(BO_2)_2$ is obtained.[91,92] Glavee also nicely pointed out the importance of working under strictly anaerobic conditions to retrieve meaningful data, especially about the alloying mechanism and the composition of amorphous MB nanoparticles. Indeed, these materials are highly sensitive to oxidation and often ignite spontaneously upon air exposure after they were synthesized in oxygen-free atmosphere. The resulting products are boron oxide and the native metal. According to Glavee et al. the most suitable conditions to obtain the highest boron content corresponding to the Co_2B composition rely on fast addition of the metal salt solution to sodium borohydride, under anaerobic conditions, followed by anaerobic handling of the resulting powders. A similar behavior was observed for nickel, yielding an amorphous compound of approximate Ni_2B composition.[96,465]

dx.doi.org/10.1021/cr400020d | Chem. Rev. XXXX, XXX, XXX−XXX

Many studies have enlightened the dependence of the final composition on the reaction temperature,[465,469] the pH, and the borohydride concentration or ratio versus the metal source.[293,294,465,469,478] These dependencies are metal-related and highly complex. For instance, the B content in Co−B amorphous alloys increases with the BH_4^- concentration,[90−92,465,471] while the opposite trend is observed with Fe−B amorphous alloys.[481] The difficulty in providing full understanding of these effects is related to the interconnection between various critical experimental parameters. For example, eqs 36 and 37 demonstrate that modifying the borohydride concentration also deeply impacts the pH of the reaction medium and therefore the kinetics of the whole process. Actually, pH can dramatically change during the addition of a borohydride aqueous solution to a metal salt solution, as clearly seen for Fe−B alloys.[35,461,467,468] Linderoth and Mørup et al.[294,464,482] identified pH as one of the key parameters for controlling the process. They adapted the typical mixing procedure by adjusting the pH during the whole addition of the borohydride solution (Figure 45). The amorphous Fe−B phase

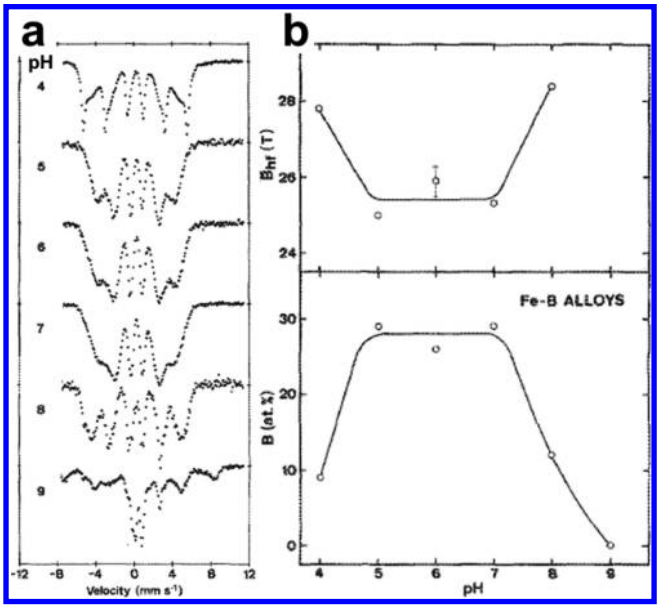

Figure 45. Structural and composition features of amorphous Fe−B samples prepared with constant pH during precipitation. (a) Mössbauer spectra at 80 K. (b) Magnetic hyperfine field for the amorphous phases in the spectra and overall boron content of the particles as a function of pH. Reprinted with permission from ref 464. Copyright 1990 American Institute of Physics.

is then obtained between pH 5 and 7 with a boron content of 28 atom %. When decreasing the pH value below 5, Mössbauer spectroscopy highlights increasing content of side product α-Fe as a side product. Thus, borohydride is mostly consumed according to eqs 33 (production of metal nanoparticles), 36, and 37 (hydrolysis of $NaBH_4$) in acidic conditions. Above pH 7−8, iron hydroxide precipitates. A similar behavior is observed for Ni−B alloys.[462] On the other side, the pH and the resulting composition of the alloy are less modified when the metal salt is added to the solution of borohydride, because the latter acts as buffer as long as it is in excess. This might be one of the reasons why this procedure provides the most reproducible synthesis of MB alloys as claimed by Glavee et al.[91,92]

3.8.1.2. Nanoscaled Ternary and Quaternary Amorphous Borides. Addition of one or more metals provides a convenient way to tune magnetic, electronic, and catalytic properties of amorphous metal−boron alloys. For instance, Dragieva and coworkers demonstrated that modifying the ratio between iron and cobalt in Fe−Co−B systems is an efficient method to adjust the hysteresis loop of magnetization.[478] More recently, Acosta showed the ability to tune the catalytic activity of Ni−M−B alloys toward hydrogenation by modifying the content and nature of the second metal.[486] Oppegard et al.[487] followed by Dragieva et al.,[478] Linderoth, Mørup et al.,[482] and Yiping et al.[488,489] showed that ternary Fe−Co−B alloys with B content of ca. 20−25 atom % could be effectively obtained by borohydride reduction of multimetallic aqueous solutions. Adjusting the initial ratio between iron and cobalt in solution enables tuning of the Fe:Co:B ratios in the solid between ca. 60:10:30 and 10:60:30,[481,490] while pH variation is the key parameter to modify the boron content.[482] Incorporation of cobalt or nickel results in a decrease of the particle size. This should be ascribed to the higher standard redox potentials of Co^{2+}/Co and Ni^{2+}/Ni compared to the Fe^{2+}/Fe couple. Ni(II) and Co(II) react easier and faster with borohydride and induce a quick nucleation step and smaller particles.[292,294] Numerous studies reported other Fe−M−B (M = Cr, Mn, Ni),[490−498] Fe−Zr−B,[230,497] Fe−Nd−B,[499] Fe−W−B, Co−Zr−B,[500] Co−Cu−B,[501] Co−Mo−B,[502] Ni−Cr−B,[503,504] Ni−Co−B,[192] Ni−Mo−B,[505] Ni−W−B, Ni−Ru−B, and Ni−La−B.[506,507] Some quaternary amorphous alloys, such as Ni−Co−W−B[508] and Co−Ni−Mo−B,[509] were also investigated in order to promote the catalytic activity of these nanomaterials for hydrogenation reactions.

3.8.1.3. Ternary Boron Phosphides. Tuning of the catalytic magnetic properties of amorphous alloys can also be achieved by incorporating both boron and phosphorus.[510−512] These ternary compositions were investigated with iron[494,513−515] and nickel[510−512,516−518] through aqueous precipitation from metal salts, sodium hypochlorite, and potassium or sodium borohydride. XPS and Mössbauer spectroscopy in the case of iron demonstrate that boron and phosphorus are mainly in their elemental states, albeit with slight oxidation of boron due to air exposure.[514,516] The compositions are usually lying in the metal-rich part of the ternary phase diagram. It is noteworthy that, as observed for binary compositions, the B and P contents can be controlled by adjusting the pH of the aqueous solution. Thermal analysis suggests stronger binding of Fe with P than with B, but to our knowledge, no further structural characterization was performed.[515]

3.8.2. Synthesis of Amorphous Metal Boride Nanoparticles in Organic Solvents. Use of organic solvents at atmospheric pressure most often leads to amorphous metal borides because the temperature range that can be reached in such conditions is not sufficient to trigger crystallization. Synthesis of nanoscaled amorphous metal boride alloys relies on the same procedures as those developed for aqueous synthesis, namely reduction of metal salts by borohydride. Actually, aqueous and organic procedures have been continuously developed in parallel since the 1950s, when Fe−B[519] and Co−B[520] alloys were obtained in diethyl ether, followed soon by Ni−B[472,521] and Co−Ni−B[522] systems in ethanol.

The nature of the solvent has a direct impact on the reactivity of borohydride and the resulting composition of amorphous alloys. Most studies focus on aprotic solvents. Syntheses by Molvinger et al.[523−525] in tetrahydrofuran at room temperature

dx.doi.org/10.1021/cr400020d | Chem. Rev. XXXX, XXX, XXX−XXX

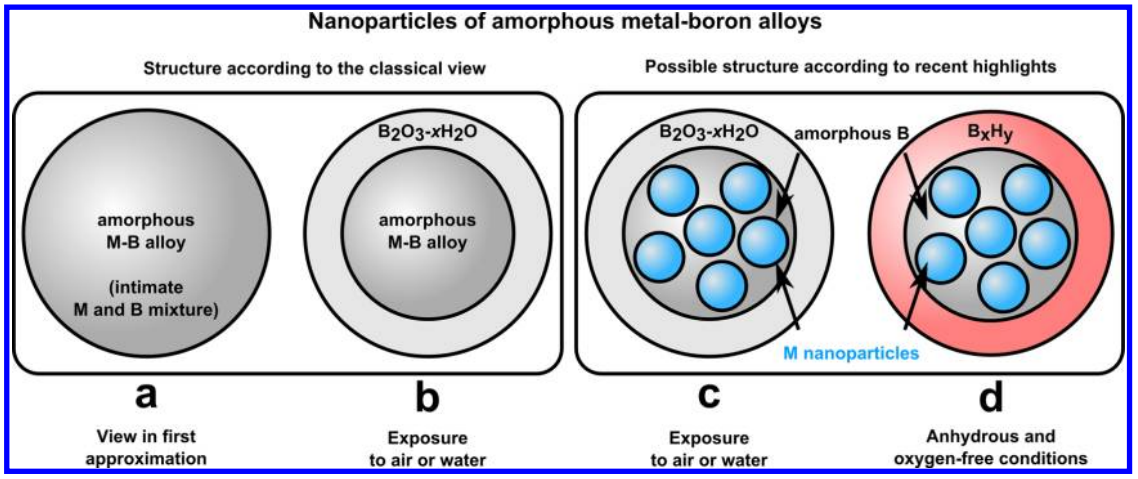

Figure 46. Schematic representations of the possible internal structure in amorphous metal boride alloys obtained by precipitation through reduction of metal salts in solution.

or under reflux lead to CoB_2, NiB_2, $FeB_{1.8}$.[523−525] The exact composition of these boron-rich compounds is nevertheless unclear, especially the hydride content, which is discussed later in subsection 3.8.3. They are most probably hydride or borohydride adducts. Surprisingly, Glavee and co-workers obtained very different compositions in diglyme: elemental Co[93] and metal-rich $Ni_{2.45}B$[96] were obtained. Fe_2B and FeB were synthesized from, respectively, $FeBr_2$ and $FeBr_3$.[94] For Ni(II), Fe(II), and Cu(II), the reaction occurs in aprotic and coordinating solvents through a two-step process.[96] First, a complex is formed by coordination of the metal ion by BH_4^- and the solvent (eq 38). Second, the metal borohydride complex decomposes through reduction of the metal and formation of elemental metal or an M−B alloy (eqs 39 and 40).

$$FeBr_x + x NaBH_4 + n\text{diglyme} \rightarrow Fe(BH_4)_x(\text{diglyme})_n + x NaBr(aq) \quad (38)$$

$$2Fe(BH_4)_2(\text{diglyme})_n + 9H_2O(l) \rightarrow Fe_2B + 3B(OH)_3(aq) + 12.5H_2(g) \quad (39)$$

$$Fe(BH_4)_3(\text{diglyme})_n + 6H_2O(l) \rightarrow FeB + 2B(OH)_3(aq) + 9H_2(g) \quad (40)$$

The reaction kinetics depend on the solvent and the metal. Cobalt(II) is immediately reduced in THF and diglyme with the production of a black colloidal dispersion of alloy nanoparticles.[525] In THF, the reduction of Ni(II) is also immediate,[525] while it occurs slowly in diglyme at room temperature (RT).[96] Similarly, reduction of Fe(II) and Fe(III) is much faster in THF[525] than in diglyme,[94] where it has to be activated thermally above 70 °C. Cu(II) reduction is also activated above 90 °C in diglyme.[96] At a given temperature, the lifetime of the intermediate BH_4^- complex depends on two parameters: the solvent and the metal. The different behaviors between highly coordinating and less complexing solvents might originate, at least partially, from the relative stabilities of the intermediate borohydride. For instance, a complex $Fe(BH_4)_2(\text{solvent})_n$ was reported in diethylether,[519] with lower stability than in more coordinating diglyme. Comparison is, however, not straightforward between the series of experiments of Glavee et al.[96] in diglyme and Molvinger et al.[523−525] in THF. Indeed, the latter are using THF to wash the precipitates, while the former are using deoxygenated water. Although oxidation of the alloys by air is of course avoided, any remaining traces of borohydride or hydride will be destroyed in contact with water. This simple example highlights that the whole synthesis and purification process should be examined with care before attempting comparative interpretations. Glavee and co-workers drew a comparison between the different products obtained in water and diglyme from Co(II), Ni(II), Fe(II), Fe(III), and Cu(II), but no trend could be clearly outlined.[96] According to the time and temperature required for decomposition, the relative stabilities of metal-borohydride complexes in diglyme follow the order Co(II) < Ni(II) < Fe(II) < Cu(II). The boron content in the alloy is however not directly related to this classification, since reduction in diglyme of Co(II) and Cu(II) yields sole elemental metals. The relative position of the redox potentials of each couples might also impact the reaction pathway.[96]

Only few reports deal with the reduction of metal cations with borohydride in organic protic solvents such as alcohols.[191,521,522,526−528] In these solvents, the reaction is believed to proceed according to a more complex scheme[527] because borohydrides have a strong tendency to react with the solvent and form borate esters, a prime example being methyl borates $H_{3-x}B(OCH_3)_x$ (x = 1−3) formed in methanol during organic reduction processes.[317,318]

3.8.3. Nature of the Amorphous Boride Nanoparticles.

Although the synthesis of amorphous metal boride nanoparticles is relatively straightforward, the exact structural nature of the products is debated since their early development.[522] A recent review from Demirci and Miele is addressing this point for Co−B alloys obtained in water.[37] X-ray diffraction,[462,491,526,529] X-ray absorption fine structure spectroscopy (EXAFS),[36,226−230,473,496,530−533] and Mössbauer spectroscopy[491] tend to indicate that nanoparticles of binary and ternary alloys are of predominantly amorphous nature. Ni−B and other M−B (Ni, Co, Fe, Pd) alloys obtained at low temperature in water were considered until recently as amorphous phases with an homogeneous elemental distribution incorporating short-range order and long-range disorder (Figure 46a,b).[191] Geng et al.[217,218] followed by Arzac et al.[245] questioned this statement for Ni−B and Co−B by providing high resolution TEM, electron energy loss spectroscopy (EELS), and electron diffraction analyses. The authors suggest a nanocomposite

dx.doi.org/10.1021/cr400020d | Chem. Rev. XXXX, XXX, XXX−XXX

structure (Figure 46c) made of nanoscaled metal (Ni or Co) clusters embedded into an amorphous boron matrix which is partially oxidized with the presence of BO_2^- groups. However, the use of high dose electron beams (acceleration voltage of 300[217,218] or 200 kV[245]) raises the question of potential crystallization and segregation during the observation. Most XPS works were dedicated to Ni−B amorphous alloys because of their specific catalytic activity and selectivity. One major XPS Ni $2p_{3/2}$ XPS peak was observed at ca. 852.2 eV and is characteristic of nickel in its metallic state.[191,217,218] The same observation was made for other metals such as Co, Fe, and Pd. The XPS data for the B 1s level in Ni−B alloys exhibit two binding energies of 188.2 and 191.7 eV.[191,217,218] The latter value corresponds to oxidized boron ($NaBO_2$ reference).[191] The binding energy of the former peak depends on the metal (Ni, Co, Fe, Pd)[191] and is close to that corresponding to elemental boron (187.5 eV). The attribution of this XPS peak is debated: while Geng et al.[217,218] argue that the shift to higher energy compared to pure elemental boron can be qualitatively ascribed to electron density withdrawing from boron by neighboring boron−oxygen species, Okamoto et al.[191] and other groups[531] consider this shift not strong enough to be attributed to B−O groups and interpret the values as an electron transfer from B to the metal. An alternative interpretation of the spectroscopic data and a description of the electronic structure based on B to M electron transfer of these amorphous alloys were suggested by Diplas et al.[182,193,194] and detailed above in subsection 2.5.3.1. According to the binding energy shifts of the M $2p_{3/2}$ (M = Ni, Co) levels, d electrons transfer from B to M and enriched d population on M atoms are more pronounced for nickel than cobalt.[534] As developed in subsection 2.5.3 for crystalline materials, a consensus has not been reached yet about the general direction of electron transfer in amorphous metal-rich boride alloys. According to first principle calculations, the M:B ratio might play a strong role.[175,535]

Reduction in aqueous or organic solutions[479,522,536] by borohydride leads to residual hydrogen in the resulting amorphous alloys. Especially, Co−B and Ni−B alloys produced in ethanol were shown to contain hydrogen with ratio H/M of, respectively, 0.6 and 1.5.[522] Okamoto showed by XPS that B−H bonds (B 1s binding energy of ca. 182 eV)[191] are present in amorphous Pd−B and Pt−B alloys synthesized in water. The corresponding peak was not observed in Co−B and Ni−B alloys.[191] The synthesis in organic solvent prevents total elimination of hydrogen.[522] This effect is intensified in aprotic solvents such as THF, with reported compositions CoB_2, NiB_2, $FeB_{1.8}$.[523−525] Fourier transform infrared spectroscopy[523] suggested a bidentate M−H−B bridging structure, similar to that observed in mononuclear metal borohydride molecular complexes, and a single terminal hydrogen B−H. All in all, hydrides can still be incorporated into the nanoscale metal boride alloys (Figure 46d). They are especially present when the synthesis is performed in organic, aprotic solvents. Interestingly, Taghavi et al. suggested recently that treatment with hydrogen below 100 °C of amorphous Ni−B nanoparticles made in water could remove part of the oxide layer and enhance the catalytic activity.[537]

3.8.4. Tuned Nanostructures of Amorphous Metal Boride Alloys. The size of M−B amorphous alloy nanoparticles can be controlled by modifying the nucleation and growth kinetics. For instance, increasing the reactant concentration and the mixing rate leads to fastened nucleation and a decrease in the particle size. Co−B nanoparticles can then be obtained in the range 40−90 nm.[292−294] Surface complexing agents and pH modifiers such as citrates give also access to controlled diameters in the same domain.[475,538] Templating based on microemulsions also yields efficient size control between 4 and 12 nm (Figure 47a).[295,539]

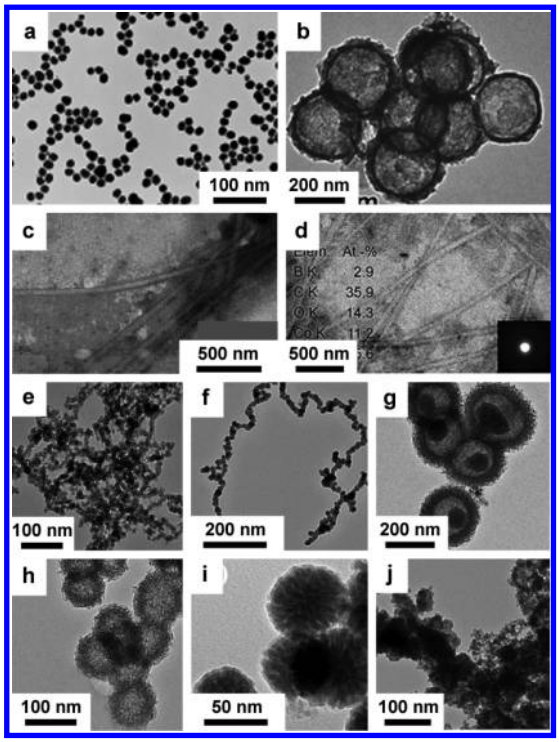

Figure 47. TEM pictures of amorphous metal boride nanostructures obtained by precipitation in solution: (a) Co−B nanoparticles obtained by templating in water/oil microemulsions;[539] (b) Co−B hollow spheres obtained by hard templating with PS spheres;[541] (c) Fe−B nanotubes,[543] (d) Co−B nanotubes[543] obtained by soft templating with a nonionic−anionic surfactant mixture organized in a nematic phase; (e−j) Ni−B spheres obtained by reacting brij-76/Ni^{2+} micelles into a KBH_4 solution with various temperatures and borohydride concentrations.[546] Reprinted, respectively, with permission from refs 539, 541, 543, 546. Copyright, respectively, 2010 Elsevier, 2009 Elsevier, 2006 John Wiley and Sons, Inc., 2010 Royal Society of Chemistry.

Besides size tuning, some current works are dedicated to the design of nanostructured amorphous metal borides for increased catalytic activity.[25] Besides scarce reports on hard templating (Figure 47b),[540,541] soft-templating is the most common route toward nanoscaled amorphous M−B alloys.[542] The process is based on the self-assembly properties of surfactants in water. Micelles or oil-in-water emulsion droplets are exposed to metal ions in the continuous aqueous phase. When the surfactants are negatively charged, the cations are located at the surface of the micelles/droplets because of attractive electrostatic interactions.[543] Then, an alkali borohydride is added to reduce metal ions and yield metal boride alloy nanoparticles localized at the interface between water and the organic phase. This process was successful in the preparation of amorphous Fe−B,[543] Ni−B,[543] Co−B,[543] and Ni−P−B[518] nanotubes (Figure 47c,d) by using a nonionic−anionic surfactant mixture organized in a nematic phase.[543] The lamellar surfactant−inorganic precursor hybrids roll-up and

dx.doi.org/10.1021/cr400020d | Chem. Rev. XXXX, XXX, XXX−XXX

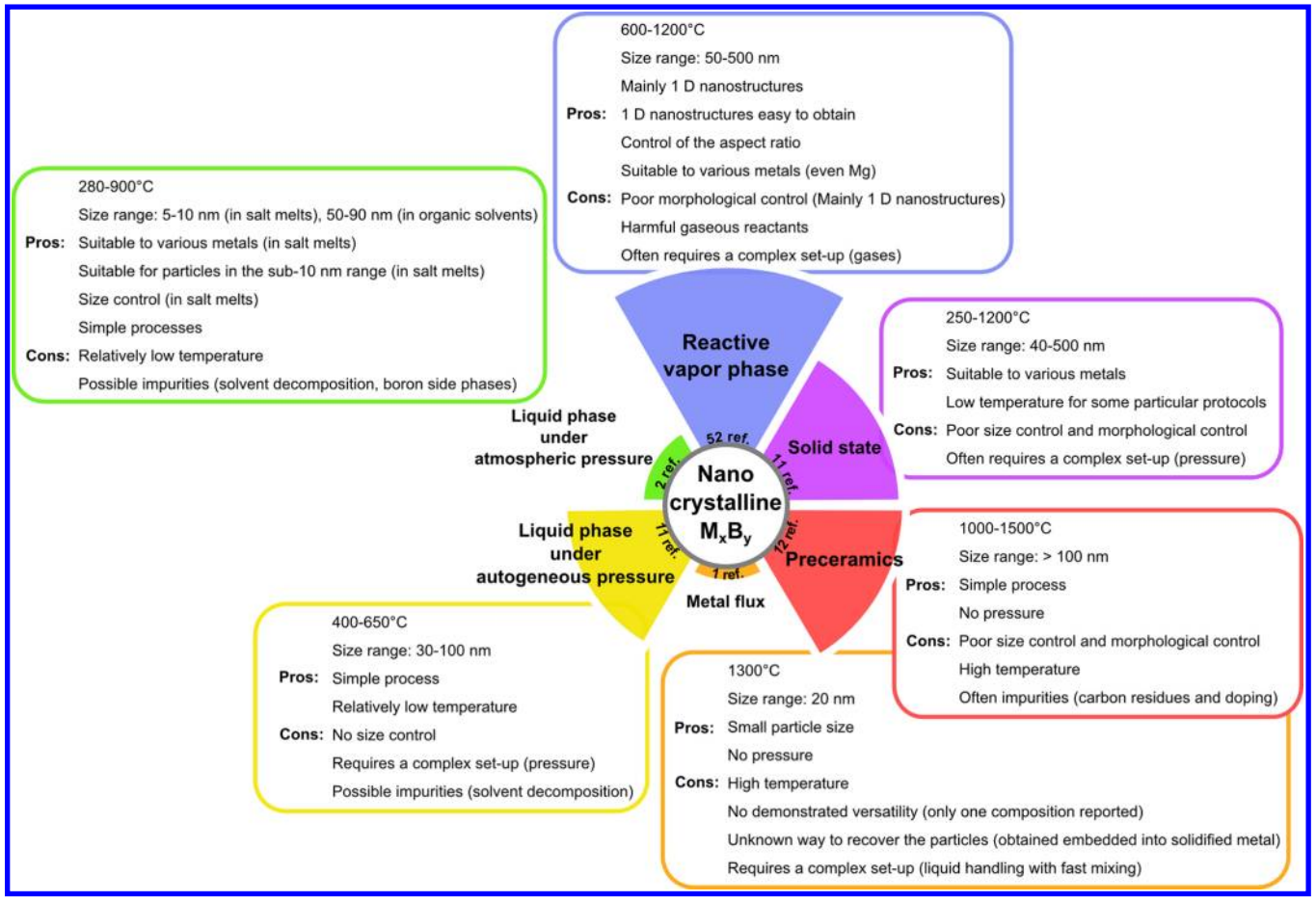

Figure 48. Summary of the different families of processes investigated for the synthesis of nanostructured crystalline metal borides. The size of each slice accounts for the number of published works (ref.) corresponding to each family. The colloidal synthesis of amorphous metal boride nanoparticles is not reported here.

yield nanotubes which are readily aligned on a silicon substrate.[543−545] The localization of Ni−B nanoparticles at the interface with water was also demonstrated when oil droplets based on a nonionic surfactant (brij-76) and containing Ni^{2+} cations were added to a borohydride aqueous solution (Figure 47e−j).[546] After formation of the porous Ni−B shell, BH_4^- anions could still diffuse into the droplets and reduce the remaining Ni^{2+} ions to form a yolk−shell mesoporous structure. Positively charged micelles based on cetyltrimethylammonium ions in water can also act as soft templates for mesoporous spheres of Ni−B and Co−B alloys.[547,548] In this case, the electrostatic double layer effect causes the accumulation of metal cations in the vicinity of the cylindrical micelles. Because of their high concentration, the micelles self-organize into a nematic phase, and the Ni^{2+} or Co^{2+} cations are reduced into M−B alloys in the space between micelles, thus resulting in a worm-like mesoporous structure.

Besides micelles or microemulsions, organic ligands which can act as both metal ion and surface complexants yield anisotropic growth, as described by Tong et al.[549] who obtained nanostructured Co−B flowers with a "wrapped paper" morphology. The authors used ethylenediamine as growth directing agent during the reduction of cobalt acetate by KBH_4 in a basic aqueous solution. Ionic liquids can also orient the formation of the solid toward a mesoporous network of Co−B.[550]

External stimuli can also be used, such as magnetic field for preferential growth of Co−B nanowires.[551]

3.8.5. Borane Adducts: Beyond Borohydrides for the Production of Nanostructures of Amorphous Metal Borides. In addition to borohydride, solution-phase reduction of metal salts is also reported with other boron based reagents. Ternary amorphous borides Ni−M−B (M = Ni, Mn, Co, Cr, Fe, and Zn) were recently obtained by using the BH_3−tetrahydrofuran complex.[486,552] Amine−borane complexes are also typically used as reductants and boron donor. Ammonia borane $H_3N{-}BH_3$ and its derivatives are currently considered as some of the most suitable compounds for chemical storage of hydrogen. Indeed, this adduct possesses a high theoretical capacity (19.6 wt % for ammonia borane) and a dehydrogenation temperature which can be lowered by chemical modification, adsorption on porous supports, and the use of additives or catalysts.[553] In the latter case, amorphous metal boride (cobalt,[554,555] nickel,[554,555] iron[556]) nanoparticles have shown high activity, whether for thermal dehydrogenation or hydrolytic dehydrogenation.[554−556] These particles are produced through in situ reduction of metal salts by ammonia borane in water[554] or organic solvents such as THF.[555,556] An additional role of the amines might be found in the coordinating ability of these molecules which could provide efficient growth confinement by stabilizing the surfaces of small nanoparticles. Au@Co@Fe triple core−shell nanoparticles were also obtained by a similar colloidal synthesis in water.[557]

dx.doi.org/10.1021/cr400020d | Chem. Rev. XXXX, XXX, XXX−XXX

Nevertheless, the presence of boron in the final nanostructure was not specifically assessed. In addition, the *tert*-butylamine−borane adduct was used as reductant for the colloidal synthesis of gold nanoparticles.[558] Palladium[559] and nickel[560] nanoparticles were produced from tributylamine−borane in oleylamine, while Pt nanocubes and nanopods[561] were obtained from morpholine−borane. Although no boron was detected in these products, Pd, Ni, and Pt particles were washed by protic solvents which may destroy the boron hydride species possibly incorporated into the nanoparticles. When the reduction of palladium salts in water is concerned, dimethylamine−borane seems more efficient as boron donor than borohydride.[562] On the opposite, tributylamine−borane does not incorporate noticeable amounts of boron when the reduction is conducted into oleylamine as solvent.[559] Such behaviors put on the forefront the extreme sensitivity of these colloidal routes from the point of view of the composition of the nanoparticles. The discrepancy between the different results lies in many experimental parameters, among others the nature of the solvent, and of the reductant and boron donor, and the washing procedure. From a general point of view, solution-phase procedures toward metal nanoparticles which involve the use of boron-containing reducing agents should always be considered with care as to the incorporation of boron in the final product.

3.8.6. Supported Systems. Supported amorphous metal borides have been intensively produced in order to target catalytic studies. Chemical reduction of solubilized metal salts with metal borohydrides in the presence of solid substrates is the most used method. Ni−B was deposited on silica,[192,532,563,564] alumina,[565,566] MgO,[567] and clays.[565] Co−B was obtained over silica,[476] carbon nanotubes,[568] and titania.[569] Other examples are given in subsection 5.3 dedicated to catalytic properties of metal borides and phosphides. Ternary compositions were also synthesized, including Ni−Co−B,[192] Ni−La−B,[566] and Ni−Ru−B.[570] Electroless plating is an alternative method for deposition[540] and can be catalyzed by silver nanoparticles predeposited on titania[569,571,572] or MgO.[567,573,574]

Electrodeposition has been widely used for metal boride synthesis.[575] However, only few reports deal with nanostructured systems. Mitov et al. deposited amorphous Mn−Co−Ni−B "microcauliflowers" on Ni foams.[576,577] These structures were made of stacked 100 nm-thick layers of $Mn_8B_{30}O_{62}$ and $Co_{62}Ni_{36}O_2$. In another method, hard templating approaches can be combined with electrodeposition for the growth of nanostructured metal borides, such as $Co_{87}Fe_5B_8$ nanowires grown in alumina pores.[578]

3.9. Summary for Nanoscaled Metal Borides

Figure 48 summarizes the different families of synthetic approaches toward nanoscaled crystalline metal borides. Recent results dealing with induction thermal plasma synthesis and arc discharge were not discussed herein since they yield mixed phases $TiB_2/TiB/Ti$[579,580] and PtB/Pt,[581] respectively, although the boride phases were of nanometer scale. Spray pyrolysis has not been developed in this section or included in Figure 48 because it usually provides sub-micrometer-scale particles,[582] although some promising results have been recently obtained by ultrasonic coupling.[583] Strikingly, many techniques involve relatively high temperatures (above 500 °C) compared to the typical protocols for metals, metal oxides, metal phosphides, and so on. This can be ascribed primarily to the strong covalency occurring in metal borides, which implies high energy input in order to get crystallization from a poorly ordered system. Other explanations are to be found in the lack of a suitable reactive elemental boron precursor, the wide range of stoichiometries available for many metals, and the sensitivity to air exposure. The latter point could also be the reason why only few crystalline metal-rich borides have been reported up to now, while less sensitive boron-rich borides are more often met at the nanoscale. High temperature syntheses (above 1000 °C for solid state and 500 °C for liquid phase routes) also raise the question of the sample purity, because decomposition of the vials or the solvent could occur. Compositional characterizations usually reported are insufficient, and too few reports have assessed this important point. Another problem to tackle is size decrease. Among the vast range of routes explored, only few provide particle sizes below 40 nm. Even rarer are those combining such small particle sizes and versatility in terms of the available compositions on one side, and simplicity, safety, and relatively low temperatures on the other side. Actually, the most recent techniques based on liquid phase synthesis under atmospheric pressure fall into this category and are opening new avenues for the controlled fabrication of nanoscaled metal borides. Interestingly, these routes are related to colloidal syntheses which are widely developed for other materials, especially crystalline metal phosphide nanoparticles. The next section deals with these nanomaterials and these approaches. The aim is to demonstrate the exquisite compositional and morphological control that can be reached by liquid phase synthesis of metal phosphides, especially through the right choice of metal and phosphorus precursors.

4. NANOSCALED METAL PHOSPHIDES

Major papers dealing with metal phosphides in the 2000−2012 period are reviewed in this section. As no dedicated review was published recently, the following record intends to be exhaustive in the 2008−2012 period, on the restricted subject of metal phosphide nanoparticles. A number of selected older works are also mentioned as starting point in order to enlighten the field evolution.[584]

4.1. From Bulk to Nanoscaled Metal Phosphides

As presented before, a wide range of processes and phosphorus precursors were available in the 1980s, for the preparation of bulk metal phosphides. However, nanoparticle synthesis requires an additional control on the surface states of these compounds. In order to limit the growth of the crystallites and to control the final size and shape of the particles, new strategies had to be designed. They relied for instance on the use of organic capping agents in wet routes, on the heterogeneous nucleation of nanoparticles from gas-phase precursors at relatively low temperature (to avoid sintering), or the fine control of reaction kinetics by an accurate tuning of the precursors reactivities.

As will be shown in the following section, the quest for designed MP nanoparticles originated from the field of III−V semiconductors, where size control allowed adjusting the band gap of the materials. However, further extension to other metals triggered the development of specific routes, better adapted to morphology control, both in terms of processes and precursors.

4.2. Short Historic Introduction: Why MP Nanoparticles?

A transition from bulk synthetic techniques to nanoparticle ones occurred in the 1960−2000 period. At first, the driving force of this renewal was the quest for tunable band gap semiconductors.

dx.doi.org/10.1021/cr400020d | *Chem. Rev.* XXXX, XXX, XXX−XXX

Table 5. Starting Stoichiometries of the Metal−Phosphine Precursor (Italicized) and Final Structure of the Nanoparticles (Indicated with Asterisk) Obtained by Thermal Decomposition in a Silica Xerogel[599]

Fe−P	Ru−P	Co−P	Rh−P	Ni−P	Pd−P	Pt−P
					$Pd_{15}P_2$, Pd_6P, $Pd_{1.8}P$	
Fe_3P				Ni_3P	Pd_3P	
				Ni_5P_2, $Ni_{12}P_5$	Pd_5P_2*	
*Fe_2P***	Ru_2P	*Co_2P**	Rh_2P*	Ni_2P*	Pd_7P_3	Pt_5P_2
			Rh_3P_2,Rh_4P_3	Ni_5P_4, $Ni_{1.22}P$		
FeP	*RuP**	*CoP*		NiP		
FeP_2	RuP_2	CoP_2	RhP_2	*NiP_2*	*PdP_2*	*PtP_2**
			RhP_3	NiP_3	PdP_3	
FeP_4	α-RuP_4,β-RuP_4					

Scheme 1. Methanolysis of Alkyl(disilylphosphido)indane Single-Source Precursors[a]

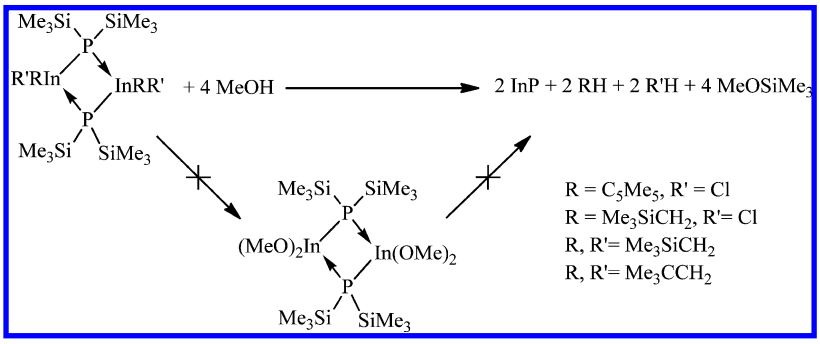

[a]The preformed In−P bonds are not maintained during polycondensation.[617]

Indeed, numerous MPs are semiconductor materials.[67,11] In 1952, H. Welker suggested that indium phosphide (InP) could be used as a semiconductor in electronic devices.[585] The possibility to grow this material in thin polycrystalline films[586] allowed its use in multilayer stacks along with other III−V materials such as GaAs or InAs. InP, GaP, and their alloys with arsenide became progressively major compounds and applications such as photoemitting diodes and microwave oscillators, but also for signal enhancement in biology.[19,587,588]

This new field of applications triggered the development of several new synthetic routes. Indeed, the need for processable materials that could be nicely deposited as regular thin films or organized architectures required softer reaction conditions (CVD, hydro- and solvothermal syntheses),[589] and the use of molecular reactive sources of materials, such as PH_3[586,590] or $P(SiMe_3)_3$.[591]

Additionally, new organometallic precursors, particularly suited for CVD,[592] were extensively developed at this period:[593] the so-called "single-source precursors" contained both the metal (In, Ga, or both) and the P source,[594] as a PH_2 ligand or a $P(SiMe_3)_2$ ligand.[595,596] They allowed for a fine control of the layer composition and doping.

4.2.1. Beyond III−V Semiconductors. Even though InP and GaP semiconductors were the most studied phosphides in the 1960−2000 period, other phases were also investigated, such as Cd_3P_2.[597] For instance, metal phosphide semiconductors were investigated as photoelectrochemical cells (CoP_8, Fe_3P, MoP_2, Ni_2P, WP_6).[11]

Moreover, metallic conductor films of TiP were also obtained from single-source precursors involving alkyl-phosphines by CVD.[598] In a different approach, the use of single-source precursors (organometallic M−phosphine complexes) allowed the incorporation of M_xP_y nanoparticles in silica xerogels by the thermal decomposition of the starting complexes, followed by diffusion and growth of the intermediate clusters.[599] The composition of the nanoparticles exhibited equal or larger M/P ratio than the precursors (Table 5). According to the authors, the stability of the phase obtained also played a role on their formation.

Using non-single-source precursor, refractory ceramics were developed using solid-state metathesis routes: several phosphides (YP, LaP, VP, NbP, MoP, etc.),[600,601] but also metastable HfP and ZrP phases,[115] were obtained by the self-propagating reaction of metal chloride precursors with Na_3P, a reaction that is driven by the formation of NaCl.

Advanced characterization tools such as solid-state NMR (MnP, RuP, WP, $Co_xMn_{1-x}P$),[602] electrochemistry (GaP),[603] magnetic measurements (Fe_2P, Cr_2P, Mn_2P, Co_2P, Ni_2P, and superconductors $LaFe_4P_{12}$, $LaRu_4P_{12}$),[604−606] and surface spectroscopies (NiP, InP)[587,191] were also utilized in this period in order to gain a better understanding of the physical properties of the metal phosphides.

Last but not least, an authentic new binary phase was synthesized in the 1990s: BiP.[607,608] Indeed, bismuth was believed not to form any binary phosphide.[67] While BiP cannot be obtained by heating Bi and red or white phosphorus (starting materials crystallize separately), the synthesis could be achieved using molecular precursors: $BiCl_3$ and $P(SiMe_3)_3$.

4.2.2. Quantum Effects in III−V Semiconductors: Toward Nanoscaled Metal Phosphides. Meanwhile, the rapid development of InP and GaP is the milestone that planted the roots for today's interest in the metal phosphides. Indeed, in solution routes developed after 1960, the products were most of the time nanocrystalline, and yielded in several occasions nonaggregated III−V quantum dots.[589,591,609−611] Nanofibers could also be obtained,[612] leading to fundamental studies of their size-dependent luminescence properties[613] and to applications in optoelectronics.[614] More complex structures

dx.doi.org/10.1021/cr400020d | Chem. Rev. XXXX, XXX, XXX−XXX

such as nanoporous III−V electrodes were thus developed for eletroluminescent devices.[615] InP−SiO_2 nanostructured materials were prepared by the CVD of $InMe_3$ inside the pores of MCM-41 silica and its further reaction with PH_3.[616]

Characteristic dimensions and 3D organization of the materials were rapidly beyond the reach of lithographic methods, leaving solution routes and molecular precursors as the only alternative for a precise size control and self-assembly at the nanoscale.[12] Gaining an intimate understanding of the molecular reaction pathways thus became crucial. Such in-depth studies were done in the 1990s for reactions employing $[M(PR_2)_2]_2$ single-source precursors (M = In, Zn, Ga, Cd; R = alkyl, aryl, SiR'_3) and have been extensively reviewed by W. E. Buhro.[617] The phosphines included in the complexes are highly reactive source of $P^{(3-)}$, easier to manipulate than PH_3. Several decomposition routes (phosphinolysis, alcoholysis, thermolysis) and reaction intermediates were identified, depending on the experimental conditions (and surprisingly, some more recent papers on the subject[618] do not mention these pioneering works). Interestingly, in several cases the integrity of the single-source precursor is not conserved, and the first step is its decomposition into a phosphorated fragment and a metallic one (Scheme 1).

However, the drawback of this route is the competitive formation of polymeric $[M(PR_2)_x]$ species that sometimes prevent a complete conversion into metal phosphide.[617] Meanwhile, their supramolecular interactions allowed the growth of InP fibers.[619]

Altogether, the strong structure−property relationship found in III−V metal phosphide prompted both physicist and chemist communities to develop new nanoparticle syntheses. They should provide well-dispersed nanoparticles of tailored size and shape, in gram scale, if possible, for further incorporation into materials, and they should avoid the use of the highly toxic PH_3 and $P(SiMe_3)_3$ precursors.

4.3. Colloidal Syntheses from Single-Source Precursors

Single-source approaches continued to be largely used in the 2000s. Clusters of Co(0) with bidentate arylphosphine were grafted on mesoporous silica (SBA-15) and decomposed into Co_2P nanoparticles, with conservation of the initial Co/P ratio.[620] Similarly, the decomposition of Fe clusters containing P^tBu moieties (Fe/P = 2) yielded Fe_2P nanoparticles with well-defined morphologies (bundles, crosses),[621] while a film of Cu_3P could be deposited by CVD from a Cu complex bearing a bidentate arylphosphine.[622] More recently, a phase-pure Fe_3P thin film was obtained from $H_2Fe_3(CO)_9PR$ (R = ^{t}Bu or Ph), a precursor in which the Fe/P ratio corresponded to the final ratio in the film.[623]

Additionally, the single-source precursor should have a temperature of decomposition low enough to avoid secondary reactions with solvent or surfactant molecules: the decomposition of $FeMn(CO)_8(\mu\text{-}PH_2)$ yielded $Fe_{2-x}Mn_xP$ nanoparticles at 220 °C while the more robust $FeMn(CO)_8(\mu\text{-}PPh_2)$ decomposed into FeO at ca. 350 °C.[624] Interestingly, the single-source approach was thus found to be able to yield ternary metal phosphide nanoparticles.

But temperature could also provide a lever to tune the phase. Both Ni_2P and Ni_2S thin films were deposited by CVD using the same precursor, a nickel complex bearing a selenide and a sulfide phosphine.[625] Factors controlling the final phase are interdependent and include in particular the type of CVD and the temperature.[626] The same family of precursors, containing $R_3P{=}S$ and $R_3P{=}Se$ ligands, also allowed the synthesis of $Ni_{12}P_5$, Ni_2P, and NiSe colloids.[627] With a similar strategy, Co_2P, CoP, and Co chalcogenide nanoparticles[628] were later prepared, along with Cd phosphides and Cd sulfide films.[629] A $PtRuP_2$/carbon composite was obtained by thermal treatment of a PPh_3-containing bimetallic precursor.[630]

Single-source precursors containing silylphosphines were progressively abandoned, since mechanistic works mentioned earlier had shown that, most of the time, their integrity was not preserved in the first steps of the reaction. Rather, $P(SiMe_3)_3$ was largely used directly, as a liquid analogue to PH_3, as described in the next section.

On the other hand, the annealing reduction of metal phosphate under H_2 was achieved and provided Rh, Ir, and Ag nanocrystalline phosphides.[631]

4.4. Substitutes for PH_3 as Safer "P" Donors

4.4.1. In Situ and ex Situ PH_3 Generation. Although the phosphine PH_3 forms spontaneously in the living sphere (at very low concentration),[632] this gas is one of the most toxic, lethal at a few ppm. It has been largely used in electronics, as mentioned before, but chemists try to avoid it. Thus, it was not used directly in solution but was rather obtained in situ from sodium hypophosphite (NaH_2PO_2) in basic hydrothermal conditions, in the synthesis of $Ni_{12}P_5$ hollow nanoparticles (Scheme 2).[633] It was also used in a ball-milling route yielding

Scheme 2. Representative Examples of One-Pot and Two-Pot Routes to MPs Using in Situ Generation of PH_3[633,635,626]

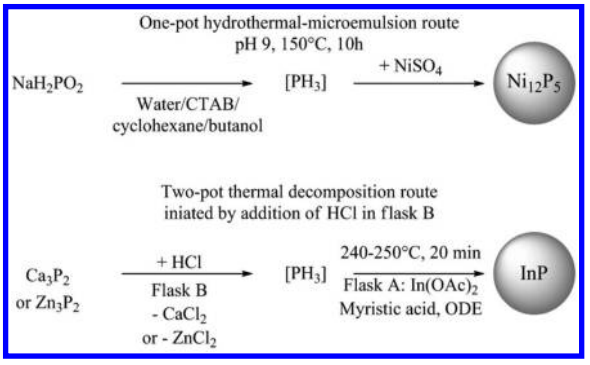

Ni_2P nanoparticles.[634] PH_3 could be alternatively generated by HCl addition on Ca_3P_2 on a secondary reaction flask connected to the main reactor, for the production of InP well-dispersed nanocrystals.[635] Zn_3P_2 itself was recently used over HCl to generate PH_3 in situ (in a separated flask connected to the main one) for the production of InP nanoparticles that were coated with ZnS in a second step.[636,637]

Phase control was recently demonstrated in the case of cadmium phosphide, using PH_3 generated in situ via decomposition of Ca_3P_2 and bubbled in the reaction mixture heated at the desired temperature (120−250 °C). Its reaction with Cd(acetate)$_2$ produced Cd_6P_7 nanocrystals instead of the more common Cd_3P_2 ones.[638] Reaction temperature could be lowered by using a more reactive metal precursor, such as $Fe(N(SiMe_3)_2)_2$, but it yielded an amorphous FeP_2 phase.[639]

4.4.2. $P(SiMe_3)_3$ as a Highly Reactive Alternative to PH_3. $P(SiMe_3)_3$ was employed in the gas phase for deposition of TiP films using dual-source CVD,[640] but also in solution: MnP nanoparticles were thus obtained from Mn(0) carbonyl complexes,[641] Cd_3P_2 nanoparticles from heteroleptic[642] or

dx.doi.org/10.1021/cr400020d | Chem. Rev. XXXX, XXX, XXX−XXX

Scheme 3. Representative Synthetic Routes to MP Nanoparticles Using TOP as a Phosphorus Donor[a]

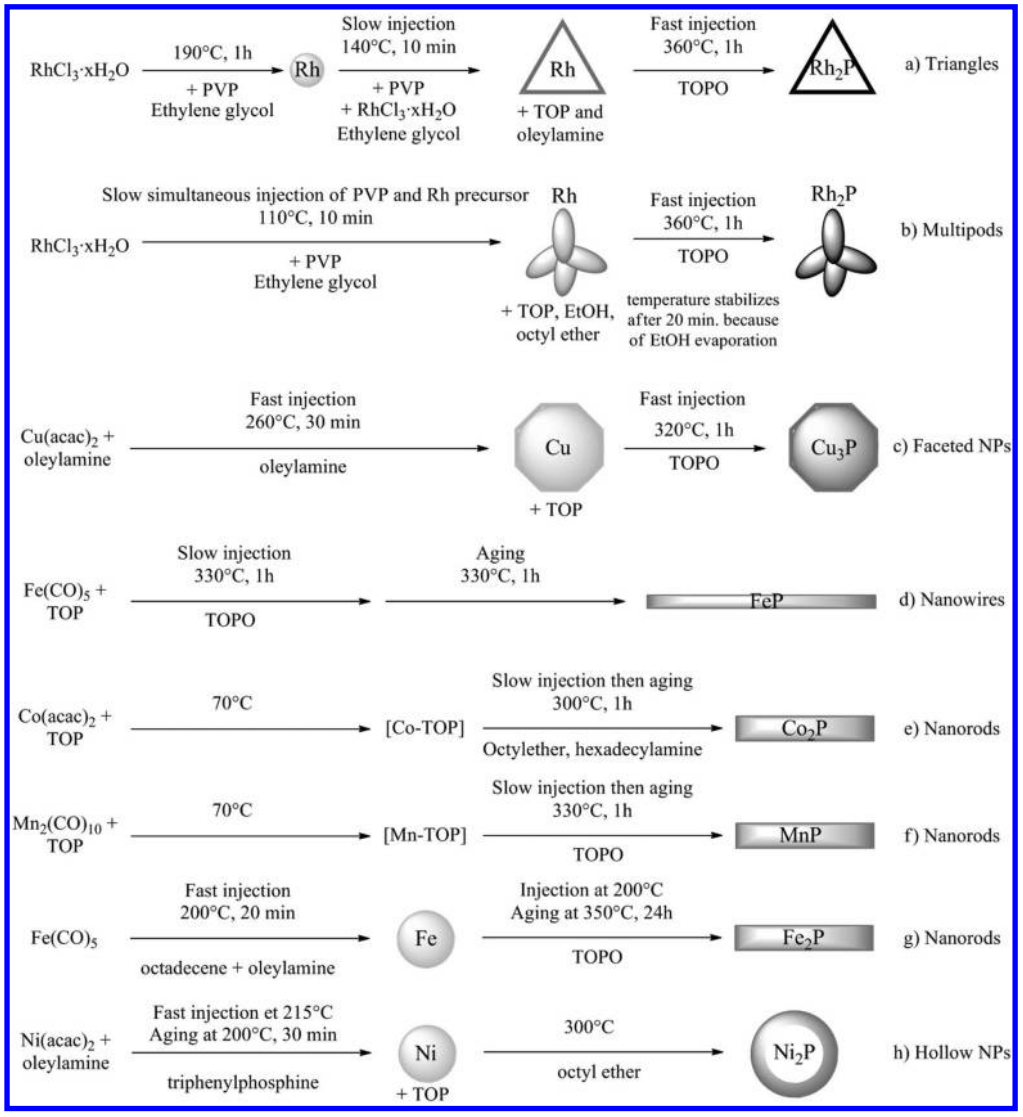

[a]See Figure 49 for the corresponding TEM pictures and references.

homoleptic[643] carboxylate precursors and from CdO,[644] and InP nanoparticles from In(acetate)$_3$,[645,646] $InCl_3$,[647] or In(myristate)$_3$.[648] The nucleation and growth kinetics of InP nanocrystals were studied in-depth in order to gain a better control on their luminescence properties.[649] Nanowires of InP and GaP were also obtained from metal−alkyl precursors.[650] It must be noted that these synthetic procedures allowed also the deposition of a ZnS passivating shell on the InP nanoparticles, in one (or two) step(s), with consequences for the precise composition of the shell (InPZnS alloy, or respectively graded interface) and thus on their luminescence properties,[651] but these properties also depend on external parameters such as the temperature.[652] The precise reaction mechanism for the decomposition of $P(SiMe_3)_3$ remains unclear even though it strongly depends on the presence of protic species in the medium,[618] on the pH, and on the metal precursors, as suggested by previous works on single-source precursors.[617]

Interestingly, Harris et al. showed recently that the analogous $P(GeMe_3)_3$ reacts four times slower than $P(SiMe_3)_3$, allowing an improved size control of InP nanoparticles.[653] More generally, a better kinetic control is expected to enhance the quality of the MP synthesis when using reactive "P" donors. This can be achieved by carefully designing the precursor (as above) and by lowering the reaction temperature. Very recently, Ojo et al. demonstrated the room-temperature reactivity of $P(SiMe_3)_3$ for the synthesis of Cd_3P_2 nanocrystals, proving that crystallization of the particles does not necessary require strong heating when using molecular precursors.[654] Excellent quantum yields (>50%) were obtained by coating the nanoparticles with a protective ZnS shell in a one-pot procedure.

$P(SiMe_3)_3$ was also used in the presence of tri-n-octylphosphine (TOP) for the synthesis of InP nanoparticles[655−657] and core−shell MnP−InP nanoparticles.[658] Here, TOP was utilized to help the dissolution of the metal precursor ($InCl_3$) and to stabilize the colloids afterward. Similarly, TOP was used as a surfactant in the synthesis of InP nanorods from In(0) nanoparticles,[659] and in the preparation of InP nanorods that were grown using $Au_{101}(PPh_3)_{21}Cl_5$ clusters[660] or Bi nanoparticles[661] as seeds.

dx.doi.org/10.1021/cr400020d | Chem. Rev. XXXX, XXX, XXX−XXX

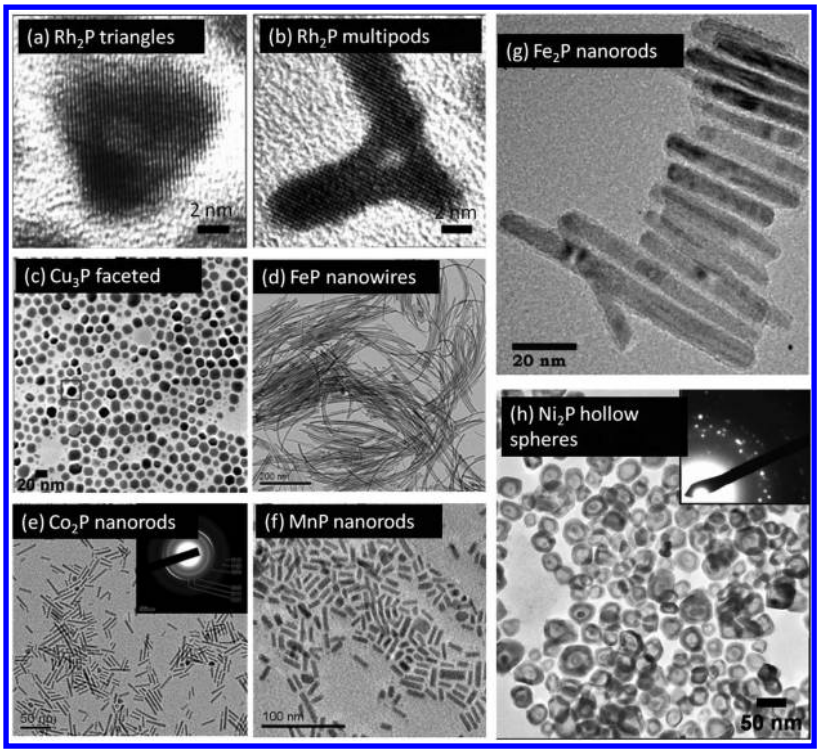

Figure 49. Selected panel of nanoparticles obtained using TOP as a phosphorus source. The morphology can be controlled (c–e) through the synthetic procedure (slow delivery of TOP using a syringe injection) or (a, b) through the shape of the metal nanoparticle precursors: for parts a and b, see ref 41; for part c, see ref 42; for parts d–f, see ref 45; for part g, see ref 44; for part h, see ref 680. Reprinted, respectively, with permission from refs 41, 42, 45, 44, 680. Copyright, respectively, 2008 American Chemical Society, 2007 American Chemical Society, 2005 American Chemical Society, 2009 American Chemical Society, 2007 American Chemical Society.

4.5. Tri-n-octylphoshine (TOP): A Versatile "P" Source

4.5.1. Reaction of TOP with M(0) Precursors. After having been used sometimes as a ligand, TOP was finally used as the "P" source in 2004, in the synthesis of Fe_2P nanorods and nanowires from an Fe(0) source $[Fe(CO)_5]$,[662,663] but also for the coating of magnetite nanoparticles with Fe_2P in a more recent study.[664]

The temperatures required for breaking the P–C bond were quite high (ca. 300 °C), but with TOP being a less toxic and less expensive reactant than $P(SiMe_3)_3$, this procedure is still very attractive. Starting also from a M(0) precursor, Ni_2P nanoparticles were obtained from Ni(cyclooctadiene)$_2$ at 345 °C.[665] An In(0) precursor, obtained from the metal or by in situ reaction of $InCl_3$ on Na, was also reacted with TOP at elevated temperatures (typically, 250 °C for 7 h) to produce InP aggregated nanoparticles:[666] the authors proposed a catalytic role of the In(0) species in the breaking of the P–C bond. Similarly, Cd_3P_2 nanoparticles were obtained from Cd(II) salts, TOP, and Na, but in this case the authors proposed the formation of Na_3P prior to the reaction with Cd.[667]

Rh(0) preformed nanoparticles with complex shapes were later converted into Rh_2P of parent shapes,[41] and Fe(0) nanoparticles were transformed into Fe_2P and FeP, with modification of morphology.[44]

4.5.2. Widening the Scope of the Reactivity of TOP. Very interestingly and likely because of its simplicity, the thermal decomposition method could be generalized to other metals, in other oxidation states (Scheme 3, Figure 49). Whether or not the metal precursor should be reduced to a M(0) species to give the phosphide is still a debatable question, which of course depends deeply on the metal, and the reaction conditions.

Nanorods at 300–360 °C (Co_2P, MnP, Fe_2P, FeP, Ni_2P),[45,668,669] nanoparticles ($Ni_{12}P_5$, Ni_2P, PtP_2, Rh_2P, Pd_5P_2, PdP_2, Cu_3P, FeP, CoP, AgP_2, $SnP_{0.94}$),[42,43,670] hollow nanoparticles ($Ni_{12}P_5$, Ni_2P),[43,47] and other shapes such as powders, wires, thin films, and foils (Ni_2P, Ni_5P_4, Cu_3P, CuP_2, InP, Rh_2P, GaP, Pd_5P_2, PdP_2, Zn_3P_2, Zn_2P_3, Au_2P_3),[42] nanowires (Ni_2P,[671] Fe_2P,[672] Zn_3P_2[48]), nanorices (Co–Fe–P),[673] and nanoneedles (InP)[46] were obtained within a few years, using high-boiling point solvents, molecular precursors, and relatively hard reaction temperatures. A fine control of the reaction conditions leads to Janus Cu–Cu_3P nanoparticles,[674] while the time evolution of CoP nanowires in solution illustrated a self-assembly process upon solvent evaporation yielding 2D and 3D stacked structures, a phenomenon that was shown to be very sensitive to the temperature in the 0–20 °C range.[675] Sonochemical synthesis allowed a remarkable lowering of the average reaction temperature of the heating bath to 70 °C in the synthesis of FeP hollow nanoparticles.[676]

Ternary alloy could also be obtained, such as $(Ni_xFe_{1-x})_2P$ nanorods.[677] Some control of the morphology could be achieved by the variation of the reaction conditions, although its origin is not yet fully rationalized but has been related to the precursors concentration:[678] nanorods, nanoplatelets, and nanowires of Ni_2P were obtained from the same Ni(acac)$_2$ precursor.[672]

Lastly, metal oxide nanoparticles were converted into phosphides (Ni_2P, CoP, and FeP, but MnP did not work) using TOP, although the reaction likely proceeds by dissolution–reprecipitation, as suggested by the authors.[679]

dx.doi.org/10.1021/cr400020d | Chem. Rev. XXXX, XXX, XXX–XXX

Table 6. Selected Synthesis of Metal Phosphide Nanoparticles Using TOP as a Phosphorus Donor[a]

M	phase	ox.	TOP equiv	process	conditions and cosolvent/surfactant	morphology	ref
Mn	MnP	0	15	solvothermal, slow injection	$Mn_2(CO)_{10}$ mixed with TOP and injected at 330 °C, TOPO	nanorods	45
Fe	Fe_2P	0	15	solvothermal, slow injection	$Fe(CO)_5$ mixed with TOP and injected at 300 °C, octylether and oleylamine	nanorods or nanowires (double injection)	662
Fe	FeP	0	15	solvothermal, slow injection	$Fe(CO)_5$ mixed with TOP and injected at 360 °C, TOPO	nanorods	45
Fe	FeP	0	29	solvothermal	$Fe(CO)_5$ mixed with TOP and injected at 300 °C, TOPO	nanowires	663
Fe	FeP and Fe_2P	0	up to 39	solvothermal	Fe nanoparticles reacted with TOP, 350–385 °C; octadecene, oleylamine	hollow particles, nanorods	44
Co, Fe	$Co_{1.5}Fe_{0.5}P$, respectively $Co_{1.7}Fe_{0.3}P$	+2, +3	7.5	solvothermal	Co(II) carbonate and $Fe(acac)_3$ mixed with TOP and oleic acid; oleylamine is quickly injected at 290 °C, respectively, 320 °C	short nanowires in bundle	673
Co	Co_2P	+2	24	solvothermal, slow injection	$Co(acac)_2$ mixed with TOP and injected at 300 °C, octylether and hexadecylamine	nanorods	45
Co	Co_2P	+2	5	solvothermal	$Co(acetate)_2$ reacted on TOP at 320 °C, oleylamine	hollow nanoparticles	47
Co	Co_2P then CoP	0	2.6 (Co_2P) 13 (CoP)	solvothermal, injection	Co nanoparticles are reacted on TOP at 300 °C (Co_2P) or 350 °C (CoP); octadecene (only for Co_2P), oleylamine	spherical nanoparticles, hollow at high temperatures	683
Rh	Rh_2P	0	large excess	solvothermal, injection	Rh nanoparticles reacted on TOP, injection at 360 °C and aging at 300–360 °C, initial morphology of the nanocrystals is mainly preserved; TOPO, EtOH, oleyamine	triangles, multipods, some hollow structures	41
Rh	Rh_2P	0	large excess	solvothermal	Rh nanoparticles are reacted on TOP at 360 °C, TOPO	spherical nanoparticles	680
Ni	Ni_2P	+2	31	solvothermal, slow injection	$Ni(acac)_2$ mixed with TOP and injected at 330 °C, TOPO	nanorods	45
Ni	Ni_2P	+2	21	solvothermal, injection or mixing	$Ni(acac)_2$ mixed with TOP and injected at 310 °C, TOPO	spherical nanoparticles	684
Ni	Ni_2P	+2	10	solvothermal	$Ni(OAc)_2$ reacted with TOP at 320 °C, octadecene and oleic acid	nanorods	47
Ni	Ni_2P	+2	2	solvothermal	$Ni(OAc)_2$ reacted with TOP at 250 °C, oleylamine and TOPO	nonhollow nanoparticles	47
Ni	Ni_2P	0	5	solvothermal	Ni nanoparticles are reacted with TOP at 320 °C, oleylamine	hollow nanoparticles	47
Ni	Ni_2P	0	large excess	solvothermal	Ni nanoparticles are reacted with TOP at 300 °C, octylether	spherical nanoparticles	680
Pd	Pd_5P_2	+2	large excess	solvothermal	$Pd(acac)_2$ is reacted with TOP at 300 °C	TEM not provided	680
Pd	PdP_2	0	large excess	solvothermal	Pd nanoparticles are reacted with TOP at 360 °C, TOPO	irregular shapes	680
Pt	PtP_2	0	large excess	solvothermal	Pt nanoparticles are reacted with TOP at 370 °C, TOPO	spherical nanoparticles	680
Cu	Cu_3P	+1	11	solvothermal, injection	CuCl prereacted with amines and injected at 370 °C and aged at 350 °C; oleylamine, octylamine, TOPO	Cu_3P nanoplate	674
Cu	Cu_3P	+1	5.6	solvothermal, injection	CuCl prereacted with amines and injected at 370 °C and aged at 350 °C; oleylamine, octylamine, TOPO	Janus Cu–Cu_3P nanoparticles, plain Cu_3P after 45 min	674
Zn	Zn_3P_2	0		vapor-phase	Zn foil exposed to TOP vapor at 350 °C	nanowires	48
In	InP	+3	90	solvothermal, injection	$InMe_3$ in octadecene injected in a TOP/TOPO solution at 200–300 °C; TOPO, octadecene	nanoneedles	46
Sn	$SnP_{0.94}$	+2	15	solvothermal	$Sn(OAc)_2$ heated at 390 °C, TOPO	tear-drop shape	670

[a]Ox. indicates oxidation degree of the metal precursor. TOP equiv indicates stoichiometry of TOP vs the metal precursor.

dx.doi.org/10.1021/cr400020d | Chem. Rev. XXXX, XXX, XXX–XXX

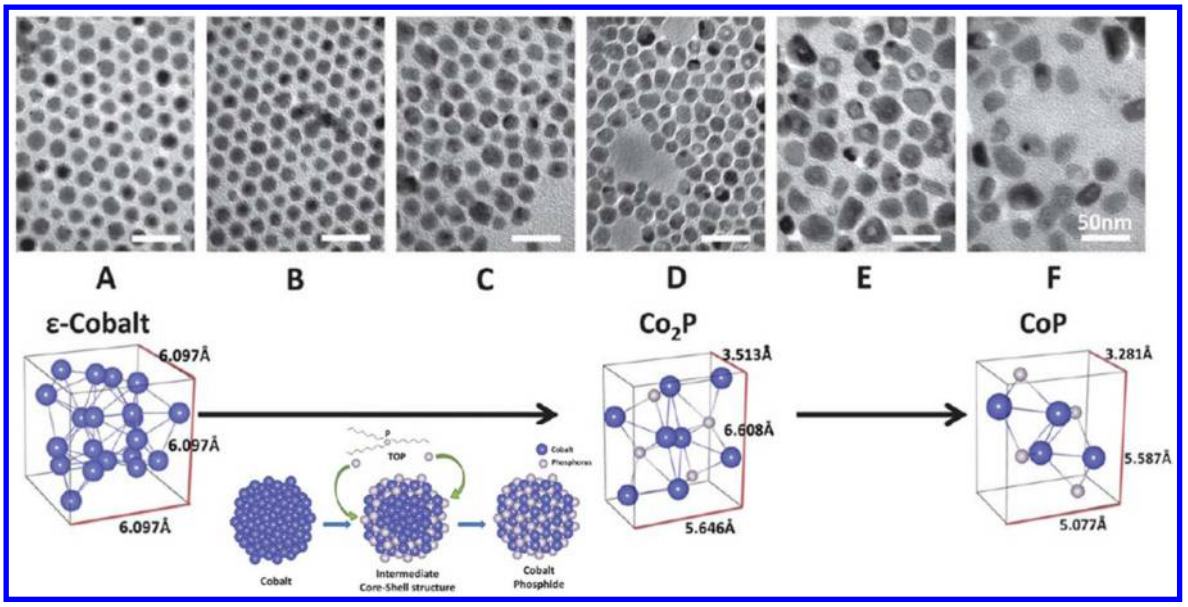

Figure 50. Step-by-step transformation of ε-Co to CoP using TOP as a P-donor. Adapted with permission from ref 683. Copyright 2011 Royal Society of Chemistry.

4.5.3. Knowledge or Know-How? This impressive list of compositions and structures was however obtained with poorly defined systems, compared with the single-source precursor syntheses. To the best of our knowledge, TOP is most often used in a large excess (in stoichiometries that are often not even calculated in the experimental section), because (i) it often serves also as a solvent for the metal precursors, (ii) it serves as a stabilizing ligand on the colloids, and (iii) its decomposition is very incomplete (and sometimes leads to very partial "P" incorporation[681]), though it was shown to occur in the earlier stage of the reaction when using nickel nanoparticles, sometimes leading to unwanted P-doping.[682]

So far, no clear relationship could be evidenced with the M/P final ratio or with the nanocrystal morphologies. Yields of the reaction (vs the metal or vs the phosphine) are not specified. It is likely that TOP plays an important role in the stabilization of metallic intermediates ($M^{(0)}$ or $M^{(+x)}$), ensuring the formation of a large reservoir of monometallic species in solution, which favors a slow growth of the nanocrystals and/or ripening and self-repairing mechanisms. As a consequence, a significant part of the metal precursor may not be incorporated in the colloids.

In Table 6 are presented a selected set of syntheses which involved TOP as a phosphorus source. As a general trend, higher reaction temperatures and larger excess of TOP promote the formation of more P-rich phase (FeP vs Fe_2P, CoP vs Co_2P), regardless of the oxidation state of the metal precursor. However, the M:P ratio also depends on the choice of surfactants and solvents, as well as on the procedure (with or without injection), likely because this affects the rate of decomposition of TOP in the reaction mixture, and so does the morphology of the nanoparticles. This still hampers the design of new syntheses leading to a chosen phase or morphology.

Surprisingly, the wide adoption of TOP as a "P" source coincided with a disinterest in mechanistic studies that had given crucial information in the study of silylphosphines.

In most cases, synthetic routes became more and more empirical, although they were very efficient in providing monodisperse nanocrystals. These synthetic routes still rely on a high degree of empirical mastery. A development of the processes gave access to more and more shapes and sizes: slow syringes injections,[662] multistep heating ramps, and the use of "batch solutions" containing partially decomposed precursors became common. The complexity of typical syntheses, in terms of number of reactants, steps, and kinetic control, hampers their understanding from the chemical point of view.

4.5.4. Recent Mechanistic Studies. However, a recent systematic study on the Ni_xP−TOP shed light on some important aspects of the reaction:[685] with high Ni/P ratio, Ni(0) nanoparticles formed as intermediate while Ni_xP_y would immediately appear with lower ratio, with consequences on the composition and morphologies of the final colloids.

A more specific study was conducted using a Pd-directed synthesis of Fe_2P nanoparticles.[686] The authors used sacrificial Pd nanoparticles to rapidly form Pd−Fe alloy from Fe nanoparticles in an ultrasound bath. These intermediate species were reacted with TOP to form Fe_2P nanorods (containing Pd atoms) that exhibited the same diameter as the starting Pd nanoparticles. Very interestingly, PH_3 and NH_3 were identified by a gas sensor and were believed to form from TOP and oleylamine under the catalytic action of Pd. Their removal by an argon stream was detrimental to the formation of Fe_2P, but a too high concentration in PH_3 (provided by an external bottle) would block the Pd active site.

Additionally, another recent study deciphered the mechanism of diffusion of the P in Co nanoparticles, by analyzing the phase evolution over time (Figure 50).[683] This study highlights that both Co_2P and CoP nanoparticles contain excess Co, and unraveled the role of surface passivation by a shell of amorphous Co−P on the final hollow morphology of the nanoparticles. In the case of Ni_2P nanoparticles, a recent study, based on EXAFS and XANES spectroscopies, revealed three steps in the decomposition: complexation, nucleation, and phosphidation.[684]

More mechanistic studies would be needed to understand in-depth the complex mechanisms at stake in the TOP route. These investigations would be easier if the synthetic processes were limited to one-step processes, and without involving sophisticated procedures such as time-controlled additions of

dx.doi.org/10.1021/cr400020d | Chem. Rev. XXXX, XXX, XXX−XXX

Table 7. Synthesis of Metal Phosphide Nanoparticles with P_4 as the Primary Phosphorus Source[a]

M	phase	process	ox.	conditions: temp, time, solvent(s), additives,	resulting morphology	ref
Fe	Fe_2P	solvothermal	+2	180 °C, 48 h, ethylenediamine	100−120 nm faceted nanoparticles	706
	FeP	thermal activation	0	180 °C/250 °C, 2 h, octadecene and oleylamine	10 nm plain amorphous (180 °C) or hollow crystallized (250 °C)	717
	FeP_2	solid-state reaction	+2	700 °C, 40 h, in sealed silica ampules	submicronic crystallites	714
Co	Co_2P	solvothermal	+2	220 °C, 30 h, EtOH	micronic hollow nanospheres or nanotubes	703
			+2	80−140 °C, ethylenediamine	aggregated nanoparticles (ca. 25 nm)	700
			+2	160 °C, 16.6 h, water, EtOH, sodium acetate, sodium dodecyl benzene sulfonate	urchin-like micronic, aggregated	705
		hydrothermal	+2	190 °C, 48 h, water, polyacrylamide	rod-like or flower-like	704
	CoP_3	solvothermal	+2	plateau at 130 °C, 15 h, 275 °C, 2 days, toluene, annealing 500 °C	aggregated nanoparticles (ca. 250−300 nm)	715
		solid-state reaction	+2	600 °C, 40 h, in sealed silica ampules	bulk pellet	714
Ni	Ni_2P	solvothermal	+2	200 °C, 16 h, EG, EtOH, and water, urea, SDS	hollow submicronic spheres	699
			+2	80−140 °C, 12 h, ethylenediamine	aggregated nanoparticles (ca. 25 nm)	700
			+2	180 °C, 12 h, glycol, water	dendritic	707
		hydrothermal	+2	160 °C, 12 h, water and ammonia liquor	aggregated nanoparticles <100 nm	232
		electroreduction	+2[b,c]	DMF, Et_4NBr, P_4, emulsified under argon at 50 °C, has to be present before the reduction	powder, surface area of 200 m^2/g	708
		thermal activation	0[c,d]	100 °C, 1 h (rt when starting from a complex) in toluene, annealing 100 °C, 4 h (respectively, 300 °C, 1 h)	dispersed nanoparticles (5−20 nm) (respectively, aggregated nanopowder)	49
	Ni_2P−Ni	thermal activation	0[d]	rt to 220 °C, 15 min to 2 h, oleylamine, TOP,	core−shell Ni_2P−Ni or amorphous Ni_xP dispersed nanoparticles	713
	$Ni_{12}P_5$	hydrothermal	+2	180 °C, 15 h, water, PEG, hexamethylenetetraamine	200 nm hollow spheres	701
	NiP_2	solvothermal	+2	plateau at 130 °C, 15 h, 275 °C, 2 days, toluene, annealing 350 °C	aggregated nanoparticles (ca. 50−100 nm)	715
		solid-state reaction	+2	500 °C, 40h. In sealed silica ampules.	100−600 nm aggregated nanoparticles	714
Pd	PdP_2, Pd_5P_2	thermal activation	+2	rt, 3 h, DMF, annealing: 400 °C, 4 h	nanopowder with a mixture of phases	720
	Pd_6P, Pd_3P_2	thermal activation	0[c]	12 h, RT THF, likely amorphous (crystallinity is not indicated)	polydispersed nanoparticles (mean size: 140 nm for Pd_3P_2, 65 nm for Pd_6P)	720
	PdP_2	solid-state reaction	+2	500 °C, 40 h, in sealed silica ampules	micronic domains	714
	PdP_2	thermal activation	0	310 °C, 2 h, octadecene, oleylamine	5−10 nm, potato shaped	717
	Pd_5P_2	thermal activation	0	310 °C, 2 h, octadecene, oleylamine	5−10 nm, potato shaped	717
Cu	Cu_3P	solvothermal	+2	80−140 °C, 12 h, ethylenediamine	aggregated nanoparticles (ca. 25 nm)	700
			+2	200 °C, 17 h, water, EtOH, ethylene glycol, EDTA	hollow micronic spheres	711
			+2	140−180 °C, 12 h, glycol, EtOH, water	ca. 100 nm hollow spheres	712
		hydrothermal	+2	140 °C, 10 h, water and ammonia liquor	sheet-like, ca. 20 nm	232
		thermal decomposition	0	250 °C, 2 h, octadecene, oleylamine	ca. 50 nm, polydispersed	717
	CuP_2	solvothermal	+2	plateau at 130 °C, 15 h, 275 °C, 2 days, toluene, annealing 350 °C	aggregated nanoparticles (ca. 100−300 nm)	715
		solid-state reaction	+2	500 °C, 40 h, in sealed silica ampules	micronic textured powder	714
Zn	Zn_3P_2	thermal activation	0[c]	rt, 15 min, THF, TOP or trioctylamine	1−5 nm amorphous dispersed nanoparticles	50
Ga	GaP	solvothermal	+3	Na_3P prepared in situ in dimethylbenzene (120 °C, 10 h), the metal is then added (100 °C, 2.5 h)	aggregated nanopowder	710
		sonochemical	+3	in situ synthesis of Na_3P (2 h, 20 kHz, 17 W/cm^2), the metal is then added (3 h, same sonication), annealing 600 °C	aggregated nanopowder	709
In	InP	solvothermal	+3	180 °C, 12 h, to get In/InP core−shell, then a treatment with HCl for 20 h at RT, water, ethanolamine, $NaBH_4$	520 nm hollow spheres, shell thickness 110 nm	702
		sonochemical	+3	in situ synthesis of Na_3P (2 h, 20 kHz, 17 W/cm^2), the metal is then added (3 h, same sonication), annealing 250 °C	aggregated nanopowder	709
		thermal activation	0[c]	rt, 15 min (respectively, 180 °C, 2 h), THF (respectively, diethylene glycol), TOP or trioctylamine (respectively, oleylamine)	2−10 nm amorphous (respectively, 5−25 nm crystallized) dispersed nanoparticles	50
		chemical reduction	+3[e]	1−5 h, 40−75 °C, EtOH, toluene, $NaBH_4$	5 nm dispersed nanoparticles	719
Pb	Pb_2P	thermal activation	0[c]	150 °C, 1 h, 1-octadecene	5−10 nm dispersed nanoparticles	50

[a]Oxidation degree of the metal precursor. [b]Ni(0) is generated in situ by electroreduction. [c]Organometallic complex. [d]Preformed nanoparticle. [e]In(0) generated in situ by chemical reduction.

dx.doi.org/10.1021/cr400020d | Chem. Rev. XXXX, XXX, XXX−XXX

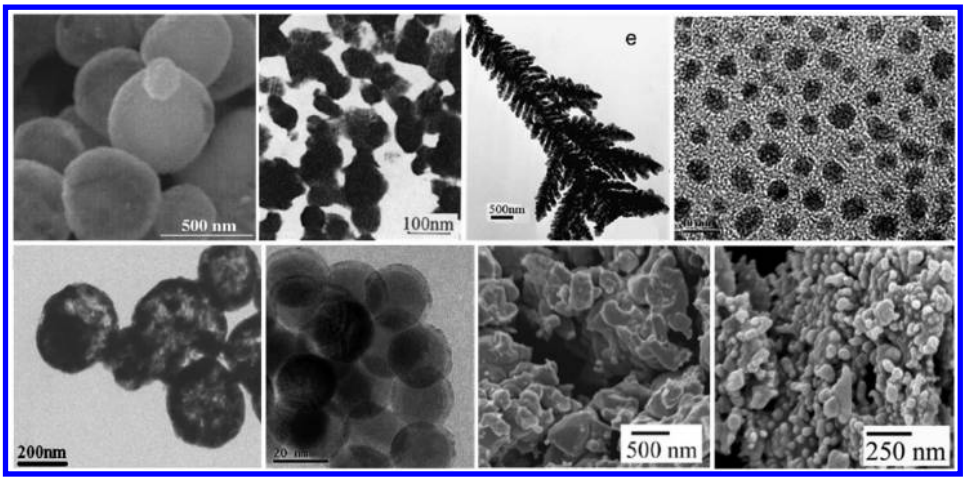

Figure 51. Ni–P nanoparticles obtained with P_4 as a primary "P" source. Top: Representative Ni_2P structures (refs from left to right: 699, 232, 707, 49). Bottom: From left to right, hollow $Ni_{12}P_5$, core–shell Ni_2P–Ni, NiP_2, and NiP_2 (refs from left to right: 701, 713, 714, 715). Reprinted, respectively, with permission from refs 699, 232, 707, 49, 701, 713, 714, 715. Copyright, respectively, 2008 Elsevier, 1999 Elsevier, 2007 Elsevier, 2008 Royal Society of Chemistry, 2009 Elsevier, 2011 American Chemical Society, 2009 American Chemical Society, 2008 American Chemical Society.

Scheme 4. Representative Reactions between Ni Precursors and White Phosphorus[a]

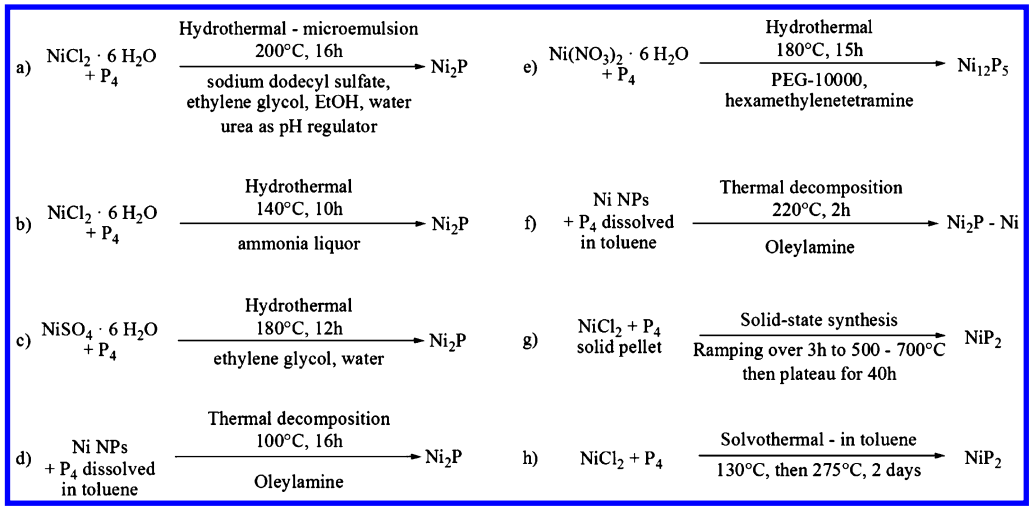

[a]Parts a–d correspond to the top row in Figure 51 and e and f to the bottom row (from left to right). See Figure 51 for references.

reactants, very strict temperature ramping rates, or the use of other process parameters that strongly affect the kinetics of the reactions.

4.6. Alternative to TOP: Other Alkyl- and Arylphosphines

Even though it largely dominates today's literature, TOP was not the only phosphine used as a "P" source. HP^tBu_2 was reacted on $ZnEt_2$ for the synthesis of Zn_3P_2 nanoparticles exhibiting a strong luminescence.[687] Co_2P nanoparticles supported on mesoporous silica were obtained by the direct decomposition of grafted Co_4-bisphosphine clusters on the silica surface.[620] GeP thin films (not pure) were obtained from primary ($CyPH_2$) and secondary (Ph_2PH) phosphines,[688] while Co–P amorphous films were deposited from $Co_2(CO)_8$ and PMe_3.[689] The sonochemical reaction of PEt_3 on a Fe(0) precursor yielded FeP nanoparticles.[690]

Similarly, WP nanoparticles were obtained from a W(0) carbonyl precursor and PPh_3 (850 °C).[691] This latter phosphine was used in the preparation of InP nanocrystallites in benzene,[692] and InP and GaP nanowires between 350 and 400 °C. Later, the reaction was extended to a solvent-free approach in vacuum sealed tubes, to other metals, and resulted in nanowires of Ni_2P, NiP_2, Fe_2P, FeP, Co_2P, and CoP where the phase was controlled by the M/P ratio.[693,694] Additionally, nickel–nickel phosphide composite nanoparticles were obtained with PPh_3, but the precise localization of both parts was not achieved.[695,696] Ni_2P hollow nanoparticles with a tunable void were prepared by changing the concentration of PPh_3.[697]

Tri(m-tolyl)phosphine was utilized to prepare InP nanofibers and GaP, MnP, CoP, and Pd_5P_2 nanocrystals in sealed ampules, at 370 °C.[698]

4.7. Elemental Phosphorus

During the past decade, the solution routes have been largely extended. First of all, historical sources of phosphorus, elemental P (white or red), have been used anew for the production of metal phosphide nanoparticles: the use of softer conditions (no annealing) and molecular metal precursors (chlorides, nitrates, etc.) prevented the aggregation of the product into large crystals.

dx.doi.org/10.1021/cr400020d | Chem. Rev. XXXX, XXX, XXX–XXX

Scheme 5. Soluble-P_4 Stoichiometric Route to Metal Phosphide Nanoparticles[a]

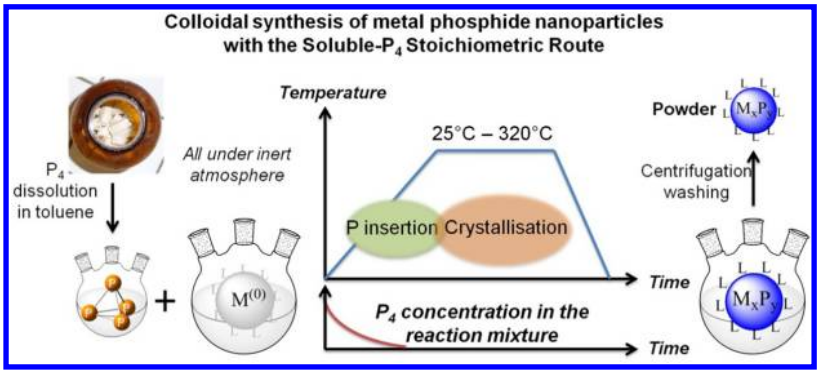

[a]Under inert atmosphere, P_4 (white solid) is dissolved into toluene and added at room temperature to a solution of M(0) nanoparticles. This solution is heated to the desired temperature. The P_4 molecules dissociate on the metal particles, and P atoms are quantitatively inserted into the particles. The crystallization of the metal phosphide nanoparticles follows. After cooling down, they are separated by centrifugation and washed to remove excess surface ligands and solvent.

4.7.1. White Phosphorus P_4. The reaction of excess amounts of P_4 in hydrothermal or solvothermal processes (usual solvent: ethylenediamine, water, EtOH, and mixtures) yielded polydispersed nanocrystallites of Ni_2P,[232,699,700] $Ni_{12}P_5$,[701] Cu_3P,[700,701] InP,[702] Co_2P[700,703,704] urchin-like Co_2P,[705] and Fe_2P[706] (see Table 7).

In these syntheses, phosphorus was introduced in large excess (typically, 1−5 equiv of P_4 vs the metal), and the precursors were at the M(II) state. Using mixtures of solvents, complex shapes such as dendrites of Ni_2P were obtained.[707] Additionally, electroreduction of Ni(II) in liquid ammonia (a traditional solvent for metal phosphide synthesis) in the presence of P_4 at 160 °C provided Ni_2P nanocrystallites.[708] Lastly, P_4 could be used as a starting material for the in situ preparation of Na_3P with Na, in the sonochemical synthesis of InP and GaP nanocrystals.[27,709,710] Selected morphologies obtained using P_4 for the synthesis of Ni_2P nanoparticles are shown in Figure 51 (see also Scheme 4). They highlight a large diversity although some of the nanoparticles were obtained in an aggregated form.

It must be noted that, in these reactions, P_4 is introduced as solid pieces and generally does not react directly with the metal source, but it is transformed into intermediate species such as phosphate or PH_3,[711,712] depending on the reaction conditions (pH, protic or aprotic solvent, etc.). In a few exceptions, that is when only the metal precursor can react with it (dry and aprotic solvent), P_4 served directly as a "P" donor.

As shown in Schemes 5 and 6 and Figure 52, starting from M(0) precursors (molecular complexes or nanoparticles), the reaction of P_4, as a molecular stoichiometric reagent dissolved in toluene, yielded well-dispersed metal phosphide nanoparticles (Ni_2P, InP, Zn_3P_2, Pb_2P) in mild conditions (room temperature to 220 °C, 15 min to 2 h) that were optimized through reaction monitoring by ^{31}P NMR of the supernatant.[49,50]

Starting from molecular metal(0) precursor could also lead to phase mixtures. Use of a Pd(0) complex [$Pd_2(dba)_3$, dba = dibenzylideneacetone] yielded polydispersed submicronic Pd_6P and Pd_3P_2 particles, yet the Pd/P initial ratio of 1 was not conserved in the product as both phases precipitate separately.[716] The difference between the nickel case, which gave a single-phase product in a stoichiometric fashion, and the palladium case discussed here are 2-fold: (i) $Pd_2(dba)_3$ is more stable, as a precursor, that [Ni(1,5-cyclooctadiene)$_2$], and thus

Scheme 6. Representative Syntheses of MP Nanoparticles Using the Soluble-P_4 Stoichiometric Route[a]

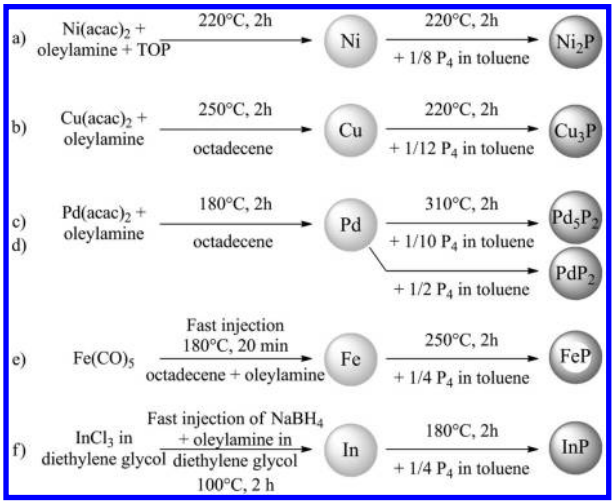

[a]TEM observations of the nanoparticles are depicted in Figure 52.

less prone to a reaction with P_4, and (ii) more strenuous conditions are required to crystallize the nanoparticle products in the case of palladium, as demonstrated in ref 717 (see below), which makes the identification of the final products more difficult when using XRD.

The route from preformed metal(0) nanoparticles was further extended to Pd, Fe, and Cu. While phase control could be demonstrated in the case of Pd (Pd_5P_2 vs PdP_2) and Cu (Cu_3P vs CuP_2) by using the corresponding M:P stoichiometries in the synthesis, differences in the propensity of the metal phosphide nanoparticles to undergo crystallization were also demonstrated. Indeed, Cu_3P and Ni_2P crystallized in mild conditions (T < 220 °C) while Pd_5P_2 and PdP_2 had to be heated to 310 °C to undergo crystallization. At this latter temperature, Pd_3P would not yet crystallize, highlighting an effect of the M:P ratio on the crystallization.[717,718]

As a natural development of this "soluble-P_4 stoichiometric route", the use of substoichiometric amounts of P_4 on Ni nanoparticles lead to core−shell Ni_2P−Ni nanoparticles with a tunable shell thickness.[713] The formation of this inverted structure, where the metal phosphide is in the core, will be discussed in subsection 6.3.1. Interestingly, direct core−shell

dx.doi.org/10.1021/cr400020d | Chem. Rev. XXXX, XXX, XXX−XXX

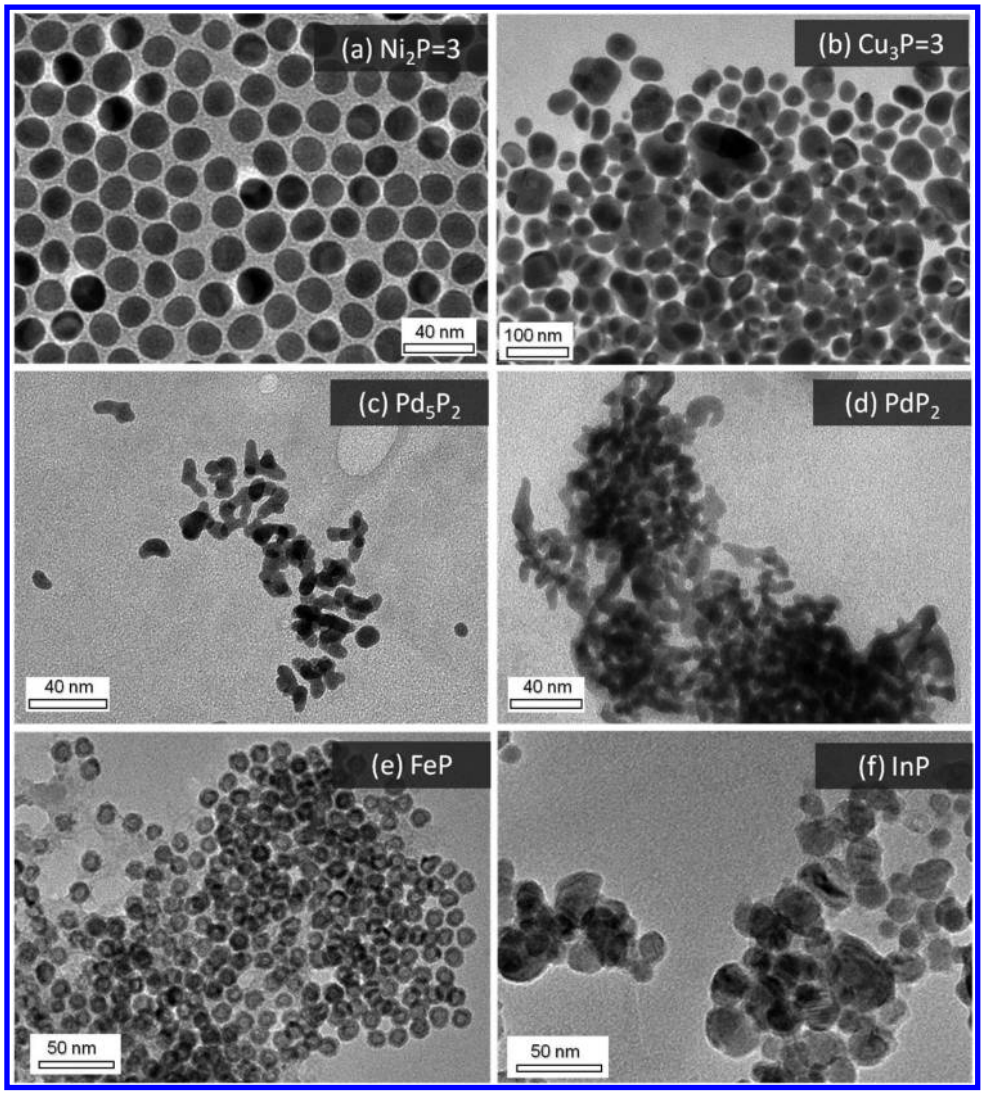

Figure 52. Selected examples of nanoparticles prepared with the soluble-P_4 stoichiometric route. References: for part a, ref 713; for parts b–e, ref 717; for part f, ref 50. Reprinted, respectively, with permission from refs 713, 717, 50. Copyright, respectively, 2011 American Chemical Society, 2012 American Chemical Society, 2010 Royal Society of Chemistry.

structures (with the metal inside and the metal phosphide outside) could also be obtained using copper nanoparticles, through a more predictable mechanism. Even under mild reaction conditions (100 °C), Cu_3P is able to crystallize. Thus, incomplete reaction of copper nanoparticles with P_4 leads to Cu–Cu_3P core–shell nanoparticles.[717]

Starting from oxidized precursors, such as metal chlorides, two routes have been used. An additional reductant ($NaBH_4$ in EtOH) was added to a solution of P_4 and $InCl_3$ in toluene, producing InP nanoparticles at 75 °C.[719] However, an excess of phosphorus (2:1) had to be added to avoid In remaining as a byproduct, thus pinpointing the occurrence of side reactions. Additionally, P_4 may also react with $NaBH_4$ before it reacts with In, meaning that it would just serve as a raw material. P_4 (excess) dissolved in DMF was also reacted with $Pd(acac)_2$, producing an amorphous product that was converted by annealing into a mixture of Pd_5P_2 and PdP_2.[720]

More elegantly, part of P_4 itself was used to reduce the metal center (and was thus added in the exact required excess), giving PCl_3 as a byproduct, while the rest reacted as the "P" donor: phosphorus-rich metal phosphide aggregated nanoparticles were obtained by this route through a reaction at 130 °C, followed by annealing for two days at 275 °C (CuP_2, CoP_3, NiP_2).[715] This reaction could be extended to using P_4 or red P in the gas phase at 500–700 °C for ca. 2 days (lower temperatures are possible, though), and yield submicronic powders of FeP_2, CoP_3, NiP_2, CuP_2, and PdP_2.[714]

4.7.2. Red Phosphorus. Red phosphorus was also used as a source of "P" in the hydrothermal synthesis of aggregated[721] or well-dispersed[722] $Ni_{12}P_5$, as well as Ni_2P nanoparticles and well-dispersed InP nanoparticles, assisted by a complexing agent (ethylenediamine tetraacetic acid).[723] In a solvothermal process, the synthesis of Ni_2P nanoparticles from $NiCl_2$ hexahydrate[724] was achieved with a long reaction time (20 h) but a relatively low temperature (180 °C). Similarly, Sn_4P_3 nanoparticles were obtained at 200 °C for 40 h.[725] These temperatures of reaction are indeed relatively low, considering that red P is quite difficult to decompose. By comparison, Ni_2P, Cu_3P, and CoP nanoparticles[726] and Ni_3P–Ni thin films were also prepared using red phosphorus, but its decomposition in a gas phase required higher temperatures (>400 °C).[727] Indeed, the lack of reactivity of red P could be compensated by the use of higher temperatures: single crystals of $Ce_3Zn_{2-x}P_4$ and $Ce_4Zn_{2-x}P$ were obtained by heating in molten salts and

dx.doi.org/10.1021/cr400020d | *Chem. Rev.* XXXX, XXX, XXX–XXX

annealing.[728] Similarly, ternary Au phosphide alloys (Hg, Pb, Tl) were obtained in liquid lead.[729]

4.8. Alternative Phosphorus Sources

PCl_3 was used as a source of phosphorus in a reaction with Na and a Ni(II) precursor to yield Ni_2P nanoparticles.[730] Similarly, InP nanocrystals were synthesized using both PCl_3 and a strong reductant ($LiBEt_3H$).[731] It was also used to convert W(0) into WP on a flat surface.[732]

Tri-n-octylphosphine oxide (TOPO) was used as a "P" source in the synthesis of Co_2P branched nanostructures at 350 °C.[733]

Oxide metal precursors such as NiO were reduced in the presence of $(NH_4)_2HPO_4$ in a nonthermal H_2 plasma to provide WP, GaP, InP, MoP, Co_2P, CoP, Ni_3P, and Ni_2P.[734,735]

Other sources of "P" include GaP, which was used in a transmetalation reaction with Zn in the gas phase (ca. 1300 °C), to produce Zn_3P_2 nanowires and "nanotrumpets"[736] or Cd_3P_2 and Zn_3P_2 nanobelts.[737]

4.9. Alternative Processes

From a fundamental point of view, In−P clusters,[738] Al−P clusters with various charges, and Cd_3P_2 clusters[739] were "synthesized" by DFT, and their bonding and physical properties were studied, as a model for larger nanoparticles.

Supercritical fluids[740] and flash evaporation technique[741] allowed the deposition of nanostructured InP thin films. Very interestingly, $P(SiMe_3)_3$ could also be used in a microfluidic reactor to produce well-controlled quantum dots at 225 °C.[742] Moreover, the synthesis conducted in a microfluidic reactor in supercritical octane provided high-quality nanocrystals in very short time (2 min) thanks to the high diffusivity of the precursors.[743]

High-temperature methods such as metal−organic vapor phase expitaxy (working at 450−700 °C) provided access to InP nanoparticles, nanowires,[744,745] nanotubes, and porous nanostructures free of surface impurities. Both the growth mechanisms[746−750] and the confinement properties could be studied from experimental and theoretical points of view.[751−758] More complex morphologies such as heterostructured pearl-like InP−ZnS nanowires,[759] Zn_3P_2−ZnS,[760] Zn_3P_2−ZnO,[761] AlP−GaP,[762] and GaInP−GaP[763] core−shell nanowires, but also twinned InP,[764,765] tripods of InP nanowires,[766] alternated zinc-blende and wurtzite InP nanowires,[767] and Zn_3P_2 nanowires,[768] were also obtained by physical routes, including the use of high-temperature induction furnace (ca. 1250 °C) (Figure 53). The use of Sn nanoparticle catalysts in CVD provided $ZnGeP_2$ nanowires in a single step, from $ZnGeP_2$ solid-source powder, at 650 °C.[769] Au nanoparticles catalysts were used to prepare GaP−ZnS nanowires from GaP−ZnS powders at 1150 °C.[770]

Carbothermal reduction of a gel allowed the incorporation of Fe_2P, Co_2P, and $Ni_{12}P_5$ nanocrystals in carbon xerogel that was pyrolized at 800 °C for 3 h under nitrogen atmosphere.[771] It also led to MoP supported on carbon.[772] Moreover, dry autoclaving methods provided easy access to metal phosphide nanopowders.[34,773]

InP polydisperse nanoparticles were also obtained by laser ablation of bulk InP in an aqueous environment.[774] The coupling of a gas-phase plasma synthesis and a colloidal step yielded InP−ZnS nanoparticles with good luminescence yield (15%).[775]

Lastly, CoWP films could also be deposited by electroreduction of sodium hypophosphite and metal precursors.[776]

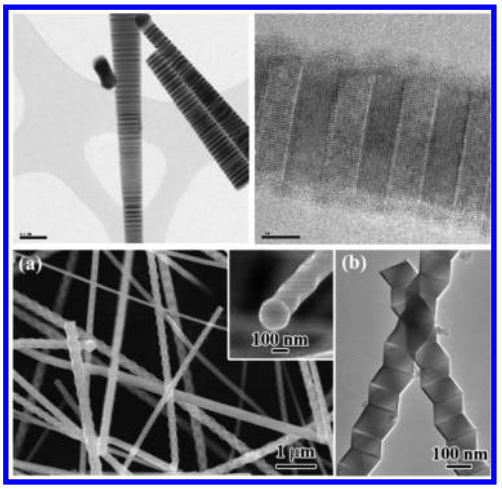

Figure 53. Top: InP twinned nanowires. Reprinted with permission from from ref 764. Copyright 2008 Nature Publishing Group. Bottom: Zn_3P_2 twinned nanowires. Reprinted with permission from ref 768. Copyright 2008 American Chemical Society.

Thin films[777] and nanowires[778] of InP were also obtained by electrochemistry. InP thin films were passivated by a controlled electrochemical oxidation in NH_3 and functionalization by a monolayer of Pt clusters.[779] Surface functionalization of GaP was chemically achieved by a preliminary Cl-functionalization using PCl_5, protecting them from oxidation in air, and a secondary functionalization using Grignard reagents.[780]

4.10. Summary for Nanoscaled Metal Phosphides

Altogether, the 2000−2012 years have seen huge progress in the synthesis of metal phosphide nanoparticles (Figure 54).

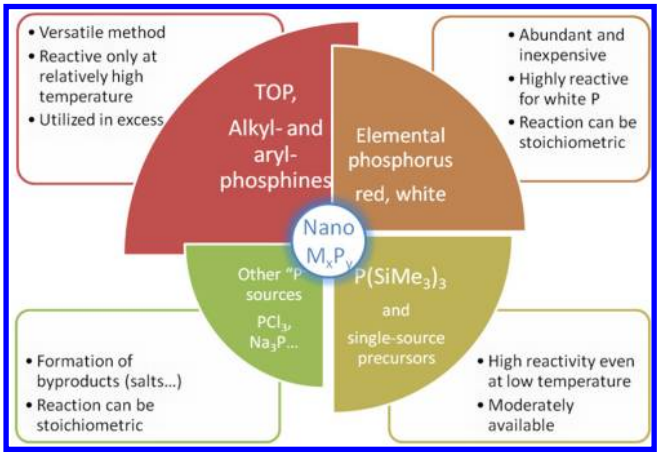

Figure 54. Overview of the main "P" sources for the synthesis of metal phosphide nanoparticles. The size of each slice accounts for the relative use of each method in the past decade.

Thermal decomposition of TOP has emerged as a powerful route to produce them at lower cost, on the lab scale, while the use of more reactive (and, ideally, stoichiometric) sources such as P_4 or $P(SiMe_3)_3$ seem more favorable to gain insight about the intermediates and mechanisms of reaction.

dx.doi.org/10.1021/cr400020d | Chem. Rev. XXXX, XXX, XXX−XXX

5. PROPERTIES OF NANOSCALED METAL BORIDES AND METAL PHOSPHIDES

5.1. Li-Ion Batteries

5.1.1. Overview. In the field of Li batteries, the distinction between bulk and nanoscaled materials is becoming of major importance. Most materials are indeed ground before being incorporated into electrodes, and thus present sizes lowered into the submicrometer or nanometer ranges. Downscaling also raises the question of the material mechanical integrity through cycling and its dependency on the size of the crystal domains and the size of the overall aggregates: electronic percolation must be guaranteed, but diffusion distances must not be too important in the solid. Additionally, interfaces are the locus of very complicated chemical and electrochemical reactions, with the electrolyte and the other components of the cell. As a consequence, the compromise between surface area and crystallinity is not the same as in catalysis for instance. With this aspect in mind, major papers of the 2000−2012 period are reviewed in this subsection (see ref 32 for a dedicated review). Although metal phosphides can be considered as a "hot topic" in the field of Li-ion batteries, it is not the case of metal borides. Surprisingly, apart from allusions about their inertness,[781] no study reports the electrochemical behavior of these compounds versus lithium, and metal borides seldom appear as Li-inactive materials in nanocomposite electrodes.

5.1.2. Major Advances in the Field: The Case of Metal Phosphides. As a matter of fact, the field of metal phosphides for lithium batteries is young since the first report was published in 2002: Nazar and co-workers described the promising Li uptake by a CoP_3 electrode through a conversion mechanism.[782] "P" was found to play the role of a redox shuttle: Li_3P was identified at the end of the discharge, and subsequent cycling occurred between this phase and the LiP phase. A redox role of the phosphorus center was later identified also in NiP_2 electrodes.[285]

More classically, MnP_4[284,783,784] and TiP_4[785,786] were found to be good intercalation materials for Li, forming Li_xMP_4 phases. Monoclinic NiP_2 exhibited a mixed behavior, starting with intercalation and ending with conversion, as evidenced by the formation of Ni nanoparticles after the discharge.[787] A similar behavior was identified later for NiP_3 electrodes, although the capacity was found to fade more rapidly.[788]

Other phases such as Mn based alloys,[789] Fe−Sb−P alloys,[790,791] Fe−Sn−Sb−P alloy,[792] Sn_4P_3,[793] Zn_3P_2,[794] ZnP_2,[795] FeP,[796,797] FeP_2 and FeP_4,[798] Ni_3P,[799] VP,[800] and VP_2[801] were then investigated.[802] Recently, a new metastable compound obtained by ball milling (tetragonal Ni_2SnP) was tested, but it transformed back into the orthorhombic thermodynamic phase upon cycling.[803]

5.1.3. Nanostructuration of the Electrodes. Nanostructuration of the electrodes[28,29] was soon envisioned as a tool to improve the kinetics of the reaction with Li (by shortening the diffusion lengths) and to manage volume expansion of the electrode upon Li incorporation.

Metal phosphides as active materials were then scaled down for both better kinetics and better mechanical accommodation of the stress generated by volume variations (NiP_2,[804] $SnP_{0.94}$,[43] GaP,[805] Cu_3P,[806] MoP_2,[807] ZnP_2[808]). Ni_3P ordered porous films exhibited enhanced electrochemical Li incorporation in terms of both capacity and reversibility due to a good contact with the electrolyte.[809] Ni_5P_4, NiP_2, and Ni_2P nanoparticles were recently investigated.[810−813] The formation of a carbon layer around the nanoparticles was found to be crucial to compensate for the lack of electronic conductivity of this latter phase.[814,815] Interestingly, amorphous electrodes of a FeP_2 nanopowder were also found to exhibit a fairly good capacity retention, although the structure of the powder after extended cycling has not yet been studied.[639] In the case of CoP, which undergoes successive insertion and conversion reactions, it was shown that the insertion potential is merely not affected by nanosizing, while the conversion reaction became strongly asymmetric in this case because of the formation of new interfaces in the electrode.[816] Interestingly, the use of shaped Co_2P and CoP nanoparticles (nanorods and plain and hollow particles) has been proposed as a way to further optimize the electrode properties.[817]

Some metal phosphides and metal borides were also used in nanocomposite electrodes, namely, a Fe_2P−$LiFePO_4$ cathode[818] and a Si−TiB_2 anode.[819] The electronically conductive MPs and MBs were inactive versus Li but acted as networks for electron conduction and as matrices for restraining volume expansion of the active materials during cycling.

5.2. Alkaline Aqueous Batteries

5.2.1. Primary Alkaline Batteries. A growing number of reports has been dedicated to metal borides and phosphides as high capacity electrodes for alkaline aqueous batteries in the past few years. The ability of these materials to undergo multielectron redox reactions is the fundamental property for such a craze.

Studies have focused first on metal borides, including crystalline TaB, TaB_2, TiB_2, VB_2,[820−823] amorphous Fe−B and Co−B, and crystalline CoB[431] anodes. Different irreversible reactions are at play, whether the corresponding metal is corroded or is passivated in the acid−base and redox conditions of the working cell:[820]

$$TiB_2 + 12OH^- \rightarrow Ti_{passivated} + 2BO_3^{3-} + 6H_2O + 6e^- \quad (41)$$

$$VB_2 + 20OH^- \rightarrow VO_4^{3-} + 2BO_3^{3-} + 10H_2O + 11e^- \quad (42)$$

Bulk TiB_2 and VB_2 reached capacities of, respectively, 1600 mA h g^{-1} and 3100 mA h g^{-1} at 100 mA h g^{-1} discharge rate in metal boride/air cells with 30% KOH aqueous electrolyte. These experimental values are approximately 70% of the theoretical ones, as compared to the calculated maximum capacity of zinc of 820 mA h g^{-1}.[820] High capacity retention at large rate was also evidenced, thus making metal diborides high energy and high power anodes. Interestingly, the example of alkaline aqueous batteries highlights the impact that alloying metal and boron can have on the electrochemical properties.[820] In the same conditions, elemental boron is totally inert, and the parent metals are inactive because of deep passivation. First, because alloyed boron in diborides is electronically enriched, it is more prone to oxidation. Also, metal borides are more electronically conductive than pure boron. Both factors favor the participation of boron atoms to the total capacity in alkaline as well as neutral electrolytes.[820,824] Second, incorporation of electronegative boron negatively shifts the electrode potential compared to pure metal. Therefore, the metal is not any more (V) or less (Ti) passivated and is readily oxidized, thus ensuring complete reaction. The counterpart of the high electrochemical activity of metal borides is their spontaneous corrosion in contact with the electrolyte. To overcome this obstacle and

dx.doi.org/10.1021/cr400020d | Chem. Rev. XXXX, XXX, XXX−XXX

increase the battery lifetime, Licht and co-workers deposited a buffer layer of ionically conductive zirconia between the electrolyte and the metal boride electrode.[821−823] The resulting VB_2/air battery exhibits a volumetric capacity even higher than that of gasoline.[823] The same group showed evidence of improved capacity for smaller metal boride particle size, presumably because of enhanced reactions kinetics.[30,31] Further feasibility studies suggested that even if metal boride/air batteries were not electrochemically rechargeable, VB_2 could be recovered from the discharged cell by Mg-mediated reduction of the oxidized anode materials.[823]

Because of their structural similarities with metal borides, metal phosphides could also turn out efficient multielectron high capacity anodes for alkaline aqueous batteries. This was shown for Sn_4P_3[825] and more recently submicroscale VP_x (x = 1, 2, 4).[826] The reported capacities are nevertheless lower than those obtained with VB_2 anodes, probably because of a larger amount of spontaneous corrosion in contact with the electrolyte.

5.2.2. Secondary Alkaline Batteries. Metal borides are also currently studied in the framework of rechargeable alkaline aqueous batteries. The presence of residual hydrogen[479,522,536] in amorphous metal-rich boride nanoparticles obtained by borohydride reduction in solution (see subsection 3.8.3) led to the early suggestion that these compounds might be suitable negative electrodes in Ni-metal hydride cells. First tests performed by Mitov et al.[827,828] and Wang et al.[829] tended to confirm this view. Some reports are still considering the formation of metal boron hydrides as plausible,[539,550,830,831] but recent works[551,832,833] nicely reviewed by Zhao et al.[834] lead to the current consensus that hydrogen sorption has only a minor contribution to energy storage. Indeed, crystalline cobalt borides Co_3B,[833] Co_2B[830,833] and CoB[431,833] have also good capacity and cycling stability, even if they do not show any significant hydrogen sorption.[431,828,835] Although differences between amorphous and crystalline metal borides[836] both in terms of crystal structure and particle size/surface area hinder direct comparison of their performances (ranging between 250 and 350 mA h g^{-1} after 100 cycles), the common mechanism seems to be similar to the oxidation−reduction process described above for boron-rich metal borides in primary alkaline batteries. The charge reaction corresponds to reduction of the Co hydroxide into elemental Co, similar to the reaction occurring in Ni−Cd batteries:

$$CoB_x + (2 + 6x)OH^- \rightarrow Co(OH)_2(s) + xBO_3^{3-} + 3xH_2O + (2 + 3x)e^- \quad (43)$$

$$Co(OH)_2(s) + 2e^- \rightarrow Co(s) + 2OH^- \quad (44)$$

Equation 44 is reversible and ensures the major part of the energy storage process after boron has been largely dissolved. The same mechanism should also be at play for amorphous[832] and crystalline[837] Fe−B nanoparticles as well as amorphous Ni−B nanoparticles.[838] The role of boron atoms is 3-fold.[829,833] First, it contributes to the discharge capacity, at least in the first cycles. Second, it activates cobalt atoms by decreasing the potential of the electrode. Third, it leaves a clean, renewed surface after each cycle and B solubilization, which limits passivation and ensures good cyclability. The ability to recharge the battery arises from the low solubility of cobalt hydroxide and its facile reduction during charge. Some additives,[839,840] core−shell structures,[831,841] and ternary compositions (Co−B−S,[842] Mg−Co−B[843]) have been suggested to limit further the $Co(OH)_2$ solubility and enhance the cycling stability at high temperature.

It is noteworthy that high capacity, cycling rate, and cycling life could be achieved by enhanced kinetics through nanostructuration of Co−B electrodes into smaller nanoparticles,[539,842] submicronic chains or rods,[844] nanorods,[551] and mesoporous structures.[550]

5.3. Catalysis

The growing interest for hydrogenation reactions and, later, for hydrotreating processes with metal borides and metal phosphides[25,35,192,845] appears as a driving force for the development of synthetic routes toward high surface area materials (nanoparticles, supported and unsupported).

Catalytic applications of metal boride and metal phosphide nanoparticles started to develop in the 1990s with hydrogenation reactions. The next decade was a difficult time for the petroleum industry, as regulation on sulfur content and NO_x emission became more and more severe. Hydrotreating reactions with metal phosphides were thus largely investigated, and represent a huge proportion of the works on metal phosphide catalysis in the past decade. Altogether, nanoscaling offered a new golden youth to the field of metal phosphides in the 2000s. Metal borides, on the other side, remained confined to the field of hydrogenation reactions for which they are highly efficient in terms of activity and selectivity. This is only in the last 10 years that the scope widened, with the emergence of works on hydrotreating and hydrogen evolution from borohydrides for hydrogen storage and release. This subsection reviews the most significant trends in catalysis for nanoscaled metal borides and metal phosphides. One should bear in mind that if most of the studies dedicated to metal phosphides address crystalline phases which enable in-depth characterization with insightful calculation approaches, it is not the case of metal borides for which nanoscaled crystalline phases are extremely rare. On the contrary, nanoscaled metal borides are met as amorphous phases in the catalysis field,[25] except for the few exceptions mentioned below. It is noteworthy that metal borides and metal phosphides can even exhibit higher activity than noble metal catalysts.

5.3.1. Hydrogenation: A Driving Force toward Metal Boride and Metal Phosphide Nanoparticles. *5.3.1.1. Historical Background.* The discovery of amorphous metal borides, from precipitation in solution,[90,312] is contemporary with the recognition of their high catalytic activity for hydrogenation of various organic substrates.[312,521,846] Later, the huge potential of metal phosphide nanoparticles in hydrogenation catalysis was revealed in the 1990s,[847,848] after a pioneering work dealing with nitrobenzene hydrogenation over bulk Ni_2P.[102] Many reviews have covered this aspect of metal boride and metal phosphide properties, including those from Chen et al.,[35] Deng et al.,[192] Ganem et al.,[849] and, more recently, Wu et al.,[36] Alexander et al.,[33] and Pei et al.[25] For more details about the industrially relevant catalysts, the reader is redirected to the recent insightful and exhaustive review of Pei et al. dealing with nanoparticles of amorphous metal−metalloid alloys.[25]

5.3.1.2. Ultrafine Amorphous Alloy Particle Activity. Various alloy compositions (Ni, Fe, Co, Pd, P, B)[33,36,526] of nanoparticles obtained by precipitation in aqueous or organic solvents were studied. The activity of these so-called "ultrafine

dx.doi.org/10.1021/cr400020d | Chem. Rev. XXXX, XXX, XXX−XXX

amorphous alloy particles" (UAAPs)[35,192] was investigated for hydrogenation of various substrates such as benzene,[227,506,508,565,850−854] cyclopentadiene,[35,855] nitrobenzene,[486,511,533,534,543,547,856−859] furfural,[510,860] cynnamaldehyde,[548,569] 2-ethylanthraquinone,[503,504] sugars,[229,486,861−864] and nitriles.[532,534] Amorphous Ni−B and Co−B are especially recognized as catalysts with higher activity, selectivity, and poison resistance than their parent metal (Raney Ni and Co)[531,548,565,569,849] for hydrogenation of alkenes,[227,473,506,508,565,850−852,854,860,865] aldehydes and ketones,[229,486,503,504,507,548,567,860−862,865] nitro-derivates,[486,533,543,544,547,857,858,866] and nitriles.[532,534] Because these nanoparticles are precipitated in nondegassed water, they are partially oxidized and nonpyrophoric (see subsection 3.8), which is a strong advantage compared for instance to Raney Ni. However, the role of partial surface oxidation on the catalytic properties has been largely uncovered. Most of the alloys contain a large proportion of metal versus the heteroatoms (typical composition: M/(P,B) = 8 in mol). The B/P heteroelement has a primary role in the superior performances of these materials by ensuring a relatively thermally stable amorphous structure, with homogeneous dispersion of unsaturated reactive metal sites.[192,473] Crystallization, induced by heating and in the course of the reaction, was perceived as disadvantageous and was studied in order to be avoided.[35,192,867,868] In this respect, ternary and quaternary compositions were shown to improve the catalytic activity,[508] first by improving the local disorder, enhancing the thermal stability of the amorphous phase, and reducing the particle size.[507,508,869−871] A second beneficial effect of the additional metals is in the incorporation of Lewis acidic sites for sorption of the substrate (Cr, W, rare earths).[229,503,504,507,508,534,857,860,870,872]

5.3.1.3. Supported Catalysts. Dispersing the UAAPs on a suitable matrix was also shown to provide enhanced activity and lifetime. Nickel phosphides were deposited on SiO_2 for naphthalene hydrogenation, and good selectivity for decalin was obtained,[873] with or without the presence of N-containing species (quinoline).[874] Supports such as silica,[850,872,875−877] alumina,[506,565,851,853,865] zirconia,[852,854,865] MgO,[567] titania,[569] clays,[565] polymers,[878] carbon nanofibers,[879] and nanotubes[880] have been investigated for amorphous metal borides. The primary role of the supporting phase on these compounds is to ensure a good dispersion, enhanced structural stability, and resistance to sintering. Another strategy for increasing the surface area and stability of amorphous metal boron alloys and their catalytic activity for hydrogenation consists in developing mesoporous structures.[540,546,548]

5.3.1.4. Specific Effects of the Metalloid on the Activity. Other effects are specific to each heteroelement, more precisely to the direction of d electron transfer between the metal and the metalloid. Indeed, besides enhancing the stability of the amorphous phase, boron transfers some of its electrons to metal atoms for providing metal sites with enriched d population (see subsection 2.5.3).[192,881] This favors back-donation from the metal d orbitals to the antibonding π^* orbitals of the unsaturated bonds and enhances the catalytic activity of metal borides.[473] Modification in the d population by alloying could also impact the adsorption strength of the substrate and play a role in the enhanced activity.[875] Moreover, electronically enriched metal sites are less subjected to sulfur and amine binding, thus ensuring good resistance to poisoning and air exposure.[192,866] Interestingly, the resistance of amorphous metal phosphides to sulfur poisoning was also noticed,[531] but to a lesser extent than metal borides,[192] presumably because the metal in MBs is more electronically enriched than in MPs. All in all, it is still difficult to distinguish geometrical (particle size, surface area) and electronic (composition, direction of the electron transfer) effects in these systems. Especially, a direct comparison between amorphous alloys differing from the nature of the metal or of the metalloid (B, P) remains arduous because the characteristics of the catalysts, such as compositions and particle size, cannot be modified independently.[33,35,192,882] For instance, although electron transfer seems to be unfavorable to the activity of metal phosphides, Ni−P amorphous phases have been shown to be more active for hydrogenation of cyclopentadiene,[192] furfural,[510] and nitrobenzene[511] than Ni and amorphous Ni−B. Actually, amorphous nanoparticles of ternary Ni−P−B seem to benefit from both metalloids for providing higher catalytic activity for hydrogenation of furfural,[510] nitrobenzene,[511] and *p*-chloronitrobenzene[518] than binary alloys. Again, the reasons for these enhanced performances are still unclear.

5.3.1.5. Selectivity. Selectivity is also improved compared to the parent metal, especially for metal borides. Propensity of Cu−B[860] to selectively hydrogenate C=O bonds prior to C=C bonds could be ascribed to acidic boron atoms acting as an adsorption site for C=O groups. The same behavior was observed for conjugated C=O/C=C bonds on Co−B.[548,569,883] On the contrary, Ni−B hydrogenates selectively C=C bonds in the conjugated C=O/C=C system of citral, before hydrogenation of the remaining C=O bond prior to unconjugated C=C.[849,875,883] Similarly, Kukula et al. reported recently different selectivities for hydrogenation of nitriles with conjugated C=C/C≡N bonds depending on the metal: Co−B and Ni−B target respectively C≡N and C=C bonds.[534] Chloronitro-aromatics are also selectively reduced by amorphous metal borides to the corresponding amines without dehalogenation.[533,857] Ru−B catalysts are especially suitable for selective hydrogenation of benzene into cyclohexene.[850,851,853,865,884] A crystalline nickel phosphide promoted with TiO_2 or CeO_2 nanoparticles was demonstrated to hydrogenate phenylacetylene in EtOH (respectively heptenes in toluene) with good selectivities for styrene (respectively heptanes).[885] Ni_2P nanoparticles were also found to selectively hydrogenate a range of functional alkynes into alkenes in milder conditions (85 °C).[886] A selective hydrogenation of acetylene was also achieved on MoP,[887] while the selective hydrogenation of pyridine on MoP(001) was investigated by DFT.[888] Similarly, Pd_xP nanophosphides hydrogenated selectively olefins and polyolefins.[720,889,890] Other substrates were selectively hydrogenated, such as cynnamaldehyde with Ni_2P on SiO_2[891] and acetonitrile with Mo_xP,[892] although in this latter case, the reaction was highly sensitive to the M/P ratio: high ratio (x = 1.1) yielded majorly ethylamine while low ratio (x = 0.9) yielded more condensed amines such as diethylamine. Like activity, the hydrogenation selectivity of metal−metalloid alloys depends on various factors,[229] including compositions (nature of the metal, boron content, and metal d electron population), particle size and surface area, thermal stability of the amorphous phase, etc.

5.3.1.6. In Situ Production of the Catalyst. An alternative method of hydrogenation is to use $NaBH_4$ as reductant with in situ production of amorphous metal boride catalysts.[849] A wide range of substituted aromatics with functional groups NO_2,

dx.doi.org/10.1021/cr400020d | *Chem. Rev.* XXXX, XXX, XXX−XXX

C═O, C═C, C−Br was hydrogenated.[563,564,849,893] Alternatively, hydrazine can also be used.[878]

5.3.1.7. Enantioselective Catalysis. Hybrid colloidal catalysts have also been reported for enantioselective hydrogenation. Adsorbing[894] or grafting[523−525,895−898] asymmetric molecules on amorphous Fe−B, Co−B, and Ni−B nanoparticles produced in an aprotic solvent afforded good opportunities for such reactions. For instance, heterogeneous oxazaborolidines are efficient catalysts for asymmetric borane reduction of prochiral ketones to the corresponding alcohols.[523−525]

5.3.1.8. Dehydrogenation. Finally, dehydrogenation catalysis can also be performed by metal borides and metal phosphides. Amorphous phases have been particularly highlighted, like a Ni−P membrane[899] and Fe−B,[900] Fe−P,[901] Fe−P−B nanoparticles.[902]

5.3.2. Hydrotreating Reactions. *5.3.2.1. Overview.* Processes based on molecular hydrogen to remove elemental contaminants such as sulfur, oxygen, and nitrogen from various substrates are embraced under the generic name hydrotreating. The ever increasing environmental concerns have led to stringent regulations concerning transportation fuels. This initiated a strong research effort from the materials and catalysis communities for hydrotreating of petroleum feedstocks, especially for sulfur removal. Hydrodesulfurization (HDS) is the primary hydrotreatment which is intensively employed and studied in order to improve petroleum-related fuels. Hydrodeoxygenation (HDO) is the second hydrotreating reaction of interest, targeting upgraded bio-oils, especially from lignocellulosic biomass, as substitutes for fossil fuels.[903,904] The objective is to reduce the oxygen content which is responsible for detrimental characteristics such as high viscosity, immiscibility with hydrocarbon fuels, poor heating value, corrosiveness, low thermal stability, and short lifetime.[903] Hydrotreating also encompasses hydrodenitrogenation for hydrocarbon feedstocks and hydrodechlorination for environmental remediation.

Current hydrotreating catalysts are mainly metal sulfides, but increasing restrictions on fuel sulfur contents calls for catalysts of even higher HDS activity, while sulfur replacement by oxygen during HDO[903] quickly deactivates metal sulfide catalysts. According to reports from the beginning of the 21st century, nanoscaled metal phosphides and metal borides could play a significant role in, respectively, hydrodesulfurization and hydrodeoxygenation.

Unsupported MoP obtained by phosphate reduction was reported to be active for hydrodenitrogenation (HDN) by Oyama et al.[905] and by Weber et al.[906] Alloys of Mo with Ni, Co, and W were then investigated.[907] Extensions to hydrodesulfurization (HDS) were reported for WP[908] and to hydrodechlorination (HDCl) for Ni_2P.[909,910] Recently, hydrodeoxygenation of anisole was also achieved with Ni_2P, MoP, and NiMoP supported catalysts.[911] After a few years, various studies converged with a model metal phosphide HDS catalyst: a nanoscaled metal phosphide supported on SiO_2, which provides a good surface area of ca. 100 m^2/g, prepared by impregnation of metal and phosphate salts and temperature-programmed reduction (TPR) under H_2. The resulting catalysts were found to be active for difficult substrates such as dibenzothiophene[912] and 4,6-dimethyldibenzothiophene,[913,914] but also for ultradeep hydrodesulfurization,[13] which makes them good candidates for industrialization. Possibilities of metal phosphides for other hydrotreating reactions (HDN, HDO, HDCl) have been much less covered than those related to HDS.

At first sight, occurences in the literature of HDS over metal borides are scarce,[915−918] despite their reported resistance to sulfur poisoning. However, other Ni−B based procedures dating back to the 1960s bear the generic name "desulfurization" and can be considered as being strongly related to hydrodesulfurization.[849,919−924] Their common base consists of the in situ production of amorphous Ni−B nanoparticles by adding sodium borohydride to a solution containing a nickel salt and the sulfur-containing substrate. A wide range of organic compounds can then be targeted.[849,919−924] Although in-depth study of the mechanism has not been performed at that time, immediate formation of a black colloidal suspension together with hydrogen bubbling shows that Ni−B UAAPs are readily formed. The H_2 byproduct can then be consumed by HDS of the substrate over the catalysts. It should however be noticed that some reports[919] suggest that preformed Ni−B nanoparticles can also catalyze desulfurization without the use of molecular hydrogen, even if this route has not been investigated further. All in all, the possibilities of metal boride for HDS have not been cleared yet.[915−918,924] On the contrary, metal borides, especially in their amorphous form, have been much more studied for two years as potential catalysts for HDO of bio-oils.[904]

5.3.2.2. Hydrodesulfurization. Metal phosphides have attracted much more attention than metal borides in the field of HDS. Crystalline Ni_2P was found to be the most active metal phosphide of the first row transition metal phosphides,[925] after in-depth comparisons with other metals (Fe_2P, CoP, Ni_2P),[926] and other phases (Ni_2P, Ni_3P, $Ni_{12}P_5$[927] and Co_2P, Co_xP, CoP[928]). The Ni-rich surface Ni_3P_2 exhibited by the $Ni_2P(001)$ facet is generally considered to be the most active one, being converted to a Ni_3PS one upon sulfur exposure.[929] However, a recent analysis of the $Ni_2P(0001)$-1 surface by LEED (low-energy electron diffaction) suggested that this surface is mainly covered by P adsorbed on the Ni_3P_2 3-fold sites, thus limiting the number of dangling bonds.[930] This implies that the activation of the catalyst requires at least one preliminary step, involving a deeper phosphorus removal.

Ternary alloys have also been particularly studied, such as $Ni_xMo_{1-x}P$,[931,932] Ni_xCo_yP,[933] and $Ni_{2-x}Fe_xP_y$.[934] A dedicated review by S.T. Oyama in 2003 highlighted the very fast progress of the field in less than 5 years, and pinpointed the excellent activity of Ni_2P.[935] More recently, noble metal phosphides such as Rh_2P,[936] $Pd_{4.8}P$, Pd_3P, Ru_2P, and PtP_2[28,937] showed better performances in HDS than pure metal catalysts with the exception of Pt. Phosphorus was found to play a key role in increasing the activity of Ru catalysts as both RuP and Ru_2P supported on MCM-41 were 2 times more active for HDS of dibenzothiophene than Ru.[938] Altogether, Rh_2P was found to be the most active catalyst among the noble-metal based phosphides.

Metal borides were only scarcely considered for HDS.[915−918,939] Skrabalak et al. studied thiophene HDS over unsupported crystalline Ni_3B and Co_2B.[917] These phases were obtained by annealing at 450 °C the corresponding UAAPs precipitated in oxygenated water. The resulting particles had a diameter of ca. 100 nm. The presence of amorphous boron oxide was not assessed. The authors showed that these phases were actually unstable in harsh HDS conditions (450 °C) and were readily sulfided and converted into the corresponding metal sulfides, which are typical HDS catalysts. Other studies

dx.doi.org/10.1021/cr400020d | Chem. Rev. XXXX, XXX, XXX−XXX

focused on amorphous metal borides, especially Ni−B and Ni−Mo−B supported on silica[918] or boehmite.[939] The crystallization temperature was shifted from 275 to 400 °C for, respectively, unsupported and supported Ni−Mo−B. This ternary alloy with partially oxidized Mo species showed enhanced resistance to deep sulfurization. Once pretreated under a mixture of H_2S/H_2 at 375 °C, the catalyst showed enhanced activity for thiophene HDS than unsupported systems and conventional supported and sulfided Ni−Mo alloy. The high activity was ascribed to the high dispersion of Ni sites and resistance to crystallization. Ternary alloys Ni−B−P are also currently considered for increased HDS activity,[940] although the role of B addition on the activity of Ni_2P is not clear yet.

In-depth spectroscopic investigation of metal phosphide surface (EXAFS, XPS,[941] and solid-state NMR[927]) and cross-studies (in situ spectroscopies and DFT)[942−944] revealed the nature of catalyst active sites. In HDS with Ni_2P catalysts, the two Ni sites were found to run different reactions, one through the direct desulfurization route, and the other one through hydrogenation.[945] Very interestingly, these studies also pinpointed the importance of partial P removal by S on Ni_2P surface that provides the active phase for HDS,[929,946,947] although S substitution occurs only on the surface. Indeed, the sulfur resistance goes further than a limited kinetic S incorporation, since a $NiPS_3$ precursor exposed to HDS conditions (340 °C) was shown to form back Ni_2P.[948] Similarly, a highly active MoP based catalyst was prepared by sulfidation of the oxide precursor followed by TPR under H_2.[949] As mentioned above, the activity of amorphous[918] and crystalline[917] metal borides for HDS seems also to be related to surface sulfidation.

5.3.2.3. Hydrodeoxygenation. Nanoscaled amorphous metal borides prepared by aqueous precipitation are economical, have a good thermal stability, and do not require any additive compared to typical metal sulfides and noble metal HDO catalysts.[950] Most catalytic tests were performed on Ni−B and Co−B based compositions, with phenol[502,505,509,951−954] as a model substrate derived from lignocellulosic biomass with a particularly robust C−O bond.[904] Benzaldehyde,[502,951] acetophenone[502,951] and cyclopentanone[502] were scarcely investigated. Because of the strong activity for hydrogenation of amorphous Co−B and Ni−B, the reaction is believed to occur according to the hydrogenation−dehydration route toward cyclohexane,[509,951,952] compared to direct hydrogenolysis for common metal sulfide catalysts leading mainly to benzene. Ternary compositions (Ni−Mo−B,[505] Co−Mo−B,[502,951] Ni−W−B, and Co−W−B[955]) are the milestone for high yield of deoxygenation: Ni or Co sites are the hydrogenation sites, with enhanced activity compared to pure metal because their d electron population is enriched by electronic transfer from boron.[951,952] The second metal is partially oxidized (e.g., molybdenum oxide Mo(IV)) and acts as the acidic site for adsorption of the C−O groups, polarization of the C−O bond, and dehydration.[505] Ni−W−B was reported as being more active than Co−W−B,[955] but differences in compositions, thermal stabilities, and surface areas make difficult the identification of the key parameter. Some quaternary compositions were also investigated to increase the activity and decrease the amount of aromatics in the products, including Ni−Co−Mo−B,[952] Ni−La−Mo−B,[952] Ni−Co−W−B,[956] La−Ni−W−B,[953] and La−Ni−Mo−B.[954] Some results suggest a higher activity than MoS_2.[509] Interestingly, an early report from Loubinoux et al.[957] suggests that amorphous metal borides can be used upstream from the primary bio-oil upgrading, for the direct conversion of wood into oil. Indeed, the authors impregnated wood meal with an aqueous solution of nickel salt and then precipitated amorphous nickel boride by addition of sodium borohydride. The in situ precipitated UAAPs catalyzed the cracking of lignin by hydrogenolysis at room temperature.[957] The yield of monomeric phenols reached 69%.

As mentioned earlier, unsupported (MoP[958]) and silica supported (Ni_2P,[911,959,960] Co_2P,[959] Fe_2P,[959] WP,[959] MoP,[911,959] and NiMoP[911]) metal phosphides[904] were also identified recently as efficient catalysts for hydrodeoxygenation of *p*-methylphenol,[958] anisole,[959,960] and guaiacol.[959] At 300 °C under 1 atm and for the HDO of 2-methyltetrahydrofuran (a biofuel model compound), the order activity of the metal phosphides supported on silica is Ni_2P > WP > MoP > CoP > FeP, all of them being better than the commercial Pd/Al_2O_3 catalyst.[961] Moreover, Ni_2P and CoP showed a higher selectivity for alkane production (pentane and butane), while the group 6 metals produced preferentially the alkenes (pentene and pentadienes).

A model experiment conducted with Ni_2P/SiO_2 for the HDO of ethanol suggested that, in the case of phosphides, the mechanism goes through hydrogenation/dehydrogenation steps, which is in contrast with zeolite HZSM-5 catalysts.[962] The evolution of the HDO conversion during the reaction suggests deactivation of the metal phosphide catalyst, presumably by partial oxidation in contact with water as a byproduct.[911] Such deactivation does not seem to take place with amorphous metal borides which exhibit higher resistance to deep oxidation.[952,955]

5.3.2.4. Hydrodenitrogenation and Hydrodechlorination. Metal borides and metal phosphides catalyze other hydrotreating reactions. Hydrodenitrogenation (HDN) was cited above for binary and ternary metal phosphides based on Mo−P compositions.[905−907] Hydrodechlorination (HDCl) was also reported for both boron and phosphorus based compounds. Ni_2P is particularly active for this kind of hydrogenolysis.[909,910] Cleavage of C−Cl bonds was reported early on with the use of sodium borohydride in the presence of amorphous Ni−B or Pd−B nanoparticles.[849] More recently, HDCl of chlorobenzene was highlighted over crystallized Ni−B deposited on silica.[882] The amorphous phase was partially crystallized by treatment under H_2 at 400 °C. The resulting catalyst was composed of Ni metal nanoparticles segregated from an amorphous boron phase. The HDCl catalytic activity of this nanocomposite was compared to a Ni/Ni_3P mixture crystallized from supported amorphous Ni−P. Higher activity was highlighted for the phosphorus based system, thus suggesting that electron deficiency of the metal sites is beneficial to the HDCl activity. However, it is difficult to draw conclusions from such a comparison of two systems with different phases, compositions, and micro- or nanostructures. Some recent reports dealt with the HDCl of chlorobenzene[572] and *p*-chlorophenol[963] over supported and unsupported Ni−B[572] and Ni−B/Pd nanocomposites.[572,963] The amorphous Ni−B phase was shown to be more active than the crystalline one, as already mentioned for hydrogenation and HDS reactions. Also, Ni−B/Pd nanocomposites were more active than Ni−B because of the promotional effect of Pd for hydrogen splitting.

Some recent reports have shown that some ternary compounds (Fe−B/Ni−B,[964,965] Fe−Pd−B[966]) obtained by

dx.doi.org/10.1021/cr400020d | *Chem. Rev.* XXXX, XXX, XXX−XXX

borohydride reduction of metal salts [Fe(II), Ni(II)] were active for dechlorination catalysis in water in the absence of introduced hydrogen. These supported catalysts were wrongly described as pure metal (Fe, Ni) or bimetallic (Fe−Ni) nanoparticles and are clearly related to metal−boron alloys.

5.3.2.5. Hot Topics. The vast majority on the works published in the 2000−2012 period and dedicated to hydrotreating processes has focused on metal phosphides, while metal borides seem to emerge since few years. The following points are receiving much attention from researchers or would be worth considering in the near future.

5.3.2.5.1. Amorphous versus Crystalline Phases. Clearly, most of the works dealing with hydrotreating over boron or phosphorus based alloys are now focusing on nanoscaled amorphous phases for metal borides and crystalline compounds for metal phosphides.[882] The former have the advantage of higher activity than their crystalline counterparts. Also, crystalline metal borides are usually made of relatively large particles, with a diameter higher than 50 nm.[917] Probably, part of the enhanced activity of amorphous metal borides compared to crystalline MBs originates from their smaller nanoparticles, higher surface area, and better dispersion of the active metal sites. Comparison between systems of the same geometrical and compositional features could provide interesting insights into the reactivity of these systems. On the other side, metal phosphides, even crystallized, show high catalytic activity. The often smaller size of crystalline metal phosphide nanoparticles compared to crystalline metal boride particles could explain their higher activity.

5.3.2.5.2. Composition. The development of binary compounds with different compositions,[927,928] and ternary[231,502,505,911,918,931,933,934,939,951,955] and quaternary[952−954,956] metal phosphide and metal boride phases, is gaining increasing interest for enhanced activity in hydrotreating.

5.3.2.5.3. Role of the Precursors and Synthetic Method. The influence of the metal precursors was also studied in the case of metal phosphides.[967] New synthetic methods were developed: the reaction of Ni oxide nanoparticles with H_2 and PH_3[968,969] (not the greenest method but the use of lower temperature avoids sintering of the starting nanoparticles), and the reduction of impregnated precursors with methane.[970] Methane produced in situ was also used for the reduction of Mo to form MoP.[971] Ni(II) dihydrogenophosphite was impregnated on a MCM-41 silica support and reduced by TPR, although the precursor itself was a precatalyst reactive enough to be converted in situ in Ni_2P during the HDS process.[972] Hypophosphite was also found to produce Ni_2P from $NiCl_2$ on the same support.[973] The potential of these new routes was confirmed by a study on Ni_2P, Cu_3P, MoP, and InP formation from oxide and hypophosphite metal precursors.[974] Metal phosphite precursors were also used for the preparation of Ni_2P and CoP catalysts active in competitive HDN−HDS reactions.[975] Additionally, catalytic properties of Ni_2P in a colloidal form were evaluated and highlighted an effect of the surface ligand.[665]

5.3.2.5.4. Supports. Many recent advances for HDS over metal phosphides[26] deal with variation of the support: SiO_2[976] including SBA-15,[977] Al_2O_3,[978−980] zeolites,[981,982] TiO_2,[979,983,984] and high area unsupported powders[969,985,986] were studied. It must be noted that phosphate reduction, by spray pyrolysis[987] or in a model flat surface,[988] also gives access to the metal phosphide: each intermediate was characterized with a combination of in situ techniques in the case of Ni_2P.[989] However, the nature of the support modifies the nanoparticle features (size, shape) and their electronic properties for very small nanoparticles. Carbon as a support[990,991] allows smaller particle size and higher dispersion after TPR than SiO_2, but also higher intrinsic activity (when normalized by the number of active sites).[991] Ni_2P supported on mesoporous carbon was obtained by a solid phase reaction and exhibited higher activities in HDS and HDN than silica supported catalysts.[992] The influence of the reduction temperature and catalyst loading were specifically investigated in the case of MoP[993] and Ni_2P.[994−996] Temperature of reduction could be lowered by using small amounts of Pd as catalysts for $Ni_2P−SiO_2$ catalysts.[997] Additives such as citric acid allowed a diminution of the mean size of the nanoparticles.[998] Supported metal borides have only been rarely reported for hydrotreating,[918,939] but the support seems to be highly beneficial for HDS catalysis when it improves thermal stability of the amorphous alloys. The impact of the support on HDO over metal borides has not been investigated so far.

5.3.2.5.5. Extension to Industrial Cases. HDN and HDS of crude oils[999,1000] and carbazole[1001] were achieved over metal phosphides as a first step toward industrialization, along with deep[1002] and ultradeep HDS on Ni_2P.[13] Finally, it was shown that the HDS of dibenzothiophene over MoP proceeded through the hydrogenation of the substrate,[1003] suggesting potential use of MoP in other hydrogenation reactions. Actually, other catalytic applications have been explored both for metal borides and metal phosphides.[33]

5.3.3. Hydrogen Generation. The potential of metal borohydrides and borane complexes for hydrogen generation has been reviewed in a number of papers.[313,1004−1007] $NaBH_4$ attracted most of the attention since the Millennium Cell company proposed in 2000 a prototype of hydrogen generator based on a sodium borohydride aqueous solution.[1008,1009] However, the U.S. Department of Energy issued in 2007 a "No Go" recommendation concerning $NaBH_4$ for "on-board vehicular hydrogen storage".[1010] This decision was based on several considerations[1005] including the too low effective H_2 storage capacities (theoretical gravimetric hydrogen storage capacities of 10.8 wt % and 7.5 wt % from, respectively, solid $NaBH_4$ and a concentrated aqueous solution; for the latter, the highest effective capacity ever reported is 6.7 wt %),[1006] inefficiency of the byproduct ($NaBO_2$) recycling, and cost. Although automotive applications seem an unrealistic goal for borohydride based applications, portable applications are still at stake.[1006] In parallel, amine borane adducts,[553,1006] ammonia borane $H_3N−BH_3$ as a primary example with high theoretical gravimetric hydrogen storage capacity of 19.5 wt %, are also envisaged as competitors for H_2 storage, including in the automotive field.[1006]

All these compounds exhibit slow kinetics of H_2 evolution which have to be overcome by a suitable catalyst for operation in realistic conditions. Amorphous metal boride nanoparticles are among the most active and priceless catalysts for this function. Two methods of hydrogen release are envisioned: hydrolysis (eq 11) and thermolysis (eq 8).

In their pioneering work, Schlesinger et al.[90] showed that hydrogen release from metastable basic $NaBH_4$ aqueous solutions could be triggered close to room temperature by addition of metal(II) chlorides (Mn, Fe, Co, Ni, Cu). The black suspension immediately formed was made of amorphous metal boride nanoparticles. These UAAPs were the actual catalysts of borohydride hydrolysis and hydrogen evolution. Among the

various alloys, amorphous Co−B is recognized as the most active catalyst,[37,90,471,476,477,1011,1012] but the Ni−B system is also highly active.[1012,1013] As already described for hydrogenation and hydrotreating, some ternary [Co−Ni−B,[1014−1016] Co−Mn−B,[576,1017] Co−Fe−B,[1018] Co−W−B,[1019] Co−M−B (M = Ni, Fe, Cu, Cr, Mo, and W),[1020] Co−Mo−B,[1021] Co−P−B[1022]] and quaternary (Co−Ni−P−B[1023]) compositions have been shown to enhance the catalytic activity for a number of reasons found in reduced particle size, increased disorder of the alloy resulting in more unsaturated metal sites, and incorporation of acidic sites.[1020,1022,1023] Supports such as Ni foams,[576,1024] silica,[761,1013] carbon,[1025,1026] and carbon nanotubes[568] have been investigated not only to assess the practical use of the catalyst, but also to improve the activity by ensuring a better dispersion of the active sites. Co−B films deposited on glass by pulsed laser deposition showed higher activity than the powdered catalyst obtained by precipitation.[1027] Surprisingly, partial crystallization of the film into Co_2B seems to increase the activity,[1027] while it often has a detrimental effect on powders.[1022] More refined M−B nanostructures (Figure 47), such as sub-10-nm nanoparticles,[245,528,1011] hollow spheres,[541] and mesoporous structures (e.g., Co−B mesostructures for hydrolysis of KBH_4[542,549]), were also suggested to provide higher surface area and activity. Interestingly, the activity of Co−B nanoparticles was improved after plasma treatment. This enhancement was ascribed to various factors, such as increased surface area and increased interaction between metal and boron sites.[1028] Some direct fuel cells using $NaBH_4$ were designed by building anodes based on Co−B catalysts.[1024] Amorphous metal phosphides have also been studied as catalysts for borohydride hydrolysis. Compositions such as Co−P,[1029−1031] Ni−P,[1029,1032] Co−Ni−P,[1033,1034] Ni−Fe−P,[1029] and Co−W−P[1035] have been studied but showed lower activity than the corresponding amorphous metal borides.[313]

Strategies to hasten the ammonia borane hydrolysis by focusing on the catalyst activity are closely related to those envisioned for borohydride hydrolysis. Co−B[5541036−1038] and Ni−B[554] are also the most investigated catalysts together with their ternary modifications (e.g., Co−P−B[1039]) and supported phases.[1038,1039] Nano- and mesostructure (hollow Co−B nanospindles,[1036] Co−B films obtained by pulsed laser ablation,[1037] Au−Co(B)−Fe(B) core−shell−shell nanoparticles[557]) phases are another hot topic. As already mentioned, works highlighting the catalytic activity of amorphous metal nanoparticles should always be considered with care because these compounds are often made by borane or borohydride reduction. The boron content is only scarcely evaluated, and the exact nature of these catalysts remains highly elusive.[553]

Thermolysis seems less realistic than hydrolysis for use of alkali borohydrides because of their high decomposition temperature (in the range 300−600 °C).[1004,1006] It is unlikely that a catalyst would provide a sufficiently strong temperature decrease for envisaging practical use. On the contrary, while the hydrolysis method for $H_3N−BH_3$ is unlikely to provide high hydrogen capacity,[1006] its thermolysis is the topic of much current research.[553,1006] Ammonia borane starts to decompose at 70 °C. $H_3N−BH_3$ loses a first equivalent of H_2 between 70 and 110 °C (theoretical gravimetric hydrogen storage capacity of 6.5 wt %), then a second equivalent in the range 110−200 °C (theoretical gravimetric hydrogen storage capacity of 13 wt %), and the last equivalent up to 500 °C.[553] Thermolytic dehydrogenation of ammonia borane can be considered as a possible way for fuel cell hydrogen feeding if at least the first 2 H_2 equivalents are recovered, which requires a decrease in the decomposition temperature down to the targeted maximum delivery temperature of 85 °C.[553] Although other amine−borane adducts are intensively investigated in this field,[553] most research has focused on ammonia borane. Again, amorphous Co−B and Ni−B catalysts combine the advantage of low cost and high activity for this dehydrogenation process.[555,1039] Ternary compositions such as Co−P−B have been shown to provide higher activity than the corresponding Co−B alloys.[1039] Metal borides not only decrease the temperature of decomposition of borohydrides[314] and ammonia borane,[556] but also modify the dehydrogenation pathway. For instance, the reduced evolution of harmful diborane from $LiBH_4$ due to the addition of metal chlorides (La(III), Ti(III))[314] probably proceeds through metal boride intermediates. Furthermore, dehydrogenation of $H_3N−BH_3$ over amorphous Fe−B nanoparticles leads to crystalline polyaminoborane instead of an amorphous phase from neat ammonia borane.[556] In addition, $Ca(BH_4)_2$ decomposition into CaH_2, CaB_6, and H_2 was recently catalyzed by TiB_2 and NbB_2 nanoparticles,[1040] presumably enabling heterogeneous nucleation of CaB_6. Interestingly, the metal boride particles enhanced the reversibility of the reaction, and rehydrogenation under H_2 pressure was possible.

Decomposition of hydrous hydrazine into H_2 and N_2 was also scarcely reported over 10−40 nm amorphous Co−B nanoparticles obtained by solution plasma processing, and crystalline MoP metal phosphides.[1041] Amorphous $Fe_{0.67}B_{0.33}$ nanoparticles of 2−5 nm diameter nicely deposited over carbon nanotubes recently showed high activity and selectivity for H_2 generation from aqueous solutions of hydrazine.[1042] MoP catalysts were found to be more active than Mo_2N catalysts for hydrazine decomposition into H_2 and N_2, because the adsorption of the intermediate NH_3 was weaker.[1043] The same reaction was run with $Ni_{2-x}Co_xP_y$ on SiO_2, which showed a better activity than the corresponding binary phosphides.[1044] Aqueous phase reforming of glycerol, ethylene glycol, and sorbitol was investigated over amorphous Ni−B catalysts,[1045] in order to assess the possibility of H_2 production from biomass-derived oxygenated molecules. The Ni−B catalyst showed higher H_2 selectivity than common Raney Ni.

5.3.4. Other Dissociative Reactions. Dissociative reactions different from hydrogen evolution have been reported. For instance, hydrogenolysis of nitrosamines over nanoscaled amorphous nickel boride leads to N_2 evolution, while the same reaction over Raney Ni proceeds through a different pathway and yields ammonia instead of N_2.[866] Hydrogenolysis of ethyl lactate to 1,2-propanediol was performed with good selectivity and yield on Ru−Sn−B supported on alumina,[1046] and Ru−B on tin-doped mesoporous silica[1047] and titania.[1048]

Other reactions have been catalyzed by crystalline metal phosphides. Fe_2P was used for the catalytic dissociation of NO and reduction to N_2 under H_2.[1049] Cracking of cellulose to sorbitol, with a 10:1 selectivity over mannitol, was achieved using both acid and metallic sites of a Ni_2P catalyst.[1050] NH_3 could also be decomposed using H_3PO_4 activated Ni and Fe catalysts: phosphides were identified and proposed as part of the catalytic cycles along with nitrides.[1051] Pd−P catalysts supported on PTFE membranes were found to be active for formic acid oxidation and toluene deep oxidation.[1052]

5.3.5. Associative Reactions. Metal borides and metal phosphides were involved in other industrially relevant reactions. Methanation of carbon monoxide, a poison of H_2

dx.doi.org/10.1021/cr400020d | Chem. Rev. XXXX, XXX, XXX−XXX

oxidation catalysts, was performed on amorphous Ni−Ru−B supported on zirconia to purify hydrogen-rich gas prior to its injection into fuel cells.[570] The catalyst was highly selective and avoided useless H_2 consumption by CO_2 methanation. Ni−B phases showed good activity for syngas fabrication from partial oxidation of methane[1053,1054] and steam methane reforming.[1055] Co−B supported on zirconia,[1056] silica,[1057] and zeoliths[1058] and nanoparticles of Co−B[1059,1060] and Fe−B[1059−1062] dispersed in water or PEG were also shown to be interesting Fischer−Tropsch catalysts. The particularly good resistance of metal borides to coke formation during steam methane reforming, partial oxidation of methane, and Fischer−Tropsch catalysis was ascribed to the high dispersion of the catalyst[1053] and the similar binding preferences of carbon and boron with metal atoms, as evaluated by DFT calculations.[1056,1063] H_2O_2 synthesis from O_2, CO, and H_2O was catalyzed by Ni−La−B supported on zirconia in the presence of phosphoric acid to stabilize hydrogen peroxide.[566] The quick deactivation was due to surface complexation by phosphates and subsequent dissolution of the active boride phase. Other processes relied on cascading reactions, such as the transformation of phenylpyruvic acid into phenylalanine in the presence of hydrogen, ammonia, and water over Ni−B supported on silica. This one-pot procedure combined hydrogenation of a conjugated ketone C═O group into an intermediate alcohol that was subsequently aminated.[1064] The catalyst was shown to be more active than typical Raney Ni. Amorphous Ni−B[1065,1066] and more recently In−B[1067] have been also investigated for other coupling reactions related to preparative organic chemistry. Nanoparticles (50 nm) of Co−B appeared recently as active catalysts of the Heck C−C coupling.[1068]

Nanoscaled metal phosphides have also been investigated in a wider range of reactions. By DFT calculation, Mo_6P_3 clusters were used as a catalyst model for syngas conversion, predicting the formation of methane as the main product.[1069] This could be verified experimentally using MoP on SiO_2.[1070] However, when the catalyst was promoted with K, the formation of heavier oxygenated products was favored.[1071] Additionally, Fischer−Tropsch synthesis was run with a $Ru/Co/ZrP/SiO_2$ catalyst: the presence of phosphorus was found to avoid the formation of large Co nanoparticles, thus improving the activity of the catalyst.[1072] Finally, the water−gas shift reaction was achieved on a model $Ni_2P(100)$ surface. The formation of Ni oxyphosphide with strong P−O interaction was revealed to be the active site.[1073]

5.4. Electrochemical and Photoelectrochemical Devices

Electrocatalytic properties have been demonstrated recently for metal phosphides and metal borides to be incorporated in fuel cells or solar cells. Hydrogen oxidation reaction was investigated on several transition metal phosphides (WP, CoP, NiP, Ni−WP, Co−WP),[1074] while PtNiP composite nanotubes were shown to be durable catalysts for methanol electro-oxidation.[1075] Pd−B compounds supported on carbon showed higher catalytic activity for formic acid electro-oxidation than a commercial Pd/C catalyst with the same catalyst loading (40 wt %). The boron-doped (B content of 6.3 atom %) crystalline Pd nanoparticles were obtained by using dimethylamine borane as a reducing agent in water. The enhanced activity and poisoning resistance was ascribed to a higher density of active sites, dilation of the Pd lattice, and electron transfer between B and Pd.[562] Electroreduction can also be catalyzed by metal phosphides: $Ni_{12}P_5$ nanoparticles embedded in graphene,[1076] and MoP as well as Ni_5P_4/C[1077] were shown to be competitive with Pt as counter-electrodes for dye-sensitized solar cells. Other electrically driven reactions were investigated, including electrocatalytic hydrogenation of lignin models on crystalline Ni_2B/carbon or amorphous Ni−B/carbon nanocomposite electrodes.[1078]

Additionally, due to their semiconductor properties, metal phosphides were also used as photoelectrochemically active components. A p-GaP photocathode[1079] (respectively a p-InP electrode)[1080] was employed for the photoelectrochemical conversion of CO_2 into methanol (respectively, C_1 and C_2 hydrocarbons) in the presence of a pyridinium catalyst (respectively Cu nanoparticles). An InP nanophotocathode was used in the visible domain for H_2 production by water splitting.[1081] The electrode was made with self-assembled InP nanoparticles that were connected with dithioaromatic moieties. Water reduction was also demonstrated to be possible under visible light with GaP nanowires, for the production of H_2.[1082]

5.5. Initiation of Nanotubes and Nanowires Growth

Metal borides are widely used as catalysts for growth of nanotubes, nanowires, and other nanostructures. CVD growth of carbon nanotubes has been reported over a Fe−B catalyst.[1083] Synthesis of boron nitride 1D nanostructures including nanotubes,[1084] whiskers,[1085] bamboo-like structures,[1086] and tubules[1087] has been the topic of few recent reviews.[60,1084,1088] Whether CVD,[1085,1087,1089] arc discharge,[1083,1084,1088] or mechano-activated[1086] syntheses are involved, metal boride nanoparticles are clearly in play as catalysts with compositions often relying on the Fe−B system,[1085−1087] more rarely on Ni−B.[1089,1090] Other nanostructures, including (core)−(shell) (Fe−B)−(BN) have been synthesized by similar methods.[1091−1093]

Metal phosphide nanoparticles were also used for the growth of 1D nanostructures, in a catalytic or a sacrificial manner. FeP nanorods allowed the growth of single-wall carbon nanotubes.[1094] A Ni−P eutectic phase supported on Ni nanoparticles was found to promote the growth of TiO_2 nanowires.[1095] Ni−Ni_3P heterostructures allowed growing carbon nanostructures[1096] and amorphous Ni−P nanoparticles carbon nanotubes.[1097] Lastly, GaP nanowires were utilized as a sacrificial template for the deposition of Si on their side. After an etching step, Si nanotubes were obtained.[765]

5.6. Electronics

Since the discovery of a high critical temperature (39 K) in bulk MgB_2 classical superconductor,[16] attempts were made to evaluate the impact of the nanoscale on the conduction behavior. Studies have focused on magnetic measurements of the critical temperature, which is generally diminished by few degrees with a broadened transition upon downscaling.[298,381,383,388,1098] Few exceptions showing highly crystalline nanostructures claim a similar critical temperature compared to that of the bulk.[236,301,386] Carbon doping was suggested to increase the critical current density,[452] while nanostructuring increased pinning as a consequence of a high density of grain boundaries.[399,419]

Applications of metal phosphides in the field of electronics also include field effect transistors (Zn_3P_2)[1099] and a Schottky device (DNA modified InP).[1100] Electronic sensors of hydrogen were obtained through the conductance measurement of InP electrodes functionalized with Pd nanoparticles.[1101]

dx.doi.org/10.1021/cr400020d | Chem. Rev. XXXX, XXX, XXX−XXX

Due to their high electrical conductivity and high chemical and thermal inertness, metal borides were soon proposed as electrodes, for instance in the form of 1 μm thick films for solar cells.[1102] Since copper has become the material of choice for interconnects in ultra-large-scale integrated circuits, strong research efforts have focused on a suitable metal barrier to avoid alloying with silicon and destruction of the conductive properties of copper. Metal diborides including HfB_2, ZrB_2, and TiB_2 are good candidates as copper diffusion barriers because of their high electrical conductivity, low themal dilatation, and stability in contact with Cu. Amorphous zirconium diboride has been proposed as barrier by Sung et al.,[24] who demonstrated plasma-assisted chemical vapor deposition of highly conformal 30 nm thick films of stoichiometric ZrB_2 from the $Zr(BH_4)_4$ precursor at 300 °C. Conformal amorphous HfB_x thin films of 12 nm thickness deposited by single source CVD at 250 °C also demonstrated efficient prevention of Cu and Si alloying.[334,336] ZrB_x films with thicknesses down to 3 nm exhibit interesting barrier properties.[1103] TiB_2 could also be deposited on silicon at a thickness of 7 nm from $Ti(BH_4)_3$(dimethoxyethane) at 175 °C.[1104] The nanocomposite films, incorporating 4 nm crystalline TiB_2 nanoparticles dispersed into an amorphous Ti-rich matrix, were also good diffusion barrier against Cu and Si alloying.

Metal diborides are also attractive substrates for epitaxial growth of metal nitride semiconductors,[1105−1107] because their lattice parameters and thermal expansion coefficients are close to those of AlN and GaN for instance. Moreover, metal diborides are electrically conductive contrary to the typical sapphire substrate, which permits researchers to envision alternative device constructions. Violet and UV light emitting diodes (LEDs) were first grown over ZrB_2 bulk crystals.[1105,1106] Interestingly, crystalline ZrB_2(0001) can be epitaxially grown on Si(111) by single source CVD above 900 °C,[1108−1112] thus suggesting that zirconium diboride could be a good buffer layer for "nitride over silicon" technologies. Furthermore, the as-grown 20−30 nm thick crystalline films are metallic with electrical conductivity close to bulk values[1112] and high reflectance in the visible to UV range.[1108] These characteristics were employed by Blake et al.[1113] who built an InGaN/GaN LED over silicon substrate with two buffer layers: ZrB_2 in contact with silicon and a $Al_xGa_{1-x}N$ stack between ZrB_2 and the photoactive part of the LED. The 30 nm thick diboride film epitaxially grown over Si(111) was deposited by single source CVD. Similar lattice parameter and thermal expansion coefficients ensured good epitaxial growth of the nitride system while the high reflectivity of ZrB_2 in the visible range overcomes the large absorption coefficient of silicon. $Hf_xZr_{1-x}B_2$ (x = 0−1) can also be epitaxially grown over silicon and provide a way to enhance reflectivity of the coating.[1114] These results could pave the way toward LEDs based on silicon substrates which are more economical than typical sapphire. Alternatively, 20 nm thick ZrB_2 films epitaxially grown on silicon are also interesting substrates for nanostructure growth: nanometer-scale islands of Ge and SiC semiconductors could be heteroepitaxially grown.[1115] Lastly, epitaxial silicene was very recently highlighted on ZrB_2 thin films grown on silicon.[1116] Epitaxial relationships led to silicene buckling and opening of an electronic band gap, thus promising interesting outcomes for the discovery of novel structural and transport properties of two-dimensional nanomaterials.

Field electron emission is another application of metal borides, which are indeed well-known by scientists in the nanomaterials field, who are often relying on electron microscopes with a LaB_6 field emitter which provides a bright, relatively coherent, and stable electron beam. Metal hexaborides are among the most used field emitters because of their low work function, low volatility at high temperature, high conductivity, high chemical inertness, and high mechanical strength.[20] These materials are still the objects of innovation for enhancement of the emission properties. From a general viewpoint, efforts are focusing on nanomaterials with high aspect ratios and sharp tips to provide higher field emission currents. These 1D nanostructures, including nanowires and nanoobelisks grown by CVD, meet all the requirements for enhanced emission. Field emission properties of metal hexaboride nanostructures were reviewed recently by Ji et al.[20] Briefly, a LaB_6 nanowire obtained by metal-catalyzed CVD showed a current density comparable to state of the art carbon nanotubes.[242] LaB_6[242,1117] and other compositions were studied, including GdB_6,[368] SmB_6,[371] PrB_6,[322,372] and CeB_6.[290]

5.7. Optics

Reports on the specific optical properties of nanoscaled metal borides are relatively rare because they behave as metals, so that no quantum confinement is expected. On the other side, plasmonics is mostly an unexplored field, and no impact of the particle size on plasmons properties was reported. The reflective behavior of metal diborides such as ZrB_2 has been already mentioned in the previous subsection addressing applications in electronics. Metal borides with metallic behavior such as HfB_2 have been suggested also as low refractive index thin layer of multilayers reflective mirrors in the wavelength range from soft X-rays to ultraviolet.[1118] In such multistack devices, the specific advantage of metal borides is their strong chemical and thermal inertness which could ensure operation even during high local heating without alloying with the adjacent layers.

Compared to metal borides, many metal phosphides have a finite band gap. This has driven a range of studies on their optical properties. Silica coated InP−ZnS quantum dots were utilized as converters in white LEDS.[1119] The intrinsic luminescent properties of an InP core were also used to probe the growth of a ZnSeS gradient shell.[1120] InP−GaP−ZnS nanoparticle mixtures were also used to obtain white LEDS, showing a better robustness than In−P−ZnS nanoparticles.[1121] Low reflectance surfaces with InP nanoporous film were also obtained.[1122] Single-nanowire analysis of InP recently revealed nonlinear optical processes for excitation and for second-harmonic generation.[1123] GaP photonic crystals nanocavities could be obtained, operating in the visible light,[1124] along with other photonic devices based on nanowires.[1125] In the teraHz domain, nanoporous conductive InP membranes were obtained.[1126]

Doped nanostructures also present original optical properties, in particular when looking at localized surface plasmon resonance (LSPR). Si nanocrystals prepared from a nonthermal plasma route, and doped with up to 50% phosphorus, exhibit a tunable LSPR in the mid-infrared.[1127] Additionally, surface doping of gold nanoparticles with phosphorus seems to render their LSPR less sensitive to modification of their ligand environment.[1128]

5.8. Magnetism

Bulk $Nd_2Fe_{14}B$ is the hardest magnet known, and research has been naturally oriented toward the impact of downscaling on its magnetic properties. Nanoparticles (50 nm) agglomerated into

dx.doi.org/10.1021/cr400020d | Chem. Rev. XXXX, XXX, XXX−XXX

aggregates bigger than 100 nm exhibited reduced coercivity compared to the bulk.[392,393,395,1129] The same observation was made for amorphous Fe−B nanoparticles coated with a silica shell.[1130,1131] Petit and Pileni performed a detailed study of reverse-micelle-derived Co−B nanoparticles as a function of their size. For diameters below 10 nm, the particles exhibit a superparamagnetic behavior.[295] The magnetic properties of 50−100 nm Co−B aggregates of 5 nm primary particles suggest strongly interacting systems with exchange coupling at the interface between the primary units.[475] Some nanostructured $Nd_2Fe_{14}B/\alpha$-Fe[392,394] and $Nd_2Fe_{14}B$/Fe−B[395,1132] hard/soft exchange coupled nanocomposites have been recently developed to enhance the energy product. Because the compositional control is especially difficult in the case of $Nd_2Fe_{14}B$ synthesis due to Fe segregation during annealing, these composites are often fortuitous materials obtained while pure $Nd_2Fe_{14}B$ was actually looked for.[393] For the rare cases where nanocrystals have been unambiguously obtained, magnetic force microscopy measurements suggest that crystalline Fe_3B nanowires exhibit single domain ferromagnetism.[239] The ⟨110⟩ long axis of the nanowires corresponds to the preferential orientation of magnetocrystalline anisotropy of the tetragonal Fe_3B phase. From a more general point of view, the impact of nanoscaling on the magnetic properties of metal borides is largely uncovered and is certainly a worthy future research field, since incorporation of boron can drastically modify the magnetic behavior of metal nanoparticles, by providing either stronger coercivity (the case of $Nd_2Fe_{14}B$) or on the contrary suppressed ferromagnetism, as in, e.g., nickel borides.[1133]

Additionally, magnetic coatings on glass silica spheres were obtained with a core/shell/shell glass/Ni−$Ni_3P/Co_2P_2O_7$ urchin-like nanocomposite.[1134] Application of this coating deals with low-density magnetic materials that absorb microwaves. Lastly, prototypes of micromachines were built with Ni−P coating on polymers: the polymer helixes could be magnetically manipulated.[1135] However, a deep understanding of the intrinsic magnetic properties of metal phosphide nanoparticles is still difficult to attain because the M:P stoichiometry can be unclear and possible contamination by carbide species is likely. This results in scattered reports that show very different Curie temperature values for instance, as exemplified for iron phosphide nanoparticles.[27,44] Even so, the use of core−shell structures allows tuning of the magnetic properties of the nanoparticles, although in some cases (Ni_2P−Ni) the phosphide phase is actually decreasing the ferromagnetic features.[713] Specific efforts to design multishell hollow magnetic particles have been made for NiP−CoFeP composite structures, and more sophisticated structures are expected to be investigated in the future.[1136]

5.9. Mechanical Properties

Boron based compounds are the focus of research on ultrahigh temperature ceramics[14] and superhard materials.[22,105,106] The well-known Hall−Petch rule indicates that the higher the density of grain boundaries, the harder the material. This relation has prompted scientists to investigate the effect of downscaling on the mechanical properties, especially for resistant coatings.[1137] Although most studies addressed submicrometer scale films,[1138] nanostructured crystalline HfB_2 films with 100−200 nm thickness, deposited by single source CVD, were demonstrated to possess high hardness, elastic modulus, and wear resistance on the macro- as well as on the nanoscale.[1139−1141] Nanoindentation studies of single silica-coated amorphous Co−B nanoparticles (diameter of ca. 100 nm), coupled with calculations, showed increased hardness but comparable modulus compared to the bulk.[474,1142] Reverse plasticity was also observed and suggested to arise from the radial nanostructure of the Co−B nanoparticles and the confinement effect of the silica shell.

5.10. Biology, Medicine, Toxicology, and Environmental Applications

The tear film exhibits a poorly understood multilayer structure that could be studied using InP quantum dots, guided by their colloidal properties.[1143] Cellular imaging was achieved with core−shell InP−ZnS nanoparticles covered with polyethylene glycol (PEG).[1144] As a diagnostic tool, InP quantum dots were utilized for imaging of a pancreatic cancer, after surface functionalization of the nanoparticles with antibodies.[1145] InP−ZnS quantum dots were recently combined with rare-earth emitters, and their surface was functionalized with a cell-penetrating peptide, in order to demonstrate the multimodal multimeric abilities of such system for cell labeling.[1146]

The toxicity of metal phosphides as labeling tools was investigated. In particular, InP−ZnS nanoparticles were demonstrated to be less toxic than CdSe−ZnS ones because of the lower toxicity of In(III) ions compared with Cd(II) ions.[1147] However, phototoxicity was found to be the major contribution to cytotoxicity by creating highly reactive radicals (ROSs) in the vicinity of the particles.[1148] The toxicity of GaP implanted in tissues was also investigated.[1149]

Lastly, Co_2P nanostructures[1150] and Ni_2P urchin-like nanoparticles[1151] were utilized for the removal of heavy metal ions. Porous $Ni_{12}P_5$ structures were also found to be active as photocatalysts for environmental treatment.[1152]

Metal borides have only been investigated in the biological field as protective coatings for implants, especially titanium pieces, due to their chemical inertness and good wear resistance.[1153] However, these films have usual thicknesses in the range of few micrometers and therefore are out of the scope of this review.

5.11. Metal Phosphides and Metal Borides as Fortuitous Compounds and Other Less Defined Compounds

In the last sections, designed routes toward nanoscaled metal borides and phosphides have been described. However, these nanoscaled materials can also occur as byproducts of other chemical or electrochemical processes, or originate from their bulk counterpart.

For instance, metal phosphides are involved as waste in solid oxide fuel cell (SOFC). Indeed, they were found to form when the feedstocks contained PH_3 or other phosphorated impurities, in particular for Ni based SOFC: nickel phosphide phases[1154] (especially Ni_3P)[1155] appeared with P impurities as low as ppb,[1156] and resulted in the degradation of SOFC anodes.[1157] In the field of catalysis, P contamination was observed in cobalt nanoparticles synthesized in the presence of TOPO, and resulted in a decrease in the rate of CO_2 reduction.[1158] Such contamination was not quantified in the case of cobalt. However, a recent work on nickel nanoparticles clearly identified the incorporation of a few percent of P in nickel nanoparticles synthesized by reduction of $Ni(acac)_2$ with oleylamine in the presence of TOP,[682] although this synthesis is particularly well-defined due to its very limited number of reactant and its simplicity.[1159,1160]

dx.doi.org/10.1021/cr400020d | Chem. Rev. XXXX, XXX, XXX−XXX

The incorporation of boron atoms into metal nanoparticles, synthesized through colloidal methods from borohydrides or borane adducts, has been already covered in subsections 3.8.5 and 5.3.3. We cannot emphasize enough the importance of specifically questioning the boron (and phosphorus) insertion in these particles, if one wants to get accurate comprehension of the structure and properties of these nanomaterials.

Considering the harsh conditions to which metal borides and other boron based materials are exposed during their use, as coatings for cutting tools or as ultrahigh temperature ceramics, it is not surprising to observe structural and morphological changes at the less inert sites, like grain boundaries. This is exemplified by the occurrence of chromium boride nanoparticles, after heat treatment at ca. 1000 °C of nickel based superalloys strengthened by boron addition.[1161] The 100 nm particles originated from boron initially incorporated in grain boundaries.

Other elusive materials have been tentatively described. Gold phosphide (Au_2P_3), for instance, is a metastable air-sensitive phase under atmospheric pressure.[1162] It was obtained in particular at the bulk scale at InP and Au electrode interfaces.[1163] Its formation at the nanoscale was also proposed in a particularly strong solvothermal procedure (6 h, 360 °C), with TOP as the phosphorus source.[680] However, no TEM observation was provided at that time: the size range of the particles remains undefined.

6. CONCLUSIVE PERSPECTIVES

6.1. Toward New Compositions and Crystal Structures

6.1.1. Amorphous State versus Crystalline State. The panel of possible compositions is constantly increased by the identification of new ternary, quaternary, or more compounds at the bulk scale.[40,132,137,140,792] Most studies on nanoscaled materials focus on crystalline phases for three main reasons: they are usually more stable than amorphous ones, the control of their composition is easier, and their characterization as well as the comprehension of their properties are facilitated, especially when one considers coupling with calculations, often dedicated to crystalline states. However, metal borides and metal phosphides in the amorphous state also provide an interesting playground for the development of new materials.

A first example is the nanoparticles of amorphous metal boron alloys highlighted in this review as efficient catalysts for a wide range of reactions. Catalytic properties of crystalline metal borides have been assessed only for bulk compounds (see subsection 5.3.1). Crystalline phases with particle size similar to those of UAAPs (10−60 nm) could exhibit new behaviors, especially in terms of activity and selectivity.

A second example is given by bulk metallic glasses (BMG). Even though they relate to more strenuous preparation conditions, they illustrate well how crucial it is to control the composition independently of the crystallization state. Metal borides and metal phosphides in particular have been identified as interesting phases for this purpose, some of them being prone to keep a glassy state, because of the possibility to prepare ternary (or more) covalent alloys with chosen stoichiometries.[1164] Pd based ($Pd_{40}Ni_{40}P_{20}$ and $Pd_{40}Cu_{30}Ni_{10}P_{20}$) and Pt based ($Pt_{42.5}Cu_{27}Ni_{9.5}P_{21}$) compounds have been identified as promising materials since monoliths with critical sizes in the 10 mm range could be prepared.[1165] They exhibited high fracture strength (>1400 MPa)[1166] and interesting rheological properties.[1167] Going to the nanoscale, it is interesting to note that the composition also strongly affects the stability of the glassy state. Actually, ultra fine amorphous alloys particles (UAAPs) could also be named "nanometallic glasses" ("NMGs"). The origin of the stability of these amorphous phases can be traced back to the strong, directional, and short metal−metalloid and metalloid−metalloid bonds which ensure relatively stable short-range order, even with long-range disorder and glass-like structure.[169,170] The case of Pd based and Pt based phosphides is a nice example of the impact of alloying on the crystallization state. These nanoparticles were shown to crystallize at much higher temperature (320 °C) than Ni−P ones for instance (ca. 150 °C), and some compositions such as Pd_3P even resisted crystallization in these harsh conditions.[717] The mechanical properties of these NMGs and of nanostructured BMGs are certainly worth investigating.

6.1.2. Control of the Stoichiometry. The control of stoichiometry in the M_xB_y and M_xP_y families remains mainly empirical. At the bulk scale, the starting stoichiometry and reaction conditions are of course of major importance for the control of the phase: temperature and pressure rule the accessible phases. FeP, FeP_2, and FeP_4 were obtained as pure phases by varying the starting stoichiometries before thermal treatment.[798] Similarly, the WP_4 phase was obtained at 1000 °C under 3 GPa from elemental W and red phosphorus (quenching of temperature was done under pressure).[1168] Interestingly, the density of the binary W−P compounds was found to decrease with increasing W:P ratio (Figure 55), which offers a nice way to tune the material property through stoichiometry control. The composition of metal borides can also be controlled to some extent in bulk compounds like in the Nb−B, W−B, and Cr−B systems[82,83] by adjusting the initial reactant ratio.

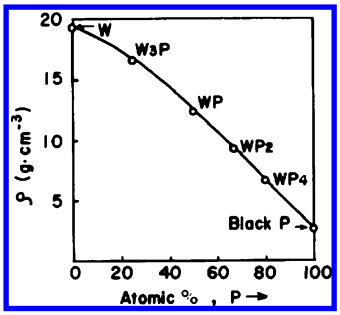

Figure 55. Density in the binary system W−P.[1168] Reprinted with permission from ref 1168. Copyright 1983 Elsevier.

Phase evolution of Cr−B (CrB and CrB_2 phases),[80] Mo−B (MoB_2 and Mo_2B_5 phases),[412] Co−P alloys,[1169] Ni−P alloys,[868] $Ni_{70}P_{30}$[1170] (main phases: Ni_2P and $Ni_{12}P_5$), and Fe_8P[1171,1172] (main phase: Fe_2P) was investigated by reactive ball milling, a solid state method that avoids the loss of P/B or M in the solvent or in the gas phase. These results at the bulk scale were oriented by the imposed stoichiometry and by thermodynamics, which predicts that some particular phases are more stable than others.[100,156] $(M_xM'_{1-x})B_2$ (M, M′ = Ti, Hf, Zr, Ta, Nb)[14] and $(Ni_xCo_{1-x})_2P$[773] solid solutions were also obtained. In the latter case, a phase segregation was observed for high Co proportions. Moreover, the preparation of pure bulk Sn_3P_4 was found to be difficult because of its high tolerance for P deficiencies, but it was finally obtained using a constant phosphorus vapor generated in a colder reservoir (isopiestic method), without Sn_4P_3 impurities.[1173]

dx.doi.org/10.1021/cr400020d | Chem. Rev. XXXX, XXX, XXX−XXX

However, it has to be anticipated that the nanoscale would give slightly different results, at least from the viewpoint of thermodynamics: (i) Surface energy may become significant and could overcome crystal cohesion which dictates the relative phase stabilities in the bulk, thus providing better tolerance to crystal defects. (ii) Overexpression of the surface energy may level energetic differences between different structures and stoichiometries, resulting in more pronounced structural flexibility, even at low temperature. It is striking to notice that, among the large variety of phases that are described at the bulk scale, very few are actually obtained as dispersed nanoparticles prepared in solvents, at low or moderate temperatures: Ni_2P and few examples of $Ni_{12}P_5$[633] (yet most of the time in mixtures of phases)[43,685] but no small nanoparticles of Ni_3P nor NiP_2, Fe_2P and FeP but no FeP_2 or Fe_3P, Co_2P and CoP but no CoP_3, InP but no InP_3, Cu_3P but no CuP_2, etc. In these cases, the stoichiometry control is basically achieved by using low excess or larger excess of a "P" donor (typically, TOP) that undergoes only a partial decomposition. The Ni−P system has been extensively studied. First, it was shown that phase transformation of crystalline $Ni_{12}P_5$ nanoparticles to the more P-rich Ni_2P nanoparticles was possible in solution, using TOP at very high temperature for a solvothermal route (350−370 °C for 3−4 h).[1174] These conditions were much stronger than the ones required for the direct synthesis of Ni_2P from the same precursors. This highlighted not only that TOP was slowly decomposed even at these temperatures, but also that crystallized $Ni_{12}P_5$ was likely a thermodynamic local minimum on the energy surface. Similar selectivities also occurred in the case of a quantitative reaction of the phosphorus source. Ni_2P−Ni nanoparticles were obtained instead of Ni_3P nanoparticles, in soft conditions:[713] it seems that some systems would prefer a phase segregation over the crystallization of the expected phase. This raises a general question about the stability of some metal phosphide phases at the nanoscale.

When solvents are used at high temperatures, reactants (TOP for metal phosphides)[1175] or even solvents (tetraethyleneglycol for metal borides)[52] led to the competitive formation of metal carbides as impurities or as a secondary phase. This point was often neglected because some of the carbide phases are not easy to distinguish from their metallic counterpart, on the basis of the XRD diffractograms.[52] Besides, EDS mounted on electron microscopes is often not reliable for carbon detection. XPS analysis nevertheless allows distinguishing carbides from ethers, alkanes, or alkenes. For instance, Ni_3C species have sometimes been wrongly assigned to hcp Ni, but XPS clearly showed a carbide contribution on the carbon spectrum,[52,1175] and it was later found that such carbidation had strong influence on the magnetic properties of the nanoparticles.[1176]

As a consequence, a subsequent "phosphidation" of metal phosphide nanoparticles may lead to carbides or carbidophosphides and not pure phosphides. Interestingly, the thermal decomposition (500 °C) of $FeCl_3$ and TOP was found to yield FeP nanoparticles.[669] However, further heating led to Fe_2P nanoparticles, suggesting that this is the most stable phase at the nanoscale, and also led to impurities that were assigned to iron carbides. It must be noted that surface carbide species could also form in these procedures, due to the appearance of carbon-containing decomposition products at the high temperatures typically utilized. Such surface carbides, that are known to have a strong influence in catalytic processes,[1177] could also change the surface energies and promote one or the other phase, or even be responsible for some of the anisotropic morphologies obtained when using TOP/TOPO mixtures.

6.1.3. Control of Polymorphism. Polymorphism is also met in metal borides and metal phosphides. Rational means to direct the reaction pathway toward one phase or the other are actually totally nonexistent at the nanoscale, as well as examples of selective synthesis of single polymorphs. In bulk systems, however, selectivity was reported: stoichiometric mixtures of Ni and red phosphorus (Ni:P = 1:2) yielded the cubic NiP_2 phase under mechanical alloying and the monoclinic one upon heating.[787] Similar cases for metal borides have not been described. For instance, selective synthesis of orthorhombic or monoclinic Ni_4B_3 is unknown.

6.2. P and B Sources: An Essential Struggle

6.2.1. Oxidation Degree of the Phosphorus Source. As presented before, metal phosphides are covalent compounds, where the electron density can easily be shifted from the metal center to the phosphorus one. In the synthesis of metal phosphide nanoparticles, there is no prerequisite on the metal or the phosphorus precursor in terms of oxidation states. However, a sufficient amount of electron density has to be given to the final compound, which is neutral.

Therefore, the phosphorus sources have to be distinguished considering not only their ability to provide "P" atoms, but also according to their oxidation state. $P(SiMe_3)_3$ is formally a P(−III) source. P_4 and other allotropes of elemental P are P(0) sources. PCl_3 is a P(III) source. PH_3, TOP, and other alkyl- and aryl-phosphines are formally P(III) sources, but H and C electronegativities are quite similar to P electronegativity. It must be noted that the reaction of PCl_3 (P(III)) with $P(SiMe_3)_3$ (P(−III)) was logically found to yield elemental phosphorus.[608]

Using zerovalent sources is straightforward, as the reaction of x M(0) with y P(0) generally yields M_xP_y compounds with a 100% yield in M and in P (see Table 7 and in particular refs49,50). Thus, a reaction between a M(II) source, for instance MCl_2, and a P(0) one would have to bring 2 electrons per metal, in addition to the stoichiometric P amount: such reaction was done using P_4 both as a "P" donor and a reductant, and yielded PCl_3 as a byproduct of the reduction step.[715,714]

When the phosphorus source is not reducing enough, it can be modified in situ to become more reducing (by forming Na_3P for instance),[709,710] and the P precursor has to be added in excess as it also plays the role of the reductant. Alternatively, an additional reductant such as $NaBH_4$[702] or Na[666,730] can be added to the solution. Yet, in this last route it is not always clear to know which part (metal or phosphorus precursor) will be reduced first, and this has strong consequences on the nucleation/growth behavior of the nanoparticles.

However, the final oxidation state of the metal in the metal phosphide structure is most of the time slightly positive, as discussed above. Thus, the phosphine source is sometimes paradoxically described as an oxidizing source, when the metal source is already reduced, such as for the synthesis of MnP nanoparticles from $Mn_2(CO)_{10}$ and $P(SiMe_3)_3$.[641] In other cases, such as the reaction of In(0) nanoparticles with $P(SiMe_3)_3$, the electrons in excess are assumed to react with solvent impurities or surface oxide impurities on the indium.[659]

In the vast majority of studies, reductive sources of phosphorus are used, which is related with the utilization of oxidized metal precursors. However, due to the complexity of

dx.doi.org/10.1021/cr400020d | Chem. Rev. XXXX, XXX, XXX−XXX

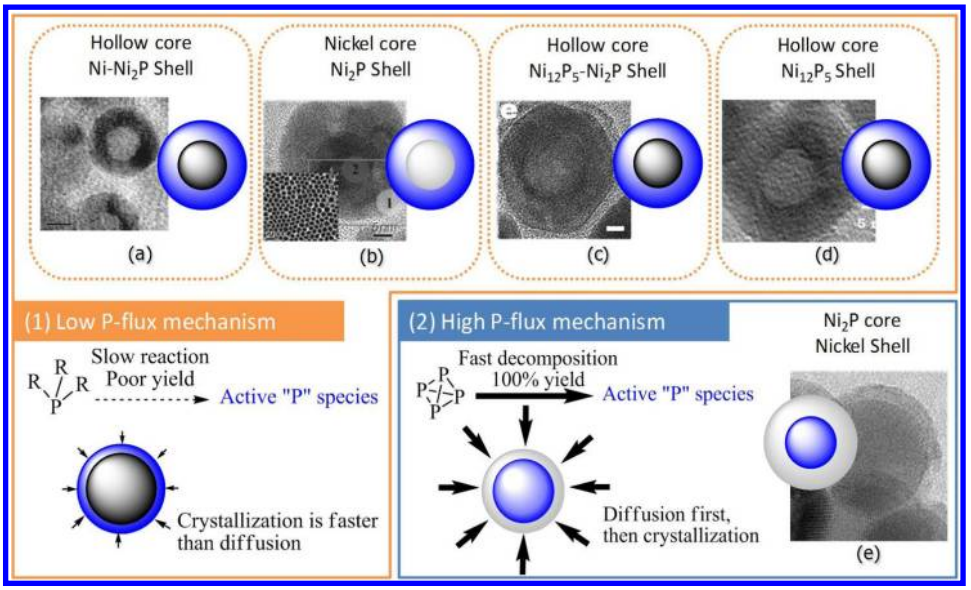

Figure 56. Hollow and core−shell structures obtained in the Ni−P system in (a) ref 696, (b) ref 695, (c) ref 685, (d) ref 679, and (e) ref 713. (1) Low P-flux mechanism leading to metal phosphides in the shell (TOP or another alkylphosphine is used as the P donor). (2) High P-flux mechanism leading to metal phosphide in the core (P_4 dissolved in the solution is used as a P donor). Adapted, respectively, with permission from refs 696, 695, 685, 679, 713. Copyright, respectively, 2010 American Chemical Society, 2009 American Chemical Society, 2009 American Chemical Society, 2010 American Chemical Society, 2011 American Chemical Society.

the reaction mixtures, it is rarely obvious to know if the electrons of the final metal phosphide come from this "P" source, or if the metal is reduced by another participant (solvent, reductant) at the high temperatures that are utilized. As a corollary, the in situ reactive source of phosphorus remains unclear in most of the cases because it often has to be severely modified before its reaction with the metal (such as in the case of TOP).

6.2.2. Oxidation Degree and Reactivity of the Boron Source. The same statement on the redox reactivity of phosphorus sources can be made for boron sources: oxidizing or reducing species can be used depending on the redox state of the metal source, as long as enough electrons are provided to the system. Use of a coreductant can be fruitful, as seen for the reaction between boron oxide and metal chlorides in the presence of magnesium.[331,406] Very often, reducing species, whether coreactant or borohydride ions, are introduced in excess (see for instance Table 4), and the final stoichiometry of the product is not controlled. Actually, the range of available boron sources is quite limited compared to P precursors: mainly boron, boranes, alkali borohydrides, boron halides, boron oxide, and boric acid. Two points clearly differenciate the B case from the P case: (i) Elemental boron is not a molecular entity and is strongly inert. This is testified by etching tests in nitric acid which showed that metal boride nanocrystals are etched faster than amorphous elemental boron,[51] a quite surprising result which is opposed to most other cases; here, an amorphous phase seems more inert, if not stable, than a crystalline one. (ii) Decomposition of the other sources follows a complex multistep scheme. Especially, even when the reaction with the metal precursor is fast, intermediate species, such as amorphous phases, are formed. The resistance to crystallization of metal borides then hinders ordering until high energy input is provided, usually through temperature increase.

Despite these difficulties, three recent routes are worth mentioning and would require more in-depth exploration. First, highly reactive boron sources are still to be found. In this respect, multidisciplinary collaborations between the communities of organic chemistry, organometallic chemistry, solid state chemistry, and nanomaterials should be highly beneficial, not only to identify single M/B sources, but even new B precursors. Second, metal sources that have been mainly left aside should be considered in more detail, since a highly reactive metal source could presumably compensate the lack of reactivity of current boron sources. Third, the use of coreactants seems promising, even if their real effect on the reaction pathway is unknown.

6.3. Toward Advanced Morphologies and Complex Nanostructures

6.3.1. Reactivity of the P Source for the Preparation of Advanced Morphologies. Core−shell morphologies of metal phosphide nanoparticles are a nice example of the exquisite control that can be reached by colloidal synthesis and rational use of the metalloid source. They were obtained through the so-called "nanoscale Kirkendall mechanism".[41,44,47,1178] It consists of the outward migration of the metal during the phosphidation process. However, the driving force for this reaction is still unclear: surface curvature, diffusion promoted by the temperature, and presence of defects are arguments that were proposed.[1179] A better understanding of this solid-state-like nanoscaled process would benefit from studies in the softest conditions possible and using a stoichiometric "P" donor.

A variety of core−shell and hollow structures could be obtained in the Ni−P system (Figure 56), containing Ni, $Ni_{12}P_5$, and/or Ni_2P in an amorphous or a crystallized state. Their localization and identification were not straightforward, first because of the relatively small size of these nanoparticles, and second because EDS and XPS analyses had to be used with caution. Indeed, the nanoparticles surface was most of the time covered with TOP (or another phosphine), which was used as the ligand to limit the size of the nanoparticles. However, a clear trend appeared when considering the effect of the phosphorus source on the final morphology. When TOP or

dx.doi.org/10.1021/cr400020d | Chem. Rev. XXXX, XXX, XXX−XXX

another low-yield P-source was employed, the flux of phosphorus across the surface was low, and long reaction times were needed to incorporate the required amount of P atoms (Figure 56, mechanism 1).[695,696,685,679] As a result, the kinetics of crystallization was fast compared to the one of P-diffusion, and the Ni−P phase (either Ni_2P, $Ni_{12}P_5$, or mixtures remained in the shell). It is interesting to note that nickel atoms also had the time to diffuse outward in some instances, resulting in hollow nanoparticles (Figure 56a,c,d).

On the contrary, when a very reactive source of P was employed (P_4 in solution), high amounts of phosphorus were rapidly incorporated into the nanoparticles and were free to diffuse to reach the center of the nanoparticles (Figure 56, mechanism 2).[713] This effect was better observed by employing substoichiometric amounts of P_4 (Ni/P = 3 or more). It resulted in the fast incorporation of P and a slower crystallization of Ni_2P in each nanoparticle, in their center (Figure 56e). Interestingly, this latter example also raised the question of phase preference at the nanoscale, since the Ni_3P phase could have been expected as the only product of the reaction. Instead, a nanoscale-induced phase segregation was observed and resulted in an original Ni_2P−Ni core−shell structure, where the Ni shell thickness could be tuned by adjusting the amount of P_4. Altogether, this example on the Ni−P system not only stressed out the impact of nanoscale on thermodynamics and phase diagrams, but it also highlighted the influence of kinetics (crystallization vs decomposition of the "P" source) for the fine control of advanced metal phosphide nanostructures.

6.3.2. Toward Complex Structures: Janus Nanoparticles as an Example of the Power of Colloidal Synthesis. Anisotropic metal phosphide nanoparticle morphologies, such as nanorods or nanowires, were obtained by tuning the surface energy through selective adsorption of ligands or surfactants on some facets. For instance, in the case of FeP, the addition of TOPO in the TOP mixture favored the growth of 1D structures.[651]

In comparison with macroscopic crystals, nanoparticles are relatively easily transformed at moderate temperatures, either to obtain new phases or to create complex architectures such as core−shell or Janus structures. This offers an additional synthetic lever for a fine-tuning of properties for catalysis, magnetism, or optics.

It was shown in the previous subsection that the kinetics of decomposition of the P donor had strong consequences on the reaction outcome. The kinetics of diffusion versus crystallization can also influence the final nanoparticle morphology, as well exemplified in the Cu−P system. Using the thermal decomposition of TOP at 350 °C, Cu nanoparticles were partially converted to Cu_3P.[674] This partial conversion was promoted by the relatively small excess of TOP employed (5.6 TOP per Cu). The nucleation of small Cu_3P domains occurred on the side of the starting nanoparticles. Upon further P insertion, these domains would grow, and the reaction could be stopped at an intermediate state where only one hemisphere of the Cu nanoparticles would have been converted to Cu_3P, as shown in Figure 57. The authors explained the appearance of an asymmetry in the nanoparticles, instead of a core−shell structure, through inhomogeneous ligand coverage on the starting Cu nanoparticles. It should also be noted that no amorphous intermediate was observed in this system, in contrast with the Ni−P one, which likely contributed to maintain spontaneous symmetry breaking. On the other hand,

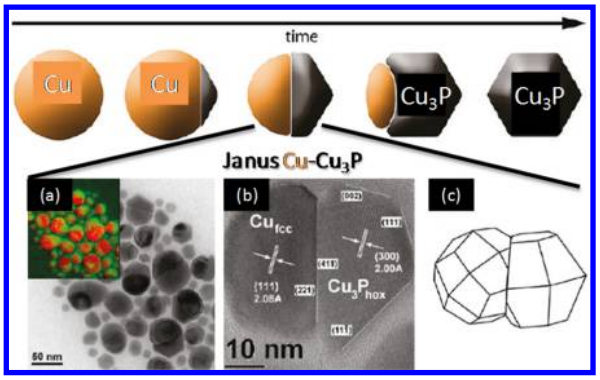

Figure 57. Formation of Cu−Cu_3P Janus nanoparticles upon reaction of TOP with Cu nanoparticles. (a) EFTEM zero-loss images of the sample, with inset showing P (green) and Cu (red) EFTEM maps of the same zone. (b) HRTEM images of the Janus nanoparticles. (c) Reconstruction of the crystalline shape of the structure shown in part b. Adapted with permission from ref 674. Copyright 2012 American Chemical Society.

the nature of the crystallographic facets in contact in the final Janus structure ensured minimizing of the interfacial energy, because the nucleation and growth of the Cu_3P grain occurred without any volume constraint.

The formation of a Janus structure instead of a core−shell one could suggest that the metal/metal phosphide interface is associated with a high energy cost in this case. The fact that the particles showed a constriction at the interface would support this idea. Yet, the use of a different soluble P source, P_4, yielded a core−shell Cu−Cu_3P structure instead of a Janus one.[717] As discussed in subsection 6.3.1, the flux of P reacting with the nanoparticles is higher when using white phosphorus than when using TOP. The core−shell structure might thus be a higher energy local minimum than the Janus one, in the case of Cu−Cu_3P structures. Another possible explanation is that the decomposition of TOP to provide P atoms is significantly faster on the defects of the surface, such as the one found at the Cu−Cu_3P interface. Annealing experiments under controlled atmosphere might be a way to get experimental insights into these questions.

Altogether, the examples of Ni−P and Cu−P highlighted the role of reaction thermodynamics and kinetics on the formation of advanced metal phosphide nanostructures (core−shell, hollow, Janus). Controlled syntheses were achieved only through detailed mechanistic studies. Further advances in this field will have to take advantage of highly reactive P-donors and spontaneous symmetry breaking to yield new structures. The phosphidation of binary metal nanoparticles will also have to be studied from this perspective.

6.3.3. Homogeneous versus Heterogeneous Nucleation: A "Trick" To Overcome Boron Lack of Reactivity. The low efficiency of current boron sources does not enable the refined morphological control reached by solvent based metal phosphide syntheses. However, a survey of the literature affords interesting examples that are different than typical spherical particles. In particular, the case of CVD and HPCVD of MgB_2 nanostructures, already detailed in subsection 3.2.5, exemplifies the additional morphological diversity (rods, prisms) that can be rationally attained by taking advantage of reactions at the interfaces. The 0D and 1D growth can be supposed to occur from, respectively, homogeneous and heterogeneous nucleation of MgB_2: micrometer scale 0D prisms[387] were obtained with

dx.doi.org/10.1021/cr400020d | Chem. Rev. XXXX, XXX, XXX−XXX

high concentration of precursors and under high temperature, two parameters favoring homogeneous nucleation. On the contrary, 1D submicronic morphologies such as pillars[386] and helices[388] resulted from lower reactant concentrations and lower temperatures, ensuring heterogeneous nucleation. Such an approach, not rationalized in the original reports, could be advantageously extended to the case of nanoscaled metal borides as well as metal phosphides.

6.4. Surface State, Surface Oxidation, and Other Surface Passivation

It must be mentioned that the surface of metal borides and metal phosphides (bulk or nanoparticles) is in some instances highly reactive toward oxygen. For instance, an amorphous oxidized shell, identified as oxide by EELS, can be clearly seen on some alkaline earth hexaboride nanowires obtained by CVD.[240] Similarly, the effects of oxygen on the passivation of InP nanowires with H and OH were studied by DFT calculation to understand its consequence on the luminescence properties.[1180] Coverage on purpose by the oxidation product is possible on InP (14% lattice mismatch with In_2O_3), in order to grow a protective In_2O_3 shell on InP. Metal boride UAAPs can also be passivated by flowing air above the powder to grow an amorphous oxide shell. Interestingly, while amorphous metal boride nanoparticles prepared under inert conditions are pyrophoric, crystalline nanoparticles seem more stable.[51,52]

In the case of colloidal syntheses, the ligands dynamics is of paramount importance for further functionalization, but also in-depth understanding of the nanoparticle reactivity. It was studied in detail on InP for which TOPO ligand equilibrium between the surface and the solution was investigated by solution NMR.[1181] Even using nonexchangeable ligands such as long chain carboxylate strongly bound to the surface, a shell of indium oxide could still exist around small InP nanoparticles (2.7 nm) strictly synthesized in air-free conditions.[1182] This was explained by the formation of water as a product of the side-reaction involving the carboxylate. Water then oxidized the surface of the nanoparticles to indium phosphate species. As a consequence, the nanoparticles exhibited a limited growth and a limited luminescence. This exemple illustrates the complexity of surface definition and characterization, since the chosen set of ligands not only influences the nature of the organic layer surrounding the nanoparticles, but also can lead to modification of the inorganic core. It should be remembered that most of the reaction mechanisms are poorly known in this field, and that such phenomenon could occur in a number of other synthetic procedures that employ metal carboxylates as precursors. Further growth of a ZnS shell was also shown to significantly oxidize the InP core.[1183]

Chemical modifications of the surface down on purpose are also possible: etching of InP synthesized with $P(SiMe_3)_3$ was achieved in a fluorinated ionic liquid under microwave irradiation, and allowed an enhancement of the photoluminescence to a quantum yield of 47% by in situ etching of the surface oxide species and fluorine passivation of the surface.[1184] This procedure avoided the use of highly toxic HF for surface passivation, highlighting the interplay between chemistry and process for the improvement of nanomaterials though surface tailoring.

6.5. Mechanistic Studies and Trails for the Design of New Synthetic Routes

We have shown in this review the numerous routes that have been uncovered for the synthesis of nanoscaled metal borides and phosphides. However, only few mechanistic studies have been proposed so far, which is largely due to the complexity of most of the reaction schemes: various precursors and reactants are generally used in complex processes, not well suited for a step-by-step analysis.

Although it is admitted that the precursors of P or B undergo several transformations, most of the time simultaneously with the metal precursor, almost nothing is known about the nature of these reaction intermediates. Therefore, how to design the precursors to trigger the formation of one phase in spite of another, to increase the yields, or to gain a rational control on the morphology and size of the product remains an unanswered question. This problem is complex and requires a combination of experimental techniques because several length scales and state of the matter have to be analyzed in the course of one process: from monometallic molecules to extended crystal lattices, from gas phase or liquid phase to condensed matter, from amorphous to crystalline and from bare surfaces to ligand-stabilized or passivated surfaces. These transformations are intimately connected. Thus the use of in situ techniques, with time-resolution and spatial resolution whenever possible, will be required to solve the interplay of all these parameters. Modelization at any scale (DFT level, molecular dynamics, etc.) will also have to be used to help select the most likely routes and interpret the experimental data.

6.5. Novel Properties and Fields of Applied Research: The Potential Fate of Nanostructured MBs and MPs as Nanomaterials

Altogether, this review summarized the wide variety of nanostructured metal boride and metal phosphide nanoparticles that can be obtained nowadays, and the strategies that researchers successfully developed to reach these nanoscaled phases. If the covalent character of metal borides and metal phosphides enables researchers to build bridges between both systems, the development of nanoscaled metal borides is clearly less mature, with a reluctance for the discovery of new routes, essentially for two reasons: the lack of highly reactive boron sources and the resistance to crystallization. Both points suggest that the solution for nanoscaled metal boride synthesis is to be found at higher temperature than metal phosphides, unless a fundamental breakthrough is made.

While mechanistic studies could shed light on the crucial experimental levers for better compositional, structural, and morphological control of nanostructured metal phosphides and metal borides, another tentalizing approach is to rethink the existing syntheses in terms of precursors, in an attempt to rationalize the stoichiometry introduced and the reaction temperature. The use of single-source precursors provides an interesting solution by bringing the constituents in the right stoichiometry and already intertwinned at the molecular scale. A third path is to use very reactive P or B sources to ensure a quantitative incorporation in the final nanomaterials. The two families of materials are not mirrored in this aspect, since elemental phosphorus P_4 is highly reactive while elemental boron allotropes are very stable. Finally, relying on specific reaction media that can enhance kinetics, like specific solvents (e.g., salt melts) for metal borides, is another tempting solution. Given the possibilities offered by modern tools, the exploration of these routes and identification of the most promising ones will certainly rely on detailed in situ monitoring of the reaction pathway.

dx.doi.org/10.1021/cr400020d | Chem. Rev. XXXX, XXX, XXX−XXX

The properties of nanoscaled metal borides and metal phosphides were shown to differ, if not outperform in some cases, those of the traditional bulk phases because of increased surface exposure or grain boundary density, and also confinement, like quantum effects in semiconductors. However, many fields described above have only been touched upon. Actually, the behavior of these nanoscaled crystalline phases in electronics, optics, magnetism, mechanics, and biomedicine are still to be explored, especially because most of these compounds have not been obtained yet at the nanoscale in the strict sense: one particle dimension below 100 nm. Future works may then first concentrate on a better rationalization of the synthetic procedures, in order to further develop applications, for instance in the field of catalysis. In order to express the full potential of nanoscaled metal borides and metal phosphides as materials, the adopted synthetic procedures should also address the practical and societal questions of safety, sustainability, and scalability, while opening the routes of shaping and processing. Most of these goals are still out of reach. Yet, they promise, together with the design of novel synthesis pathways and the discovery of new materials and new properties, many years of exciting and stimulating research, which should open new horizons of nanomaterials and nanotechnology.

AUTHOR INFORMATION

Corresponding Author

*E-mail: david.portehault@upmc.fr (D.P.); clement.sanchez@upmc.fr (C.S.).

Present Addresses

[⊥]Materials Sciences Division, Lawrence Berkeley National Lab, 1 Cyclotron Road, Berkeley, California 94720, United States.
[#]Université Paul Sabatier, Laboratoire Hétérochimie Fondamentale et Appliquée, UMR CNRS 5069, 118 Route de Narbonne, 31062 Toulouse Cedex 9, France.

Notes

The authors declare no competing financial interest.

Biographies

Sophie Carenco graduated from Ecole Polytechnique, Palaiseau, in 2008. She obtained her Ph.D. in 2011 from University Pierre and Marie Curie for her work on the synthesis and applications of metal phosphide nanoparticles, under the co-supervision of Pr. Clément Sanchez (UPMC) and Dr. Nicolas Mézailles (Ecole Polytechnique). She is, since January 2012, a postdoctoral fellow at Lawrence Berkeley National Lab, Berkeley, California, in the group of Prof. Miquel Salmeron, and she performs synchrotron based in situ spectroscopies (XPS, XAS) to study catalytic reactions at the surface of metal nanoparticles. She is the author of 15 publications and one book chapter. She was awarded the European Young Chemist Award from EuCheMS in 2010 and the C'Nano National Award in 2012 for her Ph.D. work.

David Portehault is currently full researcher at the CNRS in the Laboratoire de Chimie de la Matière Condensée de Paris (LCMCP), a mixed team affiliated with the University Pierre and Marie Curie, the CNRS, and the Collège de France. He graduated from the Ecole Normale Supérieure, Paris, in 2005. After Ph.D. work at the LCMCP under the supervision of Prof. J.-P. Jolivet, he became a fellow of the Excellence CNRS—Max Planck Society postdoctoral program for nanomaterials and performed senior postdoctorate research in the Colloids Department under the supervision of Prof. M. Antonietti in the Max Planck Institute for Colloids and Interfaces at Potsdam during 2008−2010. He was then recruited at the CNRS, where his current interests deal with the design by innovative molecular approaches, based, e.g., on "chimie douce", colloidal synthesis, and the sol−gel routes, of innovative nanoparticles and nanostructured materials with advanced properties, including binary and ternary metal oxides (titanium, manganese) and nonoxides (carbides, nitrides, borides). These materials are often developed at the interface between physics and chemistry. They are especially destined for application fields such as energy harnessing and information technologies.

Cédric Boissière is currently full researcher of the CNRS in the LCMCP, a mixed team affiliated with the University Pierre and Marie Curie, the CNRS, and the Collège de France. He was born in 1974 and graduated from Montpellier University in 1998. After Ph.D. work in inorganic ultrafiltration mesoporous membranes prepared by soft chemistry, he was recruited as a full researcher at CNRS in France in 2002. He is the author of 120 publications in nanomaterials science and 25 patents mainly focused on the synthesis and application of hierarchical functional materials processing in general and more

dx.doi.org/10.1021/cr400020d | Chem. Rev. XXXX, XXX, XXX−XXX

specifically focused on heterogeneous catalysts. His current materials of interest are nanoparticles of metal, metal oxides, and metal fluorides, and inorganic and hybrid nanocomposites, which are obtained through evaporation processes (dip-coating and spray drying for materials shaping as thin films and size controlled powders, respectively). They are destined for application fields such as energy harnessing, heterogeneous catalysis, functional optical thin films, silica based therapeutic vectors, and sensing technologies. He received the 2006 award of the European Membrane Society the Jean RIST Medal of the French Society of Metals and Materials (SF2M) in 2007.

Nicolas Mézailles is currently a Research Director at Université Paul Sabatier in the "Laboratoire Hétérochimie Fondamentale et Appliquée". After graduating from Ecole Nationale Supérieure de Chimie de Toulouse as chemical engineer, Nicolas Mézailles obtained a Ph.D. degree in 1997 from Purdue University (Indiana) under the direction of Prof. Clifford Kubiak. He came back to France to receive postdoctoral training at the Ecole Polytechnique in the group of Prof. François Mathey. He was recruited by CNRS in 1998 in the "UMR 7653" and has worked with Prof. P. Le Floch. He was promoted to Research Director in 2008. His ongoing research interests span the use of geminal dianions as precursors for the synthesis of metal carbene fragments, ligand synthesis and coordination, the mechanisms of nanoparticle synthesis, metal−phosphide nanoparticles, and more recently transition metal activation of N_2.

Clément Sanchez is Professor at the Collège de France, Chair "Chemistry of Hybrid Materials", and Director of the Laboratoire de Chimie de la Matière Condensée de Paris (mixed unit between University of Pierre and Marie Curie, Collège de France, and CNRS). He was Director of Research at the National Center for Scientific Research (CNRS) and Professor at the Ecole Polytechnique. He received an Engineer degree from the Ecole Nationale Supérieure de Chimie de Paris in 1978 and a "Thèse d'État" (Ph.D.) in physical chemistry from the University of Paris VI in 1981. He did postdoctoral work at the University of California, Berkeley, and is currently performing research at the Collège de France in Paris. He is specialized in the field of nanochemistry and physical properties of nanostructured porous and nonporous inorganic and hybrid organic inorganic materials shaped as monoliths, microspheres, and films. He is studying the resulting properties of these materials with their implications in the fields of environment, energy and nanomedicine. He was the recipient of many national and international awards. He is a member of several Academies of Sciences (French, European, Europaea, and so forth) and an MRS Fellow (for a more complete CV see http://www.labos.upmc.fr/lcmcp/?q=node/1973). He was scientific organizer of several international meetings associated with the field of soft-chemistry, hybrid materials, and related bioaspects.

ACKNOWLEDGMENTS

The authors acknowledge the University Pierre and Marie Curie, the CNRS, the Collège de France, the Ecole Polytechnique, and the Direction Générale de l'Armement for funding.

REFERENCES

(1) Jolivet, J.-P. *Metal Oxide Chemistry and Synthesis: From Solution to Solid State*; Wiley: Chichester, U.K., 2000.
(2) Niederberger, M.; Pinna, N. *Metal Oxide Nanoparticles in Organic Solvents*; Springer: London, 2009.
(3) Debecker, D. P.; Mutin, P. H. *Chem. Soc. Rev.* **2012**, *41*, 3624.
(4) Sanchez, C.; Belleville, P.; Popall, M.; Nicole, L. *Chem. Soc. Rev.* **2011**, *40*, 696.
(5) Xia, Y.; Xiong, Y.; Lim, B.; Skrabalak, S. E. *Angew. Chem., Int. Ed.* **2009**, *48*, 60.
(6) Yin, Y.; Alivisatos, A. P. *Nature* **2005**, *437*, 664.
(7) Hughes, B.; Luther, J.; Beard, M. *ACS Nano* **2012**, *6*, 4573.
(8) Rosenthal, S. J.; Chang, J. C.; Kovtun, O.; McBride, J. R.; Tomlinson, I. D. *Chem. Biol.* **2011**, *18*, 10.
(9) Mattoussi, H.; Palui, G.; Na, H. B. *Adv. Drug Deliv. Rev.* **2012**, *64*, 138.
(10) Giordano, C.; Antonietti, M. *Nano Today* **2011**, *6*, 366.
(11) Sharon, M.; Tamizhmani, G. *J. Mater. Sci.* **1986**, *21*, 2193.
(12) Trindade, T.; O'Brien, P.; Pickett, N. L. N. L. *Chem. Mater.* **2001**, *13*, 3843.
(13) Landau, M. V.; Herskowitz, M.; Hoffman, T.; Fuks, D.; Liverts, E.; Vingurt, D.; Froumin, N. *Ind. Eng. Chem. Res.* **2009**, *48*, 5239.
(14) Fahrenholtz, W. G.; Hilmas, G. E.; Talmy, I. G.; Zaykoski, J. a. *J. Am. Ceram. Soc.* **2007**, *90*, 1347.
(15) Brown, D.; Ma, B.-M.; Chen, Z. *J. Magn. Magn. Mater.* **2002**, *248*, 432.
(16) Nagamatsu, J.; Nakagawa, N.; Muranaka, T.; Zenitani, Y.; Akimitsu, J. *Nature* **2001**, *410*, 63.
(17) Glowacki, B. *Phys. C* **2003**, *387*, 153.
(18) Mori, T. In *Handbook on the Physics and Chemistry of Rare Earths*; Gschneidner, K. A., Jr., Bunzli, J. C., Pecharsky, V., Eds.; Elsevier: Amsterdam, 2007; Vol. *38*, pp 105.
(19) Pyshkin, S.; Ballato, J.; Bass, M.; Turri, G. *J. Electron. Mater.* **2009**, *38*, 640.
(20) Ji, X. H.; Zhang, Q. Y.; Xu, J. Q.; Zhao, Y. M. *Prog. Solid State Chem.* **2011**, *39*, 51.
(21) Mori, T. *J. Phys.: Conf. Ser.* **2009**, *176*, 012036.
(22) Levine, J. B.; Tolbert, S. H.; Kaner, R. B. *Adv. Funct. Mater.* **2009**, *19*, 3519.
(23) Schneider, S. B.; Baumann, D.; Salamat, A.; Konôpková, Z.; Liermann, H.; Schwarz, M. R.; Morgenroth, W.; Bayarjargal, L.; Friedrich, A.; Winkler, B.; Schnick, W. *Chem. Mater.* **2012**, *24*, 3240.
(24) Sung, J.; Goedde, D. M.; Girolami, G. S.; Abelson, J. R. *J. Appl. Phys.* **2002**, *91*, 3904.
(25) Pei, Y.; Zhou, G.; Luan, N.; Zong, B.; Qiao, M.; Tao, F. F. *Chem. Soc. Rev.* **2012**, *41*, 8140.

(26) Oyama, S. T.; Gott, T.; Zhao, H.; Lee, Y.-K. *Catal. Today* **2009**, *143*, 94.
(27) Brock, S. L.; Perera, S. C.; Stamm, K. L. *Chem.—Eur. J.* **2004**, *10*, 3364.
(28) Kanda, Y.; Temma, C.; Nakata, K.; Kobayashi, T.; Sugioka, M.; Uemichi, Y. *Appl. Catal., A* **2010**, *386*, 171.
(29) Kim, M. G.; Cho, J. *Adv. Funct. Mater.* **2009**, *19*, 1497.
(30) Licht, S.; Ghosh, S.; Wang, B.; Jiang, D.; Asercion, J.; Bergmann, H. *Electrochem. Solid-State Lett.* **2011**, *14*, A83.
(31) Licht, S.; Hettige, C.; Lau, J.; Cubeta, U.; Wu, H.; Stuart, J.; Wang, B. *Electrochem. Solid-State Lett.* **2012**, *15*, A12.
(32) Cabana, J.; Monconduit, L.; Larcher, D.; Palacín, M. R. *Adv. Mater.* **2010**, *22*, E170.
(33) Alexander, A.-M.; Hargreaves, J. S. J. *Chem. Soc. Rev.* **2010**, *39*, 4388.
(34) Pol, V. G.; Pol, S. V; Gedanken, A. *Adv. Mater.* **2011**, *23*, 1179.
(35) Chen, Y. *Catal. Today* **1998**, *44*, 3.
(36) Wu, Z.; Li, W.; Zhang, M.; Tao, K. *Front. Chem. Eng. China* **2007**, *1*, 87.
(37) Demirci, U. B.; Miele, P. *Phys. Chem. Chem. Phys.* **2010**, *12*, 14651.
(38) Greenwood, N. N.; Parish, R. V.; Thornton, P. *Q. Rev., Chem. Soc.* **1965**, 441.
(39) Shein, I. R.; Medvedeva, N. I.; Ivanovskii, a. L. *Phys. B* **2006**, *371*, 126.
(40) Albert, B.; Hillebrecht, H. *Angew. Chem., Int. Ed.* **2009**, *48*, 8640.
(41) Henkes, A. E.; Schaak, R. E. *Inorg. Chem.* **2008**, *47*, 671.
(42) Henkes, A. E.; Schaak, R. E. *Chem. Mater.* **2007**, *19*, 4234.
(43) Muthuswamy, E.; Savithra, G. H. L.; Brock, S. L. *ACS Nano* **2011**, *5*, 2402.
(44) Muthuswamy, E.; Kharel, P. R.; Lawes, G.; Brock, S. L. *ACS Nano* **2009**, *3*, 2383.
(45) Park, J.-G. J.; Koo, B.; Yoon, K. Y.; Hwang, Y.; Kang, M.; Hyeon, T. *J. Am. Chem. Soc.* **2005**, *127*, 8433.
(46) Strupeit, T.; Klinke, C.; Kornowski, A.; Weller, H. *ACS Nano* **2009**, *3*, 668.
(47) Chiang, R.-K. R.-T. *Inorg. Chem.* **2007**, *46*, 369.
(48) Bae, I.-T.; Vasekar, P.; VanHart, D.; Dhakal, T. *J. Mater. Res.* **2011**, *26*, 1464.
(49) Carenco, S.; Resa, I.; Le Goff, X.; Le Floch, P.; Mézailles, N. *Chem. Commun.* **2008**, 2568.
(50) Carenco, S.; Demange, M.; Shi, J.; Boissière, C.; Sanchez, C.; Le Floch, P.; Mézailles, N. *Chem. Commun.* **2010**, *46*, 5578.
(51) Portehault, D.; Devi, S.; Beaunier, P.; Gervais, C.; Giordano, C.; Sanchez, C.; Antonietti, M. *Angew. Chem., Int. Ed.* **2011**, *50*, 3262.
(52) Schaefer, Z. L.; Ke, X.; Schiffer, P.; Schaak, R. E. *J. Phys. Chem. C* **2008**, *112*, 19846.
(53) Ma, J.; Gu, Y.; Shi, L.; Chen, L.; Yang, Z.; Qian, Y. *Chem. Phys. Lett.* **2003**, *381*, 194.
(54) Ma, J.; Du, Y.; Wu, M.; Li, G.; Feng, Z.; Guo, M.; Sun, Y.; Song, W.; Lin, M.; Guo, X. *J. Alloys Compd.* **2009**, *468*, 473.
(55) Gu, Y.; Qian, Y.; Chen, L.; Zhou, F. *J. Alloys Compd.* **2003**, *352*, 325.
(56) Feng, X.; Bai, Y.-J.; Lü, B.; Zhao, Y.-R.; Yang, J.; Chi, J.-R. *Inorg. Chem. Commun.* **2004**, *7*, 189.
(57) Brewer, J. R.; Jacobberger, R. M.; Diercks, D. R.; Cheung, C. L. *Chem. Mater.* **2011**, *23*, 2606.
(58) Kim, J. W.; Shim, J.-H.; Ahn, J.-P.; Cho, Y. W.; Kim, J.-H.; Oh, K. H. *Mater. Lett.* **2008**, *62*, 2461.
(59) Oganov, A. R. In *Boron Rich Solids: Sensors, Ultra High Temperature Ceramics, Thermoelectrics, Armor*; Orlovskaya, N., Lugovy, M., Eds.; Springer: Dordrecht, The Netherlands, 2011; p 207.
(60) Pakdel, A.; Zhi, C.; Bando, Y.; Golberg, D. *Mater. Today* **2012**, *15*, 256.
(61) De Morveau, G.; Lavoisier, A.; Berthollet, C.; De Fourcroy, A. *Méthode de Nomenclature Chimique*; Paris, 1787.
(62) Ade, M.; Kotzott, D.; Hillebrecht, H. *J. Solid State Chem.* **2010**, *183*, 1790.
(63) Tillard, M.; Belin, C. *Inorg. Chem.* **2011**, *50*, 3907.
(64) Fokwa, B. P. T. *Eur. J. Inorg. Chem.* **2010**, *2010*, 3075.
(65) Malik, Z. P.; Sologub, O.; Grytsiv, A.; Giester, G.; Rogl, P. F. *Inorg. Chem.* **2011**, *50*, 7669.
(66) Aronsson, B.; Lundström, T.; Rundqvist, S. *Borides, Silicides, and Phosphides: A Critical Review of Their Preparation, Properties and Crystal Chemistry*; Spottiswoode Ballantyne and Co.: Colchester, U.K., 1965.
(67) Von Schnering, H. G.; Hoenle, W. *Chem. Rev.* **1988**, *88*, 243.
(68) Gaskell, P. *J. Non-Cryst. Solids* **1979**, *32*, 207.
(69) Chevallier; Fée; Guibourt; Julia Fontenelle; Laugier; Orpila; Payen; Gabriel-Pelletan; Lassaigne-ach.-Richard; Robinet; Segalas-D'Echepare. *Journal de Chimie Médicale, Pharmacie et Toxicologie* **1827**, *3*, 536.
(70) Lassaigne, J.-L. *Abrégé Élémentaire de Chimie, Considérée Comme Science Accessoire à l'Étude de la Médecine, de la Pharmacie et de l'Histoire Naturelle*; Béchet Jeune: Paris, 1829.
(71) Kiessling, R. *J. Electrochem. Soc.* **1951**, *98*, 166.
(72) Samsonov, G. V. *Usp. Khim.* **1956**, *25*, 190.
(73) Samsonov, G. V. *Usp. Khim.* **1959**, *28*, 189.
(74) Gilles, P. W. In *Borax To Boranes*; American Chemical Society: Washington, DC, 1961.
(75) Von Crell, F. *Ann. Chim.* **1800**, *35*, 202.
(76) Davy, H. *Gilb. Ann.* **1810**, *73*, 16.
(77) Gay-Lussac, L. J.; Thénard, L.-J. *Rech. Phys. Chim.* **1811**, *1*, 276.
(78) Moissan, H. *Ann. Chim. Phys.* **1895**, *6*, 296.
(79) Weintraub, E. *Trans. Am. Electrochem. Soc.* **1909**, *16*, 165.
(80) Iizumi, K.; Kudaka, K.; Maezawa, D.; Sasaki, T. *J. Ceram. Soc. Jpn.* **1999**, *493*, 491.
(81) Millet, P.; Hwang, T. *J. Mater. Sci.* **1996**, *31*, 351.
(82) Yeh, C. L.; Wang, H. J. *Ceram. Int.* **2011**, *37*, 2597.
(83) Yeh, C.; Wang, H. *J. Alloys Compd.* **2010**, *490*, 366.
(84) Tammann, G. *Der Glaszustand*; Leopold Voss: Leipzig, 1933; p 123.
(85) Nakano, K.; Hayashi, H.; Imura, T. *J. Cryst. Growth* **1974**, *24–25*, 679.
(86) Levine, J. B.; Nguyen, S. L.; Rasool, H. I.; Wright, J. a.; Brown, S. E.; Kaner, R. B. *J. Am. Chem. Soc.* **2008**, *130*, 16953.
(87) Kanatzidis, M. G.; Pöttgen, R.; Jeitschko, W. *Angew. Chem., Int. Ed.* **2005**, *44*, 6996.
(88) Andrieux, L. *C. R. Acad. Sci.* **1929**, *189*, 1279.
(89) Paul, R.; Buisson, P.; Joseph, N. *C. R. Acad. Sci.* **1951**, *232*, 627.
(90) Schlesinger, H.; Brown, H. C.; Finholt, A.; Gilbreath, J. R.; Hoekstra, H. R.; Hyde, E. K. *J. Am. Chem. Soc.* **1953**, *75*, 215.
(91) Glavee, G. N.; Klabunde, K. J.; Sorensen, C. M.; Hadjapanayis, G. C. *Langmuir* **1992**, *8*, 771.
(92) Glavee, G. N.; Klabunde, K. J.; Sorensen, C. M.; Hadjipanayis, G. C. *Langmuir* **1993**, *9*, 162.
(93) Glavee, G. N.; Klabunde, K. J.; Sorensen, C. M.; Hadjipanayis, G. C. *Inorg. Chem.* **1993**, *32*, 474.
(94) Glavee, G. N.; Klabunde, K. J.; Sorensen, C. M.; Hadjipanayis, G. C. *Inorg. Chem.* **1995**, *34*, 28.
(95) Corrias, A.; Ennas, G.; Musinu, A.; Marongiu, G.; Paschina, G. *Chem. Mater.* **1993**, *5*, 1722.
(96) Glavee, G. N.; Klabunde, K. J.; Sorensen, C. M.; Hadjipanayis, G. C. *Langmuir* **1994**, *10*, 4726.
(97) Marggraf, A. *Chymische Schriften*; Arnold Web.: Berlin, 1761.
(98) Pelletier, B.; Pelletier, C.; Sédillot, J. *Mémoires et Observations de Chimie*; Chez Croullerois: Paris, 1798; Vol. *2*, p 42.
(99) Carenco, S.; Boissière, C.; Mézailles, N.; Sanchez, C. *Actual. Chim.* **2012**, 22.
(100) Schlesinger, M. E. *Chem. Rev.* **2002**, *102*, 4267.
(101) Charles, E.; Charles, B. Y. E. *J. Am. Chem. Soc.* **1937**, *323*, 2038.
(102) Sweeny, N.; Rohrer, C.; Brown, O. *J. Am. Chem. Soc.* **1958**, *80*, 799.
(103) Albert, B. *Eur. J. Inorg. Chem.* **2000**, *2000*, 1679.
(104) Shveikin, G. P.; Ivanovskii, A. L. *Russ. Chem. Rev.* **1994**, *63*, 711.
(105) Ivanovskii, A. L. *J. Superhard Mater.* **2011**, *33*, 73.
(106) Ivanovskii, A. L. *Prog. Mater. Sci.* **2012**, *57*, 184.

(107) Caputo, R.; Guzzetta, F.; Angerhofer, A. *Inorg. Chem.* **2010**, *49*, 8756.
(108) Kortus, J.; Mazin, I.; Belashchenko, K.; Antropov, V.; Boyer, L. *Phys. Rev. Lett.* **2001**, *86*, 4656.
(109) Chen, X.; Tu, Q.; He, M.; Dai, L.; Wu, L. *J. Phys.: Condens. Matter* **2001**, *13*, L723.
(110) Burdett, J. K.; Canadell, E.; Miller, G. J. *J. Am. Chem. Soc.* **1986**, *108*, 6561.
(111) Burdett, J. K.; Canadell, E. *Inorg. Chem.* **1988**, *27*, 4437.
(112) Fehlner, T. P. *J. Solid State Chem.* **2000**, *154*, 110.
(113) Kanama, D.; Oyama, S.; Otani, S.; Cox, D. *Surf. Sci.* **2004**, *552*, 8.
(114) Knappschneider, A.; Litterscheid, C.; Kurzman, J.; Seshadri, R.; Albert, B. *Inorg. Chem.* **2011**, *50*, 10540.
(115) Gillan, E. G.; Kaner, R. B. *Chem. Mater.* **1996**, *8*, 333.
(116) Çamurlu, H. E.; Maglia, F. *J. Eur. Ceram. Soc.* **2009**, *29*, 1501.
(117) Villars, P. *Pearson's Handbook: Crystallographic Data for Intermetallic Phases*; ASM International: Materials Park, OH, 1997.
(118) Hillebrecht, H.; Ade, M. *Angew. Chem., Int. Ed.* **1998**, *37*, 935.
(119) Kotzott, D.; Ade, M.; Hillebrecht, H. *Solid State Sci.* **2008**, *10*, 291.
(120) Kotzott, D.; Ade, M.; Hillebrecht, H. *J. Solid State Chem.* **2009**, *182*, 538.
(121) Lugscheider, E.; Reimann, H.; Pankert, R. *Metallurgy* **1982**, *36*, 247.
(122) Finch, C. B.; Becher, P. F.; Tennery, V. J.; Yust, C. S. *J. Cryst. Growth* **1982**, *58*, 647.
(123) Lugscheider, E.; Krautwald, A.; Eschnauer, H.; Wilden, J.; Meinhardt, H. *Surf. Coat. Technol.* **1987**, *32*, 273.
(124) Telle, R. *Chem. Unserer Zeit* **1988**, *22*, 93.
(125) Vlaisavljevich, B.; Gagliardi, L.; Wang, X.; Liang, B.; Andrews, L.; Infante, I. *Inorg. Chem.* **2010**, *49*, 9230.
(126) Oryshchyn, S.; Babizhetskyy, V.; Zhak, O.; Stoyko, S.; Guérin, R.; Simon, A. *Intermetallics* **2011**, *19*, 1041.
(127) Philipp, F.; Schmidt, P.; Milke, E.; Binnewies, M.; Hoffmann, S. *J. Solid State Chem.* **2008**, *181*, 758.
(128) Philipp, F.; Schmidt, P.; Ruck, M.; Schnelle, W.; Isaeva, A. *J. Solid State Chem.* **2008**, *181*, 2859.
(129) Lincke, H.; Nilges, T.; Johrendt, D.; Pöttgen, R. *Solid State Sci.* **2008**, *10*, 1006.
(130) Tschulik, K.; Ruck, M.; Binnewies, M.; Milke, E.; Hoffmann, S.; Schnelle, W.; Fokwa, B. P. T.; Gillessen, M.; Schmidt, P. *Eur. J. Inorg. Chem.* **2009**, *2009*, 3102.
(131) He, H.; Stearrett, R.; Nowak, E. R.; Bobev, S. *Inorg. Chem.* **2010**, *49*, 7935.
(132) Tsujii, N.; Uvarov, C. A.; Klavins, P.; Yi, T.; Kauzlarich, S. M. *Inorg. Chem.* **2012**, *51*, 2860.
(133) Pfannenschmidt, U.; Rodewald, U. C.; Pöttgen, R. *Z. Kristallogr.* **2010**, *225*, 280.
(134) Mizusaki, S.; Adachi, Y.; Ohnishi, T.; Taniguchi, T.; Nagata, Y.; Ozawa, T.; Noro, Y.; Samata, H. *J. Alloys Compd.* **2009**, *468*, 28.
(135) Pfannenschmidt, U.; Pöttgen, R. *Intermetallics* **2011**, *19*, 1052.
(136) Feng, K.; Yin, W.; He, R.; Lin, Z.; Jin, S.; Yao, J.; Fu, P.; Wu, Y. *Dalton Trans.* **2011**, 3.
(137) Chung, I.; Biswas, K.; Song, J.-H.; Androulakis, J.; Chondroudis, K.; Paraskevopoulos, K. M.; Freeman, A. J.; Kanatzidis, M. G. *Angew. Chem., Int. Ed.* **2011**, *6163*, 2.
(138) Verozubova, G. A.; Trofimov, A. Y.; Trukhanov, E. M.; Kolesnikov, a. V.; Okunev, a. O.; Ivanov, Y. F.; Galtier, P. R. J.; Said Hassani, S. a. *Crystallogr. Rep.* **2010**, *55*, 65.
(139) Bobev, S.; Xia, S.; Bauer, E. D.; Ronning, F.; Thompson, J. D.; Sarrao, J. L. *J. Solid State Chem.* **2009**, *182*, 1473.
(140) Watkins, T.; Chizmeshya, A. V. G.; Jiang, L.; Smith, D. J.; Beeler, R. T.; Grzybowski, G.; Poweleit, C. D.; Menéndez, J.; Kouvetakis, J. *J. Am. Chem. Soc.* **2011**, *133*, 16212.
(141) Lesnyak, V.; Stratiichuk, D.; Sudavtsova, V.; Slobodyanik, M. *Russ. J. Appl. Chem.* **2001**, *74*, 1274.
(142) Sharma, D.; Chandra, K.; Misra, P. S. *Mater. Des.* **2011**, *32*, 3198.
(143) Booth, R. A.; Marinescu, M.; Liu, J.; Majetich, S. A. *J. Magn. Magn. Mater.* **2010**, *322*, 2571.
(144) Sangster, J. M. *J. Phase Equilib. Diffus.* **2009**, *31*, 73.
(145) Sangster, J. M. *J. Phase Equilib. Diffus.* **2009**, *31*, 68.
(146) Sangster, J. M. *J. Phase Equilib. Diffus.* **2009**, *31*, 62.
(147) Sangster, J. M. *J. Phase Equilib. Diffus.* **2009**, *31*, 77.
(148) Okamoto, H. *J. Phase Equilib. Diffus.* **2010**, *31*, 200.
(149) Ganesan, R.; Dinsdale, A. T.; Ipser, H. *Intermetallics* **2011**, *19*, 927.
(150) Stadler, S.; Winarski, R. P.; Maclaren, J. M.; Ederer, D. L.; Moewes, A. *J. Electron Spectrosc. Relat. Phenom.* **2001**, *111*, 75.
(151) Shein, I.; Ivanovskii, A. *Phys. Rev. B* **2006**, *73*, 1.
(152) Xiao, B.; Xing, J. D.; Ding, S. F.; Su, W. *Phys. B* **2008**, *403*, 1723.
(153) Zhou, C. T.; Xing, J. D.; Xiao, B.; Feng, J.; Xie, X. J.; Chen, Y. H. *Comput. Mater. Sci.* **2009**, *44*, 1056.
(154) Zhao, E.; Meng, J.; Ma, Y.; Wu, Z. *Phys. Chem. Chem. Phys.* **2010**, *12*, 13158.
(155) Wang, B.; Li, X.; Wang, Y. X.; Tu, Y. F. *J. Phys. Chem. C* **2011**, *3*, 21429.
(156) Delsante, S.; Schmetterer, C.; Ipser, H.; Borzone, G. *J. Chem. Eng. Data* **2010**, *55*, 3468.
(157) Pashinkin, A. S.; Malkova, A. S.; Mikhailova, M. S. *Russ. J. Phys. Chem. A* **2009**, *83*, 1051.
(158) Yang, Z.; Liu, L.; Wang, X.; Yang, S.; Su, X. *J. Alloys Compd.* **2011**, *509*, 165.
(159) Zhang, W.; Wu, W.; Cheng, X. *Phys. B* **2010**, *405*, 4536.
(160) Arbouche, O.; Belgoumène, B.; Soudini, B.; Azzaz, Y.; Bendaoud, H.; Amara, K. *Comput. Mater. Sci.* **2010**, *47*, 685.
(161) Flage-Larsen, E.; Løvvik, O. M.; Prytz, Ø.; Taftø, J. *Comput. Mater. Sci.* **2010**, *47*, 752.
(162) Wen, X.-D.; Cahill, T. J.; Hoffmann, R. *J. Am. Chem. Soc.* **2009**, *131*, 2199.
(163) Xiao, B.; Feng, J.; Zhou, C. T.; Xing, J. D.; Xie, X. J.; Cheng, Y. H.; Zhou, R. *Phys. B* **2010**, *405*, 1274.
(164) Zhang, M.; Wang, H.; Cui, T.; Ma, Y. *J. Phys. Chem. C* **2010**, *114*, 6722.
(165) Lawson, J. W.; Bauschlicher, C. W.; Daw, M. S. *J. Am. Ceram. Soc.* **2011**, *94*, 3494.
(166) Volonakis, G.; Tsetseris, L.; Logothetidis, S. *Mater. Sci. Eng., B* **2011**, *176*, 484.
(167) Hafner, J.; Tegze, M.; Becker, C. *Phys. Rev. B* **1994**, *49*, 285.
(168) Hafner, J.; Becker, C. *J. Phys.: Condens. Matter* **1999**, *8*, 5269.
(169) Hausleitner, C.; Hafner, J. *Phys. Rev. B* **1993**, *47*, 5689.
(170) Hausleitner, C.; Hafner, J.; Becker, C. *Phys. Rev. B* **1993**, *48*, 119.
(171) Lamparter, P. *Phys. Scr.* **1995**, *T57*, 72.
(172) Thijsse, B.; Sietsma, J. *Mater. Sci. Eng., A* **1994**, *180*, 438.
(173) Xia, W. S.; Fan, Y.; Jiang, Y. S.; Chen, Y. *Appl. Surf. Sci.* **1996**, *103*, 1.
(174) Ee, L.; van Thijsse, B.; Sietsma, J. *Phys. Rev. B* **1998**, *57*, 906.
(175) Zhu, J.; Dai, G.; Qiao, M.; Fan, K. *Int. J. Quantum Chem.* **2008**, *108*, 370.
(176) Li, Q.; Wang, H.; Ma, Y. M. *J. Superhard Mater.* **2010**, *32*, 192.
(177) Aydin, S.; Simsek, M. *Phys. Rev. B* **2009**, *80*, 1.
(178) Zhang, M.; Yan, H.; Zhang, G.; Wang, H. *J. Phys. Chem. C* **2012**, *116*, 8.
(179) Armstrong, D. R.; Perkins, P. G.; Cetina, E. A. V. *Theor. Chim. Acta* **1983**, *64*, 41.
(180) Mohn, P.; Pettifor, D. G. *J. Phys. C: Solid State Phys.* **1988**, *2829*, 2829.
(181) Grosvenor, A. P.; Wik, S. D.; Cavell, R. G.; Mar, A. *Inorg. Chem.* **2005**, *44*, 8988.
(182) Diplas, S.; Løvvik, O. M. *J. Phys.: Condens. Matter* **2009**, *21*, 245503.
(183) Blanchard, P. E. R.; Grosvenor, A. P.; Cavell, R. G.; Mar, A. *Chem. Mater.* **2008**, *20*, 7081.
(184) Pauling, L. *J. Electrochem. Soc.* **1951**, *212*, 518.
(185) Kiessling, R. *J. Electrochem. Soc.* **1951**, *98*, 519.

(186) Pauling, L. *Proc. R. Soc. A* **1949**, *196*, 343.
(187) Longuet-Higgins, H. C.; Roberts, M. de V. *Proc. R. Soc. A* **1954**, *224*, 336.
(188) Schmitt, K.; Stückl, C.; Ripplinger, H.; Albert, B. *Solid State Sci.* **2001**, *3*, 321.
(189) Vajeeston, P.; Ravindran, P.; Ravi, C.; Asokamanil, R. *Phys. Rev. B* **2001**, *63*, 1.
(190) Cooper, J. D.; Gibb, T. C.; Greenwood, N. N.; Paris, R. V. *Trans. Faraday Soc.* **1964**, *60*, 2097.
(191) Okamoto, Y.; Nitta, Y.; Imanaka, T.; Teranishi, S. *J. Chem. Soc., Faraday Trans. 1* **1979**, *75*, 2027.
(192) Deng, J.; Li, H.; Wang, W. *Catal. Today* **1999**, *51*, 113.
(193) Diplas, S.; Lehrmann, J.; Jørgensen, S.; Våland, T.; Watts, J. F.; Taftø, J. *Surf. Interface Anal.* **2005**, *37*, 459.
(194) Diplas, S.; Lehrmann, J.; Jørgensen, J. E.; Våland, T.; Taftø, J. *Philos. Mag.* **2005**, *85*, 981.
(195) Friedman, R. M.; Hudis, J.; Perlman, M. L.; Watson, R. E. *Phys. Rev. B* **1973**, *8*, 2433.
(196) Gelatt, C. D. J.; Ehrenreich, H. *Phys. Rev. B* **1974**, *10*, 398.
(197) Watson, R. E.; Bennett, L. H. *Phys. Rev. B* **1978**, *18*, 6439.
(198) Zintl, E. *Angew. Chem.* **1939**, *52*, 1.
(199) Klemm, W. *Proc. Chem. Soc* **1958**, 329.
(200) Derrien, G.; Tillard, M.; Manteghetti, a.; Belin, C. *Z. Anorg. Allg. Chem.* **2003**, *629*, 1601.
(201) Schwetz, K. A. In *Ullmann's Encyclopedia of Industrial Chemistry*; Wiley-VCH: Weinheim, Germany, 2006.
(202) Wang, X.-B.; Tian, D.-C.; Wang, L.-L. *J. Phys.: Condens. Matter* **1994**, *6*, 10185.
(203) Vinod, K.; Kumar, R. G. A.; Syamaprasad, U. *Supercond. Sci. Technol.* **2007**, *20*, R1.
(204) http://www.columbussuperconductors.com/docs/what%20has%20already%20been%20done.pdf http://www.columbussuperconductors.com/docs/what has already been done.pdf (accessed Apr 2, 2013).
(205) http://ir.bruker.com/phoenix.zhtml?c=121496&p=irol-newsArticle&ID=1362507&highlight= http://ir.bruker.com/phoenix.zhtml?c=121496&p=irol-newsArticle&ID=1362507&highlight= (accessed Apr 2, 2013).
(206) Ganguli, A. K.; Prakash, J.; Thakur, G. S. *Chem. Soc. Rev.* **2013**, *42*, 569.
(207) Greenwood, N. N.; Parish, R. V.; Thornton, P. *J. Chem. Soc.* **1965**, 545.
(208) Birajdar, B.; Peranio, N.; Eibl, O. *Supercond. Sci. Technol.* **2008**, *21*, 073001.
(209) Birajdar, B.; Peranio, N.; Eibl, O. *J. Phys.: Conf. Ser.* **2008**, *97*, 012246.
(210) Grivel, J. C.; Eibl, O.; Birajdar, B.; Andersen, N. H.; Abrahamsen, A.; Pinholt, R.; Grasso, G.; Hässler, W.; Herrmann, M.; Perner, O.; Rodig, C.; Pachla, W.; Ková, P.; Husek, I.; Mikheenko, P.; Abell, S.; Homeyer, J. *J. Phys.: Conf. Ser.* **2006**, *43*, 107.
(211) Adasch, V.; Hess, K.-U.; Ludwig, T.; Vojteer, N.; Hillebrecht, H. *J. Solid State Chem.* **2006**, *179*, 2916.
(212) Adasch, V.; Hess, K.-U.; Ludwig, T.; Vojteer, N.; Hillebrecht, H. *Chem.—Eur. J.* **2007**, *13*, 3450.
(213) Vojteer, N.; Schroeder, M.; Röhr, C.; Hillebrecht, H. *Chem.—Eur. J.* **2008**, *14*, 7331.
(214) Vojteer, N.; Sagawe, V.; Stauffer, J.; Schroeder, M.; Hillebrecht, H. *Chem.—Eur. J.* **2011**, *17*, 3128.
(215) Frotscher, M.; Hölzel, M.; Albert, B. *Z. Anorg. Allg. Chem.* **2010**, *636*, 1783.
(216) Albert, B.; Hofmann, K.; Fild, C.; Eckert, H.; Schleifer, M.; Gruehn, R. *Chem.—Eur. J.* **2000**, *6*, 2531.
(217) Geng, J.; Jefferson, D. A.; Johnson, B. F. G. *Chem. Commun.* **2007**, 969.
(218) Geng, J.; Jefferson, D. A.; Johnson, B. F. G. *Chem.—Eur. J.* **2009**, *15*, 1134.
(219) Jia, J. J.; Underwood, J. H.; Gullikson, E. M.; Callcott, T. A.; Perera, R. C. C. *J. Electron Spectrosc. Relat. Phenom.* **1996**, *80*, 509.
(220) Denlinger, J. D.; Clack, J. A.; Allen, J. W.; Gweon, G.-H.; Sarrao, J. L.; Bianchi, A. D.; Fisk, Z. *Phys. Rev. Lett.* **2002**, *89*, 157601.
(221) Liu, L.; Yiu, Y. M.; Sham, T. K.; Yang, D.; Zuin, L. *J. Appl. Phys.* **2010**, *107*, 043703.
(222) Capehart, T. W.; Mishra, R. K.; Herbst, J. F. *J. Appl. Phys.* **1992**, *72*, 676.
(223) Capehart, T. W.; Mishra, R. K.; Meisner, G. P.; Fuerst, C. D.; Herbst, J. F. *Appl. Phys. Lett.* **1993**, *63*, 3642.
(224) Liu, L.; Yiu, Y.-M.; Sham, T.-K. *J. Electron Spectrosc. Relat. Phenom.* **2011**, *184*, 188.
(225) Rades, S.; Kornowski, A.; Weller, H.; Albert, B. *ChemPhysChem* **2011**, *12*, 1756.
(226) Wang, W.-C.; Chen, Y.; Zhang, J.-G.; Hu, T.-D. *J. Non-Cryst. Solids* **1993**, *160*, 268.
(227) Wang, H.; Yu, Z.; Chen, H.; Yang, J.; Deng, J. *Appl. Catal., A* **1995**, *129*, 143.
(228) Forster, G. D.; Fernández Barquín, L.; Bilsborrow, R. L.; Pankhurst, Q. A.; Parkin, I. P.; Andrew Steer, W. *J. Mater. Chem.* **1999**, *9*, 2537.
(229) Li, H.; Li, H.; Wang, M. *Appl. Catal., A* **2001**, *207*, 129.
(230) Zhang, J. G.; Jin, H. J.; Xu, W. X.; Lin, Y. J.; Wang, W. C. *J. Magn. Magn. Mater.* **2002**, *245*, 621.
(231) Blanchard, P. E. R.; Grosvenor, A. P.; Cavell, R. G.; Mar, A. *J. Mater. Chem.* **2009**, *19*, 6015.
(232) Su, H.; Xie, Y.; Li, B.; Liu, X. M.; Qian, Y. T. *Solid State Ionics* **1999**, *122*, 157.
(233) Wu, Y.; Messer, B.; Yang, P. *Adv. Mater.* **2001**, *13*, 1487.
(234) Cao, L.; Hahn, K.; Wang, Y. *Adv. Mater.* **2002**, *14*, 1294.
(235) Xu, T. T.; Zheng, J.-G.; Nicholls, A. W.; Stankovich, S.; Piner, R. D.; Ruoff, R. S. *Nano Lett.* **2004**, *4*, 2051.
(236) Ma, R.; Bando, Y.; Mori, T.; Golberg, D. *Chem. Mater.* **2003**, *15*, 3194.
(237) Cao, L.; Zhang, Z.; Wen, H.; Wang, W. *Appl. Phys. Lett.* **2005**, *86*, 123113.
(238) Zhou, S.-M.; Wang, P.; Li, S.; Zhang, B.; Gong, H.-C.; Zhang, X.-T. *Mater. Lett.* **2009**, *63*, 1680.
(239) Li, Y.; Tevaarwerk, E.; Chang, R. *Chem. Mater.* **2006**, *18*, 2552.
(240) Jash, P.; Nicholls, A. W.; Ruoff, R. S.; Trenary, M. *Nano Lett.* **2008**, *8*, 3794.
(241) Jash, P.; Trenary, M. *J. Phys.: Conf. Ser.* **2009**, *176*, 012011.
(242) Zhang, H.; Tang, J.; Zhang, Q.; Zhao, G.; Yang, G.; Zhang, J.; Zhou, O.; Qin, L.-C. *Adv. Mater.* **2006**, *18*, 87.
(243) Hofmann, K.; Gruehn, R.; Albert, B. *Z. Anorg. Allg. Chem.* **2002**, *628*, 2691.
(244) Kapfenberger, C.; Hofmann, K.; Albert, B. *Solid State Sci.* **2003**, *5*, 925.
(245) Arzac, G. M.; Rojas, T. C.; Fernández, A. *ChemCatChem* **2011**, *3*, 1305.
(246) Hofmann, K.; Albert, B. *ChemPhysChem* **2002**, *10*, 896.
(247) Gao, S.-P.; Jiang, J.; Cao, M.; Zhu, J.; Yuan, J. *Phys. Rev. B* **2004**, *69*, 1.
(248) Hofmann, K.; Rocquefelte, X.; Halet, J.-F.; Bähtz, C.; Albert, B. *Angew. Chem., Int. Ed.* **2008**, *47*, 2301.
(249) Brydson, R.; Hofer, F.; Upadhyaya, D.; Kothleitner, G.; Ward-Close, M.; Tsakiropoulos, P.; Froes, S. *Micron* **1996**, *27*, 107.
(250) Jha, M.; Ramanujachary, K. V; Lofland, S. E.; Gupta, G.; Ganguli, A. K. *Dalton Trans.* **2011**, *40*, 7879.
(251) Portehault, D.; Giordano, C.; Gervais, C.; Senkovska, I.; Kaskel, S.; Sanchez, C.; Antonietti, M. *Adv. Funct. Mater.* **2010**, *20*, 1827.
(252) Reinholdt, M.; Croissant, J.; Di Carlo, L.; Granier, D.; Gaveau, P.; Bégu, S.; Devoisselle, J.-M.; Mutin, P. H.; Smith, M. E.; Bonhomme, C.; Gervais, C.; Van der Lee, A.; Laurencin, D. *Inorg. Chem.* **2011**, *50*, 7802.
(253) Mirzaei, M.; Mirzaei, M. *Monatsh. Chem.* **2011**, *142*, 111.
(254) Mauri, F.; Vast, N.; Pickard, C. *Phys. Rev. Lett.* **2001**, 87.
(255) Vast, N.; Sjakste, J.; Betranhandy, E. *J. Phys.: Conf. Ser.* **2009**, *176*, 012002.
(256) Gervais, C.; Babonneau, F. *J. Organomet. Chem.* **2002**, *657*, 75.

(257) Duperrier, S.; Gervais, C.; Bernard, S.; Cornu, D.; Babonneau, F.; Miele, P. *J. Mater. Chem.* **2006**, *16*, 3126.
(258) Brun, N.; Janot, R.; Sanchez, C.; Deleuze, H.; Gervais, C.; Morcrette, M.; Backov, R. *Energy Environ. Sci.* **2010**, *3*, 824.
(259) Silver, A. H.; Kushida, T. *J. Chem. Phys.* **1963**, *38*, 865.
(260) Roger, J.; Babizhetskyy, V.; Cordier, S.; Bauer, J.; Hiebl, K.; Le Pollès, L.; Elisabeth Ashbrook, S.; Halet, J.-F.; Guérin, R. *J. Solid State Chem.* **2005**, *178*, 1851.
(261) Paluch, S.; Żogał, O. J.; Peshev, P. *J. Alloys Compd.* **2004**, *383*, 176.
(262) Fojud, Z.; Herzig, P.; Żogał, O.; Pietraszko, a.; Dukhnenko, a.; Jurga, S.; Shitsevalova, N. *Phys. Rev. B* **2007**, *75*, 1.
(263) Kishimoto, Y.; Kawasaki, Y.; Tanabe, M.; Tanaka, T.; Ohno, T.; Ghosh, G.; Tyagi, A. K.; Gupta, L. C. *J. Magn. Magn. Mater.* **2007**, *310*, 581.
(264) Kishimoto, Y.; Kawasaki, Y.; Tanabe, M.; Ideta, Y.; Ohno, T.; Ghosh, G.; Tyagi, A. K.; Gupta, L. C. *J. Phys. Chem. Solids* **2008**, *69*, 3153.
(265) Kishimoto, Y.; Kawasaki, Y.; Ideta, Y.; Endou, S.; Tanaka, T.; Tanabe, M.; Ohno, T.; Ghosh, G.; Tyagi, A. K.; Gupta, L. C. *J. Phys.: Conf. Ser.* **2009**, *176*, 012039.
(266) Jung, J.; Baek, S.; Borsa, F.; Bud'ko, S.; Lapertot, G.; Canfield, P. *Phys. Rev. B* **2001**, *64*, 4.
(267) Kotegawa, H.; Ishida, K.; Kitaoka, Y.; Muranaka, T.; Akimitsu, J. *Phys. Rev. Lett.* **2001**, *87*, 2.
(268) Papavassiliou, G.; Pissas, M.; Fardis, M.; Karayanni, M.; Christides, C. *Phys. Rev. B* **2001**, *65*, 1.
(269) Baek, S.; Suh, B.; Pavarini, E.; Borsa, F.; Barnes, R.; Bud'ko, S.; Canfield, P. *Phys. Rev. B* **2002**, *66*, 1.
(270) Lue, C. S.; Lai, W. J. *Phys. Status Solidi B* **2005**, *242*, 1108.
(271) Bose, M.; Roy, K.; Basu, A. *J. Phys. C: Solid State Phys.* **1980**, *13*, 3951.
(272) Lue, C.; Tao, Y.; Su, T. *Phys. Rev. B* **2008**, *78*, 9.
(273) Żogał, O. J.; Fojud, Z.; Herzig, P.; Pietraszko, A.; Lyashchenko, A. B.; Jurga, S.; Paderno, V. N. *J. Appl. Phys.* **2009**, *106*, 033514.
(274) Jäger, B.; Paluch, S.; Wolf, W.; Herzig, P.; Żogał, O. J.; Shitsevalova, N.; Paderno, Y. *J. Alloys Compd.* **2004**, *383*, 232.
(275) Żogał, O. J.; Florian, P.; Massiot, D.; Paluch, S.; Shitsevalova, N.; Borshchevsky, D. F. *Solid State Commun.* **2009**, *149*, 693.
(276) Jäger, B.; Paluch, S.; Żogał, O. J.; Wolf, W.; Herzig, P.; Filippov, V. B.; Shitsevalova, N.; Paderno, Y. *J. Phys.: Condens. Matter* **2006**, *18*, 2525.
(277) Herzig, P.; Fojud, Z.; Żogał, O. J.; Pietraszko, A.; Dukhnenko, A.; Jurga, S.; Shitsevalova, N. *J. Appl. Phys.* **2008**, *103*, 083534.
(278) Creel, R. B.; Segel, S. L.; Schoenberger, R. J.; Barnes, R. G.; Torgeson, D. R. *J. Chem. Phys.* **1974**, *60*, 2310.
(279) Mali, M.; Roos, J.; Shengelaya, A.; Keller, H.; Conder, K. *Phys. Rev. B* **2002**, *65*, 1.
(280) Bastow, T. J. *Solid State Commun.* **2002**, *124*, 269.
(281) Barnes, R. G.; Creel, R. B.; Torgeson, D. R. *Solid State Commun.* **1970**, *8*, 1411.
(282) Naslain, R.; Kasper, J. S. *J. Solid State Chem.* **1970**, *1*, 150.
(283) Bekaert, E.; Bernardi, J.; Boyanov, S.; Monconduit, L.; Doublet, M.-L.; Ménétrier, M. *J. Phys. Chem. C* **2008**, *112*, 20481.
(284) Souza, D. C. S.; Pralong, V.; Jacobson, a. J.; Nazar, L. F. *Science* **2002**, *296*, 2012.
(285) Boyanov, S.; Bernardi, J.; Bekaert, E.; Ménétrier, M.; Doublet, M.-L.; Monconduit, L. *Chem. Mater.* **2009**, *21*, 298.
(286) Bates, S. E.; Buhro, W. E.; Frey, C. A.; Sastry, S. M. L.; Kelton, K. F. *J. Mater. Res.* **1995**, *10*, 2599.
(287) Portesi, C.; Borini, S.; Amato, G.; Monticone, E. *J. Appl. Phys.* **2006**, *99*, 066115.
(288) Portesi, C.; Monticone, E.; Borini, S.; Picotto, G. B.; Pugno, N.; Carpinteri, A. *J. Phys.: Condens. Matter* **2008**, *20*, 474210.
(289) Brinkman, A.; Veldhuis, D.; Mijatovic, D.; Rijnders, G.; Blank, D. H. A.; Hilgenkamp, H.; Rogalla, H. *Appl. Phys. Lett.* **2001**, *79*, 2420.
(290) Jha, M.; Patra, R.; Ghosh, S.; Ganguli, A. K. *J. Mater. Chem.* **2012**, *22*, 6356.
(291) Brewer, J. R.; Deo, N.; Wang, Y. M.; Cheung, C. L. *Chem. Mater.* **2007**, *19*, 6379.
(292) Kim, S. G.; Brock, J. R. *J. Colloid Interface Sci.* **1987**, *116*, 431.
(293) Yiping, L.; Hadjipanayis, G.; Sorensen, C.; Klabunde, K. *J. Magn. Magn. Mater.* **1989**, *79*, 321.
(294) Linderoth, S.; Mørup, S. *J. Appl. Phys.* **1991**, *69*, 5256.
(295) Petit, C.; Pileni, M. P. *J. Magn. Magn. Mater.* **1997**, *166*, 82.
(296) Guo, M.; Wang, M.; Shen, K.; Cao, L.; Li, Z.; Zhang, Z. *J. Alloys Compd.* **2008**, *460*, 585.
(297) Shi, L.; Gu, Y.; Chen, L.; Yang, Z.; Ma, J.; Qian, Y. *Inorg. Chem. Commun.* **2004**, *7*, 192.
(298) Lai, S.; Liu, S.; Lan, M. *J. Cryst. Growth* **2007**, *304*, 460.
(299) Wang, L.; Xu, L.; Ju, Z.; Qian, Y. *CrystEngComm* **2010**, *12*, 3923.
(300) Belyansky, M.; Trenary, M. *Chem. Mater.* **1997**, *9*, 403.
(301) Nath, M.; Parkinson, B. A. *Adv. Mater.* **2006**, *18*, 1865.
(302) Iyyamperumal, E.; Fang, F.; Posadas, A.-B.; Ahn, C.; Klie, R. F.; Zhao, Y.; Haller, G. L.; Pfefferle, L. D. *J. Phys. Chem. C* **2009**, *113*, 17661.
(303) Zeng, X. H.; Pogrebnyakov, a. V.; Zhu, M. H.; Jones, J. E.; Xi, X. X.; Xu, S. Y.; Wertz, E.; Li, Q.; Redwing, J. M.; Lettieri, J.; Vaithyanathan, V.; Schlom, D. G.; Liu, Z.-K.; Trithaveesak, O.; Schubert, J. *Appl. Phys. Lett.* **2003**, *82*, 2097.
(304) Xi, X.; Pogrebnyakov, a; Xu, S.; Chen, K.; Cui, Y.; Maertz, E.; Zhuang, C.; Li, Q.; Lamborn, D.; Redwing, J. *Phys. C* **2007**, *456*, 22.
(305) Amin, S. S.; Li, S.; Roth, J. R.; Xu, T. T. *Chem. Mater.* **2009**, *21*, 763.
(306) Dai, Q.; Wang, Y.; Ma, X.; Yang, Q.; Zhang, H.; Nie, R.; Feng, Q.; Wang, F. *Phys. C* **2012**, *475*, 57.
(307) Greenwood, N. N.; Greatrex, R. *Pure Appl. Chem.* **1987**, *59*, 857.
(308) Greenwood, N. N.; Kennedy, J. D. *Pure Appl. Chem.* **1991**, *63*, 317.
(309) Greenwood, N. N. *Chem. Soc. Rev.* **1992**, *21*, 49.
(310) Wirth, H. E.; Palmer, E. D. *J. Am. Chem. Soc.* **1951**, *60*, 914.
(311) Pohanish, R. P. *Sittig's Handbook of Toxic and Hazardous Chemicals and Carcinogens*, 6th ed.; William Andrew: Waltham, MA, 2012.
(312) Paul, R.; Buisson, P.; Joseph, N. *J. Ind. Eng. Chem.* **1952**, *44*, 1006.
(313) Demirci, U. B.; Akdim, O.; Andrieux, J.; Hannauer, J.; Chamoun, R.; Miele, P. *Fuel Cells* **2010**, *10*, 335.
(314) Kostka, J.; Lohstroh, W.; Fichtner, M.; Hahn, H. *J. Phys. Chem. C* **2007**, *111*, 14026.
(315) Baes, C. F.; Mesmer, R. E. *The Hydrolysis of Cations*; Wiley: New York, 1976.
(316) Shi, L.; Gu, Y.; Chen, L.; Yang, Z.; Ma, J.; Qian, Y. *Mater. Lett.* **2004**, *58*, 2890.
(317) Carey, F. A.; Sundberg, R. J. *Advanced Organic Chemistry. Part A: Structure and Mechanisms*, 5th ed.; Springer-Verlag: New York, 2007.
(318) Carey, F. A.; Sundberg, R. J. *Advanced Organic Chemistry. Part B: Reaction and Synthesis*, 5th ed.; Springer-Verlag: New York, 2007.
(319) Axelbaum, R. L.; DuFaux, D. P.; Frey, C. A.; Kelton, K. F.; Lawton, S. A.; Rosen, L. J.; Sastry, S. M. L. *J. Mater. Res.* **1996**, *11*, 948.
(320) Zhang, H.; Zhang, Q.; Tang, J.; Qin, L.-C. *J. Am. Chem. Soc.* **2005**, *127*, 8002.
(321) Xu, J.; Zhao, Y.; Zou, C. *Chem. Phys. Lett.* **2006**, *423*, 138.
(322) Xu, J.; Chen, X.; Zhao, Y.; Zou, C.; Ding, Q. *Nanotechnology* **2007**, *18*, 115621.
(323) Xu, J.; Zhao, Y.; Zou, C.; Ding, Q. *J. Solid State Chem.* **2007**, *180*, 2577.
(324) Ding, Q.; Zhao, Y.; Xu, J.; Zou, C. *Solid State Commun.* **2007**, *141*, 53.
(325) Chen, L.; Gu, Y.; Shi, L.; Yang, Z.; Ma, J.; Qian, Y. *Solid State Commun.* **2004**, *130*, 231.
(326) Li, Y.; Chang, R. P. H. *J. Am. Chem. Soc.* **2006**, *128*, 12778.
(327) Holleman, A. F.; Wiberg, E. *Inorganic Chemistry*; Academic Press: New York, 2001.

(328) Fahrenholtz, W. G. *J. Am. Ceram. Soc.* **2005**, *88*, 3509.
(329) Sevim, F.; Demir, F.; Bilen, M.; Okur, H. *Korean J. Chem. Eng.* **2006**, *23*, 736.
(330) Khanra, A. K.; Pathak, L. C.; Mishra, S. K.; Godkhindi, M. M. *Mater. Lett.* **2004**, *58*, 733.
(331) Zhang, M.; Yuan, L.; Wang, X.; Fan, H.; Wang, X.; Wu, X.; Wang, H.; Qian, Y. *J. Solid State Chem.* **2008**, *181*, 294.
(332) Jensen, J. A.; Gozum, J. E.; Pollina, D. M.; Girolami, G. S. *J. Am. Chem. Soc.* **1988**, *110*, 1643.
(333) Wayda, A. L.; Schneemeyer, L. F.; Opila, R. L. *Appl. Phys. Lett.* **1988**, *53*, 361.
(334) Jayaraman, S.; Yang, Y.; Kim, D. Y.; Girolami, G. S.; Abelson, J. R. *J. Vac. Sci. Technol., A* **2005**, *23*, 1619.
(335) Yang, Y.; Jayaraman, S.; Kim, D.; Girolami, G.; Abelson, J. *J. Cryst. Growth* **2006**, *294*, 389.
(336) Yang, Y.; Jayaraman, S.; Kim, D. Y.; Girolami, G. S.; Abelson, J. R. *Chem. Mater.* **2006**, 5088.
(337) Ye, W.; Peña Martin, P. A.; Kumar, N.; Daly, S. R.; Rockett, A. A.; Abelson, J. R.; Girolami, G. S.; Lyding, J. W. *ACS Nano* **2010**, *4*, 6818.
(338) Rice, G. W.; Woodin, R. L. *J. Am. Ceram. Soc.* **1988**, *71*, C-181.
(339) Glass, J. A.; Kher, S. S.; Spencer, J. T. *Chem. Mater.* **1992**, *4*, 530.
(340) Amini, M. M.; Fehlner, T. P.; Long, G. J.; Politowski, M. *Chem. Mater.* **1990**, *2*, 432.
(341) Jun, C. S.; Fehlner, T. P.; Long, G. J. *Chem. Mater.* **1992**, *4*, 440.
(342) Goedde, D. M.; Girolami, G. S. *J. Am. Chem. Soc.* **2004**, *126*, 12230.
(343) Yu, M. L.; Vitkavage, D. J.; Meyerson, B. S. *J. Appl. Phys.* **1986**, *59*, 4032.
(344) Belyansky, M.; Trenary, M. *Inorg. Chim. Acta* **1999**, *289*, 191.
(345) Friedhoff, W.; Milke, E.; Binnewies, M. *Eur. J. Inorg. Chem.* **2011**, *2011*, 3398.
(346) Bouix, J.; Vincent, H.; Boubehira, M.; Viala, J. C. *J. Less-Common Met.* **1986**, *117*, 83.
(347) Takahashi, T.; Kamiya, H. *J. Cryst. Growth* **1974**, *26*, 203.
(348) Takahashi, T.; Itoh, H. *J. Cryst. Growth* **1980**, *49*, 445.
(349) Besmann, T. M.; Spear, K. E. *J. Cryst. Growth* **1975**, *31*, 60.
(350) Pierson, H. O.; Randich, E. *Thin Solid Films* **1978**, *54*, 119.
(351) Pierson, H. O.; Mullendore, A. W. *Thin Solid Films* **1982**, *95*, 99.
(352) Motojima, S.; Takahashi, Y.; Sugiyama, K. *J. Cryst. Growth* **1978**, *44*, 106.
(353) Williams, L. M. *Appl. Phys. Lett.* **1985**, *46*, 43.
(354) Caputo, A.; Lackey, W. *J. Electrochem. Soc.* **1985**, *132*, 2274.
(355) Pierson, H. O.; Mullendore, A. W. *Thin Solid Films* **1980**, *72*, 511.
(356) Kher, S. S.; Spencer, J. T. *Chem. Mater.* **1992**, *4*, 538.
(357) Ueda, K.; Naito, M. *Appl. Phys. Lett.* **2001**, *79*, 2046.
(358) Ueda, K.; Naito, M. *J. Appl. Phys.* **2003**, *93*, 2113.
(359) Yamazaki, H.; Takagi, H. *J. Solid State Chem.* **2006**, *179*, 1003.
(360) Blank, D. H. A.; Hilgenkamp, H.; Brinkman, A.; Mijatovic, D.; Rijnders, G.; Rogalla, H. *Appl. Phys. Lett.* **2001**, *79*, 394.
(361) Shinde, S. R.; Ogale, S. B.; Greene, R. L.; Venkatesan, T.; Canfield, P. C.; Bud'ko, S. L.; Lapertot, G.; Petrovic, C. *Appl. Phys. Lett.* **2001**, *79*, 227.
(362) Latini, A.; Rau, J. V.; Ferro, D.; Teghil, R.; Albertini, V. R.; Barinov, S. M. *Chem. Mater.* **2008**, *20*, 4507.
(363) Ignatenko, P. I.; Goncharov, A. A.; Terpii, D. N. *Inorg. Mater.* **2007**, *43*, 344.
(364) Kher, S. S.; Tan, Y.; Spencer, J. T. *Appl. Organomet. Chem.* **1996**, *10*, 297.
(365) Kher, S.; Spencer, J. T. *J. Phys. Chem. Solids* **1998**, *59*, 1343.
(366) Kher, S. S.; Romero, J. V.; Caruso, J. D.; Spencer, J. T. *Appl. Organomet. Chem.* **2008**, *22*, 300.
(367) Wang, G.; Brewer, J. R.; Chan, J. Y.; Diercks, D. R.; Cheung, C. L. *J. Phys. Chem. C* **2009**, *113*, 10446.
(368) Zhang, H.; Zhang, Q.; Zhao, G.; Tang, J.; Zhou, O.; Qin, L.-C. *J. Am. Chem. Soc.* **2005**, *127*, 13120.
(369) Xu, J. Q.; Zhao, Y. M.; Shi, Z. D.; Zou, C. Y.; Ding, Q. W. *J. Cryst. Growth* **2008**, *310*, 3443.
(370) Xu, J.; Chen, X.; Zhao, Y.; Zou, C.; Ding, Q.; Jian, J. *J. Cryst. Growth* **2007**, *303*, 466.
(371) Xu, J. Q.; Zhao, Y. M.; Ji, X. H.; Zhang, Q.; Lau, S. P. *J. Phys. D: Appl. Phys.* **2009**, *42*, 135403.
(372) Zhang, Q. Y.; Xu, J. Q.; Zhao, Y. M.; Ji, X. H.; Lau, S. P. *Adv. Funct. Mater.* **2009**, *19*, 742.
(373) Zhang, H.; Zhang, Q.; Tang, J.; Qin, L.-C. *J. Am. Chem. Soc.* **2005**, *127*, 2862.
(374) Zou, C.; Zhao, Y.; Xu, J. *J. Cryst. Growth* **2006**, *291*, 112.
(375) Wagner, R. S.; Ellis, W. C. *Appl. Phys. Lett.* **1964**, *4*, 89.
(376) Liu, Z.-K.; Schlom, D. G.; Li, Q.; Xi, X. X. *Appl. Phys. Lett.* **2001**, *78*, 3678.
(377) Fan, Z. Y.; Hinks, D. G.; Newman, N.; Rowell, J. M. *Appl. Phys. Lett.* **2001**, *79*, 87.
(378) Kang, W. N.; Kim, H. J.; Choi, E. M.; Jung, C. U.; Lee, S. I. *Science* **2001**, *292*, 1521.
(379) Kang, W. N.; Choi, E.-M.; Kim, H.-J.; Kim, H.-J.; Lee, S.-I. *Phys. C* **2003**, *385*, 24.
(380) Yang, Q.; Sha, J.; Xu, J.; Ji, Y.; Ma, X.; Niu, J.; Hua, H.; Yang, D. *Chem. Phys. Lett.* **2003**, *379*, 87.
(381) Yang, Q.; Sha, J.; Ma, X.; Ji, Y.; Yang, D. *Supercond. Sci. Technol.* **2004**, *17*, L31.
(382) Cao, L. M.; Hahn, K.; Scheu, C.; Rühle, M.; Wang, Y. Q.; Zhang, Z.; Gao, C. X.; Li, Y. C.; Zhang, X. Y.; He, M.; Sun, L. L.; Wang, W. K. *Appl. Phys. Lett.* **2002**, *80*, 4226.
(383) Jha, A. K.; Khare, N. *Supercond. Sci. Technol.* **2009**, *22*, 075017.
(384) Fang, F.; Iyyamperumal, E.; Chi, M.; Keskar, G.; Majewska, M.; Ren, F.; Liu, C.; Haller, G. L.; Pfefferle, L. D. *J. Mater. Chem. C* **2013**, *1*, 2568.
(385) Yang, J.; Zheng, J.; Zhang, X.; Li, Y.; Yang, R.; Feng, Q.; Li, X. *Chem. Commun.* **2010**, *46*, 7530.
(386) Wang, Y.; Zhuang, C.; Gao, J.; Shan, X.; Zhang, J.; Liao, Z.; Xu, H.; Yu, D.; Feng, Q. *J. Am. Chem. Soc.* **2009**, *131*, 2436.
(387) Chen, W.; Liu, W.; Chen, C.; Wang, R.; Feng, Q. *CrystEngComm* **2011**, *13*, 3959.
(388) Nath, M.; Parkinson, B. A. *J. Am. Chem. Soc.* **2007**, *129*, 11302.
(389) Sano, N.; Kawanami, O.; Tamon, H. *J. Appl. Phys.* **2011**, *109*, 034302.
(390) Kanakala, R.; Rojas-George, G.; Graeve, O. a. *J. Am. Ceram. Soc.* **2010**, *93*, 3136.
(391) Kanakala, R.; Escudero, R.; Rojas-George, G.; Ramisetty, M.; Graeve, O. A. *ACS Appl. Mater. Interfaces* **2011**, *3*, 1093.
(392) Deheri, P. K.; Swaminathan, V.; Bhame, S. D.; Liu, Z.; Ramanujan, R. V. *Chem. Mater.* **2010**, *22*, 6509.
(393) Deheri, P. K.; Shukla, S.; Ramanujan, R. V. *J. Solid State Chem.* **2012**, *186*, 224.
(394) Jadhav, A. P.; Hussain, A.; Lee, J. H.; Baek, Y. K.; Choi, C. J.; Kang, Y. S. *New J. Chem.* **2012**, *36*, 2405.
(395) Kim, C. W.; Kim, Y. H.; Pal, U.; Kang, Y. S. *J. Mater. Chem. C* **2013**, *1*, 275.
(396) Pol, S. V.; Pol, V. G.; Gedanken, A. *Chem.—Eur. J.* **2004**, *10*, 4467.
(397) Pol, S. V.; Pol, V. G.; Kessler, V. G.; Seisenbaeva, G. A.; Solovyov, L. A.; Gedanken, A. *Inorg. Chem.* **2005**, *44*, 9938.
(398) Pol, V. G.; Pol, S. V; Gedanken, A. *Chem. Mater.* **2005**, *17*, 1797.
(399) Pol, V. G.; Pol, S. V.; Felner, I.; Gedanken, A. *Chem. Phys. Lett.* **2006**, *433*, 115.
(400) George, P. P.; Gedanken, A.; Gabashvili, A. *Mater. Res. Bull.* **2007**, *42*, 626.
(401) Zhu, Y.; Li, Q.; Mei, T.; Qian, Y. *J. Mater. Chem.* **2011**, 13756.
(402) Shi, L.; Gu, Y.; Chen, L.; Yang, Z.; Ma, J.; Qian, Y. *Chem. Lett.* **2003**, *32*, 958.
(403) Shi, L.; Gu, Y.; Qian, T.; Li, X.; Chen, L.; Yang, Z.; Ma, J.; Qian, Y. *Phys. C* **2004**, *405*, 271.

dx.doi.org/10.1021/cr400020d | *Chem. Rev.* XXXX, XXX, XXX−XXX

(404) Cai, P.; Wang, H.; Liu, L.; Zhang, L. *J. Ceram. Soc. Jpn.* **2010**, *118*, 1102.
(405) Selvan, R. K.; Genish, I.; Perelshtein, I.; Calderon Moreno, J. M.; Gedanken, A. *J. Phys. Chem. C* **2008**, *112*, 1795.
(406) Zhang, M.; Wang, X.; Zhang, X.; Wang, P.; Xiong, S.; Shi, L.; Qian, Y. *J. Solid State Chem.* **2009**, *182*, 3098.
(407) Zhang, M.; Jia, Y.; Xu, G.; Wang, P.; Wang, X.; Xiong, S.; Wang, X.; Qian, Y. *Eur. J. Inorg. Chem.* **2010**, *2010*, 1289.
(408) Suryanarayana, C. *Prog. Mater. Sci.* **2001**, *46*, 1.
(409) Kaupp, G. *CrystEngComm* **2011**, *13*, 3108.
(410) Liu, M. L.; Zhou, H. L.; Chen, Y. R.; Jia, Y. Q. *Mater. Chem. Phys.* **2005**, *89*, 289.
(411) Nishiyama, K.; Nakamur, T.; Utsumi, S.; Sakai, H.; Abe, M. *J. Phys.: Conf. Ser.* **2009**, *176*, 012043.
(412) Kudaka, K.; Iizumi, K.; Sasaki, T.; Okada, S. *J. Alloys Compd.* **2001**, *315*, 104.
(413) Calka, A.; Radlinski, A. P. *J. Less-Common Met.* **1990**, *161*, 23.
(414) Radev, D. D.; Klisurski, D. *J. Alloys Compd.* **1994**, *206*, 39.
(415) Kudaka, K.; Iizumi, K.; Sasaki, T. *J. Ceram. Soc. Japan* **1999**, *107*, 1019.
(416) Hwang, Y.; Lee, J. K. *Mater. Lett.* **2002**, *54*, 1.
(417) Iizumi, K.; Sekiya, C.; Okada, S.; Kudou, K.; Shishido, T. *J. Eur. Ceram. Soc.* **2006**, *26*, 635.
(418) Morris, M. A.; Morris, D. G. *J. Mater. Sci.* **1991**, *26*, 4687.
(419) Gümbel, a.; Eckert, J.; Fuchs, G.; Nenkov, K.; Müller, K.-H.; Schultz, L. *Appl. Phys. Lett.* **2002**, *80*, 2725.
(420) Corrias, A.; Ennas, G.; Musinu, A.; Paschina, G.; Zedda, D. *J. Non-Cryst. Solids* **1995**, *192−193*, 565.
(421) Corrias, A.; Ennas, G.; Marongiu, G.; Musinu, A.; Paschina, G.; Zedda, D. *Mater. Sci. Eng.* **1995**, *204*, 211.
(422) Begin-Colin, S.; Caër, G. L.; Barraud, E.; Humbert, O. *J. Mater. Sci.* **2004**, *39*, 5081.
(423) Barraud, E.; Bégin-Colin, S.; Le Caër, G. *J. Alloys Compd.* **2005**, *398*, 208.
(424) Çamurlu, H. E. *J. Alloys Compd.* **2011**, *509*, 5431.
(425) Setoudeh, N.; Welham, N. J. *J. Alloys Compd.* **2006**, *420*, 225.
(426) Welham, N. J. *J. Am. Ceram. Soc.* **2000**, *92*, 1290.
(427) Ricceri, R.; Matteazzi, P. *Mater. Sci. Eng., A* **2004**, *379*, 341.
(428) Bilgi, E.; Çamurlu, H.; Akgun, B.; Topkaya, Y.; Sevinc, N. *Mater. Res. Bull.* **2008**, *43*, 873.
(429) Nishiyama, K.; Ono, T.; Nakayama, A.; Sakai, H.; Koishi, M.; Abe, M. *Surf. Coat. Int., Part B* **2003**, *86*, 169.
(430) Kelly, J. P.; Kanakala, R.; Graeve, O. A. *J. Am. Ceram. Soc.* **2010**, *93*, 3035.
(431) Wang, Y.; Li, L.; Wang, Y.; Song, D.; Liu, G.; Han, Y.; Jiao, L.; Yuan, H. *J. Power Sources* **2011**, *196*, 5731.
(432) Lu, J.; Xiao, Z.; Lin, Q.; Claus, H.; Fang, Z. Z. *J. Nanomater.* **2010**, *2010*, 1.
(433) Pechini, M. P. Patent No. 3,330,697, 1967.
(434) Kang, S. H.; Kim, D. J. *J. Eur. Ceram. Soc.* **2007**, *27*, 715.
(435) Maeda, H.; Yoshikawa, T.; Kusakabe, K.; Morooka, S. *J. Alloys Compd.* **1994**, *215*, 127.
(436) Saito, T.; Fukuda, T.; Maeda, H.; Kusakabe, K.; Morooka, S. *J. Mater. Sci.* **1997**, *2*, 3933.
(437) Rees, W. S.; Seyferth, D. *J. Am. Ceram. Soc.* **1988**, *71*, C194.
(438) Mirabelli, M. G. L.; Sneddon, L. G. *Inorg. Chem.* **1988**, *27*, 3271.
(439) Mirabelli, M. G. L.; Sneddon, L. G. *J. Am. Chem. Soc.* **1988**, *110*, 3305.
(440) Seyferth, D.; Rees, W. S.; Haggerty, J. S.; Lightfoot, A. *Chem. Mater.* **1989**, *1*, 45.
(441) Seyferth, D.; Rees, W. S. *Chem. Mater.* **1991**, *3*, 1106.
(442) Seyferth, D.; Bryson, N.; Workman, D. P.; Sobon, C. A. *J. Am. Ceram. Soc.* **1991**, *74*, 2687.
(443) Su, K.; Sneddon, L. G. *Chem. Mater.* **1991**, *3*, 10.
(444) Su, K.; Sneddon, L. G. *Chem. Mater.* **1993**, *5*, 1659.
(445) Forsthoefel, K.; Sneddon, L. *J. Mater. Sci.* **2004**, *39*, 6043.
(446) Stanley, D. R.; Birchall, J. D.; Hyland, J. N. K.; Thomas, L.; Hodgetts, K. *J. Mater. Chem.* **1992**, *2*, 149.
(447) Yan, Y.; Huang, Z.; Dong, S.; Jiang, D. *J. Am. Ceram. Soc.* **2006**, *89*, 3585.
(448) Xie, Y.; Sanders, T. H.; Speyer, R. F. *J. Am. Ceram. Soc.* **2008**, *91*, 1469.
(449) Li, R.; Zhang, Y.; Lou, H.; Li, J.; Feng, Z. *J. Sol-Gel Sci. Technol.* **2011**, *58*, 580.
(450) Zhang, Y.; Li, R.; Jiang, Y.; Zhao, B.; Duan, H.; Li, J.; Feng, Z. *J. Solid State Chem.* **2011**, *184*, 2047.
(451) Portehault, D.; Maneeratana, V.; Candolfi, C.; Oeschler, N.; Veremchuk, I.; Grin, Y.; Sanchez, C.; Antonietti, M. *ACS Nano* **2011**, *5*, 9052.
(452) Hall, S. R.; Howells, J. L. F.; Wimbush, S. C. *J. Electron. Mater.* **2010**, *39*, 2332.
(453) Chen, L.; Gu, Y.; Qian, Y.; Shi, L.; Yang, Z.; Ma, J. *Mater. Res. Bull.* **2004**, *39*, 609.
(454) Kravchenko, S. E.; Torbov, V. I.; Shilkin, S. P. *Inorg. Mater.* **2010**, *46*, 614.
(455) Chen, L.; Gu, Y.; Shi, L.; Yang, Z.; Ma, J.; Qian, Y. *J. Alloys Compd.* **2004**, *368*, 353.
(456) Chen, L.; Gu, Y.; Yang, Z.; Shi, L.; Ma, J.; Qian, Y. *Scr. Mater.* **2004**, *50*, 959.
(457) Cai, P.; Yang, Z.; Shi, L.; Chen, L.; Zhao, A.; Gu, Y.; Qian, Y. *Mater. Lett.* **2005**, *59*, 3550.
(458) Lei, W.; Portehault, D.; Dimova, R.; Antonietti, M. *J. Am. Chem. Soc.* **2011**, *133*, 7121.
(459) Freitag, W. O.; Sharp, T. a.; Baltz, A.; Suchodolski, V. *J. Appl. Phys.* **1979**, *50*, 7801.
(460) Mehandjiev, D.; Dragieva, I.; Slavcheva, M. *J. Magn. Magn. Mater.* **1985**, *50*, 205.
(461) Shen, J.; Li, Z.; Fan, Y.; Hu, Z.; Chen, Y. *J. Solid State Chem.* **1993**, *106*, 493.
(462) He, Y.; Qiao, M.; Hu, H.; Pei, Y.; Li, H.; Deng, J.; Fan, K. *Mater. Lett.* **2002**, *56*, 952.
(463) Linderoth, S. *J. Magn. Magn. Mater.* **1992**, *104−107*, 128.
(464) Linderoth, S.; Mørup, S. *J. Appl. Phys.* **1990**, *67*, 4472.
(465) Saida, J.; Inoue, A.; Masumoto, T. *Metall. Trans. A* **1991**, *22*, 2125.
(466) Nafis, S.; Hadjipanayis, G. C.; Sorensen, C. M.; Klabunde, K. J. *IEEE Trans. Magn.* **1989**, *25*, 3641.
(467) Shen, J.; Li, Z.; Yan, Q.; Chen, Y. *J. Phys. Chem.* **1993**, *97*, 8504.
(468) Shen, J.; Li, Z.; Chen, Y. *J. Mater. Sci. Lett.* **1994**, *13*, 1208.
(469) Hu, Z.; Fan, Y.; Chen, F.; Chen, Y. *J. Chem. Soc., Chem. Commun.* **1995**, 247.
(470) Shen, J.; Li, Z.; Wang, Q.; Chen, Y. *J. Mater. Sci.* **1997**, *32*, 749.
(471) Levy, A.; Brown, J. B.; Lyons, C. J. *Ind. Eng. Chem.* **1960**, *52*, 211.
(472) Brown, C. A. *J. Org. Chem.* **1970**, *56*, 1900.
(473) Li, H.; Li, H.; Dai, W.; Qiao, M. *Appl. Catal., A* **2003**, *238*, 119.
(474) Rinaldi, A.; Licoccia, S.; Traversa, E.; Sieradzki, K.; Peralta, P.; Davila-Ibanez, A. B.; Correa-Duarte, M. A.; Salgueirino, V. *J. Phys. Chem. C* **2010**, *114*, 13451.
(475) Dávila-Ibáñez, A. B.; Legido-Soto, J. L.; Rivas, J.; Salgueirino, V. *Phys. Chem. Chem. Phys.* **2011**, *13*, 20146.
(476) Yang, C.-C.; Chen, M.-S.; Chen, Y.-W. *Int. J. Hydrogen Energy* **2011**, *36*, 1418.
(477) Delmas, J.; Laversenne, L.; Rougeaux, I.; Capron, P.; Garron, A.; Bennici, S.; Świerczyński, D.; Auroux, A. *Int. J. Hydrogen Energy* **2011**, *36*, 2145.
(478) Dragieva, I.; Gavrilov, G.; Buchkov, D.; Slavcheva, M. *J. Less-Common Met.* **1979**, *67*, 375.
(479) Dragieva, I.; Rusev, K.; Stanimirova, M. *J. Less-Common Met.* **1990**, *158*, 295.
(480) Dragieva, I.; Slavcheva, M.; Buchkov, D. *J. Less-Common Met.* **1986**, *117*, 311.
(481) Wells, S.; Charles, S. W.; Mørup, S.; Linderoth, S.; Wonterghem, J.; Van Larsen, J.; Madsen, M. B. *J. Phys.: Condens. Matter* **1989**, *1*, 8199.
(482) Linderoth, S.; Mørup, S.; Bentzon, M. D. *J. Magn. Magn. Mater.* **1990**, *83*, 457.

(483) Lee, D.-S.; Liu, T.-K. *J. Non-Cryst. Solids* **2002**, *311*, 323.
(484) Brown, H. C.; Brown, C. A. *J. Am. Chem. Soc.* **1962**, *84*, 1493.
(485) Brown, H. C.; Brown, C. A. *J. Am. Chem. Soc.* **1962**, *84*, 1494.
(486) Acosta, D.; Ramírez, N.; Erdmann, E.; Destéfanis, H.; Gonzo, E. *Catal. Today* **2008**, *133−135*, 49.
(487) Oppegard, A. L.; Darnell, F. J.; Miller, H. C. *J. Appl. Phys.* **1961**, *32*, S184.
(488) Yiping, L.; Hadjipanayis, G. C.; Sorensen, C. M.; Klabunde, K. J. *J. Appl. Phys.* **1991**, *69*, 5141.
(489) Yiping, L.; Hadjipanayis, G.; Sorensen, C.; Klabunde, K. *J. Magn. Magn. Mater.* **1992**, *104*, 1545.
(490) Inoue, A.; Saida, J.; Masumoto, T. *Metall. Trans. A* **1988**, *19*, 2315.
(491) Van Wonterghem, J.; Mørup, S.; Koch, C. J. W.; Charles, S. W.; Wells, S. *Nature* **1986**, *322*, 622.
(492) Hu, Z.; Hsia, Y.; Zheng, J.; Shen, J.; Yan, Q.; Dai, L. *J. Appl. Phys.* **1991**, *70*, 436.
(493) Mørup, S.; Sethi, S.; Linderoth, S.; Koch, C.; Bentzon, M. D. *J. Mater. Sci.* **1992**, *27*, 3010.
(494) Hu, Z.; Chen, Y.; Hsia, Y. *Nucl. Instrum. Meth. Phys. Res., Sect. B* **1993**, *76*, 121.
(495) Fiorani, D.; Romero, H.; Suber, L.; Testa, A. M.; Vittori, M.; Montone, A.; Dormann, J. L.; Maknani, J. *Mater. Sci. Eng., A* **1995**, *204*, 165.
(496) Zhang, J.-G. *J. Mater. Eng. Perform.* **1995**, *4*, 453.
(497) Forster, G. D.; Barquin, L. F.; Cohen, N. S.; Pankhurst, Q. A.; Parkin, I. P. *J. Mater. Process. Technol.* **1999**, *92*, 525.
(498) Zysler, R. D.; Ramos, C. A.; Romero, H.; Ortega, A. *J. Mater. Sci.* **2001**, *6*, 2291.
(499) Haik, Y.; Chatterjee, J.; Jen Chen, C. *J. Nanopart. Res.* **2005**, *7*, 675.
(500) Yuan, Z.-Z.; Chen, J.-M.; Lu, Y.; Chen, X.-D. *J. Alloys Compd.* **2008**, *450*, 245.
(501) Yuan, Z.; Zhang, D. *Intermetallics* **2009**, *17*, 281.
(502) Wang, W.; Yang, Y.; Luo, H.; Hu, T.; Liu, W. *Catal. Commun.* **2011**, *12*, 436.
(503) Liu, B.; Qiao, M.; Wang, J.; Fan, K. *Chem. Commun.* **2002**, 1236.
(504) Fang, J.; Chen, X.; Liu, B.; Yan, S.; Qiao, M.; Li, H.; He, H.; Fan, K. *J. Catal.* **2005**, *229*, 97.
(505) Wang, W.; Yang, Y.; Bao, J.; Luo, H. *Catal. Commun.* **2009**, *11*, 100.
(506) Zhang, R.; Li, F.; Shi, Q.; Luo, L. *Appl. Catal., A* **2001**, *205*, 279.
(507) Bai, G.; Niu, L.; Qiu, M.; He, F.; Fan, X.; Dou, H.; Zhang, X. *Catal. Commun.* **2010**, *12*, 212.
(508) Qiao, M.; Xie, S.; Dai, W.; Deng, J. *Catal. Lett.* **2001**, *71*, 187.
(509) Wang, W.; Yang, Y.; Luo, H.; Liu, W. *React. Kinet., Mech. Catal.* **2010**, *101*, 105.
(510) Lee, S.; Chen, Y. *Ind. Eng. Chem. Res.* **1999**, *38*, 2548.
(511) Lee, S.-P.; Chen, Y.-W. *J. Mol. Catal. A: Chem.* **2000**, *152*, 213.
(512) Lee, S.-P.; Chen, Y.-W. *Ind. Eng. Chem. Res.* **2001**, *40*, 1495.
(513) Shen, J.; Hu, Z.; Hsia, Y.; Chen, Y. *Appl. Phys. Lett.* **1991**, *59*, 2510.
(514) Shen, J.; Hu, Z.; Hsia, Y.; Chen, Y. *J. Phys.: Condens. Matter* **1992**, *4*, 6381.
(515) Hu, Z.; Fan, Y.; Wu, Y.; Yan, Q.; Chen, Y. *J. Magn. Magn. Mater.* **1995**, *140−144*, 413.
(516) Shen, J.; Hu, Z.; Zhang, Q.; Zhang, L.; Chen, Y. *J. Appl. Phys.* **1992**, *71*, 5217.
(517) Lee, S.; Chen, Y. *J. Nanopart. Res.* **2001**, *3*, 133.
(518) Mo, M.; Han, L.; Lv, J.; Zhu, Y.; Peng, L.; Guo, X.; Ding, W. *Chem. Commun.* **2010**, *46*, 2268.
(519) Schaeffer, G. W.; Roscoe, J. S.; Stewart, A. C. *J. Am. Chem. Soc.* **1956**, *78*, 729.
(520) Stewart, A. C.; Schaeffer, G. W. *J. Inorg. Nucl. Chem.* **1956**, *3*, 194.
(521) Brown, H. C.; Brown, C. A. *J. Am. Chem. Soc.* **1963**, *85*, 1005.
(522) Maybury, P. C.; Mitchell, R. W.; Hawthorne, M. F. *J. Chem. Soc., Chem. Commun.* **1974**, 534.
(523) Molvinger, K.; Lopez, M.; Court, J. *J. Mol. Catal. A: Chem.* **1999**, *150*, 267.
(524) Molvinger, K.; Lopez, M.; Court, J. *Tetrahedron: Asymmetry* **2000**, *11*, 2263.
(525) Molvinger, K.; Lopez, M.; Court, J.; Chavant, P. Y. *Appl. Catal., A* **2002**, *231*, 91.
(526) Deng, J. F.; Yang, J.; Sheng, S. S.; Chen, H. G.; Xiong, G. X. *J. Catal.* **1994**, *150*, 434.
(527) Jackelen, A. M. L.; Jungbauer, M.; Glavee, G. N. *Langmuir* **1999**, *15*, 2322.
(528) Wu, Z.; Ge, S. *Catal. Commun.* **2011**, *13*, 40.
(529) Hofer, L.; Shultz, J.; Panson, R.; Anderson, R. *Inorg. Chem.* **1964**, *3*, 1783.
(530) Forster, G. D.; Fernández Barquín, L.; Pankhurst, Q. A.; Parkin, I. P. *J. Non-Cryst. Solids* **1999**, *244*, 44.
(531) Li, H.; Li, H.; Dai, W.; Wang, W.; Fang, Z.; Deng, J.-F. *Appl. Surf. Sci.* **1999**, *152*, 25.
(532) Li, H.; Li, H.; Deng, J.-F. *Appl. Catal., A* **2000**, *193*, 9.
(533) Li, H.; Zhao, Q.; Li, H. *J. Mol. Catal A: Chem.* **2008**, *285*, 29.
(534) Kukula, P.; Gabova, V.; Koprivova, K.; Trtik, P. *Catal. Today* **2007**, *121*, 27.
(535) Fang, Z.; Shen, B.; Lu, J.; Fan, K.; Deng, J. *Acta Chim. Sin.* **1999**, *57*, 894.
(536) Dragieva, I.; Deleva, C.; Mladenov, M.; Markova-Deneva, I. *Monatsh. Chem.* **2002**, *814*, 807.
(537) Taghavi, F.; Falamaki, C.; Shabanov, A.; Seyyedi, M.; Zare, M. *Appl. Catal., A* **2013**, *453*, 334.
(538) Davila-Ibanez, A. B.; Salgueirino, V. *J. Phys. Chem. C* **2013**, *117*, 4859.
(539) Tong, D. G.; Wang, D.; Chu, W.; Sun, J. H.; Wu, P. *Electrochim. Acta* **2010**, *55*, 2299.
(540) Chen, X.; Yang, W.; Wang, S.; Qiao, M. *New J. Chem.* **2005**, *29*, 266.
(541) Ma, H.; Ji, W.; Zhao, J.; Liang, J.; Chen, J. *J. Alloys Compd.* **2009**, *474*, 584.
(542) Tong, D.; Han, X.; Chu, W.; Chen, H.; Ji, X.-Y. *Mater. Lett.* **2007**, *61*, 4679.
(543) Zhu, Y.; Liu, F.; Ding, W.; Guo, X.; Chen, Y. *Angew. Chem., Int. Ed.* **2006**, *45*, 7211.
(544) Zhu, Y.; Guo, X.; Shen, Y.; Mo, M.; Guo, X.; Ding, W.; Chen, Y. *Nanotechnology* **2007**, *18*, 195601.
(545) Zhu, Y.; Guo, X.; Mo, M.; Guo, X.; Ding, W.; Chen, Y. *Nanotechnology* **2008**, *19*, 405602.
(546) Li, H.; Zhang, D.; Li, G.; Xu, Y.; Lu, Y.; Li, H. *Chem. Commun.* **2010**, *46*, 791.
(547) Li, H.; Zhao, Q.; Wan, Y.; Dai, W.; Qiao, M. *J. Catal.* **2006**, *244*, 251.
(548) Li, H.; Yang, H. *J. Catal.* **2007**, *251*, 233.
(549) Tong, D.-G.; Han, X.; Chu, W.; Chen, H.; Ji, X.-Y. *Mater. Res. Bull.* **2008**, *43*, 1327.
(550) Tong, D.; Chu, W.; Zeng, X.; Tian, W.; Wang, D. *Mater. Lett.* **2009**, *63*, 1555.
(551) Lu, D. S.; Li, W. S.; Jiang, X.; Tan, C. L.; Zeng, R. H. *J. Alloys Compd.* **2009**, *485*, 621.
(552) Destefanis, H.; Acosta, D.; Qonzo, E. *Catal. Today* **1992**, *15*, 555.
(553) Staubitz, A.; Robertson, A. P. M.; Manners, I. *Chem. Rev.* **2010**, *110*, 4079.
(554) Kalidindi, S. B.; Indirani, M.; Jagirdar, B. R. *Inorg. Chem.* **2008**, *47*, 7424.
(555) He, T.; Xiong, Z.; Wu, G.; Chu, H.; Wu, C.; Zhang, T.; Chen, P. *Chem. Mater.* **2009**, *21*, 2315.
(556) He, T.; Wang, J.; Wu, G.; Kim, H.; Proffen, T.; Wu, A.; Li, W.; Liu, T.; Xiong, Z.; Wu, C.; Chu, H.; Guo, J.; Autrey, T.; Zhang, T.; Chen, P. *Chem.—Eur. J.* **2010**, *16*, 12814.
(557) Aranishi, K.; Jiang, H.-L.; Akita, T.; Haruta, M.; Xu, Q. *Nano Res.* **2011**, *4*, 1233.

(558) Peng, S.; Lee, Y.; Wang, C.; Yin, H.; Dai, S.; Sun, S. *Nano Res.* **2008**, *1*, 229.
(559) Mazumder, V.; Sun, S. *J. Am. Chem. Soc.* **2009**, *131*, 4588.
(560) Metin, O.; Mazumder, V.; Ozkar, S.; Sun, S. *J. Am. Chem. Soc.* **2010**, *132*, 1468.
(561) Mankin, M. N.; Mazumder, V.; Sun, S. *Chem. Mater.* **2011**, *23*, 132.
(562) Wang, J. Y.; Kang, Y. Y.; Yang, H.; Cai, W. B. *J. Phys. Chem. C* **2009**, *113*, 8366.
(563) Rahman, A.; Jonnalagadda, S. *Catal. Lett.* **2008**, *123*, 264.
(564) Rahman, A.; Jonnalagadda, S. *J. Mol. Catal A: Chem.* **2009**, *299*, 98.
(565) Zhang, R.; Li, F.; Zhang, N.; Shi, Q. *Appl. Catal.* **2003**, *239*, 17.
(566) Ma, Z.-L.; Jia, R.-L.; Liu, C.-J. *J. Mol. Catal. A: Chem.* **2004**, *210*, 157.
(567) Wu, Z.-J.; Ge, S.-H.; Zhang, M.-H.; Li, W.; Tao, K.-Y. *Catal. Commun.* **2008**, *9*, 1432.
(568) Huang, Y.; Wang, Y.; Zhao, R.; Shen, P.; Wei, Z. *Int. J. Hydrogen Energy* **2008**, *33*, 7110.
(569) Wu, Z.; Zhao, J.; Zhang, M.; Li, W.; Tao, K. *Catal. Commun.* **2010**, *11*, 973.
(570) Liu, Q.; Liu, Z.; Liao, L.; Dong, X. *J. Nat. Gas Chem.* **2010**, *19*, 497.
(571) Wu, Z.; Zhang, M.; Ge, S.; Zhang, Z.; Li, W.; Tao, K. *J. Mater. Chem.* **2005**, *15*, 4928.
(572) Wu, Z.; Zhang, M.; Zhao, Z.; Li, W.; Tao, K. *J. Catal.* **2008**, *256*, 323.
(573) Ge, S.; Wu, Z.; Zhang, M.; Li, W.; Tao, K. *Ind. Eng. Chem. Res.* **2006**, *45*, 2229.
(574) Wu, Z.; Ge, S.; Zhang, M.; Li, W.; Mu, , S.-C.; Tao, K.-Y. *J. Phys. Chem. C* **2007**, *111*, 8587.
(575) Malyshev, V. V.; Hab, A. I. *Mater. Sci.* **2003**, *39*, 87.
(576) Mitov, M.; Rashkov, R.; Atanassov, N.; Zielonka, A. *J. Mater. Sci.* **2007**, *42*, 3367.
(577) Mitov, M.; Hristov, G.; Hristova, E.; Rashkov, R.; Arnaudova, M.; Zielonka, A. *Environ. Chem. Lett.* **2008**, *7*, 167.
(578) Sharif, R.; Zhang, X.; Shamaila, S.; Riaz, S.; Jiang, L.; Han, X. *J. Magn. Magn. Mater.* **2007**, *310*, e830.
(579) Cheng, Y.; Watanabe, T. *J. Chem. Eng. Jpn.* **2011**, *44*, 583.
(580) Cheng, Y.; Shigeta, M.; Choi, S.; Watanabe, T. *Chem. Eng. J.* **2012**, *183*, 483.
(581) Ding, Z.-H.; Qiu, L.-X.; Zhang, J.; Yao, B.; Cui, T.; Guan, W.-M.; Zheng, W.-T.; Wang, W.-Q.; Zhao, X.-D.; Liu, X.-Y. *J. Alloys Compd.* **2012**, *521*, 66.
(582) Ko, J.; Yoo, J.; Kim, Y.; Chung, K.; Yoo, S.; Wang, X.; Dou, S. *Phys. C* **2006**, *445−448*, 797.
(583) Yakinci, M. E.; Aksan, M. a.; Balci, Y.; Altin, S.; Onal, Y.; Aydogdu, Y. *J. Supercond. Novel Magn.* **2010**, *24*, 235.
(584) Vasquez, Y.; Henkes, A. E.; Chris Bauer, J.; Schaak, R. E. *J. Solid State Chem.* **2008**, *181*, 1509.
(585) Welker, H. *Z. Naturforsch.* **1952**, *7a*, 744.
(586) Harrison, B. C.; Tompkins, E. H. *Inorg. Chem.* **1962**, *1*, 951.
(587) Williams, R.; McGovern, I. *Surf. Sci.* **1975**, *51*, 14.
(588) Tycko, R. *Solid State Nucl. Magn. Reson.* **1998**, *11*, 1.
(589) Yan, P.; Xie, Y.; Wang, W.; Liu, F.; Qian, Y. *J. Mater. Chem.* **1999**, *9*, 1831.
(590) Didchenko, R.; Alix, J. E.; Toeniskoetter, R. H. *J. Inorg. Nucl. Chem.* **1960**, *14*, 35.
(591) Wells, R. L.; Aubuchon, S. R.; Kher, S. S.; Lube, M. S.; White, P. S. *Chem. Mater.* **1995**, *7*, 793.
(592) Zanella, P.; Rossetto, G.; Brianese, N.; Ossola, F.; Porchia, M.; Williams, J. O. *Chem. Mater.* **1991**, *3*, 225.
(593) Maury, F. *Adv. Mater.* **1991**, *3*, 542.
(594) Cowley, A. H.; Jones, R. A. *Angew. Chem., Int. Ed. Engl.* **1989**, *28*, 1208.
(595) Douglas, T.; Theopold, K. H. *Inorg. Chem.* **1991**, *30*, 594.
(596) Barry, S. T.; Belhumeur, S.; Richeson, D. S. *Organometallics* **1997**, *16*, 3588.
(597) Green, M.; Brien, P. O. *Adv. Mater.* **1998**, *10*, 527.
(598) Lewkebandara, T. S.; Proscia, J. W.; Winter, C. H. *Chem. Mater.* **1995**, *7*, 1053.
(599) Lukehart, C. M.; Milne, S. B.; Stock, S. R. *Chem. Mater.* **1998**, *10*, 903.
(600) Hector, A. L.; Parkin, I. P. *J. Mater. Chem.* **1994**, *4*, 279.
(601) Parkin, I. P. *Chem. Soc. Rev.* **1996**, *25*, 199.
(602) Jones, E. *Phys. Rev.* **1967**, *158*, 295.
(603) Memming, R.; Schwandt, G. *Electrochim. Acta* **1968**, *13*, 1299.
(604) Chiba, S. *J. Phys. Soc. Jpn.* **1960**, *15*, 581.
(605) Fruchart, R.; Roger, A.; Senateur, J. *J. Appl. Phys.* **1969**, *40*, 1250.
(606) Meisner, G. *Physica B+C* **1981**, *108*, 763.
(607) Carmalt, C. J.; Cowley, A. H.; Hector, A. L.; Norman, N. C.; Parkin, I. P. *J. Chem. Soc., Chem. Commun.* **1994**, 1987.
(608) Allen, G. C.; Carmalt, C. J.; Cowley, A. H.; Hector, A. L.; Kamepalli, S.; Lawson, Y. G.; Norman, N. C.; Parkin, I. P.; Pickard, L. K. *Chem. Mater.* **1997**, *9*, 1385.
(609) Kher, S. S.; Wells, R. L. *Chem. Mater.* **1994**, *6*, 2056.
(610) Micic, O. I.; Sprague, J. R.; Curtis, C. J.; Jones, K. M.; Machol, J. L.; Nozik, A. J.; Giessen, H.; Fluegel, B.; Mohs, G.; Peyghambarian, N. *J. Phys. Chem.* **1995**, *99*, 7754.
(611) Green, M. *Curr. Opin. Solid State Mater. Sci.* **2002**, *6*, 355.
(612) Trentler, T. J.; Hickman, K. M.; Goel, S. C.; Viano, A. M.; Gibbons, P. C.; Buhro, W. E. *Science* **1995**, *270*, 1791.
(613) Gudiksen, M. S.; Wang, J.; Lieber, C. M. *J. Phys. Chem. B* **2002**, *106*, 4036.
(614) Duan, X.; Huang, Y.; Cui, Y.; Wang, J.; Lieber, C. M. *Nature* **2001**, *409*, 66.
(615) Föll, H.; Langa, S.; Carstensen, J.; Christophersen, M.; Tiginyanu, I. M. *Adv. Mater.* **2003**, *15*, 183.
(616) Agger, J. R.; Anderson, M. W.; Pemble, M. E.; Terasaki, O.; Nozue, Y. *J. Phys. Chem. B* **1998**, *102*, 3345.
(617) Buhro, W. E. *Polyhedron* **1994**, *13*, 1131.
(618) Allen, P. M.; Walker, B. J.; Bawendi, M. G. *Angew. Chem., Int. Ed.* **2010**, *49*, 760.
(619) Trentler, T. J.; Goel, S. C.; Hickman, K. M.; Viano, A. M.; Chiang, M. Y.; Beatty, A. M.; Gibbons, P. C.; Buhro, W. E. *J. Am. Chem. Soc.* **1997**, *119*, 2172.
(620) Schweyer-Tihay, F.; Braunstein, P.; Estournès, C.; Guille, J. L.; Lebeau, B.; Paillaud, J.-L.; Richard-Plouet, M.; Rosé, J. *Chem. Mater.* **2003**, *15*, 57.
(621) Kelly, A. T.; Rusakova, I.; Ould-Ely, T.; Hofmann, C.; Lüttge, A.; Whitmire, K. H. *Nano Lett.* **2007**, *7*, 2920.
(622) Shahid, M.; Mazhar, M.; Molloy, K. C. *Inorg. Chim. Acta* **2009**, *362*, 3069.
(623) Colson, A. C.; Chen, C.-W.; Morosan, E.; Whitmire, K. H. *Adv. Funct. Mater.* **2012**, *22*, 1850.
(624) Colson, A. C.; Whitmire, K. H. *Chem. Mater.* **2011**, *23*, 3731.
(625) Panneerselvam, A.; Malik, M. A.; Afzaal, M.; O'Brien, P.; Helliwell, M. *J. Am. Chem. Soc.* **2008**, *130*, 2420.
(626) Panneerselvam, A.; Periyasamy, G.; Ramasamy, K.; Afzaal, M.; Malik, M. A.; O'Brien, P.; Burton, N. A.; Waters, J.; Van Dongen, B. E. *Dalton Trans.* **2010**, *39*, 6080.
(627) Maneeprakorn, W.; Nguyen, C. Q.; Malik, M. A.; O'Brien, P.; Raftery, J. *Dalton Trans.* **2009**, 2103.
(628) Maneeprakorn, W.; Malik, M. A..; O'Brien, P. *J. Mater. Chem.* **2010**, *20*, 2329.
(629) Oyetunde, D.; Afzaal, M.; Vincent, M. A.; Hillier, I. H.; O'Brien, P. *Inorg. Chem.* **2011**, *50*, 2052.
(630) King, W. D.; Kwiatkowski, K. C.; Lukehart, C. M. *J. Nanosci. Nanotechnol.* **2008**, *8*, 3146.
(631) Sweeney, C. M.; Stamm, K. L.; Brock, S. L. *J. Alloys Compd.* **2008**, *448*, 122.
(632) Roels, J.; Verstraete, W. *Bioresour. Technol.* **2001**, *79*, 243.
(633) Ni, Y.; Tao, A.; Hu, G.; Cao, X.; Wei, X.; Yang, Z. *Nanotechnology* **2006**, *17*, 5013.
(634) Song, L.; Zhang, S. *Powder Technol.* **2011**, *208*, 713.
(635) Li, L.; Protière, M.; Reiss, P. *Chem. Mater.* **2008**, *20*, 2621.
(636) Zan, F.; Ren, J. *J. Mater. Chem.* **2012**, *22*, 1794.

(637) Zan, F.; Dong, C.; Liu, H.; Ren, J. *J. Phys. Chem. C* **2012**, *116*, 3944.
(638) Miao, S.; Hickey, S. G.; Waurisch, C.; Lesnyak, V.; Otto, T.; Rellinghaus, B.; Eychmuller, A. *ACS Nano* **2012**, *6*, 7059.
(639) Hall, J. W.; Membreno, N.; Wu, J.; Celio, H.; Jones, R. A.; Stevenson, K. J. *J. Am. Chem. Soc.* **2012**, *134*, 5532.
(640) Blackman, C. *Appl. Surf. Sci.* **2003**, *211*, 2.
(641) Perera, S. C.; Tsoi, G.; Wenger, L. E.; Brock, S. L. *J. Am. Chem. Soc.* **2003**, *125*, 13960.
(642) Wang, R.; Ratcliffe, C. I.; Wu, X.; Voznyy, O.; Tao, Y.; Yu, K. *J. Phys. Chem. C* **2009**, *113*, 17979.
(643) Miao, S.; Hickey, S. G.; Rellinghaus, B.; Waurisch, C.; Eychmüller, A. *J. Am. Chem. Soc.* **2010**, *132*, 5613.
(644) Xie, R.; Zhang, J.; Zhao, F.; Yang, W.; Peng, X. *Chem. Mater.* **2010**, *22*, 3820.
(645) Jasinski, J.; Leppert, V.; Lam, S.; Gibson, G.; Nauka, K.; Yang, C.; Zhou, Z. *Solid State Commun.* **2007**, *141*, 624.
(646) Xie, R.; Battaglia, D.; Peng, X. *J. Am. Chem. Soc.* **2007**, *129*, 15432.
(647) Xu, S.; Ziegler, J.; Nann, T. *J. Mater. Chem.* **2008**, *18*, 2653.
(648) Li, L.; Reiss, P. *J. Am. Chem. Soc.* **2008**, *130*, 11588.
(649) Xie, R.; Li, Z.; Peng, X. *J. Am. Chem. Soc.* **2009**, *131*, 15457.
(650) Liu, Z.; Sun, K.; Jian, W.-B.; Xu, D.; Lin, Y.-F.; Fang, J. *Chem.—Eur. J.* **2009**, *15*, 4546.
(651) Huang, K.; Demadrille, R.; Silly, M. G.; Sirotti, F.; Reiss, P.; Renault, O. *ACS Nano* **2010**, *4*, 4799.
(652) Narayanaswamy, A.; Feiner, L. F.; Meijerink, A.; Van der Zaag, P. J. *ACS Nano* **2009**, *3*, 2539.
(653) Harris, D. K.; Bawendi, M. G. *J. Am. Chem. Soc.* **2012**, *134*, 20211.
(654) Ojo, W.-S.; Xu, S.; Delpech, F.; Nayral, C.; Chaudret, B. *Angew. Chem., Int. Ed.* **2011**, *51*, 738.
(655) Talapin, D. *Colloids Surf., A* **2002**, *202*, 145.
(656) Ryu, E.; Kim, S.; Jang, E.; Jun, S.; Jang, H.; Kim, B.; Kim, S. *Chem. Mater.* **2009**, *21*, 573.
(657) Kim, M. R.; Chung, J. H.; Lee, M.; Lee, S.; Jang, D.-J. *J. Colloid Interface Sci.* **2010**, *350*, 5.
(658) Somaskandan, K.; Tsoi, G. M.; Wenger, L. E.; Brock, S. L. *J. Mater. Chem.* **2010**, *20*, 375.
(659) Nedeljković, J. M.; Mićić, O. I.; Ahrenkiel, S. P.; Miedaner, A.; Nozik, A. J. *J. Am. Chem. Soc.* **2004**, *126*, 2632.
(660) Shweky, I.; Aharoni, A.; Mokari, T.; Rothenberg, E.; Nadler, M.; Popov, I.; Banin, U. *Mater. Sci. Eng., C* **2006**, *26*, 788.
(661) Wang, F.; Buhro, W. E. *J. Am. Chem. Soc.* **2007**, *129*, 14381.
(662) Park, J.-G. J.; Koo, B.; Hwang, Y.; Bae, C.; An, K.; Park, H. M.; Hyeon, T. *Angew. Chem., Int. Ed.* **2004**, *43*, 2282.
(663) Qian, C.; Kim, F.; Ma, L.; Tsui, F.; Yang, P.; Liu, J. *J. Am. Chem. Soc.* **2004**, *126*, 1195.
(664) Lo, C.-T.; Kuo, P.-Y. *J. Phys. Chem. C* **2010**, *114*, 4808.
(665) Senevirathne, K.; Burns, A. W.; Bussell, M. E.; Brock, S. L. *Adv. Funct. Mater.* **2007**, *17*, 3933.
(666) Khanna, P. K.; Jun, K.-W.; Hong, K. B.; Baeg, J.-O.; Mehrotra, G. K. *Mater. Chem. Phys.* **2005**, *92*, 54.
(667) Khanna, P. K.; Singh, N.; More, P. *Curr. Appl. Phys.* **2010**, *10*, 84.
(668) Gregg, K. A.; Perera, S. C.; Lawes, G.; Shinozaki, S.; Brock, S. L. *Chem. Mater.* **2006**, *18*, 879.
(669) Singh, N.; Khanna, P. K.; Joy, P. A. *J. Nanopart. Res.* **2008**, *11*, 491.
(670) Kim, Y.; Hwang, H.; Yoon, C. S.; Kim, M. G.; Cho, J. *Adv. Mater.* **2007**, *19*, 92.
(671) Chen, Y.; She, H.; Luo, X.; Yue, G. H.; Peng, D. L. *J. Cryst. Growth* **2009**, *311*, 1229.
(672) She, H.; Chen, Y.; Luo, X.; Yue, G.-H.; Peng, D.-L. *J. Nanosci. Nanotechnol.* **2010**, *10*, 5175.
(673) Ye, E.; Zhang, S.-Y.; Lim, S. H.; Bosman, M.; Zhang, Z.; Win, K. Y.; Han, M.-Y. *Chem.—Eur. J.* **2011**, *17*, 5982.
(674) De Trizio, L.; Figuerola, A.; Manna, L.; Genovese, A.; George, C.; Brescia, R.; Saghi, Z.; Simonutti, R.; Van Huis, M.; Falqui, A. *ACS Nano* **2012**, *6*, 32.
(675) Zhang, S.-Y.; Ye, E.; Liu, S.; Lim, S. H.; Tee, S. Y.; Dong, Z.; Han, M.-Y. *Adv. Mater.* **2012**, *24*, 4369.
(676) Hu, C.; Li, Y.; Liu, J.; Zhang, Y.; Bao, G.; Buchine, B.; Wang, Z. *Chem. Phys. Lett.* **2006**, *428*, 343.
(677) Yoon, K. Y.; Jang, Y.; Park, J.; Hwang, Y.; Koo, B.; Park, J.-G.; Hyeon, T. *J. Solid State Chem.* **2008**, *181*, 1609.
(678) Brock, S. L.; Senevirathne, K. *J. Solid State Chem.* **2008**, *181*, 1552.
(679) Muthuswamy, E.; Brock, S. L. *J. Am. Chem. Soc.* **2010**, *132*, 15849.
(680) Henkes, A. E.; Vasquez, Y.; Schaak, R. E. *J. Am. Chem. Soc.* **2007**, *129*, 1896.
(681) Hu, X.; Yu, J. C. *Chem. Mater.* **2008**, *20*, 6743.
(682) Moreau, L. M.; Ha, D.-H.; Bealing, C. R.; Zhang, H.; Hennig, R. G.; Robinson, R. D. *Nano Lett.* **2012**, *12*, 4530.
(683) Ha, D.-H.; Moreau, L. M.; Bealing, C. R.; Zhang, H.; Hennig, R. G.; Robinson, R. D. *J. Mater. Chem.* **2011**, *21*, 11498.
(684) Seo, H.-R.; Cho, K.-S.; Lee, Y.-K. *Mater. Sci. Eng., B* **2011**, *176*, 132.
(685) Wang, J.; Johnston-Peck, A. C.; Tracy, J. B. *Chem. Mater.* **2009**, *21*, 4462.
(686) Kim, H.; Chae, Y.; Lee, D. H.; Kim, M.; Huh, J.; Kim, Y.; Kim, H.; Kim, H. J.; Kim, S. O.; Baik, H.; Choi, K.; Kim, J. S.; Yi, G.-R.; Lee, K. *Angew. Chem., Int. Ed.* **2010**, *49*, 5712.
(687) Green, M.; O'Brien, P. *Chem. Mater.* **2001**, *13*, 4500.
(688) Apostolico, L.; Mahon, M. F.; Molloy, K. C.; Binions, R.; Blackman, C. S.; Carmalt, C. J.; Parkin, I. P. *Dalton Trans.* **2004**, 470.
(689) Henderson, L. B.; Ekerdt, J. G. *Electrochem. Solid-State Lett.* **2009**, *12*, D36.
(690) Sweet, J. D.; Casadonte, D. J. *Ultrason. Sonochem.* **2001**, *8*, 97.
(691) George, P. P.; Pol, V. G.; Gedanken, A. *J. Nanopart. Res.* **2007**, *9*, 1187.
(692) Wang, J.; Yang, Q. *Chem. Lett.* **2008**, *37*, 306.
(693) Wang, J.; Yang, Q.; Zhang, Z.; Sun, S. *Chem—Eur. J.* **2010**, *16*, 7916.
(694) Wang, J.; Yang, Q.; Zhou, J.; Sun, K.; Zhang, Z.; Feng, X.; Li, T. *Nano Res.* **2010**, *3*, 211.
(695) Zheng, X.; Yuan, S.; Tian, Z.; Yin, S.; He, J.; Liu, K.; Liu, L. *Chem. Mater.* **2009**, *21*, 4839.
(696) Zafiropoulou, I.; Papagelis, K.; Boukos, N.; Siokou, A.; Niarchos, D.; Tzitzios, V. *J. Phys. Chem. C* **2010**, *114*, 7582.
(697) Zheng, X.; Yuan, S.; Tian, Z.; Yin, S.; He, J.; Liu, K.; Liu, L. *Mater. Lett.* **2009**, *63*, 2283.
(698) Wang, J.; Yang, Q.; Zhang, Z.; Li, T.; Zhang, S. *Dalton Trans.* **2010**, *39*, 227.
(699) Wang, X.; Wan, F.; Gao, Y.; Liu, J.; Jiang, K. *J. Cryst. Growth* **2008**, *310*, 2569.
(700) Xie, Y.; Su, H. L.; Qian, X. F.; Liu, X. M.; Qian, Y. T. *J. Solid State Chem.* **2000**, *149*, 88.
(701) Li, J.; Ni, Y.; Liao, K.; Hong, J. *J. Colloid Interface Sci.* **2009**, *332*, 231.
(702) Bao, K.; Liu, S.; Cao, J.; Liang, J.; Zhu, Y.; Hu, X.; Zhu, L.; Liu, X.; Qian, Y. *J. Nanosci. Nanotechnol.* **2009**, *9*, 4918.
(703) Hou, H.; Peng, Q.; Zhang, S.; Guo, Q.; Xie, Y. *Eur. J. Inorg. Chem.* **2005**, *2005*, 2625.
(704) Liu, S.; Qian, Y.; Ma, X. *Mater. Lett.* **2008**, *62*, 11.
(705) Ni, Y.; Li, J.; Zhang, L.; Yang, S.; Wei, X. *Mater. Res. Bull.* **2009**, *44*, 1166.
(706) Luo, F.; Su, H.-L.; Song, W.; Wang, Z.-M.; Yan, Z.-G.; Yan, C.-H. *J. Mater. Chem.* **2004**, *14*, 111.
(707) Liu, S.; Liu, X.; Xu, L.; Qian, Y.; Ma, X. *J. Cryst. Growth* **2007**, *304*, 430.
(708) Budnikova, Y.; Tazeev, D.; Trofimov, B.; Sinyashin, O. *Electrochem. Commun.* **2004**, *6*, 700.
(709) Li, Z.; Casadontejr, D.; Casadonte, D. J. *Ultrason. Sonochem.* **2007**, *14*, 757.

(710) Zhang, Z.-C.; Wang, B.-P. *Part. Part. Syst. Charact.* **2009**, *26*, 53.
(711) Wang, X.; Wan, F.; Liu, J.; Gao, Y.; Jiang, K. *J. Alloys Compd.* **2009**, *474*, 233.
(712) Liu, S.; Qian, Y.; Xu, L. *Solid State Commun.* **2009**, *149*, 438.
(713) Carenco, S.; Le Goff, X. F.; Shi, J.; Roiban, L.; Ersen, O.; Boissière, C.; Sanchez, C.; Mézailles, N. *Chem. Mater.* **2011**, *23*, 2270.
(714) Barry, B. M.; Gillan, E. G. *Chem. Mater.* **2009**, *21*, 4454.
(715) Barry, B. M.; Gillan, E. G. *Chem. Mater.* **2008**, *20*, 2618.
(716) Kagirov, R. M.; Voloshin, A. V.; Kadirov, M. K.; Nizameev, I. R.; Sinyashin, O. G.; Yakhvarov, D. G. *Mendeleev Commun.* **2011**, *21*, 201.
(717) Carenco, S.; Hu, Y.; Florea, I.; Ersen, O.; Boissière, C.; Mézailles, N.; Sanchez, C. *Chem. Mater.* **2012**, *24*, 4134.
(718) Carenco, S.; Hu, Y.; Florea, I.; Ersen, O.; Boissière, C.; Sanchez, C.; Mézailles, N. *Dalton Trans.* **2013**, DOI: 10.1039/c3dt50686j.
(719) Thuy, U.; Huyen, T.; Liem, N.; Reiss, P. *Mater. Chem. Phys.* **2008**, *112*, 1120.
(720) Belykh, L. B.; Skripov, N. I.; Belonogova, L. N.; Rokhin, a. V.; Shmidt, F. K. *Russ. J. Gen. Chem.* **2009**, *79*, 92.
(721) Liu, Z.; Huang, X.; Zhu, Z.; Dai, J. *Ceram. Int.* **2010**, *36*, 1155.
(722) Ni, Y.; Jin, L.; Hong, J. *Nanoscale* **2011**, *3*, 196.
(723) Yang, H.; Yin, W.; Zhao, H.; Yang, R.; Song, Y. *J. Phys. Chem. Solids* **2008**, *69*, 1017.
(724) Liu, J.; Chen, X.; Shao, M.; An, C.; Yu, W.; Qian, Y. *J. Cryst. Growth* **2003**, *252*, 297.
(725) Kovnir, K.; Kolenko, Y.; Ray, S.; Li, J.; Watanabe, T.; Itoh, M.; Yoshimura, M.; Shevelkov, A. *J. Solid State Chem.* **2006**, *179*, 3756.
(726) Song, L.; Zhang, S.; Wei, Q. *J. Solid State Chem.* **2011**, *184*, 1556.
(727) Pfeiffer, H.; Tancret, F.; Brousse, T. *Mater. Chem. Phys.* **2005**, *92*, 534.
(728) Lincke, H.; Hermes, W.; Nilges, T.; Pöttgen, R. *Solid State Sci.* **2008**, *10*, 1480.
(729) Eschen, M.; Jeitschko, W. *J. Solid State Chem.* **2002**, *165*, 238.
(730) Lü, B.; Bai, Y. J.; Feng, X.; Zhao, Y. R.; Yang, J.; Chi, J. R. *J. Cryst. Growth* **2004**, *260*, 115.
(731) Liu, Z.; Kumbhar, A.; Xu, D.; Zhang, J.; Sun, Z.; Fang, J. *Angew. Chem., Int. Ed.* **2008**, *47*, 3540.
(732) Gall, N.; Tontegode, A. Y. *Tech. Phys. Lett.* **2000**, *26*, 510.
(733) Zhang, H.; Ha, D.-H.; Hovden, R.; Kourkoutis, L. F.; Robinson, R. D. *Nano Lett.* **2011**, *11*, 188.
(734) Wang, A.; Qin, M.; Guan, J.; Wang, L.; Guo, H.; Li, X.; Wang, Y.; Prins, R.; Hu, Y. *Angew. Chem., Int. Ed.* **2008**, *47*, 6052.
(735) Guan, J.; Wang, Y.; Qin, M.; Yang, Y.; Li, X.; Wang, A. *J. Solid State Chem.* **2009**, *182*, 1550.
(736) Shen, G. Z.; Bando, Y.; Hu, J. Q.; Golberg, D. *Appl. Phys. Lett.* **2006**, *88*, 143105.
(737) Shen, G.; Chen, P.-C.; Bando, Y.; Golberg, D.; Zhou, C. *Chem. Mater.* **2008**, *20*, 7319.
(738) Longo, R. C.; Carrete, J.; Aguilera-Granja, F.; Vega, A.; Gallego, L. J. *J. Chem. Phys.* **2009**, *131*, 074504.
(739) Paliwal, U.; Joshi, K. B. *Phys. B* **2011**, *406*, 3060.
(740) Aksomaityte, G.; Cheng, F.; Hector, A. L.; Hyde, J. R.; Levason, W.; Reid, G.; Smith, D. C.; Wilson, J. W.; Zhang, W. *Chem. Mater.* **2010**, *22*, 4246.
(741) Gayen, R. N.; Das, S. N.; Dalui, S.; Paul, R.; Bhar, R.; Pal, A. K. *Thin Solid Films* **2010**, *518*, 3595.
(742) Nightingale, A. M.; De Mello, J. C. *ChemPhysChem* **2009**, *10*, 2612.
(743) Baek, J.; Allen, P. M.; Bawendi, M. G.; Jensen, K. F. *Angew. Chem., Int. Ed.* **2011**, *50*, 627.
(744) Tateno, K.; Zhang, G.; Nakano, H. *J. Cryst. Growth* **2008**, *310*, 2966.
(745) Boles, S. T.; Thompson, C. V.; Fitzgerald, E. A. *J. Cryst. Growth* **2009**, *311*, 1446.
(746) Shu, H.; Chen, X.; Zhou, X.; Ding, Z.; Lu, W. *J. Phys. Chem. C* **2010**, *114*, 10195.
(747) Kitauchi, Y.; Kobayashi, Y.; Tomioka, K.; Hara, S.; Hiruma, K.; Fukui, T.; Motohisa, J. *Nano Lett.* **2010**, *10*, 1699.
(748) Mandl, B.; Stangl, J.; Hilner, E.; Zakharov, A. a.; Hillerich, K.; Dey, A. W.; Samuelson, L.; Bauer, G.; Deppert, K.; Mikkelsen, A. *Nano Lett.* **2010**, *10*, 4443.
(749) Chiaramonte, T.; Tizei, L. H. G.; Ugarte, D.; Cotta, M. A. *Nano Lett.* **2011**, *11*, 1934.
(750) Hui, A. T.; Wang, F.-Y. F.; Han, N.; Yip, S.-P. S.; Xiu, F.; Hou, J. J.; Yen, Y.-T.; Hung, T.; Chueh, Y.-L.; Ho, J. C. *J. Mater. Chem.* **2012**, *22*, 10704.
(751) Rao, C.; Deepak, F. L.; Gundiah, G.; Govindaraj, A. *Prog. Solid State Chem.* **2003**, *31*, 5.
(752) Yu, H.; Li, J.; Loomis, R. A.; Wang, L.-W.; Buhro, W. E. *Nat. Mater.* **2003**, *2*, 517.
(753) Bakkers, E. P. A. M.; Verheijen, M. A. *J. Am. Chem. Soc.* **2003**, *125*, 3440.
(754) Delimitis, a.; Komninou, P.; Kehagias, T.; Pavlidou, E.; Karakostas, T.; Gladkov, P.; Nohavica, D. *J. Porous Mater.* **2007**, *15*, 75.
(755) Novotny, C. J.; Derose, C. T.; Norwood, R. a; Yu, P. K. L. *Nano Lett.* **2008**, *8*, 1020.
(756) Alemany, M.; Tortajada, L.; Huang, X.; Tiago, M.; Gallego, L.; Chelikowsky, J. *Phys. Rev. B* **2008**, *78*, 23310.
(757) Roy, S.; Springborg, M. *J. Phys. Chem. C* **2009**, *113*, 81.
(758) Gadret, E. G.; Dias, G. O.; Dacal, L. C. O.; De Lima, M. M.; Ruffo, C. V. R. S.; Iikawa, F.; Brasil, M. J. S. P.; Chiaramonte, T.; Cotta, M. A.; Tizei, L. H. G.; Ugarte, D.; Cantarero, A. *Phys. Rev. B* **2010**, *82*, 125327.
(759) Shen, G.; Chen, P.-C.; Bando, Y.; Golberg, D.; Zhou, C. *Chem. Mater.* **2008**, *20*, 6779.
(760) Sun, T.; Wu, P. C.; Guo, Z. D.; Dai, Y.; Meng, H.; Fang, X. L.; Shi, Z. J.; Dai, L.; Qin, G. G. *Phys. Lett. A* **2011**, *375*, 2118.
(761) Wu, P.; Sun, T.; Dai, Y.; Sun, Y.; Ye, Y.; Dai, L. *Cryst. Growth Des.* **2011**, *11*, 1417.
(762) Borgström, M. T.; Mergenthaler, K.; Messing, M. E.; Håkanson, U.; Wallentin, J.; Samuelson, L.; Pistol, M.-E. *J. Cryst. Growth* **2011**, *324*, 290.
(763) Tatebayashi, J.; Lin, A.; Wong, P. S.; Hick, R. F.; Huffaker, D. L. *J. Appl. Phys.* **2010**, *108*, 034315.
(764) Algra, R. E.; Verheijen, M. a.; Borgström, M. T.; Feiner, L.-F.; Immink, G.; Van Enckevort, W. J. P.; Vlieg, E.; Bakkers, E. P. a. M. *Nature* **2008**, *456*, 369.
(765) Algra, R. E.; Hocevar, M.; Verheijen, M. a; Zardo, I.; Immink, G. G. W.; Van Enckevort, W. J. P.; Abstreiter, G.; Kouwenhoven, L. P.; Vlieg, E.; Bakkers, E. P. a. M. *Nano Lett.* **2011**, *11*, 1690.
(766) Ikejiri, K.; Ishizaka, F.; Tomioka, K.; Fukui, T. *Nano Lett.* **2012**, *12*, 4770.
(767) Ikejiri, K.; Kitauchi, Y.; Tomioka, K.; Motohisa, J.; Fukui, T. *Nano Lett.* **2012**, *11*, 4314.
(768) Shen, G.; Chen, P.-C.; Bando, Y.; Golberg, D.; Zhou, C. *J. Phys. Chem. C* **2008**, *112*, 16405.
(769) Collins, S. M.; Hankett, J. M.; Carim, A. I.; Maldonado, S. *J. Mater. Chem.* **2012**, *22*, 6613.
(770) Liu, B.; Bando, Y.; Liu, L.; Zhao, J.; Masanori, M.; Jiang, X.; Golberg, D. *Nano Lett.* **2013**, *13*, 85.
(771) Wang, H.; Shu, Y.; Wang, A.; Wang, J.; Zheng, M.; Wang, X.; Zhang, T. *Carbon* **2008**, *46*, 2076.
(772) Yao, Z. W. *J. Alloys Compd.* **2009**, *475*, L38.
(773) Viter, V. N.; Nagornyi, P. G. *Russ. J. Appl. Chem.* **2008**, *81*, 1144.
(774) Musaev, O.; Wrobel, J.; Wieliczka, D.; Dusevich, V.; Kruger, M. *Phys. E* **2008**, *40*, 3147.
(775) Gresback, R.; Hue, R.; Gladfelter, W. L.; Kortshagen, U. R. *Nanoscale Res. Lett.* **2011**, *6*, 68.
(776) Dulal, S.; Kim, T.; Shin, C.; Kim, C. *J. Alloys Compd.* **2008**, *461*, 382.
(777) Habelhames, F.; Nessark, B.; Bouhafs, D.; Cheriet, A.; Derbal, H. *Ionics* **2009**, *16*, 177.
(778) Dorn, A.; Allen, P. M.; Bawendi, M. G. *ACS Nano* **2009**, *3*, 3260.

(779) Gonçalves, A.-M.; Mézailles, N.; Mathieu, C.; Le Floch, P.; Etcheberry, A. *Chem. Mater.* **2010**, *22*, 3114.
(780) Mukherjee, J.; Peczonczyk, S.; Maldonado, S. *Langmuir* **2010**, *26*, 10890.
(781) Huggins, R. *Solid State Ionics* **2002**, *152−153*, 61.
(782) Pralong, V.; Souza, D. C. S.; Leung, K. T.; Nazar, L. F. *Electrochem. Commun.* **2002**, *4*, 516.
(783) Bichat, M.-P.; Gillot, F.; Monconduit, L.; Favier, F.; Morcrette, M.; Lemoigno, F.; Doublet, M.-L. *Chem. Mater.* **2004**, *16*, 1002.
(784) Gillot, F.; Monconduit, L.; Morcrette, M.; Doublet, M.-L.; Dupont, L.; Tarascon, J.-M. *Chem. Mater.* **2005**, *17*, 3627.
(785) Gillot, F.; Bichat, M. P.; Favier, F.; Morcrette, M.; Tarascon, J. M.; Monconduit, L. *Ionics* **2003**, *9*, 71.
(786) Mauchamp, V.; Moreau, P.; Monconduit, L.; Doublet, M.-L.; Boucher, F.; Ouvrard, G. *J. Phys. Chem. C* **2007**, *111*, 3996.
(787) Gillot, F.; Boyanov, S.; Dupont, L.; Doublet, M.-L.; Morcrette, M.; Monconduit, L.; Tarascon, J.-M. *Chem. Mater.* **2005**, *17*, 6327.
(788) Boyanov, S.; Gillot, F.; Monconduit, L. *Ionics* **2008**, *14*, 125.
(789) Gillot, F.; Monconduit, L.; Doublet, M.-L. *Chem. Mater.* **2005**, *17*, 5817.
(790) Huang, L.; Zheng, X.-M.; Wu, Y.-S.; Xue, L.-J.; Ke, F.-S.; Wei, G.-Z.; Sun, S.-G. *Electrochem. Commun.* **2009**, *11*, 585.
(791) Cameron, J. M.; Hughes, R. W.; Zhao, Y.; Gregory, D. H. *Chem. Soc. Rev.* **2011**, *40*, 4099.
(792) Zheng, X.-M.; Huang, L.; Xiao, Y.; Su, H.; Xu, G.; Fu, F.; Li, J.-T.; Sun, S.-G. *Chem. Commun.* **2012**, *48*, 6854.
(793) Wu, J.-J.; Fu, Z.-W. *J. Electrochem. Soc.* **2009**, *156*, A22.
(794) Bichat, M.; Pascal, J.; Gillot, F.; Favier, F. *J. Phys. Chem. Solids* **2006**, *67*, 1233.
(795) Hwang, H.; Kim, M. G.; Kim, Y.; Martin, S. W.; Cho, J. *J. Mater. Chem.* **2007**, *17*, 3161.
(796) Boyanov, S.; Bernardi, J.; Gillot, F.; Dupont, L.; Womes, M.; Tarascon, J.-M.; Monconduit, L.; Doublet, M.-L. *Chem. Mater.* **2006**, *18*, 3531.
(797) Boyanov, S.; Womes, M.; Monconduit, L.; Zitoun, D. *Chem. Mater.* **2009**, *21*, 3684.
(798) Boyanov, S.; Zitoun, D.; Ménétrier, M.; Jumas, J. C.; Womes, M.; Monconduit, L. *J. Phys. Chem. C* **2009**, *113*, 21441.
(799) Cruz, M.; Morales, J.; Sánchez, L.; Santos-Peña, J.; Martín, F. *J. Power Sources* **2007**, *171*, 870.
(800) Park, C.-M.; Kim, Y.-U.; Sohn, H.-J. *Chem. Mater.* **2009**, *21*, 5566.
(801) Gillot, F.; Ménétrier, M.; Bekaert, E.; Dupont, L.; Morcrette, M.; Monconduit, L.; Tarascon, J. M. *J. Power Sources* **2007**, *172*, 877.
(802) Satyakishore, M.; Varadaraju, U. *J. Power Sources* **2006**, *156*, 594.
(803) Xia, Z.; Lin, Y.; Li, Z. *Mater. Charact.* **2008**, *59*, 1324.
(804) Boyanov, S.; Annou, K.; Villevieille, C.; Pelosi, M.; Zitoun, D.; Monconduit, L. *Ionics* **2007**, *14*, 183.
(805) Hwang, H.; Kim, M. G.; Cho, J. *J. Phys. Chem. C* **2007**, *111*, 1186.
(806) Villevieille, C.; Robert, F.; Taberna, P. L.; Bazin, L.; Simon, P.; Monconduit, L. *J. Mater. Chem.* **2008**, *18*, 5956.
(807) Kim, M. G.; Lee, S.; Cho, J. *J. Electrochem. Soc.* **2009**, *156*, A89.
(808) Park, C.-M.; Sohn, H.-J. *Chem. Mater.* **2008**, *20*, 6319.
(809) Xiang, J. Y.; Wang, X. L.; Xia, X. H.; Zhong, J.; Tu, J. P. *J. Alloys Compd.* **2011**, *509*, 157.
(810) Aso, K.; Hayashi, A.; Tatsumisago, M. *Inorg. Chem.* **2011**, *50*, 10820.
(811) Lu, Y.; Tu, J. P.; Xiang, J. Y.; Wang, X. L.; Zhang, J.; Mai, Y. J.; Mao, S. X. *J. Phys. Chem. C* **2011**, *115*, 23760.
(812) Lu, Y.; Tu, J.; Gu, C.; Wang, X.; Mao, S. X. *J. Mater. Chem.* **2011**, *21*, 17988.
(813) Carenco, S.; Surcin, C.; Morcrette, M.; Larcher, D.; Mézailles, N.; Boissière, C.; Sanchez, C. *Chem. Mater.* **2012**, *24*, 688.
(814) Lu, Y.; Tu, J.-P.; Xiong, Q.-Q.; Xiang, J.-Y.; Mai, Y.-J.; Zhang, J.; Qiao, Y.-Q.; Wang, X.-L.; Gu, C.-D.; Mao, S. X. *Adv. Funct. Mater.* **2012**, *22*, 3927.
(815) Lu, Y.; Wang, X.; Mai, Y.; Xiang, J.; Zhang, H.; Li, L.; Gu, C.; Tu, J.; Mao, S. X. *J. Phys. Chem. C* **2012**, *116*, 22217.
(816) Khatib, R.; Dalverny, A.-L.; Saubanère, M.; Gaberscek, M.; Doublet, M.-L. *J. Phys. Chem. C* **2013**, *117*, 837.
(817) Yang, D.; Zhu, J.; Rui, X.; Tan, H.; Cai, R.; Hoster, H. E.; Yu, D. Y. W.; Hng, H. H.; Yan, Q. *ACS Appl. Mater. Interfaces* **2013**, *5*, 1093.
(818) Liu, Y.; Cao, C.; Li, J.; Xu, X. *J. Appl. Electrochem.* **2009**, *40*, 419.
(819) Kim, I.; Blomgren, G. E.; Kumta, P. N. *Electrochem. Solid-State Lett.* **2003**, *6*, A157.
(820) Yang, H. X.; Wang, Y. D.; Ai, X. P.; Cha, C. S. *Electrochem. Solid-State Lett.* **2004**, *7*, A212.
(821) Licht, S.; Yu, X.; Qu, D. *Chem. Commun.* **2007**, *2*, 2753.
(822) Licht, S.; Yu, X.; Wang, Y.; Wu, H. *J. Electrochem. Soc.* **2008**, *155*, A297.
(823) Licht, S.; Wu, H.; Yu, X.; Wang, Y. *Chem. Commun.* **2008**, 3257.
(824) Wang, Y.; Guang, X. Y.; Cao, Y. L.; Ai, X. P.; Yang, H. X. *J. Appl. Electrochem.* **2009**, *39*, 1039.
(825) Zhou, W. C.; Yang, H. X.; Shao, S. Y.; Ai, X. P.; Cao, Y. L. *Electrochem. Commun.* **2006**, *8*, 55.
(826) Lambert, T. N.; Davis, D. J.; Limmer, S. J.; Hibbs, M. R.; Lavin, J. M. *Chem. Commun.* **2011**, *47*, 9597.
(827) Mitov, M.; Popov, A.; Dragieva, I. *J. Appl. Electrochem.* **1999**, *29*, 59.
(828) Mitov, M.; Popov, A.; Dragieva, I. *Colloids Surf., A* **1999**, *149*, 413.
(829) Wang, Y. D.; Ai, X. P.; Yang, H. X. *Chem. Mater.* **2004**, *7*, 5194.
(830) Liu, Y.; Wang, Y.; Xiao, L.; Song, D.; Jiao, L.; Yuan, H. *Electrochem. Commun.* **2007**, *9*, 925.
(831) Song, D.; Wang, Y.; Wang, Y.; Jiao, L.; Yuan, H. *Electrochem. Commun.* **2008**, *10*, 1486.
(832) Wang, Y.; Ai, X.; Cao, Y.; Yang, H. *Electrochem. Commun.* **2004**, *6*, 780.
(833) Liu, Y.; Wang, Y.; Xiao, L.; Song, D.; Jiao, L.; Yuan, H. *Electrochim. Acta* **2008**, *53*, 2265.
(834) Zhao, X.; Ma, L.; Shen, X. *J. Mater. Chem.* **2012**, *22*, 277.
(835) Wu, C.; Bai, Y.; Wang, X.; Wu, F.; Zhang, C. *Solid State Ionics* **2008**, *179*, 924.
(836) Anik, M.; Küçükdeveci, N. *Int. J. Hydrogen Energy* **2013**, *38*, 1501.
(837) Bai, Y.; Wu, C.; Wu, F.; Yang, L.; Wu, B. *Electrochem. Commun.* **2009**, *11*, 145.
(838) Yu, J.; Wang, L.; Wang, Y.; Dong, H.; Yang, H. *J. Electrochem. Soc.* **2004**, *151*, A1124.
(839) Lu, D.; Li, W.; Xiao, F.; Tang, R. *Electrochem. Commun.* **2010**, *12*, 362.
(840) Lu, D. S.; Li, W. S.; Tan, C. L.; Huang, Q. M. *Electrochim. Acta* **2011**, *56*, 4540.
(841) Wang, Q.; Jiao, L.; Du, H.; Huan, Q.; Peng, W.; Song, D.; Wang, Y.; Yuan, H. *Electrochim. Acta* **2011**, *58*, 437.
(842) Lu, D.; Li, W.; Tan, C.; Zeng, R. *Electrochim. Acta* **2009**, *55*, 171.
(843) Wu, C.; Bai, Y.; Wu, F.; Wang, X.; Lu, J.; Qiao, C. *Electrochem. Commun.* **2009**, *11*, 2173.
(844) Wang, Q.; Jiao, L.; Du, H.; Song, D.; Peng, W.; Si, Y.; Wang, Y.; Yuan, H. *Electrochim. Acta* **2010**, *55*, 7199.
(845) Prins, R.; Bussell, M. E. *Catal. Lett.* **2012**, *142*, 1413.
(846) Marton, J.; Adler, E. *Acta Chem. Scand.* **1961**, *15*, 370.
(847) Deng, J.; Zhang, X. *Solid State Ionics* **1989**, *32−33*, 1006.
(848) Deng, J.; Chen, H. *J. Mater. Sci. Lett.* **1993**, *12*, 1508.
(849) Ganem, B.; Osby, J. O. *Chem. Rev.* **1986**, *86*, 763.
(850) Xie, S.; Qiao, M.; Li, H.; Wang, W.; Deng, J. *Appl. Catal., A* **1999**, *176*, 129.
(851) Fan, G.-Y.; Jiang, W.-D.; Wang, J.-B.; Li, R.-X.; Chen, H.; Li, X.-J. *Catal. Commun.* **2008**, *10*, 98.
(852) Liu, S.; Liu, Z.; Wang, Z.; Zhao, S.; Wu, Y. *Appl. Catal., A* **2006**, *313*, 49.

(853) Wang, J.; Guo, P.; Yan, S.; Qiao, M.; Li, H.; Fan, K. *J. Mol. Catal A: Chem.* **2004**, *222*, 229.
(854) Liu, S. C.; Liu, Z.; Wang, Z.; Wu, Y.; Yuan, P. *Chem. Eng. J.* **2008**, *139*, 157.
(855) Wang, W.-J.; Qiao, M.-H.; Li, H.; Deng, J.-F. *Appl. Catal., A* **1998**, *166*, L243.
(856) Lee, S.-P.; Chen, Y.-W. *J. Chem. Technol. Biotechnol.* **2000**, *75*, 1073.
(857) Chen, L. F.; Chen, Y. W. *Ind. Eng. Chem. Res.* **2006**, *45*, 8866.
(858) Taghavi, F.; Falamaki, C.; Shabanov, A.; Bayrami, L.; Roumianfar, A. *Appl. Catal., A* **2011**, *407*, 173.
(859) Shen, J.-H.; Chen, Y.-W. *J. Mol. Catal A: Chem.* **2007**, *273*, 265.
(860) Liaw, B.; Chen, Y. Z. *Appl. Catal., A* **2000**, *196*, 199.
(861) Guo, J.; Hou, Y.; Yang, C.; Wang, Y.; Wang, L. *Mater. Lett.* **2012**, *67*, 151.
(862) Guo, J.; Hou, Y.; Yang, C.; Wang, Y.; He, H.; Li, W. *Catal. Commun.* **2011**, *16*, 86.
(863) Meng, Q.; Li, H.; Li, H. *J. Phys. Chem. C* **2008**, *112*, 11448.
(864) Li, H.; Yang, P.; Chu, D. *Appl. Catal., A* **2007**, *325*, 34.
(865) Narasimhan, C. S.; Deshpande, V. M.; Ramnarayan, K. *Chem. Commun.* **1988**, 99.
(866) Frierdich, A. J.; Joseph, C. E.; Strathmann, T. J. *Appl. Catal., B* **2009**, *90*, 175.
(867) Yi, G.; Zhang, B.; Wu, L.; Yang, Q. *Phys. B* **1995**, *216*, 103.
(868) Li, H.; Chen, H.; Dong, S.; Yang, J.; Deng, J. F. *Appl. Surf. Sci.* **1998**, *125*, 115.
(869) Luo, G.; Yan, S.; Qiao, M.; Fan, K. *J. Mol. Catal A: Chem.* **2005**, *230*, 69.
(870) Hou, Y.; Wang, Y.; Mi, Z. *J. Mater. Sci.* **2005**, *40*, 6585.
(871) Bai, G.; Zhao, Z.; Niu, L.; Dong, H.; Qiu, M.; Li, F.; Chen, Q.; Chen, G. *Catal. Commun.* **2012**, *23*, 34.
(872) Ji, H.-B.; Huang, Y.-Y.; Pei, L.-X.; Yao, X.-D. *Catal. Commun.* **2008**, *9*, 27.
(873) Zhang, X.; Zhang, Q.; Guan, J.; He, D.; Hu, H.; Liang, C. *Asia-Pac. J. Chem. Eng.* **2009**, *4*, 574.
(874) Zhang, X.; Zhang, Q.; Zhao, A.; Guan, J.; He, D.; Hu, H.; Liang, C. *Energy Fuels* **2010**, *24*, 3796.
(875) Chiang, S.-J.; Yang, C.-H.; Chen, Y.-Z.; Liaw, B.-J. *Appl. Catal., A* **2007**, *326*, 180.
(876) Yan, H.; Li, W.; Zhang, M.; Tao, K. *Chin. J. Catal.* **2009**, *30*, 89.
(877) Chen, X.; Wang, S.; Zhuang, J.; Qiao, M.; Fan, K.; He, H. *J. Catal.* **2004**, *227*, 419.
(878) Wen, H.; Yao, K.; Zhang, Y.; Zhou, Z.; Kirschning, A. *Catal. Commun.* **2009**, *10*, 1207.
(879) Xie, G.; Sun, W.; Li, W. *Catal. Commun.* **2008**, *10*, 333.
(880) Xu, S.; Li, F.; Wei, R. *Carbon* **2005**, *43*, 861.
(881) Luo, C.; Wang, W.; Qiao, M.; Fan, K. *J. Mol. Catal. A: Chem.* **2002**, *184*, 379.
(882) Chen, J.; Ci, D.; Wang, R.; Zhang, J. *Appl. Surf. Sci.* **2008**, *255*, 3300.
(883) Chen, Y.-Z.; Liaw, B.-J.; Chiang, S.-J. *Appl. Catal., A* **2005**, *284*, 97.
(884) Liu, Z.; Xie, S.; Liu, B.; Deng, J.-F. *New J. Chem.* **1999**, *23*, 1057.
(885) Li, X.; Zhang, Y.; Wang, A.; Wang, Y.; Hu, Y. *Catal. Commun.* **2010**, *11*, 1129.
(886) Carenco, S.; Leyva-Pérez, A.; Concepción, P.; Boissière, C.; Mézailles, N.; Sanchez, C.; Corma, A. *Nano Today* **2012**, *7*, 21.
(887) Zhou, G.; Wang, P.; Jiang, Z.; Ying, P.; Li, C. *Chin. J. Catal.* **2011**, *32*, 27.
(888) Li, Y.; Guo, W.; Zhu, H.; Zhao, L.; Li, M.; Li, S.; Fu, D.; Lu, X.; Shan, H. *Langmuir* **2012**, *28*, 3129.
(889) Belykh, L. B.; Skripov, N. I.; Belonogova, L. N.; Umanets, V. a.; Stepanova, T. P.; Schmidt, F. K. *Kinet. Catal.* **2011**, *52*, 702.
(890) Skripov, N. I.; Belykh, L. B.; Belonogova, L. N.; Umanets, V. a.; Ryzhkovich, E. N.; Schmidt, F. K. *Kinet. Catal.* **2010**, *51*, 714.
(891) Wang, H.; Shu, Y.; Zheng, M.; Zhang, T. *Catal. Lett.* **2008**, *124*, 219.
(892) Yang, P.; Jiang, Z.; Ying, P.; Li, C. *J. Catal.* **2008**, *253*, 66.
(893) Khurana, J.; Chauhan, S. *Synth. Commun.* **2001**, *31*, 3485.
(894) Yokozeki, M.; Shimokoshi, K.; Miyazaki, E. *Bull. Chem. Soc. Jpn.* **1986**, *59*, 2969.
(895) Molvinger, K.; Lopez, M.; Court, J. *Tetrahedron Lett.* **1999**, *40*, 8375.
(896) Cividino, P.; Masson, J.; Molvinger, K.; Court, J. *Tetrahedron: Asymmetry* **2000**, *11*, 3049.
(897) Molvinger, K.; Court, J.; Jobic, H. *J. Mol. Catal A: Chem.* **2001**, *174*, 245.
(898) Molvinger, K.; Court, J. *Tetrahedron: Asymmetry* **2001**, *12*, 1971.
(899) Liu, B.; Dai, W.; Wu, G.; Deng, J. *Catal. Lett.* **1997**, *49*, 181.
(900) Rajesh, B.; Sasirekha, N.; Chen, Y.; Lee, S. *Ind. Eng. Chem. Res.* **2007**, *46*, 2034.
(901) Rajesh, B.; Sasirekha, N.; Chen, Y.-W. *J. Mol. Catal A: Chem.* **2007**, *275*, 174.
(902) Rajesh, B.; Sasirekha, N.; Lee, S.-P.; Kuo, H.-Y.; Chen, Y.-W. *J. Mol. Catal A: Chem.* **2008**, *289*, 69.
(903) Huber, G. W.; Iborra, S.; Corma, A. *Chem. Rev.* **2006**, *106*, 4044.
(904) Hicks, J. *J. Phys. Chem. Lett.* **2011**, *2*, 2280.
(905) Li, W.; Dhandapani, B.; Oyama, S. *Chem. Lett.* **1998**, 207.
(906) Stinner, C.; Prins, R.; Weber, T. *J. Catal.* **2000**, *191*, 438.
(907) Stinner, C.; Prins, R.; Weber, T. *J. Catal.* **2001**, *202*, 187.
(908) Clark, P.; Li, W.; Oyama, S. T. *J. Catal.* **2001**, *200*, 140.
(909) Zhou, S.; Chen, J.; Liu, X.; Zhang, J. *Chin. J. Catal.* **2007**, *28*, 498.
(910) Liu, X.; Chen, J.; Zhang, J. *Ind. Eng. Chem. Res.* **2008**, *47*, 5362.
(911) Li, K.; Wang, R.; Chen, J. *Energy Fuels* **2011**, *25*, 854.
(912) Gong, S.; Liu, L.; He, H.; Cui, Q. *Korean J. Chem. Eng.* **2010**, *27*, 1419.
(913) Shu, Y.; Lee, Y.; Oyama, S. *J. Catal.* **2005**, *236*, 112.
(914) Cho, K.-S.; Lee, Y.-K. *Nucl. Instrum. Methods Phys. Res., Sect. A* **2010**, *621*, 690.
(915) Bonny, A.; Brewster, R.; Welborn, A. *Inorg. Chim. Acta* **1982**, *64*, L3.
(916) Bonny, A. M. *Fuel* **1984**, *63*, 1410.
(917) Skrabalak, S. E.; Suslick, K. S. *Chem. Mater.* **2006**, *18*, 3103.
(918) Parks, G.; Pease, M.; Burns, A.; Layman, K.; Bussell, M.; Wang, X.; Hanson, J.; Rodriguez, J. *J. Catal.* **2007**, *246*, 277.
(919) Truce, W. E.; Roberts, F. E. *J. Org. Chem.* **1963**, *28*, 961.
(920) Truce, W. E.; Perry, F. M. *J. Org. Chem.* **1965**, *30*, 1316.
(921) Back, T. G.; Yang, K.; Krouse, H. R. *J. Org. Chem.* **1992**, 1986.
(922) Boar, R. B.; Hawkins, D. W.; McGhie, J. F.; Barton, H. R. *J. Chem. Soc., Perkin Trans.* **1973**, 654.
(923) Back, T. G.; Yang, K. *J. Chem. Soc., Chem. Commun.* **1990**, 819.
(924) Schouten, S.; Pavlovic, D.; Damsté, J. S. S.; De Leeuw, J. *Org. Geochem.* **1993**, *20*, 901.
(925) Oyama, S.; Wang, X.; Lee, Y. K.; Bando, K.; Requejo, F. G. *J. Catal.* **2002**, *210*, 207.
(926) Wang, X.; Clark, P.; Oyama, S. T. *J. Catal.* **2002**, *208*, 321.
(927) Stinner, C.; Tang, Z.; Haouas, M.; Weber, T.; Prins, R. *J. Catal.* **2002**, *208*, 456.
(928) Burns, A. W.; Layman, K. a.; Bale, D. H.; Bussell, M. E. *Appl. Catal., A* **2008**, *343*, 68.
(929) Nelson, A.; Sun, M.; Junaid, A. *J. Catal.* **2006**, *241*, 180.
(930) Hernandez, A. B.; Ariga, H.; Takakusagi, S.; Kinoshita, K.; Suzuki, S.; Otani, S.; Oyama, S. T.; Asakura, K. *Chem. Phys. Lett.* **2011**, *513*, 48.
(931) Ma, D.; Xiao, T.; Xie, S.; Zhou, W.; Gonzalez-Cortes, S. L.; Green, M. L. H. *Chem. Mater.* **2004**, *16*, 2697.
(932) Guan, Q.; Cheng, X.; Li, R.; Li, W. *J. Catal.* **2013**, *299*, 1.
(933) Burns, A. W.; Gaudette, A. F.; Bussell, M. E. *J. Catal.* **2008**, *260*, 262.
(934) Gaudette, A. F.; Burns, A. W.; Hayes, J. R.; Smith, M. C.; Bowker, R. H.; Seda, T.; Bussell, M. E. *J. Catal.* **2010**, *272*, 18.
(935) Oyama, S. *J. Catal.* **2003**, *216*, 343.

(936) Hayes, J. R.; Bowker, R. H.; Gaudette, A. F.; Smith, M. C.; Moak, C. E.; Nam, C. Y.; Pratum, T. K.; Bussell, M. E. *J. Catal.* **2010**, *276*, 249.
(937) Bowker, R. H.; Smith, M. C.; Carrillo, B. A.; Bussell, M. E. *Top. Catal.* **2012**, *55*, 999.
(938) Guan, Q.; Sun, C.; Li, R.; Li, W. *Catal. Commun.* **2011**, *14*, 114.
(939) Qi, X.; Shi, Q.; Chen, W.; Zhang, R. *Chin. J. Catal.* **2012**, *33*, 543.
(940) Zhao, P.-F.; Ji, S.-F.; Wei, N.; Ma, Q.; Liu, H.; Li, C.-Y. *Acta Phys.-Chim. Sin.* **2011**, *27*, 1737.
(941) Oyama, S. T.; Clark, P.; Wang, X.; Shido, T.; Iwasawa, Y.; Hayashi, S.; Ramallo-López, J. M.; Requejo, F. G. *J. Phys. Chem. B* **2002**, *106*, 1913.
(942) Rodriguez, J. A.; Kim, J.-Y.; Hanson, J. C.; Sawhill, S. J.; Bussell, M. E. *J. Phys. Chem. B* **2003**, *107*, 6276.
(943) Ren, J.; Huo, C.-F.; Wen, X.-D.; Cao, Z.; Wang, J.; Li, Y.-W.; Jiao, H. *J. Phys. Chem. B* **2006**, *110*, 22563.
(944) Li, Q.; Hu, X. *Phys. Rev. B* **2006**, *74*, 035414.
(945) Oyama, S.; Lee, Y. *J. Catal.* **2008**, *258*, 393.
(946) Duan, X.; Teng, Y.; Wang, A.; Kogan, V.; Li, X.; Wang, Y. *J. Catal.* **2009**, *261*, 232.
(947) Bando, K. K.; Wada, T.; Miyamoto, T.; Miyazaki, K.; Takakusagi, S.; Koike, Y.; Inada, Y.; Nomura, M.; Yamaguchi, A.; Gott, T.; Oyama, S. T.; Asakura, K. *J. Catal.* **2012**, *286*, 165.
(948) Loboué, H.; Guillot-Deudon, C.; Popa, A. F.; Lafond, A.; Rebours, B.; Pichon, C.; Cseri, T.; Berhault, G.; Geantet, C. *Catal. Today* **2008**, *130*, 63.
(949) Teng, Y.; Wang, A.; Li, X.; Xie, J.; Wang, Y.; Hu, Y. *J. Catal.* **2009**, *266*, 369.
(950) Wang, W.; Zhang, X.; Yang, Y.; Yang, Y.; Peng, H.; Liu, W. *Chin. J. Catal.* **2012**, *33*, 215.
(951) Wang, W.; Yang, Y.; Luo, H.; Hu, T.; Liu, W. *React. Kinet., Mech. Catal.* **2010**, *102*, 207.
(952) Wang, W.; Yang, Y.; Luo, H.; Liu, W. *Catal. Commun.* **2010**, *11*, 803.
(953) Wang, W.; Yang, Y.; Luo, H.; Peng, H.; Wang, F. *Ind. Eng. Chem. Res.* **2011**, *50*, 10936.
(954) Wang, W.-Y.; Zhang, X.-Z.; Yang, Y.-Q.; Yang, Y.-S.; Peng, H.-Z.; Luo, H.-A. *Acta Phys.-Chim. Sin.* **2012**, *28*, 1243.
(955) Wang, W.; Yang, Y.; Luo, H.; Peng, H.; He, B.; Liu, W. *Catal. Commun.* **2011**, *12*, 1275.
(956) Wang, W.; Yang, Y.; Luo, H.; Peng, H.; Zhang, X.; Hu, T. *Chin. J. Catal.* **2011**, *32*, 1645.
(957) Loubinoux, B.; Heitz, M.; Coudert, G.; Guillaumet, G. *Tetrahedron Lett.* **1980**, *21*, 4991.
(958) Whiffen, V. M. L.; Smith, K. J. *Energy Fuels* **2010**, *24*, 4728.
(959) Zhao, H. Y.; Li, D.; Bui, P.; Oyama, S. T. *Appl. Catal., A* **2011**, *391*, 305.
(960) Yang, Y.; Ochoa-Hernández, C.; De la Peña O'Shea, V. A.; Coronado, J. M.; Serrano, D. P. *ACS Catal.* **2012**, *2*, 592.
(961) Bui, P.; Cecilia, J. A.; Oyama, S. T.; Takagaki, A.; Infantes-Molina, A.; Zhao, H.; Li, D.; Rodríguez-Castellón, E.; Jiménez López, A. *J. Catal.* **2012**, *294*, 184.
(962) Li, D.; Bui, P.; Zhao, H. Y.; Oyama, S. T.; Dou, T.; Shen, Z. H. *J. Catal.* **2012**, *290*, 1.
(963) Sun, C.; Wu, Z.; Mao, Y.; Yin, X.; Ma, L.; Wang, D.; Zhang, M. *Catal. Lett.* **2011**, *141*, 792.
(964) Han, Y.; Li, W.; Zhang, M.; Tao, K. *Chemosphere* **2008**, *72*, 53.
(965) Parshetti, G. K.; Doong, R.-A. *Water Res.* **2009**, *43*, 3086.
(966) Yang, L.; Lv, L.; Zhang, S.; Pan, B.; Zhang, W. *Chem. Eng. J.* **2011**, *178*, 161.
(967) Sawhill, S.; Layman, K.; Vanwyk, D.; Engelhard, M.; Wang, C.; Bussell, M. *J. Catal.* **2005**, *231*, 300.
(968) Yang, S.; Prins, R. *Chem. Commun.* **2005**, *2005*, 4178.
(969) Yang, S.; Liang, C.; Prins, R. *J. Catal.* **2006**, *237*, 118.
(970) Burns, S.; Hargreaves, J. S. J.; Hunter, S. M. *Catal. Commun.* **2007**, *8*, 931.
(971) Yao, Z. W.; Wang, L.; Dong, H. *J. Alloys Compd.* **2009**, *473*, L10.
(972) Cecilia, J. A.; Infantes-Molina, A.; Rodríguez-Castellón, E.; Jiménez-López, A. *J. Catal.* **2009**, *263*, 4.
(973) Guan, Q.; Li, W.; Zhang, M.; Tao, K. *J. Catal.* **2009**, *263*, 1.
(974) Guan, Q.; Li, W. *J. Catal.* **2010**, *271*, 413.
(975) Infantes-Molina, A.; Ceecilia, J. a.; Pawelec, B.; Fierro, J. L. G.; Rodríguez-Castellón, E.; Jiménez-López, A. *Appl. Catal., A* **2010**, *390*, 253.
(976) Lee, Y.; Oyama, S. *J. Catal.* **2006**, *239*, 376.
(977) Korányi, T. I.; Vit, Z.; Poduval, D.; Ryoo, R.; Kim, H.; Hensen, E. *J. Catal.* **2008**, *253*, 119.
(978) Song, L.; Li, W.; Wang, G.; Zhang, M.; Tao, K. *Catal. Today* **2007**, *125*, 137.
(979) Wang, K.; Yang, B.; Liu, Y.; Yi, C. *Energy Fuels* **2009**, *23*, 4209.
(980) Cho, K.-S.; Seo, H.-R.; Lee, Y.-K. *Catal. Commun.* **2011**, *12*, 470.
(981) Lee, Y.-K.; Shu, Y.; Oyama, S. T. *Appl. Catal., A* **2007**, *322*, 191.
(982) Bando, K. K.; Koike, Y.; Kawai, T.; Tateno, G.; Oyama, S. T.; Inada, Y.; Nomura, M.; Asakura, K. *J. Phys. Chem. C* **2011**, *115*, 7466.
(983) Li, X.; Lu, M.; Wang, A.; Song, C.; Hu, Y. *J. Phys. Chem. C* **2008**, *112*, 16584.
(984) Chen, J.; Zhou, S.; Ci, D.; Zhang, J.; Wang, R.; Zhang, J. *Ind. Eng. Chem. Res.* **2009**, *48*, 3812.
(985) Wang, R.; Smith, K. J. *Appl. Catal., A* **2009**, *361*, 18.
(986) Zhao, Y.; Zhao, Y.; Feng, H.; Shen, J. *J. Mater. Chem.* **2011**, *21*, 8137.
(987) Koo, K. Y.; Park, S. B. *J. Am. Ceram. Soc.* **2007**, *90*, 3767.
(988) Stamm, K. L.; Garno, J. C.; Liu, G.; Brock, S. L. *J. Am. Chem. Soc.* **2003**, *125*, 4038.
(989) Berhault, G.; Afanasiev, P.; Loboué, H.; Geantet, C.; Cseri, T.; Pichon, C.; Guillot-Deudon, C.; Lafond, A. *Inorg. Chem.* **2009**, *48*, 2985.
(990) Shu, Y.; Oyama, S. T. *Chem. Commun.* **2005**, 1143.
(991) Shu, Y.; Oyama, S. T. *Carbon* **2005**, *43*, 1517.
(992) Shi, G.; Shen, J. *Catal. Commun.* **2009**, *10*, 1693.
(993) Montesinos-Castellanos, A.; Zepeda, T. a.; Pawelec, B.; Lima, E.; Fierro, J. L. G.; Olivas, A.; De los Reyes, H., J. a. *Appl. Catal., A* **2008**, *334*, 330.
(994) Korányi, T. I.; Coumans, A. E.; Hensen, E. J. M.; Ryoo, R.; Kim, H. S.; Pfeifer, É.; Kasztovszky, Z. *Appl. Catal., A* **2009**, *365*, 48.
(995) Wang, R.; Smith, K. J. *Appl. Catal., A* **2010**, *380*, 149.
(996) Zhao, Y.; Xue, M.; Cao, M.; Shen, J. *Appl. Catal., B* **2011**, *104*, 229.
(997) Da Silva, V. T.; Sousa, L. a.; Amorim, R. M.; Andrini, L.; Figueroa, S. J. a.; Requejo, F. G.; Vicentini, F. C. *J. Catal.* **2011**, *279*, 88.
(998) Ibeh, B.; Zhang, S.; Hill, J. M. *Appl. Catal., A* **2009**, *368*, 127.
(999) Abu, I. I.; Smith, K. J. *Appl. Catal., A* **2007**, *328*, 58.
(1000) Lan, L.; Ge, S. H.; Liu, K. H.; Hou, Y. D.; Bao, X. J. *J. Nat. Gas Chem.* **2011**, *20*, 117.
(1001) Abu, I. I.; Smith, K. J. *Catal. Today* **2007**, *125*, 248.
(1002) Fuks, D.; Vingurt, D.; Landau, M. V; Herskowitz, M. *J. Phys. Chem. C* **2010**, *114*, 13313.
(1003) Bai, J.; Li, X.; Wang, A.; Prins, R.; Wang, Y. *J. Catal.* **2012**, *287*, 161.
(1004) Li, H.-W.; Yan, Y.; Orimo, S.; Züttel, A.; Jensen, C. M. *Energies* **2011**, *4*, 185.
(1005) Demirci, U. B.; Akdim, O.; Miele, P. *Int. J. Hydrogen Energy* **2009**, *34*, 2638.
(1006) Demirci, U. B.; Miele, P. *Energy Environ. Sci.* **2009**, *2*, 627.
(1007) Muir, S. S.; Yao, X. *Int. J. Hydrogen Energy* **2011**, *36*, 5983.
(1008) Amendola, S. C.; Onnerud, P.; Kelly, M. T.; Petillo, P. J.; Sharp-Goldman, S. L.; Binder, M. *J. Power Sources* **1999**, *84*, 130.
(1009) Amendola, S.; Sharp-Goldman, S. L.; Janjua, M. S.; Spencer, N. C.; Kelly, M. T.; Petillo, P. J.; Binder, M. *Int. J. Hydrogen Energy* **2000**, *25*, 969.
(1010) U.S. Department of Energy Hydrogen Program. *Independent Review. Go/No-Go Recommendation for Sodium Borohydride for On-*

Board Vehicular Hydrogen Storage; http://www.hydrogen.energy.gov/; 2007; pp NREL/MP-150-42220.
(1011) Liu, B.; Li, Q. *Int. J. Hydrogen Energy* **2008**, *33*, 738.
(1012) Liu, B. H.; Li, Z. P.; Suda, S. *J. Alloys Compd.* **2006**, *415*, 288.
(1013) Chen, Y.; Kim, H. *Fuel Process. Technol.* **2008**, *89*, 966.
(1014) Ingersoll, J. C.; Mani, N.; Thenmozhiyal, J. C.; Muthaiah, A. *J. Power Sources* **2007**, *173*, 450.
(1015) Fernandes, R.; Patel, N.; Miotello, A.; Filippi, M. *J. Mol. Catal., A: Chem.* **2009**, *298*, 1.
(1016) Wu, C.; Bai, Y.; Liu, D.-X.; Wu, F.; Pang, M.-L.; Yi, B.-L. *Catal. Today* **2011**, *170*, 33.
(1017) Yuan, X.; Jia, C.; Ding, X.-L.; Ma, Z.-F. *Int. J. Hydrogen Energy* **2012**, *37*, 995.
(1018) Liang, Y.; Wang, P.; Dai, H.-B. *J. Alloys Compd.* **2010**, *491*, 359.
(1019) Dai, H.; Liang, Y.; Wang, P.; Yao, X.; Rufford, T.; Lu, M.; Cheng, H. *Int. J. Hydrogen Energy* **2008**, *33*, 4405.
(1020) Patel, N.; Fernandes, R.; Miotello, A. *J. Catal.* **2010**, *271*, 315.
(1021) Zhuang, D.-W.; Kang, Q.; Muir, S. S.; Yao, X.; Dai, H.-B.; Ma, G.-L.; Wang, P. *J. Power Sources* **2013**, *224*, 304.
(1022) Patel, N.; Fernandes, R.; Miotello, A. *J. Power Sources* **2009**, *188*, 411.
(1023) Fernandes, R.; Patel, N.; Miotello, A. *Int. J. Hydrogen Energy* **2009**, *34*, 2893.
(1024) Li, S.; Yang, X.; Zhu, H.; Chen, Y.; Liu, Y. *J. Power Sources* **2011**, *196*, 5858.
(1025) Zhao, J.; Ma, H.; Chen, J. *Int. J. Hydrogen Energy* **2007**, *32*, 4711.
(1026) Xu, D.; Dai, P.; Guo, Q.; Yue, X. *Int. J. Hydrogen Energy* **2008**, *33*, 7371.
(1027) Patel, N.; Fernandes, R.; Guella, G.; Kale, A.; Miotello, A.; Patton, B.; Zanchetta, C. *J. Phys. Chem. C* **2008**, *112*, 6968.
(1028) Tong, D. G.; Luo, Y. Y.; Chu, W.; Hu, J. Y.; Wu, P. *Plasma Chem. Plasma Process.* **2010**, *30*, 663.
(1029) Paseka, I.; Velicka, J. *Electrochim. Acta* **1997**, *42*, 237.
(1030) Cho, K. W.; Kwon, H. S. *Catal. Today* **2007**, *120*, 298.
(1031) Eom, K.; Cho, K.; Kwon, H. *J. Power Sources* **2008**, *180*, 484.
(1032) Burchardt, T. *Int. J. Hydrogen Energy* **2002**, *27*, 323.
(1033) Podesta, J. J.; Piatti, R. C. V.; Arvia, A. J.; Ekdunge, P.; Jüttner, K.; Kreysa, G. *Int. J. Hydrogen Energy* **1992**, *17*, 9.
(1034) Kim, D.-R.; Cho, K.; Choi, Y.-I.; Park, C. *Int. J. Hydrogen Energy* **2009**, *34*, 2622.
(1035) Guo, Y.; Dong, Z.; Cui, Z.; Zhang, X.; Ma, J. *Int. J. Hydrogen Energy* **2012**, *37*, 1577.
(1036) Tong, D. G.; Zeng, X. L.; Chu, W.; Wang, D.; Wu, P. *J. Mater. Sci.* **2010**, *45*, 2862.
(1037) Patel, N.; Fernandes, R.; Guella, G.; Miotello, A. *Appl. Catal., B* **2010**, *95*, 137.
(1038) Patel, N.; Fernandes, R.; Edla, R.; Lihitkar, P. B.; Kothari, D. C.; Miotello, A. *Catal. Commun.* **2012**, *23*, 39.
(1039) Patel, N.; Kale, A.; Miotello, A. *Appl. Catal., B* **2012**, *111*−*112*, 178.
(1040) Minella, C. B.; Pellicer, E.; Rossinyol, E.; Karimi, F.; Pistidda, C.; Garroni, S.; Milanese, C.; Nolis, P.; Baró, M. D.; Gutfleisch, O.; Pranzas, K. P.; Schreyer, A.; Klassen, T.; Bormann, R.; Dornheim, M. *J. Phys. Chem. C* **2013**, *117*, 4394.
(1041) Tong, D. G.; Zeng, X. L.; Chu, W.; Wang, D.; Wu, P. *Mater. Res. Bull.* **2010**, *45*, 442.
(1042) Tong, D. G.; Chu, W.; Wu, P.; Gu, G. F.; Zhang, L. *J. Mater. Chem. A* **2013**, *1*, 358.
(1043) Cheng, R.; Shu, Y.; Zheng, M.; Li, L.; Sun, J.; Wang, X.; Zhang, T. *J. Catal.* **2007**, *249*, 397.
(1044) Ding, L.; Shu, Y.; Wang, A.; Zheng, M.; Li, L.; Wang, X.; Zhang, T. *Appl. Catal., A* **2010**, *385*, 232.
(1045) Guo, Y.; Liu, X.; Azmat, M. U.; Xu, W.; Ren, J.; Wang, Y.; Lu, G. *Int. J. Hydrogen Energy* **2012**, *37*, 227.
(1046) Luo, G.; Yan, S.; Qiao, M.; Zhuang, J.; Fan, K. *Appl. Catal., A* **2004**, *275*, 95.
(1047) Luo, G.; Yan, S.; Qiao, M.; Fan, K. *Appl. Catal., A* **2007**, *332*, 79.
(1048) Fan, G.-Y.; Zhang, Y.; Zhou, Y.-F.; Li, R.-X.; Chen, H.; Li, X.-J. *Chem. Lett.* **2008**, *37*, 852.
(1049) Yao, Z. W.; Dong, H.; Shang, Y. *J. Alloys Compd.* **2009**, *474*, L10.
(1050) Ding, L.-N.; Wang, A.-Q.; Zheng, M.-Y.; Zhang, T. *ChemSusChem* **2010**, *3*, 818.
(1051) Donald, J.; Xu, C.; Hashimoto, H.; Byambajav, E.; Ohtsuka, Y. *Appl. Catal., A* **2010**, *375*, 124.
(1052) Byeon, J. H.; Kim, Y.-W. *ACS Appl. Mater. Interfaces* **2011**, *3*, 2912.
(1053) Chen, L.; Lu, Y.; Hong, Q.; Lin, J.; Dautzenberg, F. M. *Appl. Catal., A* **2005**, *292*, 295.
(1054) Choudhary, T. V; Choudhary, V. R. *Angew. Chem., Int. Ed.* **2008**, *47*, 1828.
(1055) Xu, J.; Chen, L.; Tan, K. F.; Borgna, A.; Saeys, M. *J. Catal.* **2009**, *261*, 158.
(1056) Saeys, M.; Tan, K. F.; Chang, J.; Borgna, A. *Ind. Eng. Chem. Res.* **2010**, *49*, 11098.
(1057) Tan, K. F.; Chang, J.; Borgna, A.; Saeys, M. *J. Catal.* **2011**, *280*, 50.
(1058) Wang, Y.; Wu, H.; Zhang, Q.; Tang, Q. *Microporous Mesoporous Mater.* **2005**, *86*, 38.
(1059) Fan, X.-B.; Tao, Z.-Y.; Xiao, C.-X.; Liu, F.; Kou, Y. *Green Chem.* **2010**, *12*, 795.
(1060) Fan, X.-B.; Yan, N.; Tao, Z.-Y.; Evans, D.; Xiao, C.-X.; Kou, Y. *ChemSusChem* **2009**, *2*, 941.
(1061) Cheng, X.; Wu, B.; Yang, Y.; Xiang, H.; Li, Y. *J. Mol. Catal A: Chem.* **2010**, *329*, 103.
(1062) Cheng, X.; Wu, B.; Yang, Y.; Li, Y. *Catal. Commun.* **2011**, *12*, 431.
(1063) Xu, J.; Saeys, M. *J. Catal.* **2006**, *242*, 217.
(1064) Liang, Q.; Zhang, A.; Li, L. *J. Nat. Gas Chem.* **2008**, *17*, 303.
(1065) Sim, T. B.; Choi, J.; Joung, M. J.; Yoon, N. M. *J. Org. Chem.* **1997**, *62*, 2357.
(1066) Joung, M. J.; Ahn, J. H.; Lee, D. W.; Yoon, N. M. *J. Org. Chem.* **1998**, *63*, 2755.
(1067) Li, H.; Dong, F.; Xiong, M.; Li, H.; Li, P.; Zhou, X. *Adv. Synth. Catal.* **2011**, *353*, 2131.
(1068) Zhu, Z.; Ma, J.; Xu, L.; Xu, L.; Li, H.; Li, H. *ACS Catal.* **2012**, *2*, 2119.
(1069) Zaman, S. F.; Smith, K. J. *Mol. Simul.* **2008**, *34*, 1073.
(1070) Zaman, S.; Smith, K. *Catal. Commun.* **2009**, *10*, 468.
(1071) Zaman, S. F.; Smith, K. J. *Appl. Catal., A* **2010**, *378*, 59.
(1072) Bae, J. W.; Kim, S.-M.; Park, S.-J.; Lee, Y.-J.; Ha, K.-S.; Jun, K.-W. *Catal. Commun.* **2010**, *11*, 834.
(1073) Liu, P.; Rodriguez, J. a.; Takahashi, Y.; Nakamura, K. *J. Catal.* **2009**, *262*, 294.
(1074) Izhar, S.; Nagai, M. *Catal. Today* **2009**, *146*, 172.
(1075) Ding, L.-X.; Wang, A.-L.; Li, G.-R.; Liu, Z.-Q.; Zhao, W.-X.; Su, C.-Y.; Tong, Y.-X. *J. Am. Chem. Soc.* **2012**, *134*, 5730.
(1076) Dou, Y. Y.; Li, G. R.; Song, J.; Gao, X. P. *Phys. Chem. Chem. Phys.* **2012**, *14*, 1339.
(1077) Wu, M.; Bai, J.; Wang, Y.; Wang, A.; Lin, X.; Wang, L.; Shen, Y.; Wang, Z.; Hagfeldt, A.; Ma, T. L. *J. Mater. Chem.* **2012**, *22*, 11121.
(1078) Dabo, P.; Cyr, A.; Lessard, J.; Brossard, L.; Ménard, H. *Can. J. Chem.* **1999**, *77*, 1225.
(1079) Barton, E. E.; Rampulla, D. M.; Bocarsly, A. B. *J. Am. Chem. Soc.* **2008**, *130*, 6342.
(1080) Kaneco, S.; Ueno, Y.; Katsumata, H.; Suzuki, T.; Ohta, K. *Chem. Eng. J.* **2009**, *148*, 57.
(1081) Nann, T.; Ibrahim, S. K.; Woi, P.-M.; Xu, S.; Ziegler, J.; Pickett, C. J. *Angew. Chem., Int. Ed.* **2010**, *49*, 1574.
(1082) Sun, J.; Liu, C.; Yang, P. *J. Am. Chem. Soc.* **2011**, *133*, 19306.
(1083) Liu, Y.; Pan, Y.; Chi, W.; Shen, Z. *Appl. Surf. Sci.* **2011**, *257*, 9403.
(1084) Golberg, D.; Bando, Y.; Tang, C. C.; Zhi, C. Y. *Adv. Mater.* **2007**, *19*, 2413.

(1085) Zhong, B.; Huang, X.; Wen, G.; Xia, L.; Yu, H.; Bai, H. *J. Phys. Chem. C* **2010**, *114*, 21165.
(1086) Li, L.; Li, L. H.; Chen, Y.; Dai, X. J.; Xing, T.; Petravic, M.; Liu, X. *Nanoscale Res. Lett.* **2012**, *7*, 417.
(1087) Loh, K. P.; Lin, M.; Yeadon, M.; Boothroyd, C.; Hu, Z. *Chem. Phys. Lett.* **2004**, *387*, 40.
(1088) Sun, C.; Yu, H.; Xu, L.; Ma, Q.; Qian, Y. *J. Nanomater.* **2010**, *2010*, 1.
(1089) Lourie, O.; Jones, C.; Bartlett, B. M.; Gibbons, P. C.; Ruoff, R. S.; Buhro, W. E. *Chem. Mater.* **2000**, *12*, 1808.
(1090) Tang, C.; Bando, Y.; Sato, T. *Chem. Phys. Lett.* **2002**, *362*, 185.
(1091) Bokhonov, B.; Korchagin, M.; Borisova, Y. *J. Alloys Compd.* **2004**, *372*, 141.
(1092) Tokoro, H.; Fujii, S.; Oku, T. *Solid State Commun.* **2005**, *133*, 681.
(1093) Zhang, L.; Zhang, G.; Chen, C.; Li, L.; Xia, T.; Shi, K. *CrystEngComm* **2011**, *13*, 7153.
(1094) Huang, S.; Bai, Y.; Chen, J.; Wang, S.; Wang, Z. *Chem. Phys. Lett.* **2008**, *464*, 49.
(1095) Kim, M. H.; Baik, J. M.; Zhang, J.; Larson, C.; Li, Y.; Stucky, G. D.; Moskovits, M.; Wodtke, A. M. *J. Phys. Chem. C* **2010**, *114*, 10697.
(1096) Zhou, L.; Kong, Y.; Du, Y.; Wang, J.; Zhou, Y. *Appl. Surf. Sci.* **2010**, *256*, 7692.
(1097) Mandel, K.; Dillon, F.; Koos, A. a; Aslam, Z.; Jurkschat, K.; Cullen, F.; Crossley, A.; Bishop, H.; Moh, K.; Cavelius, C.; Arzt, E.; Grobert, N. *Chem. Commun.* **2011**, *47*, 4108.
(1098) Ko, J.-W.; Yoo, J.; Kim, Y.-K.; Chung, S.-J.; Yoo, S. I. *Phys. C* **2004**, *412−414*, 1194.
(1099) Liu, C.; Dai, L.; You, L. P.; Xu, W. J.; Ma, R. M.; Yang, W. Q.; Zhang, Y. F.; Qin, G. G. *J. Mater. Chem.* **2008**, *18*, 3912.
(1100) Güllü, O.; Çankaya, M.; Barış, O.; Türüt, A. *Appl. Phys. Lett.* **2008**, *92*, 212106.
(1101) Cernohorsky, O.; Zdansky, K.; Zavadil, J.; Kacerovsky, P.; Piksova, K. *Nanoscale Res. Lett.* **2011**, *6*, 410.
(1102) Feldman, C.; Charles, H. K.; Satkiewicz, F. G. Patent No. 4,313,254, 1982.
(1103) Takeyama, M. B.; Noya, A.; Nakadai, Y.; Kambara, S.; Hatanaka, M.; Hayasaka, Y.; Aoyagi, E.; Machida, H.; Masu, K. *Appl. Surf. Sci.* **2009**, *256*, 1222.
(1104) Kumar, N.; Yang, Y.; Noh, W.; Girolami, G. S.; Abelson, J. R. *Chem. Mater.* **2007**, *19*, 3802.
(1105) Kinoshita, H.; Otani, S.; Kamiyama, S.; Amano, H.; Akasaki, I.; Suda, J.; Matsunami, H. *Jpn. J. Appl. Phys.* **2001**, *40*, L1280.
(1106) Kamiyama, S.; Takanami, S.; Tomida, Y.; Iida, K.; Kawashima, T.; Fukui, S.; Iwaya, M.; Kinoshita, H.; Matsuda, T.; Yasuda, T.; Otani, S.; Amano, H.; Akasaki, I. *Physica Status Solidi A* **2003**, *200*, 67.
(1107) Bera, S.; Sumiyoshi, Y.; Yamada-Takamura, Y. *J. Appl. Phys.* **2009**, *106*, 063531.
(1108) Tolle, J.; Roucka, R.; Tsong, I. S. T.; Ritter, C.; Crozier, P. a.; Chizmeshya, a. V. G.; Kouvetakis, J. *Appl. Phys. Lett.* **2003**, *82*, 2398.
(1109) Tolle, J.; Kouvetakis, J.; Kim, D.-W.; Mahajan, S.; Bell, a.; Ponce, F. a.; Tsong, I. S. T.; Kottke, M. L.; Chen, Z. D. *Appl. Phys. Lett.* **2004**, *84*, 3510.
(1110) Hu, C.-W.; Chizmeshya, a. V. G.; Tolle, J.; Kouvetakis, J.; Tsong, I. S. T. *J. Cryst. Growth* **2004**, *267*, 554.
(1111) Roucka, R.; D'Costa, V.; An, Y. J.; Canonico, M.; Kouvetakis, J.; Menéndez, J.; Chizmeshya, A. *Chem. Mater.* **2008**, *20*, 1431.
(1112) Yamada-Takamura, Y.; Bussolotti, F.; Fleurence, A.; Bera, S.; Friedlein, R. *Appl. Phys. Lett.* **2010**, *97*, 073109.
(1113) Blake, A. H.; Caselli, D.; Durot, C.; Mueller, J.; Parra, E.; Gilgen, J.; Boley, A.; Smith, D. J.; Tsong, I. S. T.; Roberts, J. C.; Piner, E.; Linthicum, K.; Cook, J. W.; Koleske, D. D.; Crawford, M. H.; Fischer, A. J. *J. Appl. Phys.* **2012**, *111*, 033107.
(1114) Roucka, R.; An, Y.; Chizmeshya, A. V. G.; Tolle, J.; Kouvetakis, J.; D'Costa, V. R.; Menéndez, J.; Crozier, P. *Appl. Phys. Lett.* **2006**, *89*, 242110.
(1115) Trivedi, R.; Liu, P.-L.; Roucka, R.; Tolle, J.; Chizmeshya, A. V. G.; Tsong, I. S. T.; Kouvetakis, J. *Chem. Mater.* **2005**, *82*, 4647.
(1116) Fleurence, A.; Friedlein, R.; Ozaki, T.; Kawai, H.; Wang, Y.; Yamada-Takamura, Y. *Phys. Rev. Lett.* **2012**, *108*, 245501.
(1117) Xu, J. Q.; Zhao, Y. M.; Zhang, Q. Y. *J. Appl. Phys.* **2008**, *104*, 124306.
(1118) Fukudan, Y.; Watanabe, Y.; Ogura, S.; Iizuka, T. Patent No. 5,433,988, 1995.
(1119) Ziegler, J.; Xu, S.; Kucur, E.; Meister, F.; Batentschuk, M.; Gindele, F.; Nann, T. *Adv. Mater.* **2008**, *20*, 4068.
(1120) Lim, J.; Bae, W. K.; Lee, D.; Nam, M. K.; Jung, J.; Lee, C.; Char, K.; Lee, S. *Chem. Mater.* **2011**, *23*, 4459.
(1121) Kim, S.; Kim, T.; Kang, M.; Kwak, S. K.; Yoo, T. W.; Park, L. S.; Yang, I.; Hwang, S.; Lee, J. E.; Kim, S. K.; Kim, S.-W. *J. Am. Chem. Soc.* **2012**, *134*, 3804.
(1122) Sato, T.; Yoshizawa, N.; Hashizume, T. *Thin Solid Films* **2010**, *518*, 4399.
(1123) Wang, F.; Reece, P. J.; Paiman, S.; Gao, Q.; Tan, H. H.; Jagadish, C. *Nano Lett.* **2011**, *11*, 4149.
(1124) Rivoire, K.; Faraon, A.; Vuckovic, J. *Appl. Phys. Lett.* **2008**, *93*, 063103.
(1125) Yan, R.; Gargas, D.; Yang, P. *Nat. Photonics* **2009**, *3*, 569.
(1126) Merchant, S. K. E.; Lloyd-Hughes, J.; Sirbu, L.; Tiginyanu, I. M.; Parkinson, P.; Herz, L. M.; Johnston, M. B. *Nanotechnology* **2008**, *19*, 395704.
(1127) Rowe, D. J.; Jeong, J. S.; Mkhoyan, K. A.; Kortshagen, U. R. *Nano Lett.* **2013**, *13*, 1317.
(1128) Carenco, S.; Florea, I.; Ersen, O.; Boissière, C.; Mézailles, N.; Sanchez, C. *New J. Chem.* **2013**, 1231.
(1129) Brunsman, E. M.; Scott, J. H.; Majetich, S. a.; McHenry, M. E.; Huang, M.-Q. *J. Appl. Phys.* **1996**, *79*, 5293.
(1130) Saiyasombat, C.; Petchsang, N.; Tang, I. M.; Hodak, J. H. *Nanotechnology* **2008**, *19*, 085705.
(1131) Mustapic, M.; Pajic, D.; Novosel, N.; Babic, E.; Zadro, K.; Cindric, M.; Horvat, J.; Skoko, Z.; Bijelic, M.; Shcherbakov, A. *Croat. Chem. Acta* **2010**, *83*, 275.
(1132) Bick, J.-P.; Honecker, D.; Döbrich, F.; Suzuki, K.; Gilbert, E. P.; Frielinghaus, H.; Kohlbrecher, J.; Gavilano, J.; Forgan, E. M.; Schweins, R.; Lindner, P.; Birringer, R.; Michels, A. *Appl. Phys. Lett.* **2013**, *102*, 022415.
(1133) Legrand, J.; Gota, S.; Guittet, M.-J.; Petit, C. *Langmuir* **2002**, *18*, 4131.
(1134) An, Z.; Zhang, J.; Pan, S. *Dalton Trans.* **2010**, *39*, 3378.
(1135) Wang, W.; Sun, Z.; Zheng, M.; Dong, X.; Zhao, Z.; Duan, X. *J. Phys. Chem. C* **2011**, *115*, 11275.
(1136) An, Z.; Zhang, J. *ACS Appl. Mater. Interfaces* **2013**, *5*, 989.
(1137) Andrievski, R. a. *Int. J. Refract. Met. Hard Mater.* **2001**, *19*, 447.
(1138) Chatterjee, A.; Jayaraman, S.; Gerbi, J. E.; Kumar, N.; Abelson, J. R.; Bellon, P.; Polycarpou, A. A.; Chevalier, J. P. *Surf. Coat. Technol.* **2006**, *201*, 4317.
(1139) Jayaraman, S.; Gerbi, J. E.; Yang, Y.; Kim, D. Y.; Chatterjee, A.; Bellon, P.; Girolami, G. S.; Chevalier, J. P.; Abelson, J. R. *Surf. Coat. Technol.* **2006**, *200*, 6629.
(1140) Chatterjee, A.; Kumar, N.; Abelson, J. R.; Bellon, P.; Polycarpou, A. A. *Wear* **2008**, *265*, 921.
(1141) Chatterjee, A.; Kumar, N.; Abelson, J. R.; Bellon, P.; Polycarpou, A. A. *Tribol. Trans.* **2010**, *53*, 731.
(1142) Rinaldi, a.; Correa-Duarte, M. a.; Salgueirino-Maceira, V.; Licoccia, S.; Traversa, E.; Dávila-Ibáñez, a. B.; Peralta, P.; Sieradzki, K. *Acta Mater.* **2010**, *58*, 6474.
(1143) Khanal, S.; Millar, T. J. *Nanomed.: Nanotechnol., Biol., Med.* **2010**, *6*, 707.
(1144) Hussain, S.; Won, N.; Nam, J.; Bang, J.; Chung, H.; Kim, S. *ChemPhysChem* **2009**, *10*, 1466.
(1145) Yong, K.-T.; Ding, H.; Roy, I.; Law, W.-C.; Bergey, E. J.; Maitra, A.; Prasad, P. N. *ACS Nano* **2009**, *3*, 502.

(1146) Stasiuk, G. J.; Tamang, S.; Imbert, D.; Poillot, C.; Giardiello, M.; Tisseyre, C.; Barbider, E. L.; Fries, P. H.; De Waard, M.; Reiss, P.; Mazzanti, M. *ACS Nano* **2011**, *5*, 8193.
(1147) Brunetti, V.; Chibli, H.; Fiammengo, R.; Galeone, A.; Malvindi, M. A.; Vecchio, G.; Cingolani, R.; Nadeau, J. L.; Pompa, P. P. *Nanoscale* **2013**, *5*, 307.
(1148) Chibli, H.; Carlini, L.; Park, S.; Dimitrijevic, N. M.; Nadeau, J. L. *Nanoscale* **2011**, *3*, 2552.
(1149) Linsmeier, C. E.; Wallman, L.; Faxius, L.; Schouenborg, J.; Bjursten, L. M.; Danielsen, N. *Biomaterials* **2008**, *29*, 4598.
(1150) Ni, Y.; Li, J.; Jin, L.; Xia, J.; Hong, J.; Liao, K. *New J. Chem.* **2009**, *33*, 2055.
(1151) Ni, Y.; Mi, K.; Cheng, C.; Xia, J.; Ma, X.; Hong, J. *Chem. Commun.* **2011**, *47*, 5891.
(1152) Ni, Y.; Liao, K.; Li, J. *CrystEngComm* **2010**, *12*, 1568.
(1153) Lee, C.; Sanders, A.; Tikekar, N.; Chandran, K. S. R. *Wear* **2008**, *265*, 375.
(1154) Liu, W.; Sun, X.; Pederson, L. R.; Marina, O. A.; Khaleel, M. A. *J. Power Sources* **2010**, *195*, 7140.
(1155) Demircan, O.; Zhang, W.; Xu, C.; Zondlo, J.; Finklea, H. O. *J. Power Sources* **2010**, *195*, 3091.
(1156) Haga, K.; Shiratori, Y.; Nojiri, Y.; Ito, K.; Sasaki, K. *J. Electrochem. Soc.* **2010**, *157*, B1693.
(1157) Marina, O. A.; Coyle, C. A.; Thomsen, E. C.; Edwards, D. J.; Coffey, G. W.; Pederson, L. R. *Solid State Ionics* **2010**, *181*, 430.
(1158) Iablokov, V.; Beaumont, S. K.; Alayoglu, S.; Pushkarev, V. V; Specht, C.; Gao, J.; Alivisatos, A. P.; Kruse, N.; Somorjai, G. A. *Nano Lett.* **2012**, *12*, 3091.
(1159) Carenco, S.; Boissière, C.; Nicole, L.; Sanchez, C.; Le Floch, P.; Mézailles, N. *Chem. Mater.* **2010**, *22*, 1340.
(1160) Carenco, S.; Labouille, S.; Bouchonnet, S.; Boissière, C.; Le Goff, X.-F.; Sanchez, C.; Mézailles, N. *Chem.—Eur. J.* **2012**, *18*, 14165.
(1161) Zhang, H. R.; Ojo, O. A.; Chaturvedi, M. C. *Scr. Mater.* **2008**, *58*, 167.
(1162) Okamoto, H.; Massalski, T. B. *Bull. Alloy Phase Diagrams* **1984**, *5*, 490.
(1163) Fatemi, N. S.; Weizer, V. G. *J. Appl. Phys.* **1990**, *67*, 1934.
(1164) Takeuchi, A.; Ranganathan, S.; Murty, B. S.; Inoue, A. *Rev. Adv. Mater. Sci* **2008**, *18*, 56.
(1165) Li, Y.; Poon, S. J.; Shiflet, G. J.; Xu, J.; Kim, D. H.; Löffler, J. F. *MRS Bull.* **2007**, *32*, 624.
(1166) Inoue, A.; Nishiyama, N. *MRS Bull.* **2007**, *32*, 651.
(1167) Johnson, W. L.; Demetriou, M. D.; Harmon, J. S.; Lind, M. L.; Samwer, K. *MRS Bull.* **2007**, *32*, 644.
(1168) Kinomura, N.; Terao, K.; Kikkawa, S.; Koizumi, M. *J. Solid State Chem.* **1983**, *48*, 306.
(1169) Souza, S. M.; Trichês, D. M.; De Lima, J. C.; Grandi, T. A.; Campos, C. E. M. *J. Appl. Phys.* **2007**, *102*, 063523.
(1170) Alleg, S.; Rihia, G.; Bensalem, R.; Sunol, J. *Ann. Chim. Sci. Mater.* **2009**, *34*, 267.
(1171) Tebib, W.; Alleg, S.; Bensalem, R.; Bensebaa, N.; Bentayeb, F. Z.; Suñol, J. J.; Grenèche, J. M. *J. Nanosci. Nanotechnol.* **2008**, *8*, 2029.
(1172) Bensalem, R.; Tebib, W.; Alleg, S.; Suñol, J. J.; Bessais, L.; Greneche, J. M. *J. Alloys Compd.* **2009**, *471*, 24.
(1173) Ganesan, R.; Richter, K. W.; Schmetterer, C.; Effenberger, H.; Ipser, H. *Chem. Mater.* **2009**, *21*, 4108.
(1174) Muthuswamy, E.; Brock, S. L. *Chem. Commun.* **2011**, *47*, 12334.
(1175) Goto, Y.; Taniguchi, K.; Omata, T.; Otsuka-Yao-Matsuo, S.; Ohashi, N.; Ueda, S.; Yoshikawa, H.; Yamashita, Y.; Oohashi, H.; Kobayashi, K. *Chem. Mater.* **2008**, *20*, 4156.
(1176) Schaefer, Z. L.; Weeber, K. M.; Misra, R.; Schiffer, P.; Schaak, R. E. *Chem. Mater.* **2011**, *23*, 2475.
(1177) Sautet, P.; Cinquini, F. *ChemCatChem* **2010**, *2*, 636.
(1178) Cabot, A.; Ibáñez, M.; Guardia, P.; Alivisatos, A. P. *J. Am. Chem. Soc.* **2009**, *131*, 11326.
(1179) Fan, H. J.; Gösele, U.; Zacharias, M. *Small* **2007**, *3*, 1660.
(1180) Dionízio Moreira, M.; Venezuela, P.; Schmidt, T. M. *Nanotechnology* **2008**, *19*, 065203.
(1181) Moreels, I.; Martins, J.; Hens, Z. *Sens. Actuators, B* **2007**, *126*, 283.
(1182) Cros-Gagneux, A.; Delpech, F.; Nayral, C.; Cornejo, A.; Coppel, Y.; Chaudret, B. *J. Am. Chem. Soc.* **2010**, *132*, 18147.
(1183) Virieux, H.; Le Troedec, M.; Cros-Gagneux, A.; Ojo, W.-S.; Delpech, F.; Nayral, C.; Martinez, H.; Chaudret, B. *J. Am. Chem. Soc.* **2012**, *134*, 19701.
(1184) Lovingood, D. D.; Strouse, G. F. *Nano Lett.* **2008**, *8*, 3394.